BIOGEOCHEMICAL MECHANISMS OF RARE EARTH ELEMENT ENRICHMENT IN MINING-AFFECTED AQUEOUS ENVIRONMENTS

BY

ELIZABETH ASHBY

A thesis submitted to the Department of Earth and Environmental Science in partial fulfillment of requirements for the degree Master of Science

University of Ottawa
Faculty of Science
Department of Earth and Environmental Science
Ottawa, Ontario, Canada
September, 2017

uOttawa

ABSTRACT

One of the largest environmental liabilities facing the Canadian and international mining industry is the effect of acidic drainage to water resources. This thesis sought to determine mechanisms of rare earth element and yttrium (REY) enrichment in mine drainage, linkages between REYs and microbial populations, and whether REYs in water or biofilm occur at mineable quantities or toxic levels. Water and co-occurring biofilm samples were collected from North and South American mining and control sites, with detailed sampling at a coal mine passive water treatment system in Pennsylvania. REY concentrations within mineralized biofilm were observed to occur at borderline mineable quantities in coal mine biofilm (1,000 mg/kg dry weight total REYs), where REYs were bound predominately to particulate organic matter, manganese and iron, limiting their bioavailability. Within the passive treatment system, REYs showed the largest maximum water-biofilm partitioning coefficients after Al and Fe, and a strong inverse relationship with aqueous REY concentration. Photosynthetic eukaryotes were observed to occur within biofilms that contained an abundance of neutrophilic iron oxidizing bacteria.

RÉSUMÉ

Une des plus grandes responsabilités auxquelles font face les industries minières canadiennes et internationales est la contamination des réserves d'eau douce par le drainage acide généré par les mines. Cette thèse avait pour but de déterminer les mécanismes qui expliquent l'enrichissement en terres rares et en yttrium (Y) du drainage minier, les liens qui existent entre les terres rares et Y et les populations bactériennes ainsi que la possibilité que les biofilms présents dans les eaux de mines contiennent assez de terres rares pour permettre leur extraction ou si elles étaient présentes à des niveaux toxiques. Des échantillons d'eau et des biofilms ont été échantillonnés dans des sites miniers en Amérique du Nord et du Sud, des sites contrôles et dans un bassin de traitement passif d'une mine de charbon en Pennsylvanie. Les concentrations de terres rares et de Y dans les biofilms collectés dans le traitement passif étaient vraiment près des concentrations pouvant être extraites (1000 mg/kg de poids sec de terres rares et de Y). Les terres rares et le Y étaient associés au matériel organique particulaire et aux oxydes de Fe et Mn, limitant ainsi leur biodisponibilité. Dans le traitement passif, les terres rares et le Y ont présenté le plus grand coefficient de partage entre le biofilm et l'eau, suivi par le Fe et Al, et une relation inverse avec les concentrations solubles. Des organismes photosynthétiques ont été observés dans les biofilms qui contenaient des bactéries neutrophiles capables d'oxyder le fer.

ACKNOWLEDGEMENTS

This work would not have proceeded without the contribution of expertise, time, and ideas from a large group of people. First, I would like to thank my supervisor, Dr. Danielle Fortin, who gave me the idea to examine the partitioning coefficients of rare earth elements between water and biofilm, and the freedom to explore this interesting research area. I am also indebted to the entire Fortin lab group, particularly Maeve Moriarty, Tarek Najem, Brandon Khan and Emily Meyers. I would also like to heartily thank my USGS collaborator, Dr. Charles Cravotta. Dr. Cravotta has been a very supportive collaborator that has invested much expertise and time into the kinetic modelling of the Silver Creek drainage. Without his expertise, enthusiasm and access to the extremely interesting Silver Creek field site, my thesis would be a much different document. Maeve Moriarty, Dr. Danielle Fortin, Natalia Baranova and Emily Meyers all assisted with field sampling, thank-you! I am also indebted to Dr. Jamieson (Queen's University), Lori Manoukian (Queen's University) and Kristen Gault (AMEC Foster Wheeler) for provision of rare earth element data at field sites located in South America and the Yukon. I would also like to thank all of the members of the University of Ottawa Geochemistry laboratory, including Ping Zhang, Smita Mohanty and Nimal De Silva, who were instrumental in completing analyses via inductively coupled plasma mass and emission spectroscopy. In addition, I would like to thank the members of the University of Ottawa Hatch Lab: Pau Middlestead, Wendy Abdi, Patricia Wickham and Kerry Klassen, who provided their expertise in determining appropriate methods for quantifying organic carbon concentrations.

A final thank-you to Dr. Jack Cornett, Dr. Paul Gammon and Dr. Richard Goulet who formed my thesis defense committee, and provided comments that improved this manuscript.

TABLE OF CONTENTS

PAGE

TABLES

FIGURES

APPENDICES

ABBREVIATIONS

ARD ..... acid rock drainage
CMD ..... coal mine drainage
DIC ..... dissolved inorganic carbon
DOC ..... dissolved organic carbon
NMD ..... neutral mine drainage
ICP-MS ..... Inductively Coupled Plasma – Mass Spectroscopy
ICP-ES ..... Inductively Coupled Plasma – Optical Emission Spectroscopy
REY ..... rare earth elements and yttrium
LED ..... light-emitting diode
LREE ..... light rare earth elements (La-Sm)
HREY ..... heavy rare earth elements (Eu-Lu and Y)
MREE ..... middle rare earth elements (Sm-Ho)
HFO ..... hydrous ferric oxide (HFO)
IC ..... ion chromatography
NASC ..... North American shale composite
PAAS ..... Post-Archean average shale
PZC ..... point of zero charge
PCO_2 ..... partial pressure of carbon dioxide

TABLE OF CONTENTS

PAGE

TABLES

FIGURES

ABBREVIATIONS

ARD ..... acid rock drainage
BIOS ..... bacteriogenic iron oxides
BCF ..... bioconcentration factor
BAF ..... bioaccumulation factor
CMD ..... coal mine drainage
CO_2 ..... coal mine drainage
ddPCR ..... droplet digital PCR
DIC ..... dissolved inorganic carbon
DOC ..... dissolved organic carbon
EPS ..... extracellular polymeric substances
HREY ..... heavy rare earth elements (Eu-Lu and Y)
HFO ..... hydrous ferric oxide (HFO)
IC ..... ion chromatography
ICP-MS ..... Inductively Coupled Plasma – Mass Spectroscopy
ICP-ES ..... Inductively Coupled Plasma – Optical Emission Spectroscopy
LED ..... light-emitting diode
LREE ..... light rare earth elements (La-Sm)
MREE ..... middle rare earth elements (Sm-Ho)
NASC ..... North American shale composite
NMD ..... neutral mine drainage
PAAS ..... Post-Archean average shale
PZC ..... point of zero charge
PCO_2 ..... partial pressure of carbon dioxide
rRNA ..... ribosomal ribonucleic acid
REY ..... rare earth elements and yttrium
SEM ..... scanning electron microscopy

INTRODUCTION AND STATEMENT OF PURPOSE

Legacy effects of previous metal and coal mining activities are a large and costly environmental problem in Canada, the U.S.A. and around the world. In particular, acidic drainage is considered by some to be one of the largest environmental liabilities facing the Canadian and international mining industry[1]. The USGS estimates that 3,000 miles of streams and associated ground waters in Pennsylvania alone are affected from mine-affected waters, with an estimated cost for clean-up equalling $5 to $15 billion dollars[2]. Acidic drainage results when sulphide containing rock, such as pyrite, oxidizes and generates sulphuric acid, which dissolves metals present in surrounding rock. If sufficient buffering capacity is absent in adjacent rock (such as calcium carbonate materials), acidic drainage will result. Acidic drainage may occur immediately as sulfide-containing rock is oxidized, or after a long period of time, when buffering capacity in adjacent rock is eventually diminished. As a result, drainage from mining-affected areas often has low pH and high amounts of aluminum, iron, trace metals, sulphate and suspended solids[3]. Acidic drainage poses a threat to aquatic environments and often requires costly remediation. Depending on the chemistry and the flow rate of water requiring treatment, sites have used both passive and mechanised treatment. This treatment generally involves neutralization of acid through interaction with carbonate materials, such as lime or limestone.

Review of published geochemical literature reveals that acidic water from previous metal and coal mining activities can have elevated concentrations of yttrium, scandium and lanthanides[1], collectively referred to in this paper as 'Rare Earth Elements and Yttrium' (REY) (range 31 ug/L to 3091 ug/L)[2-5]. Elevated levels of REYs have also been identified within sediments/precipitates downstream of mining-affected areas that are characterized by more neutral pH[4]. Previous investigations within the Iberian Pyrite belt in Spain and Portugal and the coal-mining regions of Pennsylvania, suggest REYs in mine-affected water and sediments/precipitates may occur at such elevated concentrations and large quantities that they represent a mineable source of REYs[4,7]. Review of sparse toxicological data indicates that elevated concentrations of REYs in water and solid phase may potentially pose a toxicological threat, especially considering the high partitioning coefficient that have been observed between water/bacteria, water/algae and water/arthropods[8]. Speciation of REYs in aqueous and solid phases is key to understanding the mechanism of their enrichment in solid and aqueous phases, which influences both REY's potential mineable utility and their fate and effect on biota.

REYs have become an important commodity, as they are required for manufacturing a variety of modern technologies. REYs are less rare in terms of crustal abundance than their name indicates; however, deposits with sufficient concentration of REYs are less common than for other base metals. REYs crustal abundance is higher than Ag, Cd, Se, and Sn and two orders of magnitude higher than the truly rarest metals, like Pd, Pt, Ir, Au, and Re[9]. REYs are often associated with green technology; they are used to manufacture powerful magnets in wind turbines, as alloys for rechargeable batteries in hybrid vehicles and phosphors in light-emitting diodes and plasma and liquid crystal screens[1]. In 2015, according to China's Rare Earth Industry Association, rare-earth oxide consumption in China alone was expected to increase from the 2015 value of 98,000 tons to approximately 149,000 tonnes in 2020[10].

[1] IUPAC uses both lanthanides and lanthoides in reference to chemical elements with atomic numbers 57 through 71. In this paper, the more commonly used "lanthanides" will be used.

Study of the geochemical behaviour of REYs is not new. REYs have been used as geochemical tracers for close to 50 years, to examine a variety of geologic processes including: ore genesis, magma genesis, cosmogenic evolution, mantle and crustal evolution and sedimentary petrology[11]. The study of REY aqueous geochemistry is more recent. Recently, emphasis has been placed on understanding water-rock interactions within a variety of pristine and contaminated environments. Many authors have examined REY distribution patterns in acidic mine drainage, as a tool for understanding remediation approaches[12–14], while others have focused on REY sorption and speciation in acidic drainage from metal and coal mines[5,7,15–17]. Very acidic water (<pH 5.1) contains the highest proportion of aqueous REYs and has been found to indicate the geochemical signature of source rock along flow paths. Above a pH of approximately 5.1, REY are attenuated into solid phase and their fractionation patterns become of interest[11]. Ce and Eu have several oxidation states, and under certain conditions their speciation provides an indication of changes in redox conditions[18]. Also of interest are studies that have examined REY partitioning to hydrous ferric oxides[11,18,19], to manganese oxides[20], and within passive treatment systems[1,4,21]. In addition, evidence of large diurnal differences in REY concentrations at various sites indicates the importance of iron oxides[22,23].

Recently, several authors have proposed that REYs represent a mineable source in acidic mine drainage within the Iberian Pyrite Belt and in precipitates from bituminous coal mine drainage[1,4]. **Chapter 1: REY Geochemistry in mining-affected aqueous environments** of this thesis seeks to evaluate several different metal and coal mine drainage sites in North America, and compare these with neutral mine drainage and control sites, to understand which mining-affected environments have the highest aqueous and solid REYs. Early laboratory and field experiments identified REY partitioning to iron oxides as the predominant mechanism of solid-phase enrichment in iron-rich precipitates[11,18,19]. Specifically, schwertmannite was commonly identified as the predominant iron mineral present in these iron-rich systems that showed greatest REY solid accumulations[11,19]. Recently, Ayora and colleagues examined REY aqueous chemistry within an iron and aluminum-rich acid mine passive treatment system with schwertmannite present as the most common iron mineral[1]. Results from Ayora's field and laboratory work indicated that REYs accumulated exclusively within the aluminum-sulphate mineral present (basaluminite) and did not accumulate in the schwertmannite[1]. In addition, there is come debate on the role of organic matter in both aqueous and solid REY speciation. Previous studies have indicate REY-organic aqueous complexes form the majority of REY colloidal material; however, there is also debate that current modelling programs overestimate the proportion of REY-organic complexes[24,25]. As a result, **Chapter 1: REY Geochemistry in mining-affected aqueous environments** examines the speciation of REYs within aqueous and solid phases. Note that very recently, Stewart and colleagues examined non-synoptically collected solid and aqueous samples predominately from the bituminous region of Pennsylvania to understand the relative rates of REY enrichment[4]. This thesis augments their work by providing synoptically collected aqueous and additional precipitate samples within the anthracite region, as well as more detailed examination of the solid speciation of REYs.

Chapter 2: REY toxicity, bioaccumulation and linkages to microbial community composition, focuses on characterizing the microbial portion of the heterogeneous iron-rich biofilm/precipitate sampled within the passive treatment system. This chapter examines whether REYs pose a toxicological threat to algae and bacteria within the treatment system, and whether there are linkages between the algal and bacterial composition and magnitudes of REY partitioning coefficients. The

chapter goes on to explore any linkages between the diversity and abundance of naturally occurring microbes, and patterns of REY fractionation.

1.1 OBJECTIVES

The three main objectives of this chapter include:

- Comparison of REY aqueous and solid concentrations at a variety of control, acidic rock drainage (ARD), coal mine drainage (CMD) and neutral mine drainage (NMD) locations to understand large-scale trends of REY accumulation mechanisms in aqueous and solid REY enrichment in mining-affected environments.
- Determination REY speciation within aqueous and solid phases of a passive treatment system with elevated iron, aluminum and organic matter.

1.2 HYPOTHESES

This research tests the following alternate hypotheses:

(1) REYs in mine-affected water and precipitates occur at such elevated concentrations and large quantities within certain watersheds that mining-affected water and precipitates could represent a mineable source of REYs.

(2) pH is the key parameter controlling REY concentrations in the aqueous and solid phase.

(3) Sorption of REYs with iron oxides (as opposed co-precipitation of REY minerals, or sorption to organic matter or Al or Mn oxides) is the primary method of REY enrichment within iron-rich substrate, often found downstream of mining-affected environments.

CHAPTER 1: REY GEOCHEMISTRY IN MINING-AFFECTED AQUEOUS ENVIRONMENTS

1 – BACKGROUND

1.1 RARE EARTH ELEMENTS CHEMICAL AND PHYSICAL PROPERTIES

Rare earth elements are defined by the International Union of Pure and Applied Chemistry as seventeen elements: yttrium (Y), scandinum (Sc) and group IIIA lanthanides, from atomic number 57 (lanthanum (La)) through 71 (lutetium(Lu))[26]. Within this document, the acronym "REY" is used to refer to this entire group, including lanthanides, Y and Sc. In general, this group of elements is characterized by similar oxidation state (+III) and size, resulting in similar geochemical behaviour. Several REYs can occur in two oxidation states, depending on redox conditions[8]. REYs show important distinctions from other well-known metals like Cd, Cu and Zn: they have a strong affinity for oxygen containing ligands, do not form insoluble sulphides and commonly precipitate or complex with other ions. The electron configuration for REYs results in shielding of the 4f electrons by the 5s2 and 5p6 sub-shell, which leads REYs to act uniformly despite variation in the number of 4f electrons (Table 1)[24].

Ionic radius decreases with increasing atomic number as a result of attraction between nucleic protons and orbital electrons. This effect is called the 'lanthanide contraction'. The general consensus is that ionic radius is the main characteristic that differentiates the behaviour of individual REYs. As a result, rare earth elements are commonly divided into light rare earth elements (LREE), from La to Gd and heavy rare earth elements, (HREY) from Tb to Lu plus Y. The literature is not consistent with respect to these definitions; some authors consider Eu to be a member of the HREY grouping[24]. A third grouping is also used: middle rare earth elements (MREE). Again, there is some disagreement within the literature, but most studies assign elements Sm through Ho to this group.

Lanthanides with smaller ionic radii (greater atomic number) substitute more easily for major cations, than their larger ionic radii equivalents [27]. Due to their similar valence and ionic radii size, REYs are classified as hard ions that preferentially complex with hard, electronegative ligands (i.e., fluoride, carbonate, sulphate, phosphate, hydroxide)[24]. REYs are naturally occurring analogs for radioactive actinides and have been used to model actinide fate and effects[24]. In solid form, REYs are lithophilic and substitute for other cations of comparable radius and charge the mineral structures of silicates, carbonates, oxides, phosphates and oxyhydroxysalts [27].

In aqueous solution, lanthanides have a very similar radius to Ca^{2+} and occasionally act as its replacement. Previous studies have found that REYs have a relatively high affinity for sediments and low solubility in water, due to low the solubility products of REY-complexes. Mobility of REYs in aqueous solutions is controlled by pH, redox potential (only certain REYs), salinity, total suspended solids and the proportion of organic and inorganic ligands[28]. REYs occur as complexes with organic ligands (dissolved organic carbon (DOC), clays, fulvic and humic acids) and inorganic ligands (halides, sulphate, phosphate, hydroxides, carbonate), adsorb to the surface of Fe, Mn and Al oxides or occur as aqueous/free ions. In addition, REYs undergo fractionation between colloidal and dissolved fractions. Recent work by Purdy and Jamieson within circumneutral water showed that less than 2% of REYs were available in aqueous ion form and that LREEs occurred as aqua ions more frequently than HREYs[29]. This supports the commonly held assumption that LREEs are slightly more soluble than HREYs and that REY complexation with various complexes controls REY solubility[8]. Unlike other cationic materals, REY-sulphate complexes are soluble[30].

Table 1 Rare Earth Element Properties

	La	Ce	Pr	Nd	Sm	Eu	Gd	Tb	Dy	Y	Ho	Er	Tm	Yb	Lu	Sc
Atomic Number	57	58	59	60	62	63	64	65	66	39	67	68	69	70	71	21
Atomic Mass	138.91	140.12	140.91	144.24	150.36	151.96	157.25	158.93	162.5	88.91	164.93	167.26	168.93	173.05	174.05	44.96
Valence	3+	3+, 4+	3+	3+	2+, 3+	2+, 3+	3+	3+, 4+	3+	3+	3+	3+	3+	2+, 3+	3+	3+
Electron Config.	$5d6s^2$	$4f5d6s^2$	$4f^36s^2$	$4f^46s^2$	$4f^66s^2$	$4f^76s^2$	$4f^86s^2$	$4f^96s^2$	$4f^{10}6s^2$	$4d5s^2$	$4f^{11}6s^2$	$4f^{12}6s^2$	$4f^{13}6s^2$	$4f^{14}6s^2$	$4f^{14}5d5s^2$	$3d4s^2$
Abundance – Cont. Crust (ppm)	30	60	6.7	27	5.3	1.3	4	0.65	3.8	144.3	0.8	2.1	0.3	2.0	0.3	26
Ionic radius – CN6 (Å)	1.032	1.101	0.99	0.983	0.958	0.947	0.938	0.923	0.912	0.900	0.901	0.890	0.880	0.868	0.861	0.745
Ionic radius – CN8 (Å)	1.160	1.143	1.126	1.109	1.079	1.066	1.053	1.040	1.027	1.109	1.015	1.004	0.994	0.985	0.977	0.870

NOTES:

1. SNELLER ET AL. 2000 AND TAYLOR AND McLENNAN 1988[8,31].

REY are no exception to the Oddo-Harkins rule, which states even atomic-numbered elements are an order of magnitude more abundant than adjacent odd-numbered elements[27]. Since REYs are commonly portrayed together graphically, REY concentrations are usually normalized to reference sedimentary rock datasets to remove the influence of atomic number on abundance. Common normalization datasets include: North American shale composite (NASC)[32], the post-Archean Australian sedimentary rock (PAAS)[33] and average upper continental crust[34].

1.2 RARE EARTH ELEMENTS IN FRESHWATER AQUEOUS ENVIRONMENTS

Pokrovsky and colleagues were among the first to identify that freshwater rivers with high pH have a lower concentration of total aqueous REYs, and a depletion of LREEs when compared to low pH waters[35]. Subsequent work by Verplanck and colleagues found that above pH ~5, with significant iron oxidation, REYs do not behave conservatively, and their behaviour is strongly influenced by pH. Depending primarily on pH and secondarily on other water chemistry parameters, such as temperature and concentration of organic and inorganic ligands, aqueous REYs are predominately found as: carbonate complexes, sulphate complexes, organic complexes, and less commonly found as hydroxide complexes, phosphate complexes, fluoride complexes, chloride complexes[24].

Carbonate complexes are the dominant inorganic species within low temperature natural waters with pH greater than 6[24]. Luo and Byrne found MCO_3^+ dominates for pH 5.5 to 8, $M(CO_3)^{2-}$ dominates for pH>8 and the aqueous ion dominates at pH<5.5, depending on ionic strength[36]. REY-sulphate complexes are not common in natural surface and groundwater, due to low sulphate concentrations and relative weakness of sulphate ligands when compared to carbonate, hydroxide, fluoride and organic ligands. Sulphate-REY complexes are common, however, in areas downstream of coal and metal mines, where oxidation of sulphide containing rock creates sulphate-rich water[5,23,37]. Stability constants for sulphate complexes are slightly elevated for MREEs, but this is not expected to be the cause of MREE enrichment[24].

Organic ligands, and particularly organic colloids are known to be an important complexing ligands for REYs, and recent evidence suggests organics may a play chief role in REY complexation. Tang and Johannesson found that in natural waters with MREE-enrichment, high molecular weight dissolved organic matter, like humic acid, predominates; whereas, HREY-enriched waters tend to be dominated by low molecular weight dissolved organic matter, such as fulvic acids[38]. The degree to which organic matter binds to REY continues to be an active area of research; as a result current WHAM models have been found to be somewhat inaccurate[25].

Hydroxide complexes are only expected to play an important role in REY complexation in natural, low temperature waters at pH levels far above neutral in very alkaline environments. Hydroxide stability constants increase with atomic number, in a pattern similar to stability constants for carbonate and phosphate[24]. Phosphate complexes are also not expected to be an important ligand in natural waters, due to low concentration of phosphates. REY-phosphate stability constants are in fact greater than stability constants for REY-carbonate complexes, but low phosphate concentrations and competition by calcium and magnesium for phosphates negates this thermodynamic favourability[24].

Fluoride complexes are not expected to play a large role in most low temperature, natural waters with the exception of waters that have a high amounts of fluoride and are slightly acidic[24]. Importantly, total digestions for REYs are not possible with hydrofluoric acid, due to the REYs strong complexing affinity

for fluoride. REYs are very weakly complexed by chloride and as a result, chloride-REY complexes do not play an important role in REY aqueous speciation.

1.3 RARE EARTH ELEMENTS IN SOLID PHASES

1.3.1 Rare earth element and iron minerals / oxides

Iron oxides and oxyhydroxides, ranging from amorphous to crystalline (aka hydrous ferric oxides (HFO)), are among the most common suspended, colloidal and particulate material found downstream of mining environments. Iron oxides and oxyhydroxides may also be found in natural seep environments as well as where anoxic groundwater come in contact with the atmosphere. In such environments, reduced and dissolved iron (Fe(II)) oxidizes to its higher oxidation state (Fe(III)) and precipitates as a solid. The speed and mechanism of iron oxidation determines the resulting iron mineral. Common amorphous iron minerals that are found within and downstream of acid mine environments include: ferrihydrite, hematite, goethite, lepidocrocite, jarosite, and schwertmannite Table 2.

Rare earth element transport and fate is often intertwined with HFOs; however, mechanisms of co-precipitation, isomorphous substitution and sorption to iron oxides have all been proposed[39]. Isomorphous substitution[2] can occur in any of the iron oxide minerals by other trivalent metal cations, including aluminum, manganese, chromium, vanadium, and possibly REYs. Other elemental substitutions also occur via various divalent, trivalent and tetravalent elements. Iron oxide precipitation and dissolution plays a key role in the transport and fate of metal cations in natural waters.

Within very acidic waters (pH < 2.8) enriched with iron and sulphate, common to mine drainage, jarosite ($KFe_3(OH)_6(SO_4)_2$; dark yellow/yellow-brown) is often formed. When pH increases slightly but remains very acidic (pH 2.8-4.5) and enriched in iron and sulphate, schwertmannite ($Fe_8O_8(OH)_6(SO_4)\cdot nH_2O$; yellow-orange) often forms, and is generally biologically mediated due to slow kinetics of abiotic oxidation at this pH (although schwertmannite may also be formed abiotically)[11]. When the pH rises above 5, the most thermodynamically stable iron oxides in aerobic conditions are goethite (α-FeOOH; yellow-brown) and hematite (α-Fe_2O_3; orange-red) (pKs 40 – 44), although other less crystalline iron minerals like ferrihydrite and schwertmannite may be kinetically favored[40]. Goethite is thought to precipitate directly from solution, whereas hematite requires the presence of ferrihydrite as a precursor[40]. Ferrihydrite ($Fe_5HO_8\cdot 4H_2O$; brown) predominately occurs in aqueous environments (pH above 5) where Fe(II) is oxidized rapidly and/or where crystallization inhibitors are present (organics, phosphate and silicate species) and may be biologically mediated by microbes (e.g., *Gallionella sp.* and *Leptothrix sp.*). Ferrihydrite (pKs 37-39) is characterized by its poorly crystalline structure, small particle size and corresponding large surface area (200 – 600 m^2/g), which makes it particularly effective sorbent of cation species[40]. Lepiodocrocite (γ-FeOOH; orange), a polymorph of geothite, requires anoxic water with reduced Fe(II) in abundance (and pH>5), to form. Major Fe minerals are summarized within Table 2.

[2] Isomorphous substitution can be said to occur when one element substitutes for another within a mineral and no significant change in the crystal structure occurs.

Table 2 Common Iron Oxides and Oxyhydroxides

Iron-Oxyhydroxides[1]			Iron-Oxides[1]			Iron-oxyhydroxysulphates[1]		
Formula	**Mineral**	**Structure**	**Formula**	**Mineral**	**Structure**	**Formula**	**Mineral**	**Structure**
α-FeOOH	Goethite	Hexagonally close-packed	α-Fe_2O_3	Hematite	Hexagonally close-packed	$KFe_3(OH)_6(SO_4)_2$	Jarosite	Trigonal crystal structure
β-FeOOH	Akaganeite		γ-Fe_2O_3	Maghamite	Cubic close-packed	$Fe_8O_8(OH)_6(SO_4)\cdot nH_2O$	Schwertmannite	'Pin cushion' morphology
γ-FeOOH	Lepidocrocite	Cubic close-packed	Fe_3O_4	Magnetite				
$Fe_5O_3\cdot(OH)_9$	Ferrihydrite[2]							

NOTES:

1. Reference: Cornell and Schwertmann, 2000[40].
2. There is still debate on the chemical formula of ferrihydrite. It was previously considered $Fe_5HO_8\cdot 4H_2O$ and may also be Fe_2O_3*0.5(H_2O).

Iron oxidation may occur via chemical oxidation or it may be biologically-induced through microbial metabolism. The relative importance of each process, and the rate at which they occur depend on the physicochemical parameters of the water. In anoxic environments, ferrous iron is stable, but susceptible to chemical oxidation by molecular conditions. Temperature, pH, oxygen concentration, and ferrous iron concentration all dictate the rate at which chemical oxidation occurs (Equation 3). Field observations indicate that the reaction of Fe(II) with oxygen is not observed under a pH of 4[39]. As a result, Fe(II) is predominately oxidized by microbial mechanisms in solutions with pH less than 4. As pH increases above 4, increasing amounts of solid iron minerals form, at increasingly faster rates. Chemical, abiotic oxidation of iron occurs very rapidly in pH-neutral waters that are oxygen-rich. At higher pH, the greater abundance of protons influences the hydrolysis of iron, and therefore increases the reaction rate further[39]. Dissolved cation species, such as Cu^{2+}, Fe^{3+}, Al^{3+}, Co^{2+} and Mn^{2+} may also catalyze this reaction. The solubility of these ions is pH-related, and therefore, high concentrations of these metals occur in very acidic waters. Chemical iron oxidation can be either heterogeneous or homogenous; however, within natural waters homogeneous oxidation rates most often exceed heterogeneous oxidation rates[41].

The main iron oxidation equations include:

Equation 1 $\mathbf{Fe^{2+}(aq) + 1/4O_2 + H^+ \rightarrow Fe^{3+}(aq) + 1/2H_2O}$

Equation 2 $\mathbf{Fe^{3+}(aq) + 3H_2O \rightarrow Fe(OH)_3(s) + 3H^+}$

Equation 3 (combined) $\mathbf{Fe^{2+} + 1/4O_2 + 5/2H_2O \rightarrow Fe(OH)_3(s) + 2H^+}$

Table 3 Rates of Iron Oxidation

Equation	Reference	Rates
1	Heterogeneous oxidation (Martin, 2005[39])	$r_{hetero}=(d[Fe^{2+}]/dt)hetero=$ $-k^*(\beta_s[Fe^{2+}][>SOH](_{mol/m2})/[H+]^*(K_H{}^*P_{O2})(A(_{m2})/V(_L))$ k=0.7 (M/s) for $Fe^{2+}/)2$ reaction on FeOOH
2	Homogeneous oxidation (Martin, 2005[39])	$r_{homo}=k_0[O_2][Fe^{2+}] + k_1[O_2][Fe(OH)^+] + k_2[O_2][Fe(OH)^2]$
3	Abiotic iron oxidation (Stumm and Lee, 1961[42])	pH 6.5 to 7.5: $r_{abiotic} = d[Fe(II)]/dt = -k_{abiotic}{}^*[Fe^{2+}]^*[O^2]/[H^+]^2$ • Where k=temperature dependent constant ($3x10^{-12}$ mol/l/min at 20 degrees) pH < 2: $d[Fe(II)]/dt = -k[O_2][Fe(II)]$
4	Biologically-mediated iron oxidation (Pesic et al., 1989[43]; Kirby et al., 1999[44])	$r_{biol} = d[Fe^{2+}]/dt$ $r_{biol} = -k_{bio}{}^*C_{bact}[Fe^{2+}][O_2][H^+]$ $r_{biol} =[A_{bio} \exp(-E_{a,bio}/RT)\}C_{bact}[Fe^{2+}][O_2][H^+]$ Where Cbact= concentration of T. ferrooxidans in mg/L (dry weight); k_{bio} = L3/mg/mol2/s
5	Total iron oxidation (Kirby et al., 1999[44])	$R_{total} = -r_{abiotic} - r_{biol}$

NOTES:

1. REFERENCE: STUMM AND LEE, 1961 AND MARTIN, 2005.

1.3.1.1 HFO Individual Element Anomalies

In 1999, Bau examined normalized REY concentrations during iron oxide precipitation in laboratory experiments with waters between pH 3.6 to 6.2. Precipitation of HFOs increased with increasing pH, and Y, La, and Gd showed low affinity for iron oxides and a commensurate enrichment in associated waters; whereas, Ce depletion in waters indicated that oxidative scavenging of cerium was occurring on the iron oxide[19]. In addition, Bau's experiments indicated that a smaller Y_n/Ho_n ratio was associated with more iron oxidation. Vesper and Smilley examined diel patterns within coal mine drainage passive treatment systems[22]. These sites were characterized by low pH at the source, and increased pH as a result of carbon dioxide degassing. At these sites, aluminum, iron and REYs were removed to a greater extent than manganese, cobalt and nickel, and strong diel cycles noted for silica, manganese, iron, cobalt, nickel, arsenic, and REYs. As samples were collected at increasingly downstream sites, NASC normalized patterns in waters close to acidic source were not fractionated, but anomalies of Ce and Y were observed downstream.

1.3.1.2 HREYs, LREEs or MREEs HFO enrichment

There is general consensus within the literature that middle rare earth element (MREE) enrichment is often observed in acidic mine drainage, and naturally acidic waters[17,23,45]. REY patterns normalized to the NASC show enriched MREE patterns in mildly acidic natural surface waters, acid brines, an acid lake and dilute acid groundwater associated with acid-mine drainage[37]. There is debate regarding whether the enriched MREE pattern observed in acidic waters is related to dissolution of MREE

enriched materials in surrounding rocks (i.e., source patterns), or whether this is a result of water chemistry, including the presence of complexing agents (i.e., sulphates and carbonates), and sorption processes (i.e., process patterns). There is also debate as to which elements exactly are included within the overlapping MREE group; generally elements from samarium to holminium are included.

Zhao and colleagues examined REYs in acid mine drainage from a coal mine in Northern China[46]. NASC normalized water concentrations showed 'convex-up' patterns of MREE and HREY enrichment, without cerium or europium anomalies, in waters dominated by sulphate-REY aqueous complexation[46]. Zhao and colleagues proposed REY sulphate complexes could be adsorbed to Fe-Al-Mn-oxide/hydroxide colloids and subsequently co-precipitate.

Ferreira da Silva and colleagues identified a variety of processes affecting geochemical cycling of trace metals and REYs downstream of acidic mine drainage, including weathering, mineral dissolution, secondary dispersion, precipitation of Fe-oxyhydroxides, sulphates and adsorption of metals to surfaces of recently formed minerals[6]. They found moderate MREE enrichment relative to LREE within sediments and most waters during the spring, and positive correlations between sulphate and total aqueous REYs. In addition, sites with significant aqueous manganese or aluminum enrichment were associated with strong HREY enrichment within waters. Waters examined by Ferreira da Silva and colleagues were significantly affected by efflorescent sulphates, which could be grouped into MREE-enriched Fe-rich efflorescent sulphates and HREY-enriched magnesium and aluminum efflorescent minerals. Stewart and colleagues examined precipitates within coal mine drainage, and grouped them into three categories: silica-aluminum oxide precipitates, Fe oxide precipitates and calcium-magnesium oxide precipitates[4]. Fe oxide precipitates showed MREE and HREY enrichment.

Johannesson and Zhou concluded that Fe-Mn oxides were responsible for the MREE enrichment observed in a naturally occurring dilute acidic lake[37]. Specifically, within acid mine drainage affected areas, either aqueous samples or solid samples include a middle rare earth element enrichment. In 2014, Grawunder and colleagues examined acid-mine drainage affected areas in particular, and identified pyrite dissolution as the cause for the MREE enrichment observed within the water[13].

In 2004, Verplanck and colleagues examined an acid mine drainage environment (Uncle Sam Gulch, Montana) with high amounts of iron oxides and determined that REYs behave conservatively when pH is less than 5.1, but show strong inter-element partitioning between pH 5.1 and 6.6[11]. Verplanck's work determined that HREYs partitioned more strongly to freshly formed HFO at pH 6.6 than LREEs. The precipitates in this study were predominately composed of iron (jarosite, schwertmannite and goethite) and minor amounts of Al, SiO_2, Ca and Mg (quartz, gypsum and copiate) and the dominant aqueous speciation of REY was REY-sulphate[11]. Colloidal particles were found to be enriched in HREY. Gammons and colleagues also found that HREYs partitioned more strongly to HFO than LREEs at another creek in Montana (Fisher Creek) in 2005[23]. Within Fisher Creek, Montana, REYs behaved conservatively above pH 5.5 and they found increasing REY abundance within the sorbed phase was observed across the lanthanide series (pH 6.8).

1.3.2 Rare earth elements and aluminum oxides / sulphates

Investigations by Ayora and colleagues of ARD environments within the Iberian Pyrite belt, have identified REY concentrations within ARD that may be of economic grade[1]. High amounts of REY were observed to concentrate in the calcite-based passive remediation used for ARD. Both laboratory and field measurements support the finding that at pH below 5, REYs and Cu are predominately

sequestered in basaluminite (aluminum sulphate mineral), and do not precipitate in schwertmannite. These findings are in contrast with other studies that suggest iron oxides are the principal method of sequestering REYs.

1.3.3 Rare earth elements and organic material

In addition to strong affinity to aquatic plants, arthropods and bacteria, REY show strong affinity to organic acids and ligands. Work completed by Tosiani and colleagues identified organic carbon as key player in the sequestration of REYs to the particulate phase and identified a negative linear relationship between the partitioning of dissolved REYs to suspended REYs vs. dissolved organic carbon (DOC)[16]. Other studies found strong linkages between REY concentration, organic carbon, aluminum and iron, and evidence of temporal and seasonal variability[35,47,48]. These and other studies demonstrate that within tropical and boreal rivers, with high amounts of organic carbon, iron-rich and/or organic colloids play an important role in REY distribution. Within streams characterized by lower amounts of organics, Leybourne and Johannesson found selective iron extractions indicated that approximately 21-29% of REYs were associated with iron[18].

Detailed discussion on the effect of organic matter on REY fractionation is included **in Chapter 2: REY toxicity, bioaccumulation and linkages to microbial community composition**.

1.3.4 Rare earth elements and manganese oxides

At neutral pH, the chemical oxidation of Mn(II) is at least 10^6 slower than Fe(II). Similar to iron, speciation of manganese is redox-dependent, and aqueous concentrations of Mn(II) are significant only within natural water in absence of oxygen[39]. In addition, similar to iron oxides, manganese oxides exhibit amphoteric behaviour as a result of inner-sphere and outer-sphere surface complexation with ions. The isoelectric point for a generic manganese oxide, the pH at which the positive and negative charge on the mineral surface is equal, is lower (approximately pH 4) when compared to iron oxides (approximately pH 7)[39]. This is significant because when the pH of water surrounding the oxide is above the isoelectric point, surface charge on the oxide is negative. It follows that when surface charge is negative, cationic species are able to adsorb. As a result, in natural waters with circumneutral pH, where iron and manganese oxides with ‘standard isoelectric points’ occur, preferential sorption to manganese oxides over iron oxides is expected to occur. It should be noted, however, that the uncatalyzed rates of manganese oxidation are low below pH 8[39].

1.4 RARE EARTH ELEMENTS SEASONAL AND DIEL CYCLING

In low pH environments, diel metal cycling is well documented and the mechanism is predominately related to light-sensitive Fe redox reactions. In neutral to alkaline pH environments, dissolved metal cations tend to increase at night and decrease during the day. These variations are hypothesized to be caused by reversible pH and temperature-dependent adsorption to particulate matter[23].

In 2005, Morris and colleagues investigated the diel variation of zinc in some mining-impacted streams in Montana [49]. Over two years they observed diel cycling of dissolved and total zinc at several sites, where the concentrations were approximately twice as low during the late afternoon, when compared with the morning ones[49]. Biofilm showed the inverse trend and the cycling was attributed to uptake in photosynthetic biofilms, and was negatively correlated with pH, water temperature and solar radiation.

In 2005, Gammons and colleagues investigated diel cycling in a small, high altitude mountain stream with natural ARD in Montana that ranges from low pH to nearly neutral[23]. Precipitates of HFO in the headwaters, and a mixture of HFO and aluminum precipitates were observed further downstream. Diel differences in REY concentrations were noted between pH 5.5 and 6.3. At the pH 6.3 site, "dissolved" (<0.1 um) concentrations for all REYs increased during the night by an average of 380%, and the greatest solid partitioning occurred during the late afternoon. La had the smallest percentage increase (190%), whereas Eu had the largest increase (840%). For some REYs, particulate water samples showed an inverse pattern to dissolved water samples, but total water samples showed no diurnal fluctuations. In general, light REYs partitioned to a lesser degree to solids than heavy REYs.

Previous work has suggested selective complexation of the heavy REY by carbonate ions to explain the weaker tendency of heavy REY (relative to light REY) to adsorb onto hydrous Fe and Mn precipitates forming in seawater[50]; however, the opposite pattern is shown in the Fisher Creek[23]. In 2004, Verplanck and colleagues used theoretical modeling to indicate that fractionation of REY could occur between acidic water in the absence of systemic difference in aqueous speciation across lanthanide series[11]. Theoretical modelling indicated that the role of mineral precipitation was minimal and although not proven, the role of phosphate complexes in controlling REY stability was ruled out.

2 – METHODS

2.1 FIELD SITES AND SAMPLING

2.1.1 Acid rock drainage, coal mine drainage and neutral mine drainage site comparison

Data used for this analysis was derived from a variety of sources and designed to provide samples across a wide cross-section of physicochemical parameters from mining-affected sites, with a range of pH from 2.6 through 7.8. Samples were collected from sites in both North and South America to represent: anthropogenic ARD, natural ARD, NMD, CMD drainage, CMD passive treatment, and a control site (Table 4).

South America samples represent warm climate anthropogenic ARD, and were collected downstream of three different sites including (1) a historic mine with high sulphidation epithermal Cu-Au-Ag deposit; (2) an active epithermal Au-Ag deposit, with principal ore host consisting of mature quartz sandstone; (3) an active high sulphidation epithermal Au-Ag deposit, with mineralized zones within pumiceous tuffs, residual vuggy silica and quartz-alunite alteration. The water and biofilm samples were collected by H. Jamieson, L. M. Manoukian and D. Fortin.

Yukon samples represent cold climate natural ARD and were collected within one ARD creek at 11 various locations downstream of the Zn-Pb sedimentary exhalative XY deposit, located within Howard's Pass district, straddling the Yukon and Northwest Territory borders within Canada (~62.27N; 129.11W). The Zn-Pb mineralization contains sulphidic horizons (sphalerite, galena, and pyrite with accessory chalcopyrite) interbedded with carbonaceous cherty mudstone and argrillaceous cherty limestone[51]. This data was previously collected, and a portion of this data, excluding data on REYs, was previously published by Gault and colleagues[51].

The New Calumet Mine, located within the Outaouais region of Western Quebec on Ile du Grand Calumet (~578815E; 4983437N), approximately 120 km northwest of Ottawa, Ontario, was sampled to represent sites with NMD[52]. The site is within the Canadian Shield and was a historic massive sulphide Zn-Pb mine (0.34-0.42% zinc; 0.20-0.23% lead), with smaller amounts of Cu and Au. Ore materials consisted of sphalerite, galena, pyrrhotite and calcite within a gneissic, marble unit[52]. In spite of the sulphidic ore materials, pH of the tailings is slightly alkaline due to carbonate-rich host rock.

Sampling of various coal mine discharges and passive treatment systems was completed within the anthracite coal region of Pennsylvania (~400000E, 4510000N) which is located in east-central and northeastern Pennsylvania. Pennsylvania's Anthracite Coalfield lies within the Ridge and Valley Physiographic Province, where mineable coal beds are steeply folded and fractured in synclinal troughs[53]. Shale, siltstone, sandstone, conglomerate and local limestone are interbedded with mineable coals. Coal mine discharges (PENN1) were sampled as part of this research during August 2015, and were previously sampled in August 2001 and March 2001 (water only).

The control site is located in Duhamel, Quebec. Duhamel is also within the Outaouais region of Western Quebec and is approximately 120km northeast of Ottawa, Ontario (~500000N; 5097048E). Duhamel sits within the Canadian Shield and represents a pristine site, with groundwater characterized by high levels of ferrous iron. There are no mining activities directly in vicinity to Duhamel, and the site is located just east of the Réserve Faunique de Papineau-Labelle, which is a wildlife reserve that has a previous history of logging, but no mining activities.

Table 4 Summary of Sampling Locations

Number of discrete sites	Total number of sampling locations	Location	Type of Mine Drainage	pH range	Sampling dates	Samplers
3	11	South American (SA)	Anthropogenic ARD	pH 2.6-6.4	May 2014	H. Jamieson, L. Manoukian and D. Fortin.
1	11	XY Deposit, Yukon (XY)	Natural ARD	pH 3.5-5	July 2008	K. Gault (Feige)
10	10	Anthracite region, Pennsylvania (PENN1)	CMD drainage sites	pH 3.6-6.4	March 2001 (water only); August 2001; December 2015	C. Cravotta, E.J. Ashby, N. Baranova
1	1	Duhamel, Quebec (DU)	Control	pH 6.2-6.5	August 2015; September 2015; November 2015	M. Moriarty, E.J. Ashby.
1	4	New Calumet Mine, Ontario (CA)	NMD	pH 5.7-7.8	June 2015; September 2015	E.J. Ashby, M.Moriarty.
2	12	Anthracite region, Pennsylvania (PENN2)	CMD passive treatment	pH 5.8-7.6	December 2015 August 2016 AM August 2016 PM	C. Cravotta, E.J. Ashby, N. Baranova, E. Myers.

NOTES:
1. ARRANGED FROM LOWEST pH TO HIGHEST pH.

2.1.2 Coal mine drainage passive treatment site

A subset of 6 sites in the Silver Creek passive treatment system (40.718749; -70.17662), located near New Philadelphia, Pennsylvania, were sampled during low-flow conditions in both December 2015 and August 2016 to understand seasonal and diurnal variability (SC6, SC5, SC4, SC3, SC2, SC1). Construction of the Silver Creek facility was completed in July 2010, coordinated by the Schuylkill Headwaters Association, and funded by an EPA 319 Grant. The project was designed to prevent low pH, metal-laden waters from Silver Creek mine from directly entering Schuylkill River waters using passive remediation techniques.

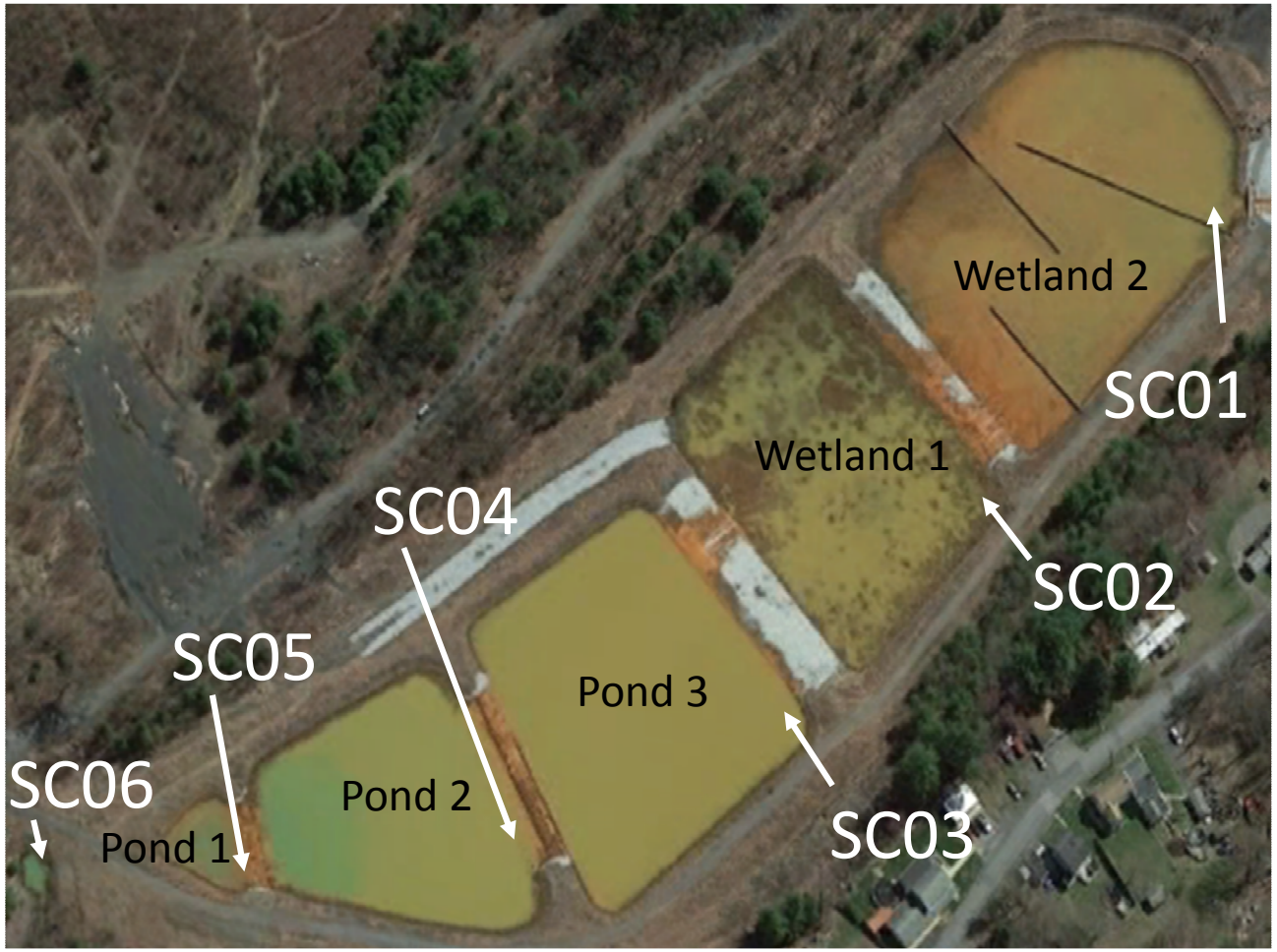

NOTES:

1. POND 1 IS THE MINE DISCHARGE AND SCOUR POOL.
2. POND 2 IS THE AERATION POND.
3. POND 3 IS THE SETTLINE POND, WITH THE LONGEST RETENTION TIME OF ALL OF THE POOLS.

Figure 1 Silver Creek Site Passive Remediation Site (image from Google earth©)

The Silver Creek passive treatment system represents a combination of treatment ponds and aerobic wetlands, located at the anoxic mine discharge outflow (~pH 5.8). At the discharge point, mine water contains elevated ferrous iron (14-17 ppm) and slightly acidic pH conditions (5.94 to 5.86), which rise to circumneutral at the terminus of the treatment system (7.13 to 6.76). The treatment site is composed of three ponds and two wetlands with one discharge location: water first passes through mine discharge and scour pool (Pond 1), then it enters the aeration pond which facilities CO_2 outgassing, raising pH (Pond 2). Subsequently water enters Pond 3, designed to precipitate aqueous iron to into solid phase; this pool has the longest retention time (see Figure 1). Water then flows through the two wetlands and is discharged. There is only one discharge exiting the facility. The facility is designed to discharge 4.5 L/min over the 20 year life of the facility[54]. Samples at this site were collected during the afternoon in December 2015 and then sampled twice in August 2016, during the afternoon and early in the morning.

Table 5 Silver Creek Site Details and Sampling Sites

Feature	Description of Feature	Sampling Sites	Surface Area (m^2)	Design Depth (m)	Geometric Design volume (m^3)	Residence Time
Inflow	Silver Creek shaft	Inflow: SC06	N/A	N/A	N/A	Assumed no residence time
Pond 1	Mine discharge and scour pool	Outflow: SC05	551	0.93	117	0.689 hr
Pond 2	Aeration basin	Outflow: SC04	5,962	3.21	14,182	83.45 hr
Pond 3	Settling basin	Outflow: SC03	7,892	3.97	24,239	142.63 hr
Wetland 1	Wetland cell	Outflow: SC02	6,972	0.62	3,233	19.03 hr
Wetland 2	Variable level pond	Outflow: SC01	8,954	0.61	4,082	24.02 hr

NOTES:

1. REFERENCE: PERSONAL COMMUNICATION WITH C. CRAVOTTA, 2017.
2. A LIMESTONE SPILLWAY (NOW COATED IN HFO) CONNECTS PONDS AND WETLAND CELLS TO EACHOTHER.
3. SAMPLING SITE SC5 IS THE MOST UPSTREAM OF THE SAMPLING SITES AND DISCHARGES AT A NATURAL SEEP THAT IS NOT MODELLED. ALL INFLUENT FROM THIS POND REPORTS TO POND 1.

2.2 BULK WATER SAMPLE CHEMICAL ANALYSIS

Water sample collection and analysis were completed by various researchers, at four different facilities, according to standard methods. Samples collected in South America were analyzed by the Analytical Services Unit at Queen's laboratory (Kingston, Canada), which is ASU accredited by the Canadian Association for Laboratory Accreditation. Samples collected in the Yukon were analyzed at the Geological Survey of Canada (GSC) Inorganic Geochemical Research Laboratory (Ottawa, Canada), and the University of Ottawa (Ottawa, Canada); a portion of this data was recently published by Gault and colleagues[51]. Samples collected within Quebec (Duhamel control site and the Calumet NMD site) and within Pennsylvania during December 2015 and August 2016 were analyzed at the University of Ottawa Geochemistry Laboratory (Ottawa, Canada).

2.2.1 Field sampling and *in situ* measurements

At each site, water grab samples were collected, in addition to *in situ* water chemistry measurements, photographs and global positioning system (GPS) coordinates. At certain sites, instantaneous flow rate was computed from wading measurements with a flow meter or calculated based on existing weirs. Clean techniques were used for all collection, handling, storing, preparation, and analysis of collected grab samples. All sample bottles were pre-cleaned by rinsing with deionized water, soaking for 24 h in 10% v/v HNO_3 (Fisherbrand ACS-Pur UN2031) and rinsing three or more times with deionized water. Sample bottles were placed within clean plastic bags in coolers for transport to various sites. During each sampling event, 10% field duplicate samples were taken for quality assurance and control, in addition to an equipment blank, which tested for any contamination within filters, syringes, deionized water or other equipment used for sampling. Although different multi-parameter probes were used by each of the sampling teams, each probe was calibrated 24h prior to sampling and included, at minimum, temperature (˚C), pH and oxidation-reduction potential (ORP) probes. These measurements were taken upstream of grab samples, or nearest to anoxic discharge point after grab samples had been taken, so as to minimize the influence of added turbidity to the measurements.

During the December 2015 and August 2016 sampling events in Pennsylvania, *in situ* parameters were collected using a YSI 556 multi-parameter probe with temperature, specific conductance, dissolved oxygen and combination pH/ORP probes. All parameters measured by the probe were calibrated the morning prior to sampling and pH buffers were checked at various times during sampling. Pt and Ag/AgCl electrodes calibrated to pH 4.0, 7.0, and 10.0 buffer solutions, and in Zobell's solution. Field measured ORP values were corrected relative to the standard hydrogen electrode (SHE) and reported as Eh according to the methods of Nordstrom[55]. A one-point calibration was completed for specific conductance, measured using 1000 µS/cm KCl standard solution calibrated to Wheatstone bridge, and checked with other KCl solutions with conductivities of 500 and 1,800 µS/cm. Flow measurements during the December 2015 and August 2016 Pennsylvania sampling event were collected with a pygmy meter, based on all discharge from the treatment facility (no bypass).

2.2.2 Alkalinity

Alkalinity measurements were taken within 12h to 24h of sampling using a digital titrator (Orion Model 290A), 50 mL of water filtered through a 0.45 um hydrophilic polyethersulfone filter (Acrodisc® syringe

filters with Supor® membrane), 1.6N H_2SO_4, and a calibrated pH meter (Thermoscientific ROSS Sure-flow pH). The 1.6N H_2SO_4 was added incrementally at approximately 10 digit intervals. The number of digits and corresponding stabilized pH were recorded.

2.2.3 Dissolved Inorganic Carbon and Dissolved Organic Carbon

Samples to be analyzed for total dissolved carbon (DC) and dissolved organic carbon (DOC) were collected in sterile 60 mL syringes, filtered through a 0.2 um filter (Acrodisc® syringe filters with Supor® membrane), into a 40 mL amber borosilicate vial. Samples were overfilled with a convex meniscus to eliminate headspace and then stoppered with an impermeable septa and screw cap to minimize loss of organics during transport and holding time prior to analysis. Samples were run on an OI Analytical TIC-TOC Analyzer (Aurora Model 1030) to determine the organic and inorganic carbon. Data was output in parts per million (ppm) and normalised using internal standards. The 2sigma analytical precision was 2% of concentration. Samples were generally analyzed within two to three weeks of collection.

Note that, where possible, DIC was used to calculate alkalinity in place of measured alkalinity values, due to high precision associated with the TIC-TOC Analyzer

2.2.4 Anions

Anion analysis was completed by either ion chromatography or spectrophotometry, depending on the research group. Samples collected in the Yukon were analyzed by ion chromatography (Dionex 600) for sulphate (SO_4^{-2}), chloride (Cl^-), bromide (Br-), nitrate (NO_3^-), and phosphate (PO_4^{-3}). Prior to analysis, samples were processed through ion exchange columns to remove divalent and trivalent metals that adversely affected the Dionex 600 machine. By this method, field duplicates showed relative percent differences less than 5%, and sulphur molarity was ±5% of that measured by ICP-OES. Samples collected in South America were analyzed by ion chromatography (Dionex ICS3000) for sulphate (SO_4^{-2}), chloride (Cl^-), fluoride (F^-), nitrate (NO_3^-), and nitrite (NO_2^-). Laboratory QAQC was within ±2% of targeted values.

Water samples from the Quebec and Pennsylvania sites were collected in sterile 60 mL syringes, filtered through a sterile 0.45 um hydrophilic polyethersulfone filter (Acrodisc® syringe filters with Supor® membrane) and stored in 500 mL polycarbonate Nalgene bottles with minimal headspace until analysis. Using separate subsamples of filtered water, nitrate (NO_3^-), nitrite (NO_2^-), orthophosphate (PO_4^{-3}) and sulphate (SO_4^{-2}) were analyzed with a spectrophotometer (Hach™ SpectroPhotometer DR-2800). A 10 mL subsample, matched glass cuvettes and the following powder pillows were used to perform nitrate, nitrite, orthophosphate and sulphate analysis, respectively: NitraVer 5 Nitrate Reagent Powder Pillows (10 mL; Method 8039), NitriVer® 3 Reagent Powder Pillows (10 mL; method 8507), PhosVer3® (Ascorbic Acid) Method (10 mL; method 8048) and SulfaVer® 4 Sulphate Reagent Powder Pillows (10 mL; method 8051). Dilutions were used when samples read out-of-range; however, sulphate was the only analysis that consistently required dilution for all analyzed samples. Samples were analyzed within 24 h to 72 h after collection. Anion concentrations were verified for one sampling event by ion chromatography. In addition, sulphur values were calculated by ICP-OES to verify validity for sulphate analysis. ICP-OES values for sulphate were used if discrepancy arose between the ICP-OES and spectrophotometer results.

2.2.5 Ferrous Iron

Water collected at all sites was analyzed for concentration of ferrous iron at the University of Ottawa (Ottawa, Canada) using the colorimetric Stookey method[56]. Two pre-labelled, sterile 10 mL falcon tubes were labelled with site information, and filled with 0.5mL of 0.5M HCl (Fisher chemical Hydrochloric Acid Trace Metal Grade; A508-4). For measurement of total ferrous iron, 0.5mL of unfiltered water was collected in a 1mL syringe, and 0.5mL was added to 0.5mL of 0.5 HCl in a sterile, pre-labelled 10mL falcon tubes. For measurement of filtered (dissolved) ferrous iron, sample water was collected in 1mL syringe and used to purge a WhatmanTM Puradisk nylon filter (0.2µm pore size; WHT67512502) prior to adding 0.5mL of filtered sample to 0.5mL of HCl in a pre-labelled falcon tube. Samples were analyzed using the Stookey ferrozine method within 24 hours of collection using a Hach™ SpectroPhotometer DR-2800.

2.2.6 Major and Minor Ions

Determination of major ions, including Al, Ca, Fe, K, Mg, Mn, Na, P, S and Si were obtained at three different laboratories, using inductively coupled plasma-optical emission spectroscopy (ICP-OES) according to standard methods. Analytical methods were consistent with USEPA Method 200.7, Revision 4.4: Determination of Metals and Trace Elements in Water and Wastes by Inductively Coupled Plasma-Atomic Emission Spectrometry and 200.15: Determination of Metals and Trace Elements in Water by Ultrasonic Nebulization Inductively Coupled Plasma-Atomic Emission Spectroscopy. Water samples were collected via grab samples or with sterile 60 mL syringes, stored in sterile polypropylene containers and acidified to pH 2 with Trace Metal Grade nitric acid (Fisher Chemical A509-P212, Lot 1115080). Water samples were either filtered (0.45µm and 0.2µm Acrodisc® syringe filters with Supor® membrane) or unfiltered, and were analyzed “as is” to ensure the lowest detection limits (no dilution or additional acids added); unfiltered water samples were centrifuged prior to analysis. The purpose of filtration is to isolate the fraction of water that is completely aqueous, or ‘dissolved’, and not attached to colloidal size particles. Generally, 0.45µm filtration is operationally defined as representing ‘dissolved’ material; however, many studies have identified a significant role of colloidal particles in general, and bound with REYs <0.45µm[24]. As a result, samples filtered to 0.2µm and 0.45µm were compared to verify whether analyzing 0.45µm filtered water, a lower level of effort, was sufficient.

A Varian Vista Pro-axial CCD Simultaneous ICP-OES (now Agilent) was used to analyze the South American samples processed by the Queen’s Laboratory Analytical Services Unit whereas samples collected in Quebec and Pennsylvania were processed by the University of Ottawa Geochemistry Laboratory with a Varian Vista PRO™ ICP-OES (now Agilent). The Yukon samples were analyzed by the GSC Inorganic Geochemical Research Laboratory with a Spectro Arcos ICP-OES. Note that, in addition to the major elements mentioned above, the GSC Inorganic Geochemical Research Laboratory also analyzed for Br, Cl, Ni, Sc, Y and Zn.

Standard quality assurance and control methods were employed. The instrument detection limit was determined by multiplying the standard deviation by three of ten replicate calibration blanks, composed of 1% nitric acid, prepared with concentration nitric acid (Fisher Chemical; Trace Metal Grade A509-P212) and deionized water. Internal standards and certified USGS reference standard (T-201) were run every 10 samples to correct for any instrument drift, and an extended rinse cycle was used between samples (90 seconds). A field reagent blank was run with every set of samples, in addition to field

sample duplicates and laboratory duplicates (10%). Calibration standards were prepared from ISO 9001 certified single and multi-element standards. All standards were gravimetrically prepared and compared against both internal and external standards, as well as previously prepared standards (Table 6). Periodic lab fortified sample matrix spike tests were employed.

For accurate detection of sulphur, ICP-OES runs were completed with a nitrogen gas in the reaction cell, in addition to the argon gas flow, and analyze using the wavelengths listed in Table 7. The auxiliary flow, nebulizer flow and other setting were optimized for sulphur; see Table 8 for a description of the setting used for sulphur optimization on the Varian Vista PROTM ICP-OES at the University of Ottawa Geochemistry Laboratory.

Table 6 Standards Used for ICP-OES at the University of Ottawa Geochemistry Laboratory

Element	Standard 1	Standard 2	Standard 3	Standard 4	Standard 5	Multi-element standard mix
Al	0	2.5	5	10		Mix A
Ca	0	2.5	5	10		Mix A
Fe	0	12.5	25	50	100	Fe, Mn
K	0	2.5	5	10	20	Mix B
Mg	0	2.5	5	10		Mix A
Mn	0	12.5	25	50	100	Fe, Mn
Na	0	2.5	5	10	20	Mix B
P	0	2.5	5	10	20	Mix B
S	0	2.5	5	10	20	Mix B

NOTE:

1. MIX A INCLUDES A NUMBER OF PARAMETERS, THAT WERE OFTEN ANALYZED FOR, BUT ULTIMATELY ICP-MS DATA WAS USED FOR THEIR CONCENTRATION. MIX A INCLUDED Al, As, B, Ba, Ca, Cd, Co, Cr, Cu, Fe, Mg, Mn, Mo, Ni, Pb, Si, Sr, Ti, Zn, Sc, V.

Table 7 ICP-OES Wavelengths Analyzed

Parameter	Wavelength 1	Wavelength 2	Wavelength 3
Al	Al 308.215	Al309.271	Al394.401
Ca	Ca393.366	Ca396.847	NA
Fe	Fe234.350	Fe238.204	Fe259.940
K	K766.491	K769.897	NA
Mg	Mg279.553	Mg280.270	Mg285.213
Mn	Mn257.610	Mn259.372	Mn260.568
Na	Na588.995	Na589.592	NA
P	P177.434	P178.222	P213.618
S	S180.669	S181.972	S182.562
Si	Si251.432	Si251.611	Si288.158

NOTES:

1. WAVELENGTHS ANALYZED AT THE UNIVERSITY OF OTTAWA GEOCHEMISTRY LABORATORY USING THE VARIAN VISTA PRO™ ICP-OES.

Table 8 ICP-OES Parameters Optimized for Sulphur

Parameter	Unit	Value
Power	kW	1.4
Plasma Flow	L/min	15
Auxiliary Flow	L/min	1.5
Nebulizer Flow	L/min	0.90
Viewing Height	Mm	10
Replicate read time	s	10.00
Instrument stabilization delay	s	15
Sample uptake delay	s	35
Pump rate	s	15
Rinse time	s	90
Fast pump	Sample delay/rinse	Y

NOTES:

1. ICP-OES OPERATING PARAMETERS OPTIMIZED FOR SULPHUR AT THE UNIVERSITY OF OTTAWA GEOCHEMISTRY LABORATORY USING THE VARIAN VISTA PRO™ ICP-OES. ANALYSIS FOR SULPHUR REQUIRED USE OF THE

2.2.7 Trace and Ultra-trace Elements

Determination of minor, trace and ultra-trace metals was obtained by inductively coupled plasma mass spectrometry (ICP-MS) by three different laboratories, using standard methods. Here, we define trace constituents as composing 100ppm to 1 ppb and ultra-trace components composing <1ppb of the sample. Trace constituents analyzed by ICP-MS include: 27Al, 137Ba, 63Cu, 59Co, 60Ni, 66Zn. Ultra-trace elements analyzed by ICP-MS include: ^{75}As (+He), ^{11}B, ^{111}Cd, ^{52}Cr, ^{95}Mo, ^{208}Pb, ^{88}Sr, 232Th, 47Ti, 238U, 51V and the REYs (^{139}La, ^{140}Ce, ^{141}Pr, ^{146}Nd, ^{147}Sm, ^{151}Eu, ^{153}Eu, ^{157}Gd, ^{159}Tb, ^{163}Dy, ^{165}Ho, ^{166}Er, ^{169}Tm, ^{172}Yb, ^{175}Lu, ^{89}Y, ^{45}Sc). Analytical methods were consistent with USEPA Method 200.8, Revision 5.4: Determination of Trace Elements in Waters and Wastes by Inductively Coupled Plasma-Mass Spectrometry and USEPA Method 6020A: Inductively Coupled Plasma-Mass Spectrometry. Water samples were collected via grab samples or with sterile 60 mL syringes, stored in sterile polypropylene containers and acidified to pH 2 with Trace Metal Grade nitric acid (Fisher Chemical A509-P212, Lot 1115080). Water samples were either filtered (0.45µm and 0.2µm Acrodisc® syringe filters with Supor® membrane) or left unfiltered, and analyzed to obtain the most accurate results at the lowest detection limit.

Samples collected in South America, analyzed by the Queen's University Analytical Services Unit, were analyzed with an Agilent 7700x ICP-MS spectrometer with an ASX-500 series auto-sampler and clean enclosure. Samples collected in the Yukon, analyzed by the Geological Survey of Canada (GSC) Inorganic Geochemical Research Laboratory (Ottawa), were analyzed with a Thermo-Scientific X Series II spectrometer. Note that in addition to the parameters analyzed above, Li, Be, Ga, Ge, Se, In, Sn, Sb, Te, Cs, Hf, Ta, W and Re were also analyzed. For these analyses, Rh and Ir were used as internal standards. Analysis of the samples collected in Quebec and Pennsylvania, done at the

University of Ottawa Geochemistry Laboratory, was performed with an Agilent 8800 Inductively Coupled Plasma Mass Spectrometry (ICP-MS) Triple Quad.

All sample dilutions and standards were completed gravimetrically. Where possible, water samples were run without dilution, but in cases where the measured concentrations were expected to exceed prepared standard curves, water samples were diluted to 1:10. Standard quality assurance and control methods were employed. The instrument detection limit was determined by multiplying the standard deviation by three of ten replicate calibration blanks, composed of 1% nitric acid, prepared with concentrated nitric acid (Fisher Chemical; Trace Metal Grade A509-P212) and deionized water. Every ten samples, internal standards and certified USGS reference standards (T-201) were run for every parameter to correct from instrumentation drift, in addition to a calibration blank. A field reagent blank was run with every set of samples, in addition to field sample duplicates and laboratory duplicates (10%). Calibration standards were prepared from ISO 9001 certified single and multi-element standards. All standards were gravimetrically prepared and compared against both internal and external standards, as well as previously prepared standards (Table 6). Periodic laboratory fortified sample matrix spike tests were employed. A helium collision cell (flow rate 1.6-2 mL/min) was used for analysis of arsenic, iron and REYs to remove polyatomic interferences.

Water and solid samples were normalized after converting their concentrations to µg/g and using the rock, North American Shale Composite (NASC) normalization and the Post Archean Average Shale (PAAS) values listed in Table 9.

Table 9 Rare Earth Element Normalization Standards

Normalization	La	Ce	Pr	Nd	Sm	Eu	Gd	Tb	Dy	Y	Ho	Er	Tm	Yb	Lu	Sc
Pennsylvania Anthracite-Mammoth No 8 (Schuylkill County) (ug/g)	13	25.5	1.95	12.675	1.5	0.435	1.95	0.71	1.185	10.65	0.23	0.6	0.225	0.8025	0.225	3.7
NASC (ug/g)	31.1	66.7	7.7	27.4	5.59	1.18	4.9	0.85	4.17	27	1.02	2.84	0.48	3.06	0.456	27
PAAS (ug/g)	41	83	10.1	38	7.5	1.61	6.35	1.23	5.5	27.31	1.34	3.75	0.63	3.53	0.61	15.89

NOTES:

1. DATA FOR THE PENNSYLVANIA ANTHRACITE-MAMMOTH NO. 8 (SCHUYLKILL COUNTY) WAS AN AVERAGE OF ALL SURFACE SAMPLES COLLECTED AND PRESENTED IN THE USGS COAL QUALITY DATABASE: VERSION 2.0, ACCESSED APRIL 2017[57].
2. DATA FOR NASC NORMALIZATION STANDARD DERIVED FROM GROMET ET AL.[32]. PAAS AND NASC VALUES USED THAT ARE SUMMARIZED IN PIPER AND BAU[33].

2.3 BIOFILM SAMPLE CHEMICAL ANALYSIS

2.3.1 %Total Organic and Inorganic Carbon

Loss on ignition (LOI) was completed to provide an estimate of organic matter in collected samples. Following standard methods, aluminum weigh pans (1.375 fl. oz.) were heated at 400˚C for 1 hour and allowed to cool in a desiccator and weighed. Biofilm samples for LOI analysis were sieved through a 2 mm sieve, placed wet into aluminum weigh pans and heated at 100˚C for 24 hours, placed in desiccator and weighed. After low temperature oven-drying, all samples were weighed and then heated at 500˚C for 24 h, placed in desiccator and weighed.

To verify LOI data, elemental analysis was conducted with the Vario Elementar Isotope Cube© to determine %N, %C, %H and %S. Elemental analysis was used to determine both total carbon (TC) content and organic carbon content (OC). To determine total carbon content, 1-2 mg of air dried sample was added to a tin capsule, and combined with tungstic oxide (WO_3), which acts as a combustion catalyst. The sample was agitated to completely mix the sample and tungstic oxide, and was weighed on a microbalance. To determine the organic carbon content, methods from Freslon and colleagues were followed[58]. A sample between 30 to 90 mg was leached with 4 M-HNO_3 to remove carbonates, dried overnight at 50 ℃ and analyzed the following day for organic carbon. As per the TC samples, the digested dry sample was combined with tungstic oxide (WO_3) in a tin capsule and weighted on a microbalance. Both TC and OC samples were flash combusted at 1800℃ with the addition of oxygen. Ultra-pure helium then carries the gases through the column, and they are measured by a thermoconductivity detector (TCD). The analytical precision of the instrument for this analysis is +/- 0.1%. Freslon and colleagues recognize that while this method is expected to completely remove carbonates, it may also lead to partial dissolution of less refractory organic compounds and thereby underestimating %OC[58].

2.3.2 Aqua regia total digestion

All solid samples collected in the Yukon, South America, Quebec and Pennsylvania were analyzed for total metal content by aqua regia digestion, using a standard 1:3 HNO_3: HCl ratio. This standard method was used to determine the total metal content of the biofilm samples and was completed by three laboratories: GSC Inorganic Geochemical Research Laboratory, Queen's University Analytical Services Unit, and the University of Ottawa Geochemistry Laboratory. The aqua regia method provides a good estimation of total labile chemical content associated with the samples, but does not digest refractory compounds, such as SiO_2, TiO_2 and Al_2O_3. As a result, aqua regia is often combined with hydrofluoric acid (HF) for total digestions; however, due to the strong binding affinity of HF to REYs, this method was not used for this study. The method for the digestion is a slight modification to the USEPA Method 200.7 Trace Elements in Water, Solids and Biosolids by Inductively Coupled Plasma Atomic Emission Spectrometry.

Biofilm samples were collected at various sites using plastic implements, such as plastic spatulas, spoons and scrapers. Solid samples were placed in 500mL HDPE bottles and transported to the designated laboratory in 0˚C cooler. Upon receipt at the laboratory, samples were promptly refrigerated and stored in the dark with coeval waters prior to further processing. During sample processing, samples were sieved with plastic sieve to remove impurities, air dried for 24 h - 48 h or oven dried below 50˚C until completely dry. Queen's University Analytical Services Unit combined

0.5 g of solid with 25 mL trace grade aqua regia at a 1:3 volumetric ratio of HNO_3:HCl. The mixture was digested on a digiprep block at 50˚C, with sealed cap for 300 minutes. Subsequently, the container cap was removed and acid was boiled off until approximately 2 mL of acid remained and double deionized water was then added to make up the volume to 25 mL. The University of Ottawa Geochemistry Laboratory used the same method, except that a slightly smaller sample volume was used (0.1 g) and the capped sample was heated overnight. The GSC Inorganic Geochemical Research Laboratory, split subsamples of precipitates into two aliquots, one of which was digested by aqua regia and the second was air dried at room temperature to calculate a wet-dry correction factor.

For quality assurance and control purposes, 10% laboratory duplicates were completed for all aqua regia digestions. In addition, a variety of solid standard reference materials were used by each laboratory. Queen's University Analytical Services Unit used the TORT-2 reference standard, to verify the aqua regia digestion method. The GSC Inorganic Geochemical Research Laboratory verified accuracy and precision of digestions and ICP-MS with certified reference materials Fe_2O_3, GXR-1, GXR-3 and Till-2. The University of Ottawa Geochemistry Laboratory used certified reference materials TORT-2, GXR-3, TILL-2 and REE-1.

Aqua regia digestions were compared with nitric acid-peroxide digestions completed on a subset of samples analyzed by the University of Ottawa Geochemistry Laboratory. Briefly, biofilm samples were collected in the same manner as described for the aqua regia digestions, and completely dried, either at room temperature or within an oven at 50˚C. Using glass digiprep tubes, 0.1 g of dried sample was added to 6 mL of double deionized water and 4 mL of trace grade 30% H_2O_2 and allowed to react. After the reaction subsided, 2 mL of trace grade HNO_3 was added. The digestion tube was placed in the digiprep heating block overnight at ~100˚C with cap loosely tightened. If the digestion was not complete, an additional 2 mL of HNO_3 was added and allowed to react. Once the digestion was complete, the samples were diluted and run on ICP-OES and ICP-MS.

2.3.3 Quantification of metals associated with iron-bearing fractions

To quantify the REYs and other metals associated with the iron and manganese fraction, a non-sequential oxalate extraction was completed on a subset (n=13) of the Pennsylvania samples according to the methods of Kostka and Luther[59]. The amount of iron extracted by oxalate is operationally defined as representing amorphous Fe(III) oxides, crystalline Fe(III) oxides and acid volatile sulphides[59]. Using completely dried sample material, ~0.01 g was weighed into 20 mL scintillation vials wrapped in aluminum foil, with small stir bar, and combined with 10 mL of oxalate solution (0.2 M ammonium oxalate and 0.2 M oxalic acid, pH 2.5). The vial was placed on a stir plate for 48 hours and then diluted to run on ICP-OES and ICP-MS. Lab duplicates and field duplicates were analyzed to represent 15% of samples collected.

Dithionite extractions were completed on a smaller subset of samples, to verify the oxalate extractions. As per oxalate extractions, dithionite extractions are expected to represent amorphous Fe(III) oxides, crystalline Fe(III) oxides and acid volatile sulphides. Methods for the dithionite extraction follow those mentioned in Kostka and Luther: each vial contained 0.01 g so sample, 0.5 g sodium dithionite in 10 mL of 0.35 M acetate/0.2 M sodium citrate (pH 4.8). Dry sample was added to 20 mL scintillation vial with 0.35 M acetate/0.2 M sodium citrate and allowed to react at 70˚C for 1 hour. After this reaction period, 0.5 g dithionite powder is added directly to scintillation vial and allowed to react at 70˚C for another hour. After the reaction was completed, the samples were diluted and run on ICP-OES and ICP-MS.

2.3.4 X-Ray Diffraction

Bulk mineral composition of collected biofilm samples was determined by powder X-ray diffraction (XRD). Prior to analysis, a subset of unfiltered solid sample was air-dried, finely ground using a mortar and pestle and compressed onto a sample plate. XRD analysis was completed using a Rigaku Ulitma IV X-ray diffractometer, operating with x-ray tube voltage of 40 kV and X-ray tube current of 44 mA, using Cu-Kα radiation. The goniometer was set up to scan 5-80˚ 2Θ range, using a step size of 0.02˚, and a scanning speed of 1˚ per second. In contrast to crystalline minerals, XRD is not very effective at quantifying iron minerals in sediment or samples with significant amorphous minerals[59]. Peaks were both identified manually and using the HighScorePlus© software, employing following steps:

1. HighScore Plus© 'Search peaks' function used to find peaks automatically.
2. Review automated peak generation and manual insertion of peaks.
3. HighScore Plus© 'Fit peaks' function used to optimize peak fit.
4. Review automated peak fit and manually adjust, as needed.
5. HighScore Plus© 'Search and match' function used to identify peaks. Used in three different ways: a) use automatic ‘Search and match’ without any constraints; b) ‘Search and match’ function constrained by string identifiers from solids bulk XRD; c) ‘Search and match’ function constrained by string identifiers identified in manual XRD; and, d) ‘Search and match’ function constrained by top 5 parameters identified in ICP-MS analysis (generally over 1,000 mg/kg abundance).

2.3.5 Energy Dispersive Spectroscopy (EDS)

Using the Oxford INCA large area SDD detector, Energy Dispersive Spectroscopy (EDS) was used to analyze the SC05-Dec sample and the SC04-Aug sample. Analysis was completed to determine the homogeneity of the samples with respect to aluminum, silica, sulphur, and iron.

2.4 COMPUTATIONAL ANALYSIS

2.4.1 Individual Element Anomalies

Individual element anomalies for REYs can either reflect source-related signatures, or they can reflect process-related signatures, such as sorption. For waters with pH less than 4 or 5, REY water signatures are expected to closely match those of adjacent rocks since REYs remain dissolved within the aqueous phase[11]. As pH increases above 4 or 5 and approaches neutrality, REYs behave non-conservatively, and are observed to fractionate as a result of other processes, such as precipitation or adsorption. To identify individual element anomalies in water where REYs behave non-conservatively, a frequently used method to correct for source-related REY signatures is to normalize to adjacent rock concentrations. In absence of a host rock for normalization, REYs are frequently normalized to a reference standard representative of rock in the area sampled, such as the North American Shale Composite (NASC) or the Post Archean Australian Shale (PAAS). Normalization is essential not only to interpret individual element anomalies, but to interpret REY results in general, since elements with even atomic numbers have higher abundance than those with odd atomic numbers, as per the Oddo-Harkins rule.

Process-related REY anomalies can be useful in determining dominant metal sorption mechanisms within water bodies. REY anomalies are calculated by dividing measured normalized concentration of a REY by the normalized interpolated value calculated using neighbouring elements. Values greater than

1, indicate a positive anomaly and values less than one indicate a negative anomaly. Although this seems straightforward, the anomaly calculations are made complicated by the fact that elements used to calculate interpolated values must not be anomalous themselves[60]. As a result, cerium, europium, lanthanum and gadolinium are often avoided when completing these calculations and a different adjoining neighbour is used. For example, to calculate the interpolated europium value, one would expect to use normalized values of samarium and gadolinium, neighbours to europium; however, instead of normalized gadolinium values, normalized terbium values are used. This is because gadolinium anomalies are frequently observed, as gadolinium is used commonly within hospitals as an imaging agent.

The interpolated normalized values can be calculated assuming a linear method or a geometric average method. The linear method is most commonly used in previous literature; however, the method that best represents a particular dataset in a linear fashion should be selected. To test which method to use, normalized interpolated values can be plotted against measured normalized values to ensure linear relationship. Based on calculations compiled by Lawrence and colleagues, methods of calculating linear and geometric average individual element anomalies are presented in Table 10[60].

Table 10 Individual element anomaly calculations

Individual element anomaly	Lawrence et al., 2006 (Linear relationship equation)	Lawrence et al., 2006 (Geometric relationship equation)	Worral and Pearson (2001)	Bau and Dulski, 1996
La_n	$=Pr_n + 2*(Pr_n - Nd_n)$	$=Pr_n * (Pr_n/Nd_n)^2$		
Ce_n	$=Pr_n + (Pr_n - Nd_n)$	$=Pr_n * (Pr_n/Nd_n)$	$=Ce_n/(SQR(La_n*PR_n))$	$=Ce_n/(0.5*La_n + 0.5*Pr_n)$
Eu_n	$=(2/3)*Sm_n + (1/3)*Tb_n$ or; $=(3/2)Sm_n - (1/2)Nd_n$	$=(Sm_n^2 * Tb_n)^{1/3}$ or; $=Smn * (Sm_n/Nd_n)^{1/2}$	$=Eu_n/(SQR(Sm_n*Gd_n)$	$=Eu_n/(0.67*Sm_n+0.33*Tb_n)$
Gd_n	$=(2/3)Tb_n + (1/3)Sm_n$ or; $=Tb_n + (Tb_n + Dy_n)$	$=(Tb_n^2 * Sm_n)^{1/3}$ or; $=Tb_n * (Tb_n/Dy_n)$		
Lu_n	$=Yb_n + (Yb_n - Tm_n)$	$=Yb_n * (Yb_n/Tm_n)$		

NOTES:

1. WHERE 'n' INDICATES VALUES THAT HAVE BEEN NORMALIZED TO A CONSTANT, IN THIS CASE, THE NASC.
2. REFERENCE: LAWRENCE et al., 2006[60]; WORRAL AND PEARSON, 2001[61] AND BAU AND DULSKI, 1996[62].

2.4.2 HREYs, LREEs or MREEs Enrichment

To determine patterns in LREE (lanthanum to gadolinium), HREY (terbium to lutetium and lutenium) and MREE (samarium to holmium) enrichment, a variety of strategies can be used. First, NASC normalized values can be plotted according to the atomic number, and observation of the resulting patterns can be

made. This can help identify both anomalies and patterns of enrichments within groups of elements. Alternately, enrichments can be quantified by creating ratios between portions of elements, such as the ratio of the sum of LREE/sum of HREY or the sum MREE/total REY. A third approach is to take representative elements from different element groups and create ratios, such as those described in Table 11. Note that this approach differs substantially between authors and may not be effective if the representative elements selected are anomalous themselves. To determine accuracy of these methods, it is suggested to complete all three methods and select enrichment calculations that are representative of data.

Table 11 LREE, HREY and MREE enrichment calculations

Variable	Lawrence et al., 2006	Ferreira da silva et al, 2009	Grawunder et al., 2014
LREE/HREY enrichments	$=Pr_n/Yb_n > 1$	$=La_n/Yb_n > 1$	$=La_n/Lu_n > 1.2$
HREY/LREEY enrichments	$=Pr_n/Yb_n < 1$	$=La_n/Yb_n < 1$	$=Lu_n/La_n > 1.2$
MREE/LREE enrichments	$=Pr_n/Tb_n < 1$	$=La_n/Gd_n < 1$	$=Tb_n/La_n > 1.2$
MREE/HREY enrichments	$=Tb_n/Yb > 1$		$=Tb_n/Lu_n > 1.2$

2.4.3 Sorption Isotherms

Sorption isotherms indicate the relationship between adsorbed and dissolved solute concentrations at a fixed temperature[63]. Sorption is a general term that combines the processes of ion exchange, surface complexation and precipitation. Precipitation occurs when dissolved components adsorb to a surface with the same chemical composition as solutes. For the purposes of this study, total solid concentrations normalized to dry weight are used to represent adsorbed materials, and may represent REYs in the solid phase that occur via ion exchange, surface complexation and precipitation. Sorption is a commonly observed process associated with various mineral oxides, where pH dependent deprotonation can remove hydrogen ions from oxygen ions, which results in a negatively charged surface. Sorption of cations, generally favoured at high pH, is usually irreversible, compared with anions, which may be reversible.

Three methods are commonly used to describe sorption isotherms: linear, Freundlich and Langmuir. In all three cases, equations are fitted to experimental/field data and the fit of the isotherm can be measured according to error calculations. Various error calculations are used, including: absolute weighting, logarithmic weighting and relative weighting. Each sampling event: December, August morning, and August afternoon were plotted with respect to these three isotherms. Isotherms with the lowest relative error were selected as the best fit. Isotherms are presented together with pH and temperature information, which are key variables affecting sorption. Generally, isotherms are plotted for experimental data where key parameters like temperature and pH are held constant, and aqueous concentration is adjusted. Despite the fairly controlled nature of our field experiment, these variables changed depending on the site. The influence of these variables on overall sorption patterns is of particular interest in determining the mechanisms of enrichment of REYs within the solid phase.

The linear isotherm is the simplest isotherm, a simple linear regression, which assumes a linear relationship between the mass of solute sorbed/mass solid and the mass solute dissolved in mass of solution. Linear isotherms assume no limit to sorption capacity, and were calculated using Equation 4.

Equation 4 $s = mc + b$

Where: q= solid concentration (ug/g)
m=slope of the line
c=solute concentration (ug/L)
b=y-intercept of the line

The Freundlich isotherm is similar to the linear isotherm, as there is no upper limit to sorption; however, the exponential equation shows less sorption at higher concentrations when compared to the linear isotherm. Equation 5 provides the equation used, as stated in Appelo and Postma[63].

Equation 5 $s = Kf * c^n$

Where: s= solid concentration (ug/g)
Kf=constant
C=solute concentration (ug/L)
n=constant

The Langmuir isotherm differs from both the linear and Freundlich isotherms, as it calculates an upper limit to sorption, resulting from saturation of surface sites. The Langmuir equation is derived from the law of mass action for the sorption reaction, and mass balance for sorption sites. Equation 6 provides the equation used for the Langmuir isotherm, as stated in Appelo and Postma[63].

Equation 6 $s = smax * \frac{KL*C}{1+KL*C}$

Where: s= solid concentration (ug/g)
Smax=constant (maximum number of sorption sites)
KL=constant
C=solute concentration (ug/L)

2.4.4 Thermodynamic modelling

The geochemical program Phreeqc-i was used to complete all thermodynamic modelling (version 3.3.22)[64]. Either the WATEQ and llnl databases were used to determine aqueous speciation, saturation indices and to complete kinetic modelling (further described below).

2.4.4.1 Aqueous speciation modelling and saturation indices calculation

Aqueous speciation modelling was completed using both the WATEQ and llnl databases in Phreeqc-i[65,66]. The WATEQ database was used to calculate saturation indices for major carbonate, iron, manganese, sulphate and aluminum minerals, and the llnl database was used to calculate saturation indices for REY-related minerals (Table 12). In both cases, pe values calculated from measured ORP and associated Eh values were used to specify the redox conditions of the solution. To include consideration of kinetics and provide results more representative of field conditions, the thermodynamic model calculating aqueous speciation and saturation indices was forced to equilibrate with $Al(OH)_3$, $Fe(OH)_3$ and manganite, which are the most kinetically favoured aluminum, iron and manganese minerals.

To calculate pe, ORP values were collected *in situ* with a multi-parameter probe. Using measured temperature and a conversion factor measured for the specific probe (-8.6), the measured ORP values were converted to standard hydrogen electrode (SHE) values. Using this Eh, the Nernst equation (Equation 7) was re-arranged to calculate pe.

Equation 7 $$Eh = \frac{2.303 * R * T}{F} * pe$$

Where: R=8.314 J/k/mol
T= temperature (Kelvin)
F= 9.65E4 colombs/mol
Eh=oxidation reduction potential (V)

Table 12 Minerals in WATEQ and llnl Phreeqc-i database

Minerals in WATEQ	Minerals in llnl
Alunite, AlumK, Basaluminite, BoehmiteManganite, Mn3(PO4)2, Mn2(SO4)3, Mn3(AsO4)2:8H2O MnHPO4, MnSO4, MnS(Green), Fe(OH)2.7Cl.3, Fe(OH)3(a), Fe2(SeO3)3, Fe3(OH)8, FeS(ppt), Goethite, Strengite, Maghemite, Magnetite, Jarosite-K, Jarosite-Na, Jurbanite, Kaolinite, Calcite, Dolomite, Siderite, Rhodochrosite, Rhodochrosite(d), MnSO4, CupricFerrite, CuprousFerrite, Diaspore, Gibbsite, Halloysite, Illite, Kmica, Pyrophyllite, Montmorillonite-Aberdeen, Montmorillonite-Ca, Bixbyite, Hausmannite, Hematite, Talc, Tremolite, ZnSiO3, Quartz, SiO2(a), Chalcedony, Smithsonite, Cerrusite, and Witherite.	Al2(SO4)3, Al2(SO4)3:6H2O, Alunite, Fe(OH)2, Fe(OH)3, Fe2(SO4)3, FeF2, FeF3, FeO, Kaolinite, Gibbsite, Ce(OH)3, Ce(OH)3(am), Ce2(CO3)3:8H2O, Ce2O3, Ce3(PO4)4, CeF3:.5H2O, CePO4:10H2O, CeO2, Celadonite, Celestite, Dy, Dy(OH)3, Dy(OH)3(am), Dy2(CO3)3, Dy2O3, DyF3:.5H2O, DyPO4:10H2O, Er(OH)3, Er, Er2(CO3)3, Er(OH)3(am), Er2O3, ErF3:.5H2O, ErPO4:10H2O, Eu, Eu(IO3)3:2H2O, Eu(NO3)3:6H2O, Eu(OH)2.5Cl.5, Eu(OH)2Cl, Eu(OH)3, Eu2(CO3)3:3H2O, Eu2(SO4)3:8H2O, Eu2O3(cubic), Eu2O3(monoclinic), Eu3O4, EuBr3, EuCl2, EuCl3, EuCl3:6H2O, Eucryptite, EuF3:0.5H2O, EuO, EuOCl, EuOHCO3, EuPO4:10H2O, EuS, EuSO4, FeSO4, FeV2O4, Gd, Gd(OH)3, Gd(OH)3(am), Gd2(CO3)3, Gd2O3, GdF3:.5H2O, GdPO4:10H2O, Goethite, Hematite, Ho, Ho(OH)3, Ho(OH)3(am), Ho2O3, Ho2(CO3)3, HoF3:.5H2O, HoPO4:10H2O, Hopeite, Jarosite, Jarosite-Na, K-Feldspar, La(OH)3, La, La(OH)3(am, La2O3, La2(CO3)3:8H2O, LaCl3, LaCl3:7H2O, LaF3:.5H2O, Lammerite, Lanarkite, Lansfordite, LaPO4:10H2O, Magnesite, Magnetite, Pr(OH)3(am), Pr2(CO3)3, Pr2O3, Prehnite, PrF3:.5H2O, PrPO4:10H2O, Sm, Sm(OH)3, Sm(OH)3(am, Sm2(CO3)3, Sm2(SO4)3, Sm2O3, Yb, Yb(OH)3, Yb(OH)3(am), Yb2(CO3)3, Yb2O3, YbF3:.5H2O, YbPO4:10H2O, Nd(OH)3, Nd(OH)3(am), Nd(OH)3(c), Nd, Nd2(CO3)3, Nd2O3, NdF3:.5H2O, NdOHCO3, NdPO4:10H2O, Pm, Pm(OH)3, Pm(OH)3(am), Pm2(CO3)3, Pm2O3, PmF3:.5H2O, PmPO4:10H2O, Pr(OH)3, Tb(OH)3, Tb(OH)3(am),, Tb2(CO3)3, Tb2O3, TbF3:.5H2O, TbPO4:10H2O, Tm(OH)3, Tm(OH)3(am), Tm2(CO3)3, Tm2O3, TmF3:.5H2O, TmPO4:10H2O, Lu, Lu(OH)3, Lu(OH)3(am), Lu2(CO3)3, LuF3:.5H2O, Lu2O3, LuPO4:10H2O.

2.4.5 Windermere Humic Aqueous Model, version 7 Modelling

2.4.5.1 Overview

The Windermere Humic Aqueous Model (WHAM, version 7) is an equilibrium chemical speciation model for surface and soil waters that includes a surface chemistry assemblage model for particles[67]. The WHAM model is in fact three submodels: one sub-model (Model VII) considers aqueous speciation with respect to dissolved inorganic and organic ligands (fulvic acid and humic acid). The second sub-model (surface complexation assemblage model for particles, SCAMP) considers adsorption of protons and metals to aluminum, silica, manganese and iron oxides, in addition to particulate and colloidal organic matter. There is a third model, the cation exchange model; however, this model is not used in subsequent

analysis and is not discussed further. As indicated by Lofts and Tipping, on a weight-for-weight basis, metal binding strength is greatest for manganese oxides, then humic substances, then iron oxides and aluminum oxides (equal) and finally silica oxides[68].

2.4.5.2 Surface Complexation Assemblage Model Assumptions

Using a surface complexation approach similar to the Dzombak and Morel to model sorption to oxides, key properties of the oxides are required for input to the model including: surface area, site density and surface acid-base properties[69]. Oxide mass (g) is input for every sample, while surface area per gram (m^2/g), bulk density (kg/m^3) and surface acid-base properties (electrostatic parameter for protons) are assumed constant for a given oxide. In fact, due to lack of comprehensive datasets, the site density for all oxides is set at 8.33 $\mu mol/m^2$, which corresponds to 5 sites per nm^2. Table 13 indicates the key input assumptions for sorption calculations to manganese, iron and aluminum oxides. Note that the pk1 and pk2 values here are the equilibrium constants for protons binding to strong and weak site on the metal oxide. Ideally, these properties are determined empirically by laboratory measurements, because these values are expected to vary widely. For example, surface areas are often measured via nitrogen gas adsorption via Brunauer-Emmett-Teller (BET) analysis; however, these measurements were beyond the scope of the current investigations. The WHAM model has utilized assumptions for Fe-oxide surface area consistent with those of Dzombak and Morel (600 m^2/g)[69].

Table 13 Key input properties for iron oxides

Parameter	Mn-oxide	Fe-oxide	Al-oxide
Surface area (m^2/g)	400	600	400
Bulk density (kg/m^3)	5.03×10^6	3.57×10^6	3×10^6
pK1	0.36	6.26	6.45
pK2	4.21	9.66	9.96
delta 1	-3	-2	-2.2
delta 2	-6	-4	-4.4
% type 0 sites	90.9	90.9	90.9
% type 1 sites	9.09	9.09	9.09
% type 2 sites	0.909	0.909	0.909

NOTES:
1. WHERE pK1 IS EQUILIBRIUM CONSTANT FOR PROTONS WITH OXIDE: $=SOH_2^+ \rightarrow =SOH + H^+$.
2. WHERE pK2 IS EQUILIBRIUM CONSTANT FOR PROTONS WITH OXIDE: $=SOH_2^+ \rightarrow =SO^- + H^+$.

To calculate the equilibrium constants between metals and hydroxide, the information in Table 14 is combined through several equations to calculate the equilibrium binding constants for different metal binding sites models. Although this surface complexation model follows the approach of Dzombak and Morel, Dzombak and Morel utilize a two-site metal ion binding model (weak and strong), whereas the WHAM model utilized a three-site metal ion binding model (weak, strong and medium). Ideally, equilibrium constant values can be estimated using empirical or semi-empirical data; however, empirical and semi-empirical data are not available to calculate these values for rare earth elements.

Due to an absence of empirical data, linear free energy models (LFERs) are used to calculate equilibrium constant values. The theory of hard and soft acids and bases (namely that hard acid acids preferentially

bind hard bases, like OH^-) provides the theoretical background whereby regression techniques can be used in combination with the first hydrolysis constant to provide an estimate of metal-binding equilibrium values[69]. Specifically, there is a tight linear relationship between cation hydrolysis (i.e., relationship between cations with hydroxyl ions in solution) and hydroxyl groups on the oxide surface. Using this relationship, simple linear equations can be used to calculate different binding values. Equilibrium constants for REYs with the weakest oxide-metal binding sites (type 0 sites; $pK_{MH,0}$) were calculated using the equations below (results of these calculations in Table 14)[68]:

Equation 8 AlOx: $pK_{MH,0} = 1.17pK_{hydrol} - 7.34$

Equation 9 MnOx: $pK_{MH,0} = 0.48pK_{hydrol} - 2.87$

Equation 10 FeOx: $pK_{MH,0} = 0.84pK_{hydrol} - 4.23$

Type 0 binding sites, which are the weakest, are also the most abundant binding sites on the oxides (Table 14). Type 1 and 2 binding sites are increasingly strong, and less abundant. Metal-oxide equilibrium constants for type 1 and type 2 binding sites were calculated as follows:

Equation 11 $pK_{MH,1}$ (type 1) = $pK_{MH,0}$ + delta1

Equation 12 $pK_{MH,2}$ (type 2) = $pK_{MH,0}$ + delta2

2.4.5.3 Model VII Assumptions

In 2011, Tipping and colleagues revised the calculations for the sub-model that considers humic and fulvic acids. These changes simplified the previous model and only considered monodentate binding to strong- and weak-acid oxygen-containing ligands[67]. As a result, the binding of each metallic cation to organic matter is modelled using just one equilibrium constant for monodentate binding to carboxylate groups (strong acids; KMA). These values are internally consistent and were obtained by fitting 248 published datasets for 40 metals. More details on the inputs can be found directly within the 2011 publication by Tipping and colleagues[67].

Table 14 Metal-oxide equilibrium constants for REYs using Linear Free Energy Relationships and the first hydrolysis constant

Ion	$logK_{MOH}$	pK_{hydrol}	Iron Oxides/Hydrous Ferric Oxides					Manganese Oxides			Aluminum Oxides		
			Dzombak and Morel, 1990		Lofts and Tipping, 1998			Lofts and Tipping, 1998			Lofts and Tipping, 1998		
			$pKa1_{init}$ STRONG	$pKa2_{init}$ WEAK	$pK_{MH,2}$ STRONG	$pK_{MH,1}$ MIDDLE	$pK_{MH,0}$ WEAK	$pK_{MH,2}$ STRONG	$pK_{MH,1}$ MIDDLE	$pK_{MH,0}$ WEAK	$pK_{MH,2}$ STRONG	$pK_{MH,1}$ MIDDLE	$pK_{MH,0}$ WEAK
LFER y-intercept:			4.374	7.893	-4	-2	-4.23	-6	-3	-2.87	-4.4	-2.2	-7.34
LFER Slope:			-1.166	-1.299	$logK_{MH,0}$	$logK_{MH,0}$	0.84	$logK_{MH,0}$	$logK_{MH,0}$	0.48	$logK_{MH,0}$	$logK_{MH,0}$	1.17
La^{3+}	5.19	8.81	-1.68	1.15	-0.8	1.2	3.2	-4.6	-1.6	1.4	-1.4	0.8	3.0
Ce^{3+}	5.66	8.34	-2.22	0.54	-1.2	0.8	2.8	-4.9	-1.9	1.1	-2.0	0.2	2.4
Pr^{3+}	5.67	8.33	-2.23	0.53	-1.2	0.8	2.8	-4.9	-1.9	1.1	-2.0	0.2	2.4
Nd^{3+}	5.82	8.18	-2.41	0.34	-1.4	0.6	2.6	-4.9	-1.9	1.1	-2.2	0.0	2.2
Sm^{3+}	6.16	7.84	-2.81	-0.10	-1.6	0.4	2.4	-5.1	-2.1	0.9	-2.6	-0.4	1.8
Eu^{3+}	6.20	7.80	-2.86	-0.16	-1.7	0.3	2.3	-5.1	-2.1	0.9	-2.6	-0.4	1.8
Gd^{3+}	6.17	7.83	-2.82	-0.12	-1.7	0.3	2.3	-5.1	-2.1	0.9	-2.6	-0.4	1.8
Tb^{3+}	6.36	7.64	-3.04	-0.37	-1.8	0.2	2.2	-5.2	-2.2	0.8	-2.8	-0.6	1.6
Dy^{3+}	6.41	7.59	-3.10	-0.43	-1.9	0.1	2.1	-5.2	-2.2	0.8	-2.9	-0.7	1.5
Ho^{3+}	6.44	7.56	-3.14	-0.47	-1.9	0.1	2.1	-5.2	-2.2	0.8	-2.9	-0.7	1.5
Er^{3+}	6.48	7.52	-3.18	-0.52	-1.9	0.1	2.1	-5.3	-2.3	0.7	-2.9	-0.7	1.5
Tm^{3+}	6.61	7.39	-3.33	-0.69	-2.0	0.0	2.0	-5.3	-2.3	0.7	-3.1	-0.9	1.3
Yb^{3+}	6.76	7.24	-3.51	-0.89	-2.1	-0.1	1.9	-5.4	-2.4	0.6	-3.3	-1.1	1.1
Lu^{3+}	6.73	7.27	-3.47	-0.85	-2.1	-0.1	1.9	-5.4	-2.4	0.6	-3.2	-1.0	1.2
Sc^{3+}	9.70	4.30	-6.94	-4.71	-4.6	-2.6	-0.6	-6.8	-3.8	-0.8	-6.7	-4.5	-2.3
Y^{3+}	6.30	7.70	-2.97	-0.29	-1.8	0.2	2.2	-5.2	-2.2	0.8	-2.7	-0.5	1.7

NOTES:

1. FOR COMPARISON, FOR IRON OXIDES, DZOMBAK AND MOREL VALUES WERE ALSO CALCULATED: y=slope*log KMOH +y-intercept.
2. LOFT AND TIPPING CALCULATIONS ARE CALCULATED AS PER EQUATIONS 13 TO 16 WITHIN THE TEXT.

3 – RESULTS

3.1 SCREENING LEVEL SITE COMPARISON

As discussed above, REYs were identified as a parameter of interest downstream of mining-affected areas. Few studies have looked comprehensively at major trends in REY chemistry downstream of a variety of types of mining sites, and under a variety of pH conditions. The trilinear piper plot completed for collected data indicates that all sites had similar major ion chemistry: water sampled was generally high in Ca-Mg and sulphate (Figure 2). Water that falls into the top quadrant of the trilinear piper plot is generally characteristic of mine drainage.

Sulphate is the dominant cation and all sites have less than approximately 30% of bicarbonate (HCO_3). The control site shows the lowest levels of sulphate and the greatest levels of bicarbonate. There is more variability within the composition of the major cations. Sites sampled range from approximately 50% to 100% calcium and anywhere from 10% to 80% magnesium. Sodium and potassium levels were also observed to exhibit a wide range in concentrations.

Filtered water samples (0.45 µm) were collected from sites that exhibited a wide range of pH. When pH was plotted vs. the sum of aqueous REYs, there was a general trend of decreasing aqueous REY concentration with increasing pH (Figure 3). There were large differences between sites; however, and regressions could not be fit for the entire dataset. Regressions with elevated R^2 values were observed for the Yukon site (R^2=0.76) and the S.American site(R^2=0.80). Filtered water samples (0.45 µm) were collected from sites that exhibited a wide range of pH. When pH was plotted vs. the sum of aqueous

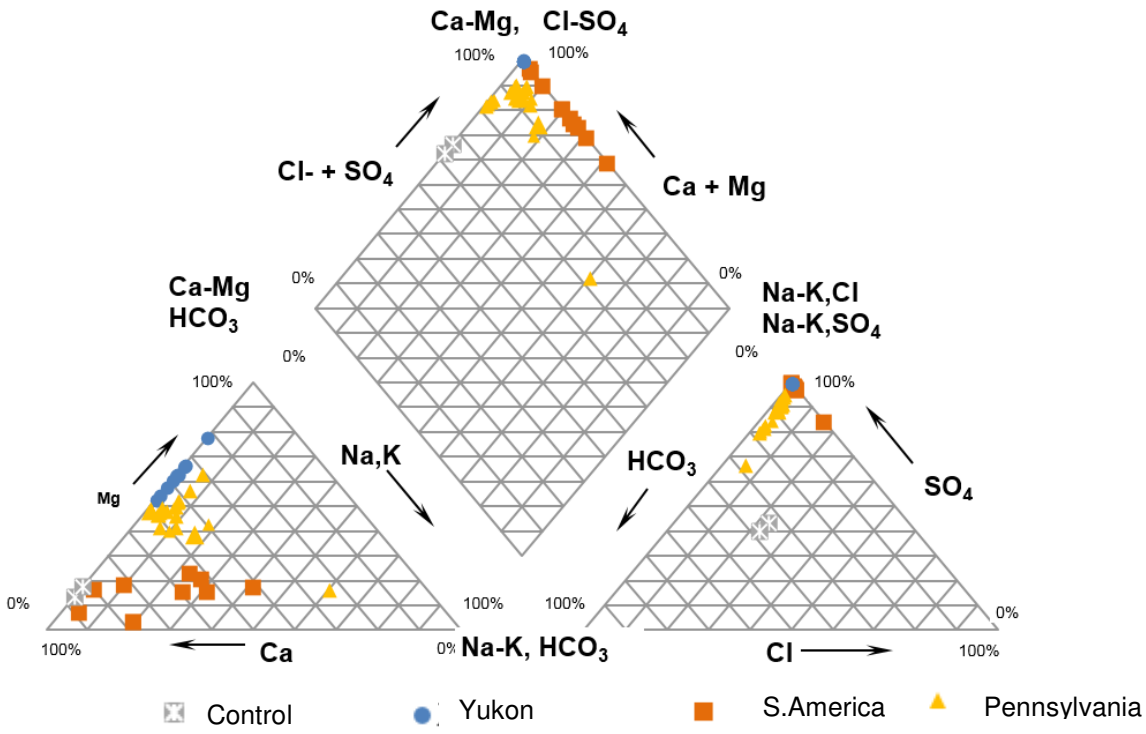

Figure 2 Trilinear Piper Plot for samples under a variety of pH conditions

REYs, there was a general trend of decreasing aqueous REY concentration with increasing pH (Figure 3). There were large differences between sites; however, and regressions could not be fit for the entire dataset. Regressions with elevated R^2 values were observed for the Yukon site (R^2=0.76) and the S.American site(R^2=0.80). While the strong correlation observed within the Yukon dataset is expected, since the water was collected within one stream, the tight correlation of the S.American dataset, which originates within three different sites was not expected. After a ph of approximately 5.5, a predictable pattern of aqueous REY enrichment with pH is hard to discern.

An inverse trend was expected within the mineralized biofilm/solid data. The biofilm data shows much greater scatter, but a loose trend of increasing REY concentrations in the biofilm with decreasing pH (Figure 3). Unlike the water data, the biofilm data shows that solids collected from low pH sites also have a large variability. Of particular interest within the biofilm dataset is the apparent inverse relationship of solid REY content at sites with elevated pH sampled from the anthracite coal region of Pennsylvania. These trends are inverse to previous literature and the patterns observed at other sites. These sites also contain the greatest amount of solid REYs, which may pose a potential toxic threat or a potential economic resource. As a result, the next chapter examines a handfull of sites within the anthracite region of Pennsylvania to understand the mechanisms that enable this solid enrichment.

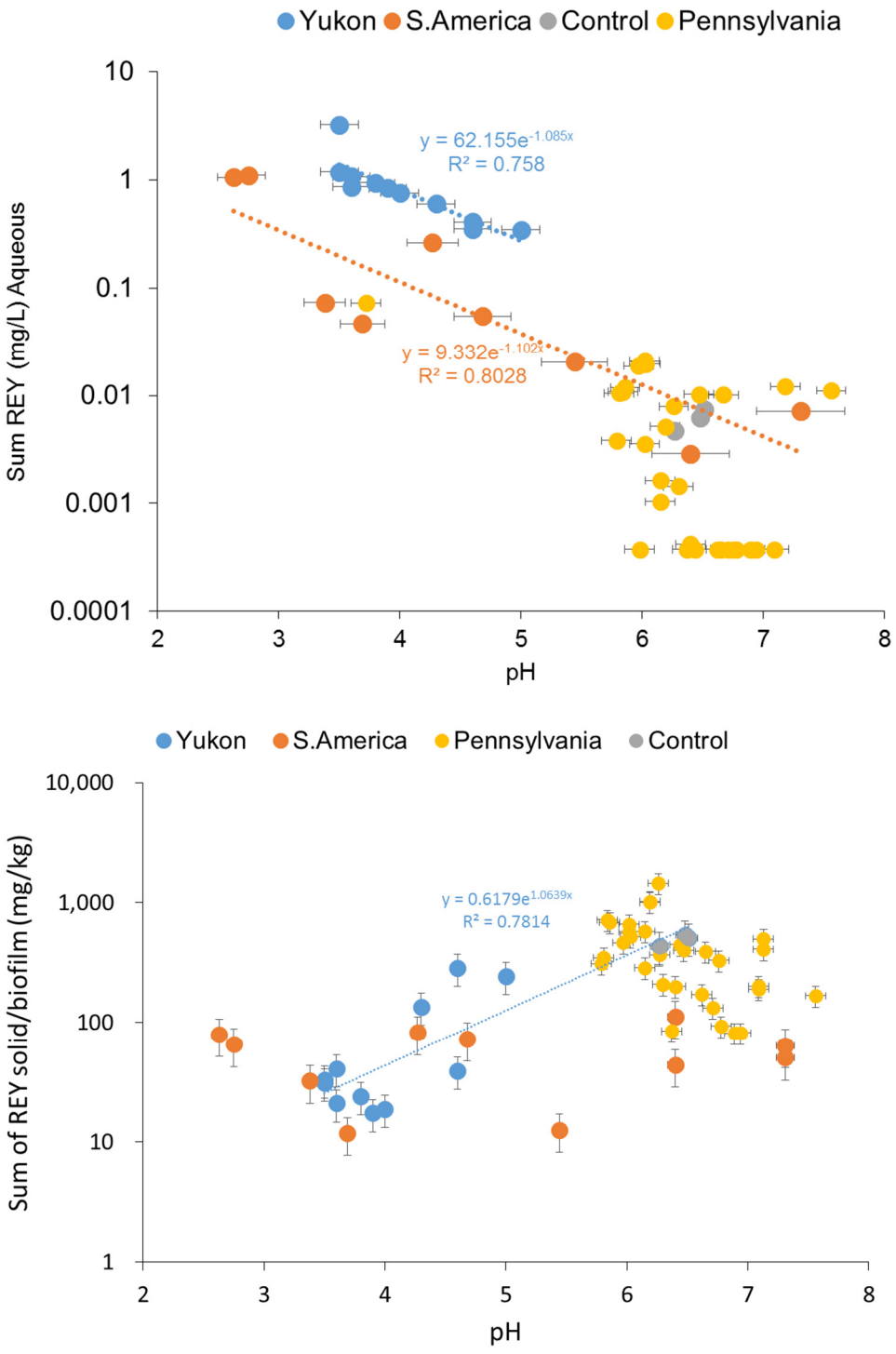

Figure 3 Comparison of aqueous REY and solid/biofilm REY vs. pH

3.2 COAL MINE DRAINAGE PASSIVE TREATMENT SITE – REY SPECIATION IN WATER ENRICHED WITH IRON, ALUMINUM AND ORGANICS

3.2.1 Bulk water sample chemical analysis

3.2.1.1 *In situ* parameters

In situ parameters were measured at each of the six sampling sites within the Silver Creek Passive treatment system (Table 15). Samples were collected under a variety of physicochemical parameters during summer low flow and winter low flow conditions; a set of diurnal samples in August were also collected. Diurnal effects on water chemistry were expected to be greatest in August due to high daytime temperatures. To assess any effects of diurnal cycling on REY concentrations, samples were collected in the late afternoon and early in the morning the following day. Of note, the measured flow rate was slightly lower in August (28.78 L/s and 28.21 L/s) than in December (47.24 L/s). As a result, the cumulative retention times in December were lower than in August.

One of the key characteristics of the Silver Creek site is the pH gradient within the passive treatment facility. The pH of the outflow of the mine seep increases from slightly acidic (5.86-6.03) to circumneutral (6.76-7.56) at the outlet. Changes in pH can vary between treatment stages on a given sampling date from 0.95 to 1.75 pH units. In general, the pH changes from low pH near the seep, to higher pH at subsequent treatment stages. December sampling event, sites SC06 and SC05 measured the lowest pH. In August, the lowest pH during both the morning and afternoon sampling events was recorded at SC04, with sites SC06 and SC05 showing very similar pH values. The outflow of the mine seep contains pCO_2 concentrations ($10^{-1.1}$ and $10^{-1.29}$ atm) equal to approximately 150-200 times that of the atmosphere ($10^{-3.5}$ atm) (pCO_2 values were calculated from DIC values). As water travels through the passive treatment system, the pCO2 values decrease. During the December sampling event, the furthest downstream sample (SC01) contained pCO_2 values ~10X the atmospheric concentrations ($10^{-2.4}$ atm), while pCO_2 values at SC01 during the afternoon August sampling event were close to atmospheric levels ($10^{-3.3}$ atm).

Temperature was the *in situ* parameter that showed the greatest variability between the August and December sampling events, as expected. The largest body of water (Wetland 2, sampling point SC01), showed a 20℃ change in temperature between the December sampling event, and the afternoon August sampling event**.** Dissolved oxygen levels are strongly linked to temperature; the solubility of oxygen decreases as water temperature increases. As a result, as temperature increases, the saturation of oxygen increases even if the measured amount of dissolved oxygen (mg/L) remains constant. At the sites most affected by temperature increases (SC01, SC02 and SC03), temperatures recorded in the afternoon in August were consistently the highest of the three sampling events; these sites also had the highest percentage of dissolved oxygen, with SC02 and SC01 displaying supersaturation. While under-saturated, the concentrations of dissolved oxygen were consistently highest in the December samples (maximum of 12.06 mg/L at SC01), where the temperatures were the lowest.

There is a consistent trend of decreasing specific conductivity from mine outflow (SC06) to passive treatment outflow (SC01). Specific conductivity values were consistently slightly lower during the December sampling event when compared to August sampling events, which is consistent with the higher flow rates; however the difference for most sites is within instrument error.

Redox potential was consistently elevated in August samples when compared to the December samples, particularly at the downstream sites most affected by changes in temperature (SC01, SC02, SC03). A general trend of increasing redox potential was noted from mine outflow (SC06) to the passive treatment outflow (SC01) for the August sampling events. Calculated pe values were slightly greater in August, when compared to December and showed a general, but not completely consistent, increasing trend from mine outflow (SC06) to passive treatment outflow (SC01).

A manual ion balance was calculated using major cations (calcium, magnesium, sodium and potassium) and anions (sulphate, nitrate, bicarbonate and chloride), in addition to ion balances calculated through the WHAM and PHREEQC-i modelling programs. For these balances, the value of 4 mg/L was used to represent chloride, since this parameter wasn't sampled. This value was taken from previous chemical data recorded at the site. The percentage error for the manual ion balance was less than 0.2% for all sites sampled (Appendix B1, Table B1.1) .

Table 15 *In Situ* parameters measured at the Silver Creek site during December 2015 and August 2016

Site	Date	Time	Flow (L/s)	Cum. Residence Time (hr)	Temperature (˚C)	Specific Conductivity (µS/mL)	Dissolved oxygen (%)	Dissolved oxygen (mg/L)	pH	Eh (mv)	pe	pCO_2 (atm)	Alkalinity (mg/L)
SC06-Dec	12/12/2015	1205	47.2	0.0	11.89	487	5.2	0.57	5.86	236.8	4.19	0.078	39.4
SC06-Aug-PM	08/08/2016	1820	28.8	0.0	12.12	502	5.5	0.56	6.03	291.3	5.15	0.051	35.7
SC06-Aug-AM	09/08/2016	0835	28.2	0.0	11.93	501	7.8	0.83	5.94	294.0	5.20	NA	NA
SC05-Dec	12/12/2015	1215	47.2	0.7	11.98	471	17.3	1.86	5.84	281.3	4.98	0.073	35.5
SC05-Aug-PM	08/08/2016	1800	28.8	1.1	13.91	498	11.4	1.18	6.02	299.3	5.25	0.047	33
SC05-Aug-AM	09/08/2016	0825	28.2	1.2	12.10	494	19.8	2.12	5.97	319.0	5.64	0.040	24.5
SC04-Dec	12/12/2015	1225	47.2	84.1	10.28	465	74.9	8.34	6.15	293.2	5.22	0.026	26.7
SC04-Aug-PM	08/08/2016	1715	28.8	138.1	17.93	463	35.9	3.40	5.81	358.5	6.21	0.035	15.5
SC04-Aug-AM	09/08/2016	0810	28.2	140.9	14.79	462	54.9	5.56	5.86	378.9	6.63	NA	NA
SC03-Dec	12/12/2015	1235	47.2	226.8	8.81	451	90.4	10.49	6.44	297.8	5.33	0.011	22.6
SC03-Aug-PM	08/08/2016	1700	28.8	372.2	25.23	452	95.8	7.89	6.47	322.1	5.44	0.0057	12.8
SC03-Aug-AM	09/08/2016	0755	28.2	379.7	20.37	455	86.3	7.78	6.27	384.1	6.59	NA	NA
SC02-Dec	12/12/2015	1245	47.2	245.8	8.73	447	97.6	11.34	6.65	286.1	5.12	0.0062	21.6
SC02-Aug-PM	08/08/2016	1650	28.8	403.5	25.55	457	124.9	10.21	7.18	367.1	6.19	0.0017	20
SC02-Aug-AM	09/08/2016	0740	28.2	411.6	21.08	458	75.9	6.74	6.67	391.8	6.71	0.0056	19.7
SC01-Dec	12/12/2015	1255	47.2	269.8	8.46	441	102.5	12.01	6.76	283.1	5.07	0.0043	19.3
SC01-Aug-PM	08/08/2016	1630	28.8	442.9	28.97	446	125.6	9.64	7.56	342.2	5.71	0.00047	13.4
SC01-Aug-AM	09/08/2016	0730	28.2	451.8	20.47	454	85.6	7.70	7.13	460.2	7.90	NA	NA

NOTES:

1. SITES ARE ARRANGED FROM UPSTREAM TO DOWNSTREAM.
2. IN SITU WATER CHEMISTRY MEASUREMENTS WERE TAKEN USING CALIBRATED YSI 556 PROBE.
3. ALKALINITY VALUES WERE CALCULATED FROM DIC, SINCE THIS WAS DEEMED MORE ACCURATE THAN ALKALINITY TITRATIONS.

3.2.1.2 Major ion chemistry - 0.45 µm Filtered Water

The major ion chemistry of the Silver Creek passive remediation site was consistent between the December 2015 and August 2016 sampling events (Figure 4). The cation composition at the site is almost equally composed of magnesium (~50%) and calcium (~45%), with minor amounts of sodium and potassium (~5%). The anion composition is almost exclusively composed of sulphate (~80-90%), with bicarbonate and carbonic acid making up the remainder of the anions (~10-20%). In general, the major ion chemistry of the Silver Creek site, falling within the top quadrant of the trilinear piper plot, is characteristic of calcium-magnesium sulphate rich waters associated with mine drainage.

Note that diurnal differences in major ion chemistry were not observed between the samples collected during the afternoon in August (green) and those collected during the morning (grey). Seasonal differences in sulphate concentrations between the August and December sampling event, however, were observed on a small scale (±10%). For values of major ion chemistry, refer to Table 16.

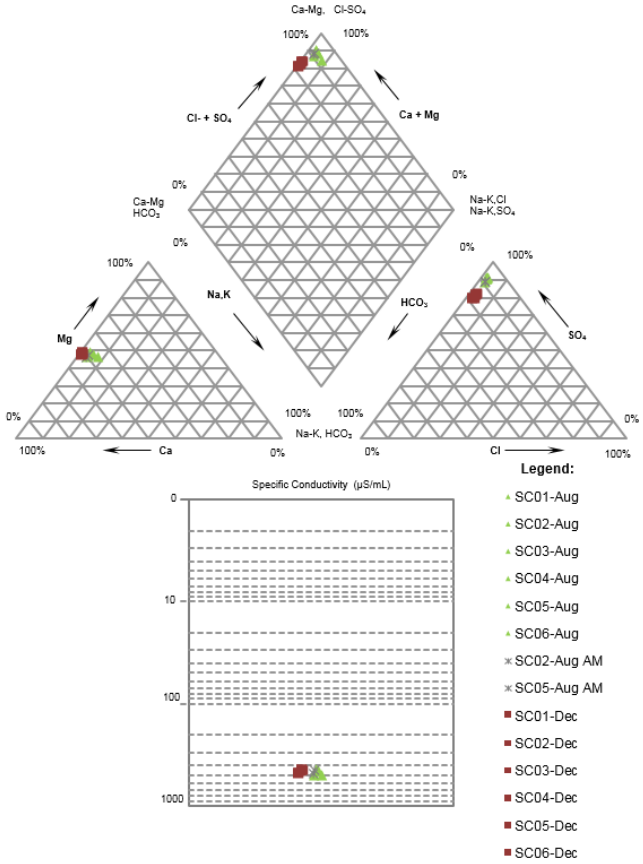

NOTES:

1. PIPER DATA ARE PLOTTED IN %meq/L.
2. TOTAL ALKALINITY WAS USED FOR HCO3 VALUES.

Figure 4 Trilinear Piper plot of Silver Creek water chemistry

3.2.1.3 REY chemistry - 0.45 µm Filtered Water

Aqueous REY concentrations in the Silver Creek passive treatment system, obtained by filtration of grab water samples through a 0.45µm filter, range from <0.007 µg/L to 9.2 µg/L. In general, concentrations of each individual REY (and the sum of REYs) are highest at the more acidic upstream sites closer to the mine seep (SC06 and SC05), and decrease at sites further downstream in the passive treatment system (

Table 17). As water travels further from the mine seep, REY concentrations decrease one order of magnitude at the SC04 and SC03 sampling points, which are located at the outlets of ponds 2 and 3, respectively. REY concentrations further decrease another order of magnitude at the SC02 and SC01 sampling sites, which are located at the outlet of wetland 1 and 2, respectively. Ce, La, Lu, Nd, Y and Sc were the most abundant REYs, measuring 1 to 8 µg/L. With the exception of measurements at SC06 during the morning sampling event in August, in general, there were little seasonal difference in REY concentration; however, most REY concentrations, except Ho, Lu and Sc, were most elevated in water collected during the August afternoon sampling event. Enrichment of REYs in the water during the afternoon August sampling event is particularly noted at sites SC05 and SC06, with site SC05 containing slightly more REYs than SC06.

Detection limits complicated analysis of samples from the December sampling event, at downstream sites SC04, SC03, SC02, and SC01. Samples during December were initially diluted, raising detection limits and samples SC03, SC02, and SC01 were re-run without dilution. Samples were run on several different runs of ICP-MS, and detection limits are provided in Appendix B1, Table B1.2.

Despite a wide range in concentration of individual REYs at sites sampled, REYs are known to act as a unit. To quantify pairwise correlations between REY parameters, scatterplot matrices were created together with correlation coefficients (0-1.0). Results of these scatterplots and correlation coefficients indicate that the Sum of REY parameter (µg/L) is highly correlated (0.96-1.0) with all LREEs, MREEs, and HREYs, and is less correlated with: Ho (0.92), Er (0.93), Sc (0.63) and Lu (0.23). Excluding Ho, Er, Sc and Lu, REYs have high within group correlation coefficients (0.96-1.0), while LREEs have especially high within group correlation coefficients (0.99-1.0).

Table 16 Silver Creek Water Major and Minor Ions data (mg/L)

Sample	DIC	DOC	$N0_2^-$	$N0_3^-$	$P0_4^{3-}$	SO_4^{2-} (Calc)	Al	Ca	Fe	Mg	Mn	K	Na	P	S	Si
SC06-Dec	40.14	4.16	0.007	4.6	0.13	180	0.12	41	17	24	2.2	<0.1	0.41	<0.03	60	5.6
SC06-Aug	29.8	2.3	0.013	3.8	0.21	204	0.17	40	20	25	2.9	0.82	2.2	<0.003	68	6.4
SC06-Aug-AM	NA	NA	0.007	1.5	0.19	219	0.0046	39	14	22	2.1	0.58	3.6	<0.03	73	6.3
SC05-Dec	37.53	2.89	0.007	3.5	0.19	180	0.10	41	17	24	2.3	<0.1	0.41	<0.03	60	5.6
SC05-Aug	27.5	1.8	0.012	2.5	0.23	225	0.018	40	19	24	2.6	0.86	2.50	<0.003	75	6.6
SC05-Aug-AM	22.6	0.8	0.006	2.3	1.24	216	0.14	44	21	26	2.9	0.96	2.4	<0.003	72	6.8
SC04-Dec	17.07	1.58	0.006	3.7	0.3	189	<0.0008	43	9.3	25	2.2	0.23	0.5	<0.03	63	5.5
SC04-Aug	17.8	1.8	0.005	0.8	0.08	213	0.10	42	12	26	3	0.57	3.3	<0.003	71	6.3
SC04-Aug-AM	NA	NA	0.005	1.5	0.17	231	0.013	38	3.6	23	2.1	1.1	2.6	<0.03	77	6.2
SC03-Dec	9.92	1	0.009	2.7	0.22	186	<0.0008	43	5	24	2.1	0.2	0.5	0.034	62	5.1
SC03-Aug	5.4	1.7	0.007	1	0.21	213	0.00130	44	0.79	26	3	0.88	2.3	<0.003	71	5.9
SC03-Aug-AM	NA	NA	0.005	0.9	0.18	249	0.00042	40	0.24	24	2.10	1.2	2.8	<0.03	83	6.2
SC02-Dec	7.68	0.88	0.006	1.7	0.16	189	<0.0008	43	2	25	2	0.27	0.5	<0.03	63	4.9
SC02-Aug	5.5	2.3	0.004	0.7	0.16	219	<0.001	41	0.28	23	1.3	0.68	2.1	<0.003	73	4.3
SC02-Aug-AM	7.1	1.8	0.003	0.9	0.12	207	0.00076	47	0.29	26	1.6	0.78	2.4	<0.003	69	4.5
SC01-Dec	6.28	1	0.009	1.6	0.12	189	<0.0008	43	1.2	25	2.1	0.47	0.58	<0.03	63	4.9
SC01-Aug	3.4	2.3	0.002	0.8	0.08	207	0.0062	44	0.27	25	2.0	0.72	2.3	<0.003	69	5.1
SC01-Aug-AM	NA	NA	0.002	0.9	0.12	267	0.0045	42	0.012	25	1.5	1.1	3.00	<0.03	89	5.9

NOTES:

1. ALL VALUES ARE PROVIDED IN mg/L, AND ALL MEASUREMENTS WERE MADE WITH FILTERED WATER (0.45 µm FOR ANIONS AND METALS; 0.2 µm FOR DIC AND DOC).
2. DIC REPRESENTS DISSOLVED INORGANIC CARBON AND DOC REPRESENTS DISSOLVED ORGANIC CARBON.
3. MOLAR CONCENTRATIONS ARE PROVIDED IN APPENDIX B, TABLE B1.3.

Table 17 Silver Creek Water Rare Earth Element Data (0.45µm filtered; µg/L)

Sample	La	Ce	Pr	Nd	Sm	Eu	Gd	Tb	Dy	Er	Ho	Tm	Yb	Lu	Y	Sc	Sum REY + Sc
Mass	139	140	141	146	147	153/151	157	159	163	166	165	169	89	175	172	45	
SC06-Dec	2.5	5.2	0.59	2.3	0.44	0.11	0.51	0.078	0.33	0.058	0.16	0.020	0.13	2.4	1.7	1.1	17.6
SC06-Aug-PM	3.9	8.1	0.95	3.8	0.68	0.17	0.86	0.12	0.58	0.31	0.11	0.042	0.24	0.037	2.9	1.3	24.1
SC06-Aug-AM	1.4	1.8	0.18	0.71	0.07	0.034	0.092	0.010	0.058	0.049	0.016	0.0077	0.037	0.0057	0.65	0.78	5.9
SC05-Dec	2.3	4.8	0.53	2.1	0.41	0.094	0.5	0.068	0.29	0.061	0.14	0.012	0.093	2.1	1.5	1.1	16.1
SC05-Aug-PM	4.5	9.2	1.00	4.1	0.66	0.16	0.84	0.12	0.55	0.29	0.11	0.037	0.21	0.034	3.1	1.1	26.0
SC05-Aug-AM	3.9	8.0	0.94	3.8	0.69	0.16	0.8	0.11	0.56	0.31	0.10	0.035	0.24	0.035	2.9	1.3	23.9
SC04-Dec	0.65	0.62	0.033	0.11	<0.03	0.011	<0.05	<0.01	<0.04	<0.01	<0.01	<0.01	<0.03	<0.9	0.13	1.00	3.6
SC04-Aug-PM	0.68	0.48	0.03	0.087	<0.009	0.045	0.017	0.0017	0.008	0.18	0.0081	0.0029	0.0012	0.0071	0.0020	1.00	5.5
SC04-Aug-AM	1.3	1.5	0.13	0.41	0.062	0.0175	0.11	0.016	0.0820	1	0.062	0.021	0.0076	0.037	0.0071	0.73	2.6
SC03-Dec	0.24	<0.05	0.012	0.051	<0.01	0.0034	0.012	<0.002	0.013	0.0085	<0.002	<0.004	0.0067	<0.004	0.18	1	1.4
SC03-Aug-PM	0.50	0.32	0.02	0.053	<0.009	0.0069	0.022	0.0041	0.017	0.0120	0.0061	0.0018	0.0069	0.0023	0.35	1	2.3
SC03-Aug-AM	0.36	0.19	0.014	0.045	0.005	0.0039	0.012	<0.002	0.009	0.0072	<0.004	<0.003	0.0041	<0.003	0.23	0.76	1.7
SC02-Dec	0.030	<0.05	<0.002	<0.006	<0.01	<0.002	<0.01	<0.002	<0.007	<0.005	<0.002	<0.004	<0.006	<0.004	0.024	1	1.0
SC02-Aug-PM	0.023	0.018	<0.001	<0.009	<0.009	0.0024	0.002	0.00100	0.00260	0.0014	0.00086	0.00095	0.0013	0.0014	0.021	0.71	0.8
SC02-Aug-AM	0.036	0.024	<0.001	<0.009	<0.009	0.00405	0.0035	0.0009	0.00330	0.0016	0.0017	0.001	0.002	0.0013	0.03	0.85	1.0
SC01-Dec	0.020	<0.05	<0.002	<0.006	<0.01	<0.002	<0.01	<0.002	<0.007	<0.005	<0.002	<0.004	<0.006	<0.004	0.021	1.00	1.0
SC01-Aug-PM	0.029	0.026	<0.001	<0.009	<0.009	0.0036	0.0032	0.00087	<0.001	0.0015	0.0019	0.0014	0.0021	0.0013	0.026	0.82	0.9
SC01-Aug-AM	0.032	0.018	0.0022	0.009	<0.002	0.0019	<0.004	<0.002	<0.003	<0.002	<0.004	<0.003	<0.004	<0.003	0.025	0.68	0.8

NOTES:

1. ALL VALUES WERE FILTERED WITH 0.45 µm FILTER, ACIDIFIED ON SITE, MEASURED ON THE ICP-MS AND PROVIDED IN µg/L.
2. DETECTION LIMITS PROVIDED IN APPENDIX B1, TABLE B1.2.
3. MOLAR CONCENTRATIONS ARE PROVIDED IN APPENDIX B1, TABLE B1.4.
4. EUROPIUM VALUES REPRESENT AN AVERAGE OF EU153 AND EU151 VALUES.

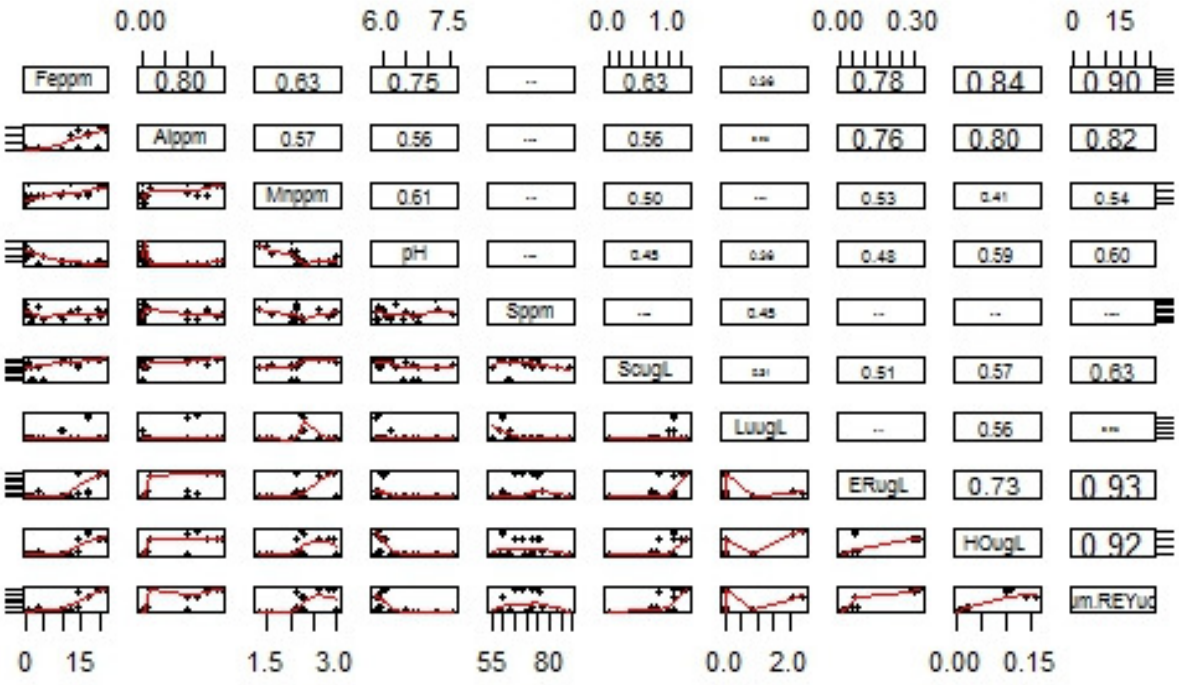

Figure 5 Pairwise Scatterplots and Correlation Coefficients for select REYs and Major Ions at the Silver Creek site (2015-2016)

Correlation coefficients indicate that the sum of REY parameter is a representative proxy for the majority of REYs, excluding Lu and Sc, and to a lesser extent Er and Ho. To understand the influence of major ions on REY chemistry, pH, Fe, Al, Mn and S were plotted for each sampling event from inflow to the Silver Creek passive treatment system (SC06) to outflow (SC01). As would be expected from carbon dioxide outgassing, pH and DIC show inverse trends. Dissolved Fe and Al decrease towards the outflow, similar to the behaviour of REYs. Seasonal differences in data are not pronounced or widespread; the December data has higher amounts of DIC than the August data as expected due to generally lower pH. In addition, the December data show much less variation in manganese than the August data. REY concentrations at the upper sampling sites showed greater concentrations during August, except for the Aug-AM sampling point at SC06. Iron levels at this site were slightly lower than other sampled sites, and, Al concentrations were much lower at this site than other sites. Diurnal differences in data include an inverse pattern in aluminum concentrations at the three most upstream sites, and nearly inverse manganese patterns.

Correlation coefficients calculated support these observations (Appendix B1.1 – Figure B2.1, Figure B2.2). The sum of REYs is correlated with iron (coefficient 0.90), aluminum (coefficient 0.82), silica (0.67), pH (0.60), and manganese (0.54), but does not show a strong correlation with sulphur (~0.1). Ho, Er, Sc, and Lu are: less correlated with iron than the Sum of REYS (correlation coefficients 0.80, 0.76, 0.56 and 0.36, respectively), slightly less correlated with Al than the sum of REYs (0.81, 0.77, 0.57, 0.27) and slightly less correlated with pH than the sum of REYs (0.59, 0.48, 0.45 and 0.36). Sc and Er are more strongly correlated with Mn (0.68, 0.53) than other REYS, and Lu is more strongly correlated with S (0.45) than other REYs.

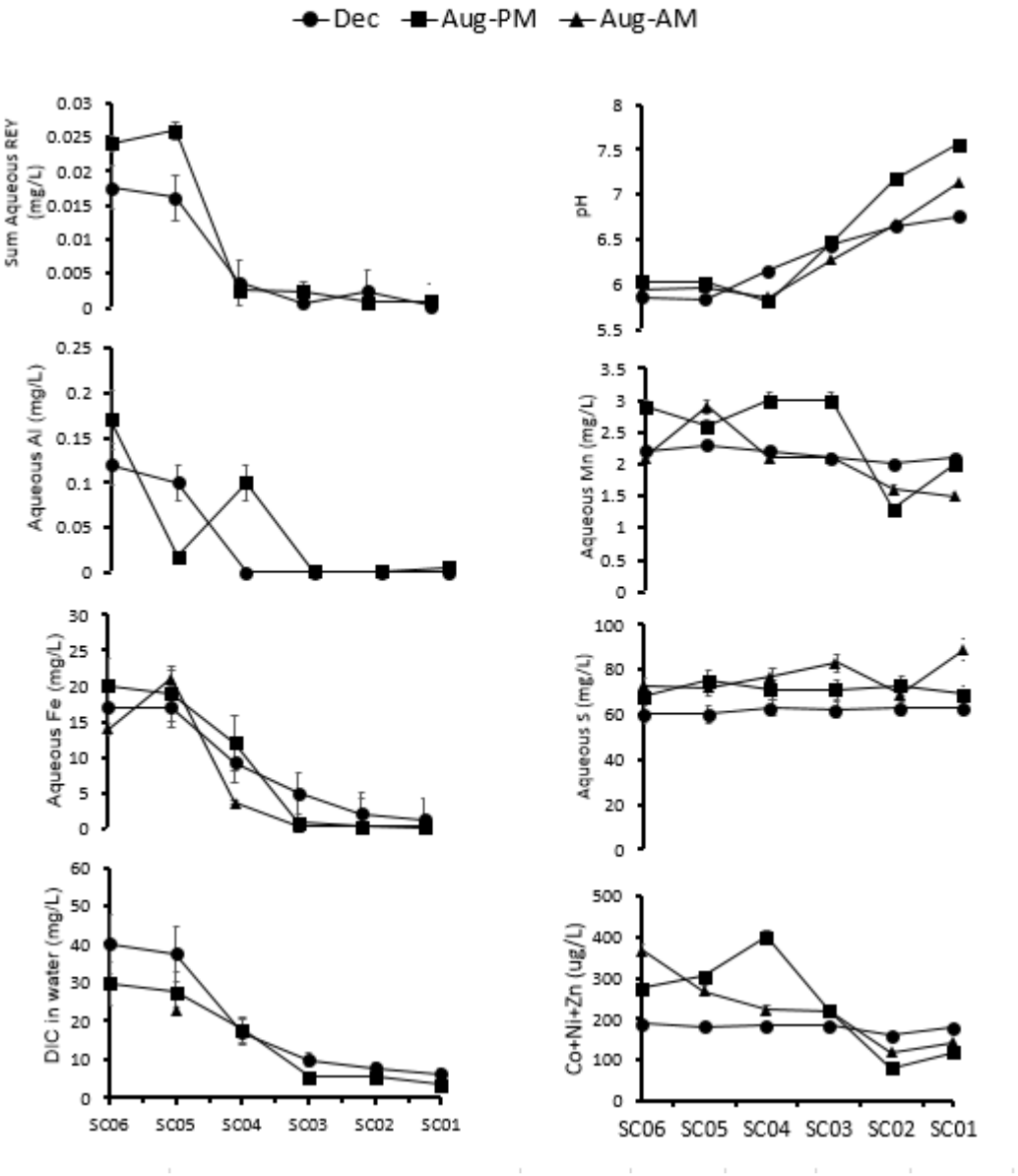

NOTE:

1. SITES ARE ARRANGED FROM UPSTREAM TO DOWNSTREAM (SC06-SC01).

Figure 6 Major Ion chemistry and Aqueous REY Concentration

For a better understanding of REY fractionation, normalized REY patterns were plotted from lowest to highest atomic number (with Y plotted between Dy and Ho) for water samples collected at each site at Silver Creek, during three sampling events representing low-flow conditions: morning August 2016, evening August 2016 and middle of the day December 2015 (Figure 7). REYs were normalized to NASC (table of normalized values in Appendix B1.5), PAAS (table of normalized values in Appendix B1.6) and rock adjacent to the area, Pennsylvania Anthracite-Mammoth No. 8 (Schuylkill

County) (table of normalized values in Appendix B1.7). Graphs of the normalized patterns are presented in Figure 7 and values used for normalization were presented in Table 9.

In general, the sites showed consistent trends in REY normalized patterns and REY normalized magnitude at different sampling points between different sampling events. In addition, the choice of normalization did not have a pronounced effect on REY patterns, with the exception that samples normalized to adjacent rock (Mammoth No. 8) showed greater variation in REY patterns. Regardless of season or time of sampling, SC05 or SC06 sites had the greatest concentration of REY in water sampled and that SC01 or SC02 sites have the lowest concentrations of REY in water sampled. The amount of dissolved REYs generally decreased from upstream (SC06) to downstream (SC01); however, during both August sampling events SC05 had greater aqueous REY concentrations than SC06.

Interference of the SC01 and SC02 sampling sites with detection limits was noted for all sampling dates, with the greatest interference observed in the December 2015 sampling event. In addition, interference of certain REYs within the SC03 and SC04 sites is also observed for the December 2015 sampling event. Numerical values for water quality sampled at all sites are provided in

Table 17, and detection limits at all sites are provided in Appendix B1, Table B1.2.

During all seasons and sampling times, the heaviest REYs show greater fractionation than MREEs or LREEs. All water samples show HREY enrichment over LREE or MREE enrichment; however, when Tm, Yb, Lu, and Sc are removed from a NASC normalized plot, the characteristic MREE enriched pattern is noted at most SC05 and SC06 sites (Figure 8). All sites seem to have a negative Er anomaly, a positive Tm anomaly and a positive Lu anomaly; however, the Tm anomaly shows some detection limit interference. An obvious and consistent positive Eu anomaly, positive Y anomaly and positive La anomaly seem to occur, without detection limit interference. Anomaly calculations are provided in the next section.

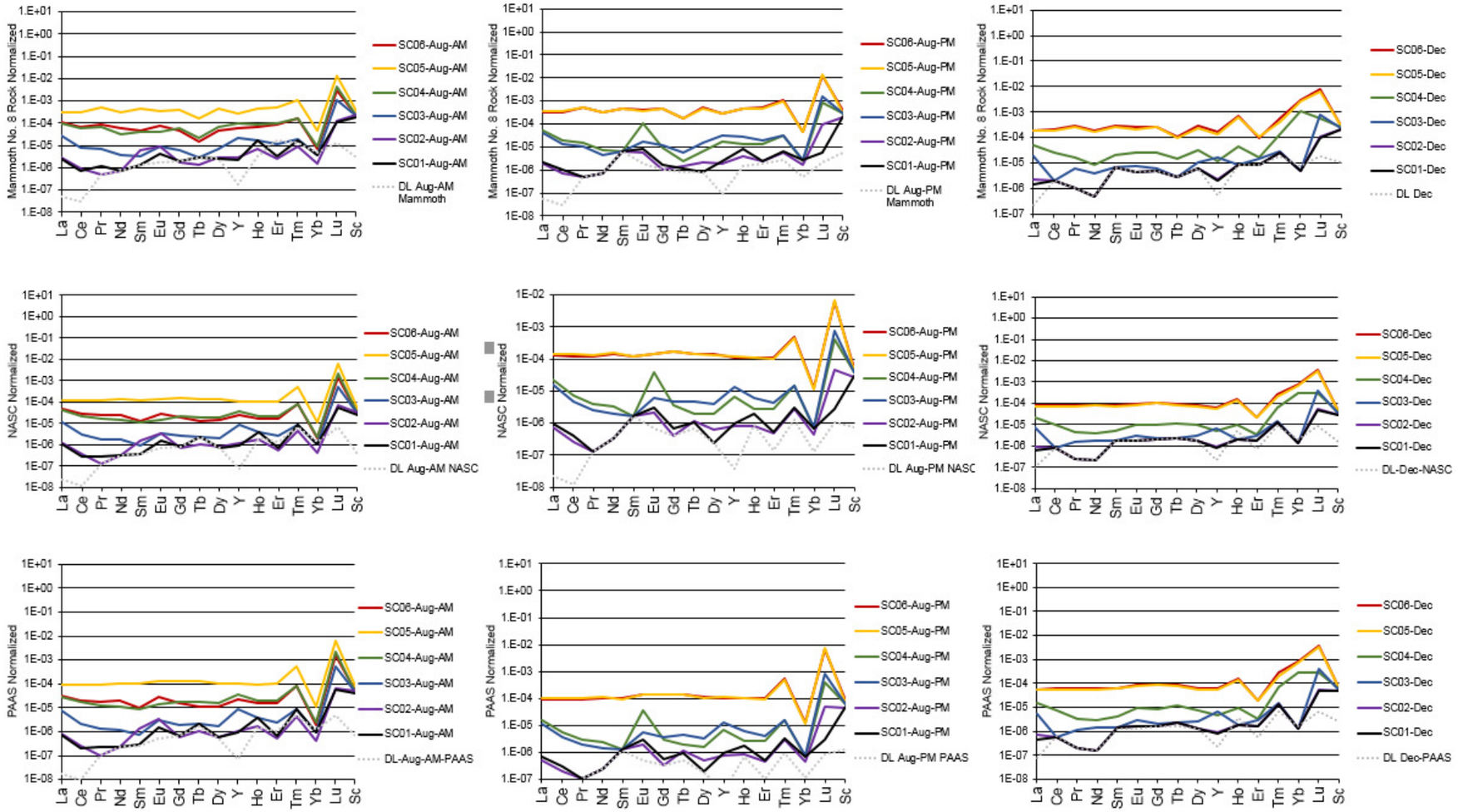

NOTE:

1. ALL VALUES WERE IN µg/L PRIOR TO NORMALIZATION; NORMALIZATION VALUES ARE PROVIDED IN SECTION 2.2.7; VALUES AT DETECTION LIMIT ARE PLOTTED AT DETECTION LIMIT

Figure 7 Silver Creek Water Mammoth No. 8, NASC, and PAAS Normalized REY data (µg/L; log scale)

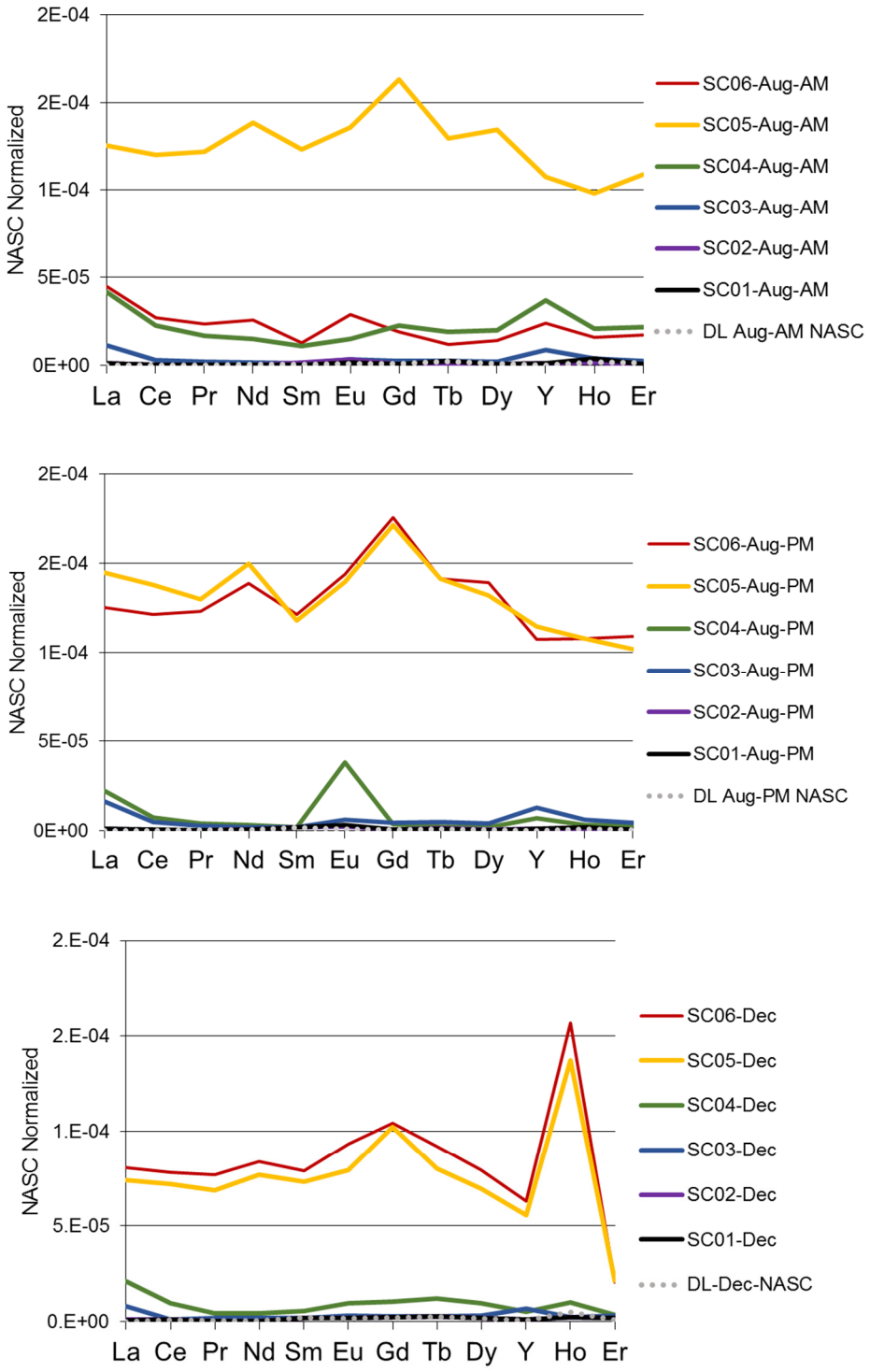

Figure 8 NASC Normalized Pattern of 0.45µm filtered Water (µg/L) – excluding Tm, Yb, Lu and Sc (not log scale)

To quantify trends in REY fractionation, REY anomalies for water and sediment were calculated, using NASC normalized data together with percentages and fractions of LREE, MREE and HREY (not normalized), and as described in Section 2.3. To determine the appropriate anomaly calculations, calculations in Table 10 were completed and resulting calculations were plotted against measured, normalized calculations (Appendix B1, Figure B2.3). Anomaly calculations that best represented a linear 1:1 trend were selected and results of these calculations are included in Table 18.

As is evidenced by the calculated percentage of LREE/total REYs and HREY/total REYS and the Pr_n/Yb_n ratio, there is an increasing proportion of dissolved phase HREY compared to dissolved phase LREE in the system with increased pH or progress downstream. MREE values seem to follow a similar trend, with increased dissolved MREE in the water at lower pH, and less MREE within the water at higher pH, in further downstream sampling locations. All sites show a positive fractionation of Y/Ho, with sites SC04 and SC03 showing the greatest values for Y/Ho fractionation (up to 90).

A lanthanum anomaly within the water was noted for all sites. Sites closer to the mine effluent discharge, with lower pH, had the lowest relative lanthanum anomaly. As water traveled downstream, pH increased, the total amount of REYs in the water decreased and the La anomaly increased. The SC01 and SC02 sites sampled in the morning of August 2016 have an extremely high lanthanum anomaly (equal to 36, 46), that is far greater from the other August and December sampling events.

Cerium anomaly calculations were completed using two different methods (linear and geometric, see Table 18). There was some variation between the two methods (±0.3); however, in spite of variation, most sites showed a positive cerium anomaly. The only exception was the SC03 December sampling event, which indicated a negative europium anomaly. There were similarly two calculations used for europium anomalies, which differed slightly, but generally showed that all sites were characterized by a positive europium anomaly.

In contrast to lanthanum which has an increasing anomaly along the flow path, the gadolinium anomaly decreased along the flow. The occurrence of a gadolinium anomaly was calculated using two methods and both methods yielded similar results. Both methods took a geometric based on the methods of Lawrence and colleagues[60]. Both calculations tend to agree, and indicate that a positive gadolinium anomaly is observed at sites closest to the discharge (SC06, SC05, SC04) and that a negative gadolinium anomaly is observed at sites furthest from the discharge (SC01 and SC02). The methods differ in that depending on the calculation method, site SC03 does not show the occurrence of an anomaly.

Yttrium anomalies have been used by other authors, in tandem with Y/Ho ratios to act as a proxy for iron oxidation. Yttrium anomalies were calculated using two different methods, which obtained similar results (average relative percent different of 26%). Considering relative error, all sites showed a yttrium anomaly, with the central sites (SC04 and SC03) showing the greatest yttrium anomaly. This reflects the general trends in the Y/Ho fractionation mentioned earlier.

Table 18 Silver Creek REY Anomaly Calculations

Site	Sum REY + Sc (ug/L)	pH	Y/Ho	LREY/ total	HREY/ total	LREY/ HREY	MREY/ HREY	LREYn/ HREYn	LREYn/ MREYn	MREYn/ HREYn	La/La*	Ce/Ce*		Eu/Eu*		Gd/Gd*		Y/Y*	
								Prn/Ybn	Prn/Tbm	Gdn/Ybn	Lan/(Prn* Prn/Ndn)	Ce/SQRT (La*Pr)	Ce/(0.5*La + 0.5*Pr)	Eu/(0.67* Sm + 0.33*Tb)	Eu/(SQRT(Sm*Gd))	Gdn/(Tbn* (Tbn/Dyn))	Gdn/(Tbn2* Smn)1/3	[2/3]*Dyn + [1/3]Hon	[1/3]*Dyn + [2/3]*Hon
SC06-Dec	17.6	5.86	10.6	66%	34%	1.9	0.6	1.8	0.8	2.4	1.3	1.0	1.0	1.1	1.0	0.98	1.19	0.88	0.98
SC06-Aug-PM	24.1	6.03	26.4	77%	23%	3.3	1.0	1.6	0.9	2.2	1.3	1.0	1.0	1.1	1.0	1.22	1.31	1.02	1.49
SC06-Aug-AM	5.9	5.94	40.6	73%	27%	2.7	0.6	1.9	2.0	1.6	2.4	0.8	0.8	2.3	1.9	1.89	1.56	2.16	2.87
SC05-Dec	16.1	5.84	10.7	67%	33%	2.0	0.6	2.3	0.9	3.4	1.3	1.0	1.0	1.0	0.9	1.11	1.31	0.88	0.99
SC05-Aug-PM	26.0	6.02	28.2	79%	21%	3.7	1.1	1.9	0.9	2.5	1.5	1.0	1.0	1.1	1.0	1.13	1.29	1.14	1.65
SC05-Aug-AM	23.9	5.97	29.0	77%	23%	3.3	1.0	1.6	0.9	2.1	1.3	1.0	1.0	1.1	1.0	1.31	1.28	1.06	1.57
SC04-Dec	3.6	6.15	13.0	41%	59%	0.7	0.1	0.4	0.4	1.0	4.3	1.0	0.7	1.2	1.3	0.71	1.13	0.64	0.87
SC04-Aug-PM	2.6	5.81	62.1	53%	47%	1.1	0.2	1.7	1.9	1.5	3.7	0.8	0.6	21.9	16.1	1.66	1.86	4.12	5.05
SC04-Aug-AM	5.5	5.86	47.6	64%	36%	1.8	0.7	1.4	0.9	1.9	1.9	0.8	0.8	1.1	0.9	1.25	1.42	2.38	3.23
SC03-Dec	1.6	6.44	90.0	24%	76%	0.3	0.2	0.7	0.7	1.1	7.1	0.2	0.2	1.5	1.4	1.38	1.14	2.88	4.42
SC03-Aug-PM	2.3	6.47	57.4	40%	60%	0.7	0.3	1.2	0.5	2.0	3.4	0.7	0.5	2.2	2.2	0.79	1.34	3.78	4.64
SC03-Aug-AM	1.7	6.27	57.5	38%	62%	0.6	0.3	1.4	0.8	1.8	5.2	0.6	0.4	2.4	2.2	0.92	1.44	4.58	5.21
SC02-Dec	1.2	6.65	12.0	9%	91%	0.1	0.1	0.1	0.1	1.0	3	1.5	1.2	0.9	0.9	0.62	0.95	0.66	0.86
SC02-Aug-PM	0.8	7.18	24.4	8%	92%	0.1	0.1	0.3	0.1	1.0	36	0.9	0.6	1.4	2.5	0.18	0.31	1.51	1.90
SC02-Aug-AM	1.0	6.67	17.6	9%	91%	0.1	0.1	0.2	0.1	1.1	57	0.9	0.6	2.4	3.2	0.50	0.59	1.53	1.68
SC01-Dec	1.2	6.76	10.5	9%	91%	0.1	0.1	0.1	0.1	1.0	2	1.8	1.7	0.9	0.9	0.62	0.95	0.57	0.76
SC01-Aug-PM	0.9	7.56	13.7	9%	91%	0.1	0.1	0.2	0.1	1.0	46	1.1	0.7	2.2	3.0	0.15	0.55	2.52	1.83
SC01-Aug-AM	0.8	7.13	6.3	9%	91%	0.1	0.1	0.2	0.1	0.6	5	0.5	0.4	1.6	3.0	0.11	0.65	0.98	0.79

NOTES:

1. FRACTIONS OF Y/HO AND LREE/TOTAL; HREY/TOTAL; LREE/HREY AND MREE/HREY WERE COMPLETED WITH DATA THAT WAS NOT NORMALIZED. THE REMAINING CALCUATIONS (LREEn/HREYn etc.) WERE COMPLETED WITH NASC NORMALIZED DATA.

3.2.1.4 Diurnal Variability

Strong, diurnal variability was noted at sampling site SC06, when water samples collected during the morning sampling event (7:30AM-8:30AM) were compared with samples collected during the afternoon/evening (16:30-18:20). The maximum diurnal change was noted for Tb (169%), whereas the smallest diurnal change occurred for La (94%). At SC06, the August afternoon water samples were consistently elevated; however, this trend was not consistent at subsequent sites further downstream (Appendix B1, Table B1.8). SC05, the site just downstream of SC06, showed very little variability between morning and evening samples, and certain REYs (Sm, Dy, Er, Yb and Lu) were elevated during the morning sampling event. Sample site SC04 is almost in direct contrast to SC06, with the SC04 August morning samples being consistently elevated by 63% to 164% over the evening samples. Site SC01 showed a similar pattern to SC04, with the morning August samples moderately elevated when compared to evening samples (4% to 100%). Sample sites SC03 and SC02 show less diurnal variability, with afternoon samples at SC03 indicating general enrichment when compared to morning samples. Analysis of SC02 was complicated due to detection limits, and did not show a consistent trend.

Table 19 Diurnal Variability of REYs at SC06 during August diel cycle experiment

Sample	SC06-Aug-PM	SC06-Aug-AM	Variation (ug/L)	Average (ug/L)	% change
La	3.9	1.4	2.5	2.65	94%
Ce	8.10	1.8	6.3	4.95	127%
Pr	0.95	0.18	0.77	0.565	136%
Nd	3.8	0.71	3.09	2.255	137%
Sm	0.68	0.07	0.61	0.375	163%
Eu	0.17	0.034	0.136	0.102	133%
Gd	0.86	0.092	0.768	0.476	161%
Tb	0.12	0.01	0.11	0.065	169%
Dy	0.58	0.058	0.522	0.319	164%
Er	0.31	0.049	0.261	0.1795	145%
Ho	0.11	0.016	0.094	0.063	149%
Tm	0.042	0.0077	0.0343	0.02485	138%
Yb	0.24	0.037	0.203	0.1385	147%
Lu	0.037	0.0057	0.0313	0.02135	147%
Y	2.9	0.65	2.25	1.775	127%

NOTES:

1. BOLD HIGHLIGHTING INDICATES THIS VALUE WAS HIGHER.

3.2.1.5 Comparisons of 0.45 µm and 0.2 µm Filtered Water

Water from sampling sites SC06 and SC05 was filtered with both 0.45um and 0.2um filters to test whether the 0.45um filtered water truly represented the dissolved fraction, or if it contained significant colloidal material. Results indicate that 0.45um is an accurate representation of dissolved REYs, with

the exception of Lu. Lu water samples that were filtered with 0.2um, and contained two orders of magnitude less Lu (Table 20). Filter blanks were run for the samples through the 0.45 µm filter in December and Lu values measured below detection (<0.09 µg/L).

Table 20 Comparison of Lu concentrations from 0.45um and 0.2um filtration

Filter size	SC06-Dec	SC05-Dec
0.45µm	2.4	2.1
0.2 µm	0.027	0.024

NOTES:
1. UNITS IN ug/L.

3.2.1.6 Water Chemistry Speciation

Speciation calculations were completed using PHREEQC-i (llnl database), exclusive of any organics data. In addition, water quality modelling was completed in WHAM with measured DOC input as 50% fulvic acid. Modelling was completed for all the December 2015 and August 2016-PM samples and select samples collected August 2016-AM. Graphs depicting the results of the speciation modelling for December are included in Figure 9- Figure 11. Speciation modelling indicates that $LnCO_3^+$, $LnSO_4^+$ and Ln^{3+} are the most common species of REYs throughout the system, with the exception that Sc consistently has Ln^{3+} speciation.

When examining the exclusively inorganic data, sampling sites SC06, SC05, SC04 and SC03 tend to have similar aqueous speciation during both December and August sampling events (Figure 9). At these sites, there is a fairly even distribution between the proportion of $LnSO_4^+$, and Ln^{3+} (~30% and ~20% respectively), with $LnCO_3^+$ as the dominant form at most sites (~50%). With the exception of Sc, and anomalous behaviour for Ce, Pr and Gd, there is a decreasing trend for Ln^{3+} with atomic number, and an increasing trend for $LnCO_3^+$ with atomic number. This perhaps means that HREYs are more likely to be found as $LnCO_3^+$ and LREEs are more likely to be found as Ln^{3+}. Anomalous behaviour for Ce, Pr and Gd is noted within the water chemistry. At these sites, $LnSO_4^+$ and Ln^{3+} complexes are preferentially formed over $LnCO_3^+$, unlike what is seen with the other REYs where $LnCO_3^+$ is generally dominant (~50%). At sites SC01 and SC02, where the pH is greater than further upstream sites (SC06-SC04), despite a decrease in alkalinity, REYs are dominantly complexed as $LnCO_3^+$ and $LnHCO_3^{2+}$..

Addition of colloidal dissolved oxygen is predicted by WHAM to play a key role in REY adsorption, and adsorb a greater proportion of HREs, when compared to LREY parameters. For lower atomic number REYs (i.e., La and Ce), colloidal organic speciation is inversely proportional to sulphate complexes (Figure 10 and Figure 12). For La and Ce, REY-sulphate complexes are observed to dominate at SC06 and SC05; however, at further downstream sites colloidal organics are expected to dominate. For HREYs, such as Gd and Yb, WHAM predicts close to 100% adsorption to colloidal particles, even when measured pH is less than 6.

Results plotted in Figure 8 indicate that there is a general patterns for aqueous speciation within the REYs: light REYs act similarly, heavy REYs act similarly, and anomalous behaviour is noted for Ce, Pr and Gd (Figure 10 to Figure 13). La acts as the LREY representative, Yb acts as the HREY representative and anomalous concentrations for Ce and Pr are represented by plots of Ce, and Gd is also plotted for comparison. Plots of La speciation (Figure 9; representative of general LREY

speciation) indicate aqueous inorganic LREY speciation is dominated by $LaSO_4^+$ and La^{3+}, with increasing influence of $LaCO_3^+$ at the most downstream sites (SC01 and SC02). The WHAM model that considers organic matter predicts that REY-organic colloid speciation is dominant downstream of site SC03 (pH 6.5). These results for lanthanum are similar to predicted results for cerium. Yttrium concentrations are dominated by either $YbCO_3^+$ or $YbSO_4^+$, when only inorganic ligands are considered. With the addition of organic colloids, the WHAM model predicts the vast majority of minerals associated with manganese. This behaviour is noted to be similar to the results observed for Gd.

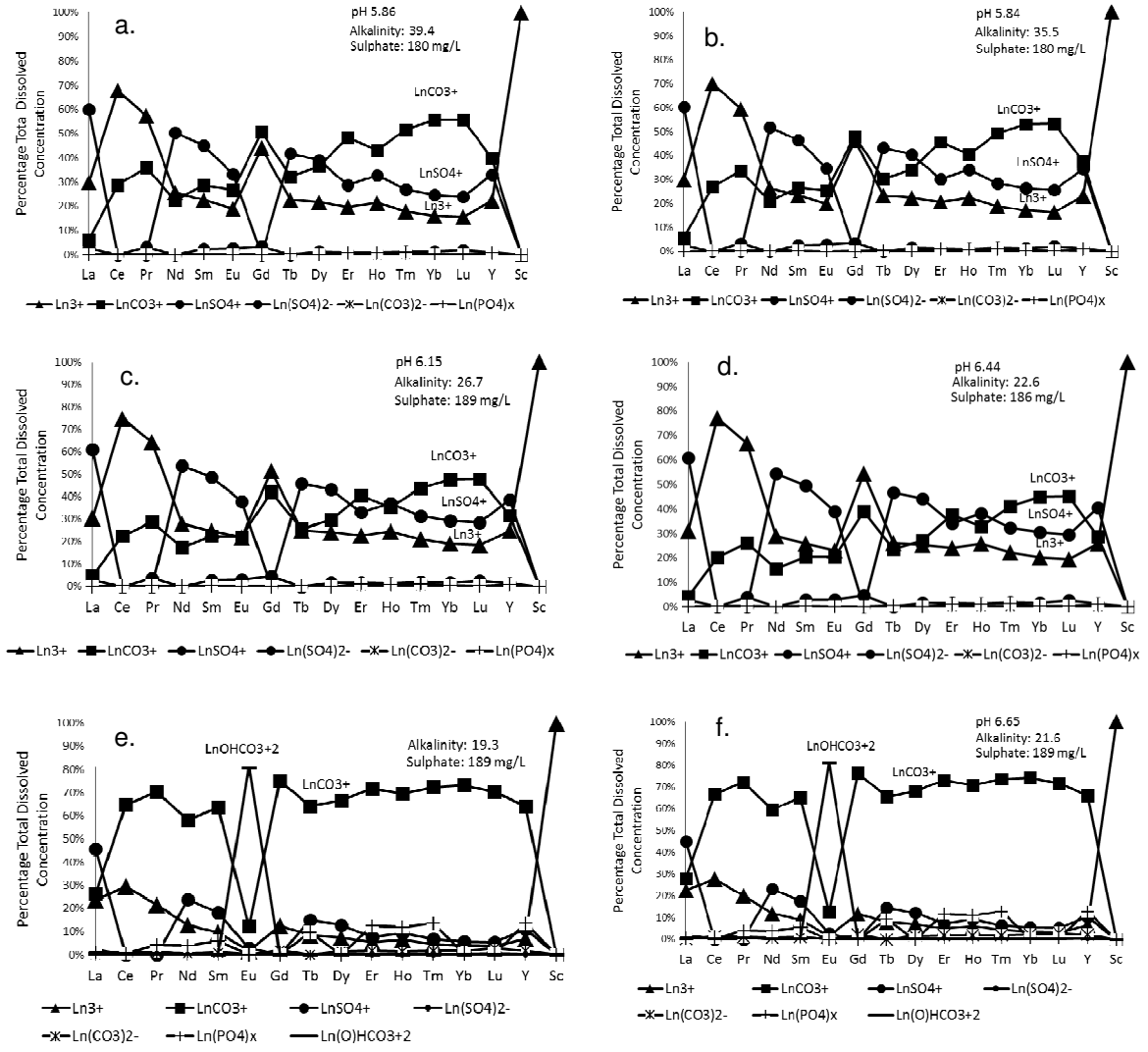

Figure 9 Aqueous Speciation for December 2015 sampling event (a) SC06; (b) SC05; (c) SC04; (d) SC03; (e) SC02; (f) SC01

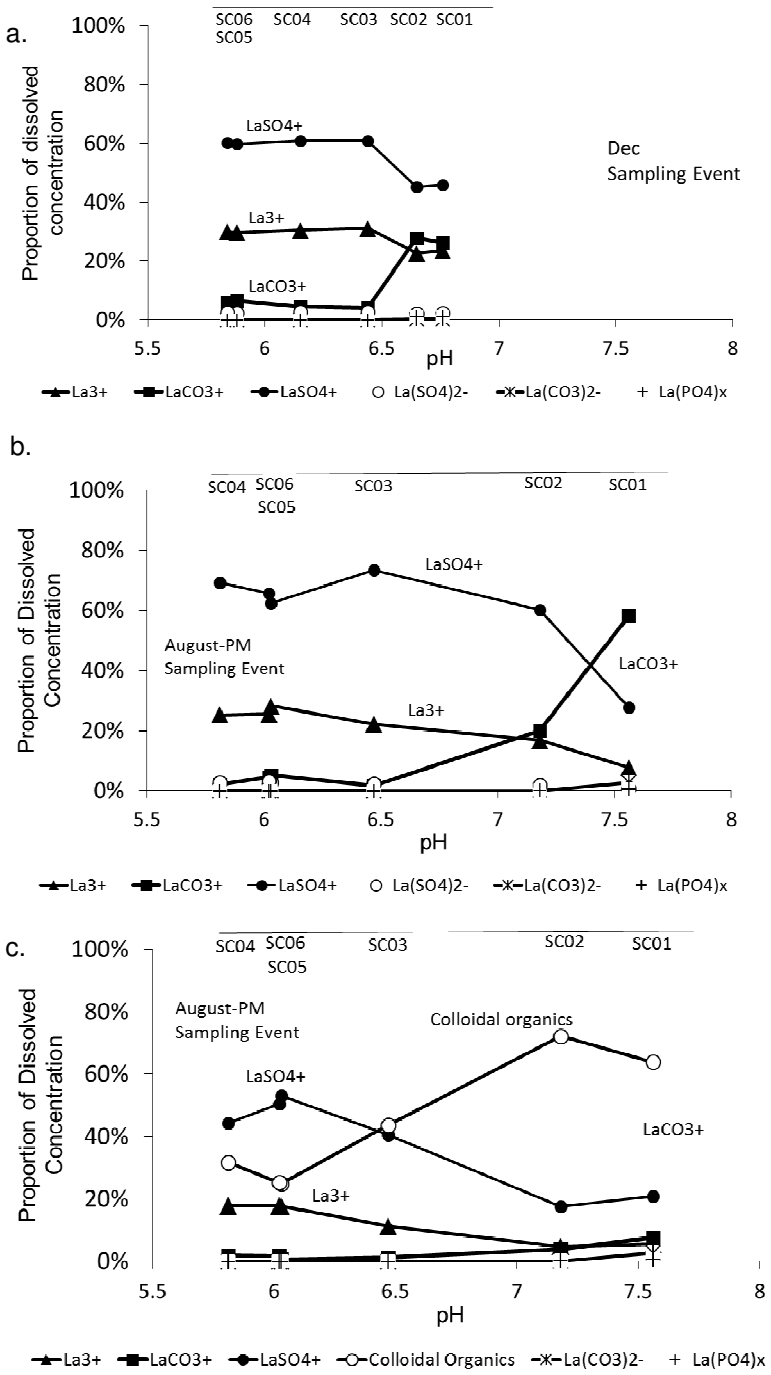

Figure 10 Modelled La aquatic speciation (a) December 2015 (PHREEQC-I, no organics), (b) August 2016-PM (PHREEQC-I, no organics) (c) August 2016-PM (WHAM, with organics)

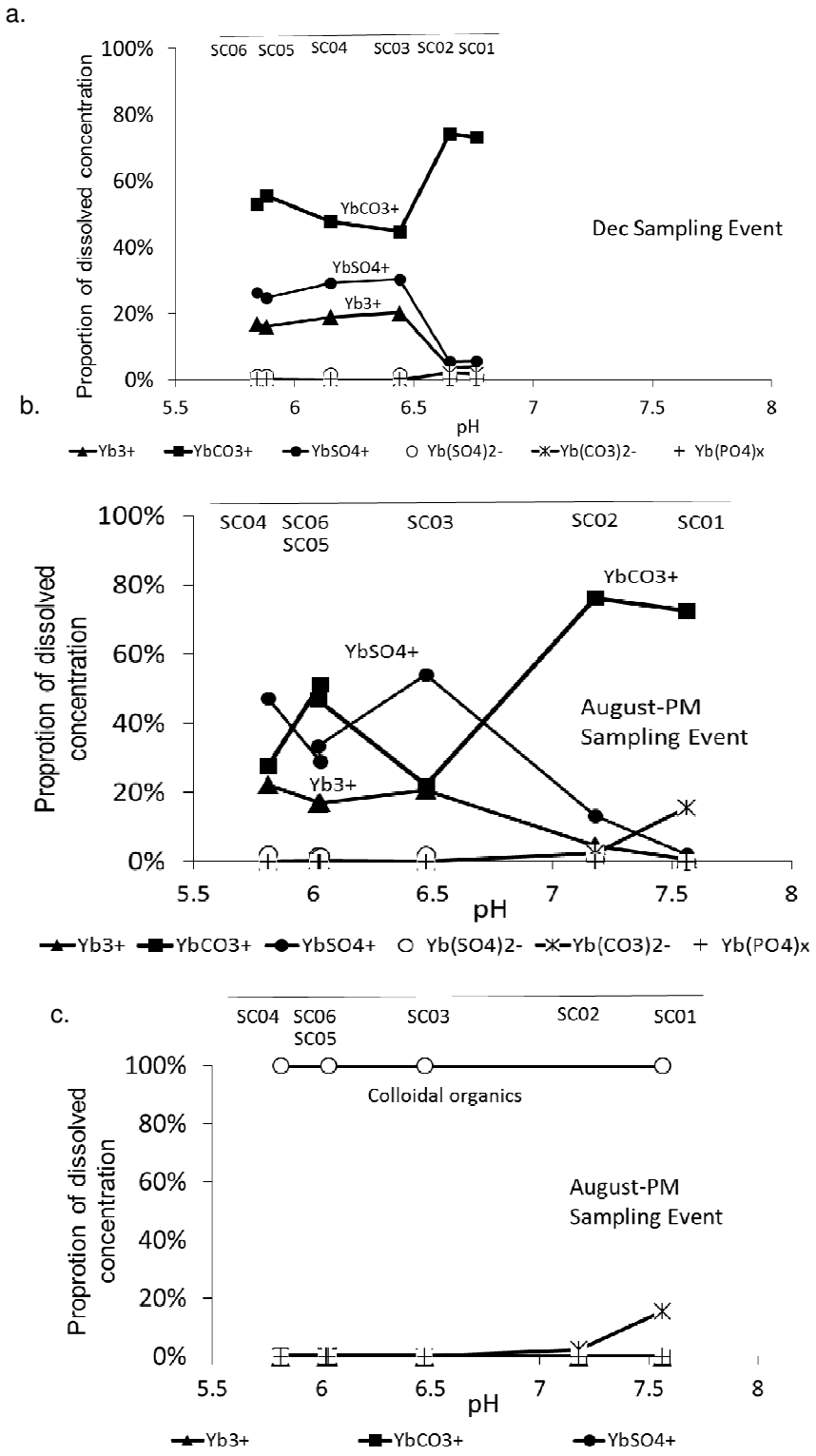

Figure 11 Modelled Yb aqueous speciation (a) December 2015 (PHREEQC-I, no organics), (b) August 2016-PM (PHREEQC-I, no organics) (c) August 2016-PM (WHAM, with organics)

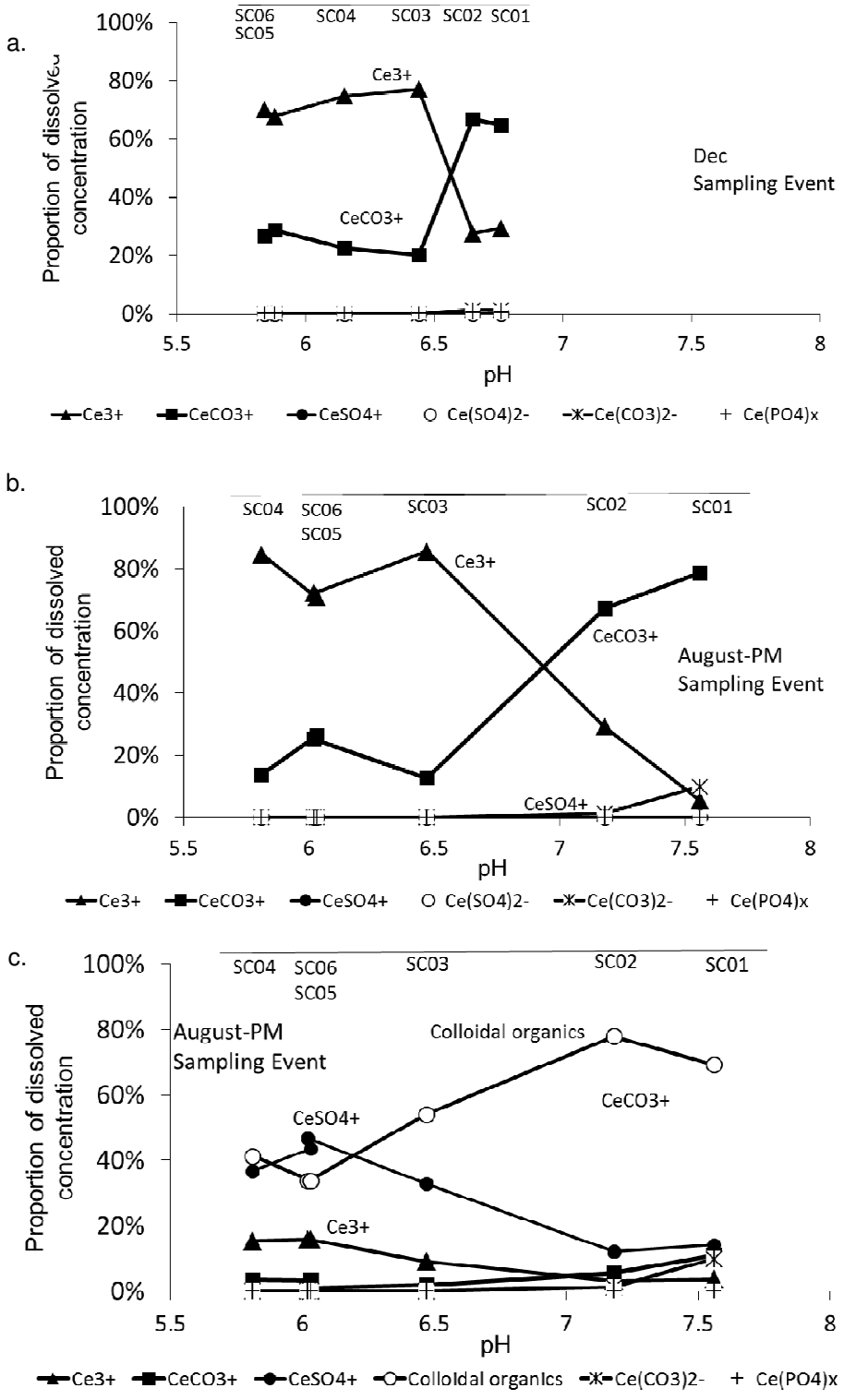

Figure 12 Modelled Ce aqueous speciation (a) December 2015 (PHREEQC-I, no organics), (b) August 2016-PM (PHREEQC-I, no organics) (c) August 2016-PM (WHAM, with organics)

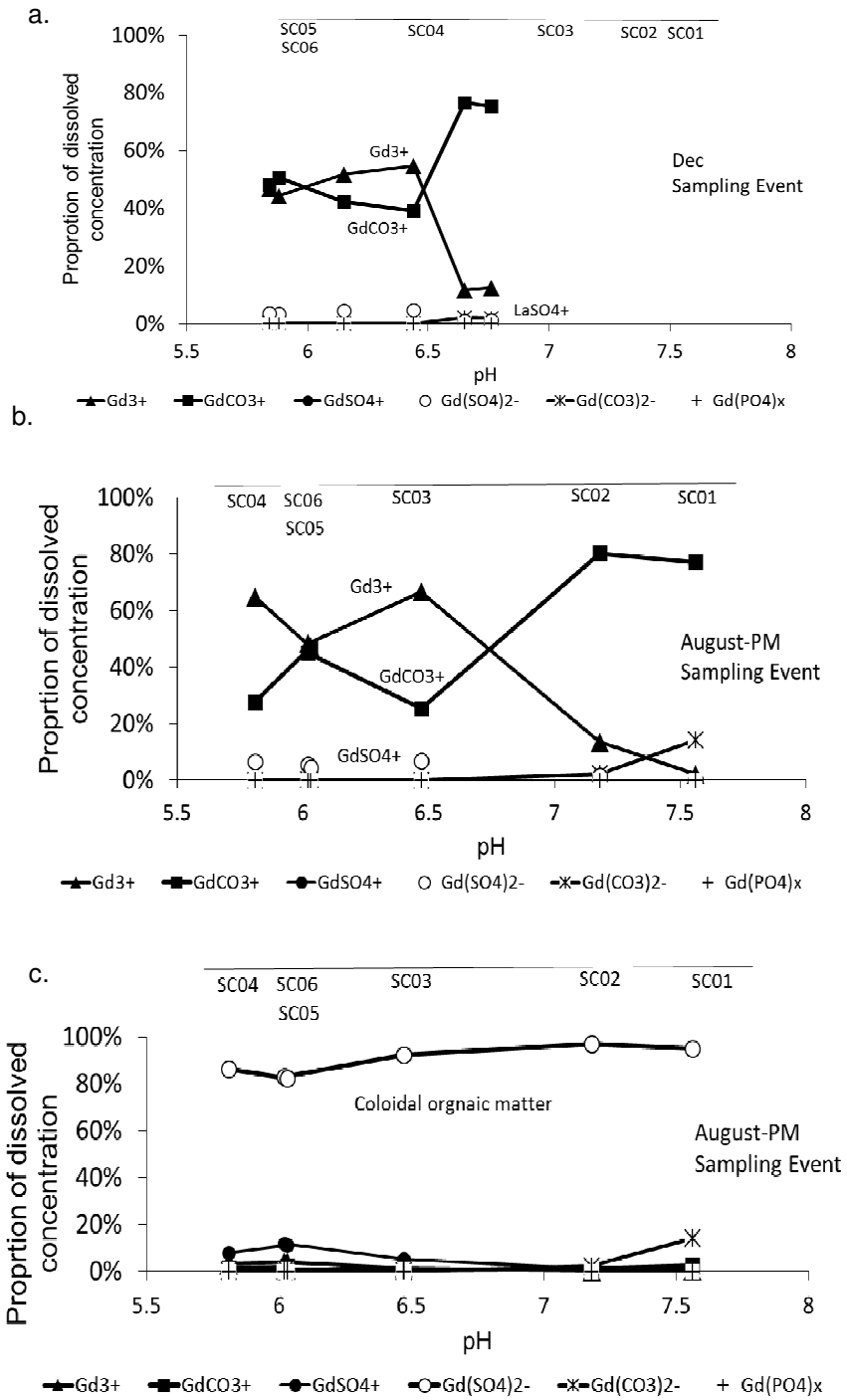

Figure 13 Modelled Gd aqueous speciation (a) December 2015 (PHREEQC-I, no organics), (b) August 2016-PM (PHREEQC-I, no organics) (c) August 2016-PM (WHAM, with organics)

3.2.2 Biofilm sample analysis

3.2.2.1 X-Ray Diffraction

X-Ray diffraction (XRD) was completed on all samples collected during the December 2015 sampling event, and the afternoon August 2016 sampling event (Figure 14). Generally, results of X-Ray diffraction indicated an abundance of amorphous iron minerals, with increasingly crystalline minerals noted at the most upstream sites. The diffraction patterns contain two broad reflections found proximate to the ˚2Theta positions 36 and 63-64, indicative of 2-line ferrihydrite, a poorly ordered iron mineral[70]. Additional peaks were noted that belong to the crystalline iron oxides, goethite and schwertmannite. Other sharp peaks were observed that correspond to silicate minerals. No manganese oxides were observed, and would not be identifiable with XRD.

The dominant mineral composition at the two sites during the December and August sampling event was quite similar; however, the August sampling event shows the presence of more crystalline iron and silica phases at upstream sites SC06 and SC04. Within the December sampling event, there are fewer sharp peaks, and a more even progression of decreasing crystallinity from the upstream SC06 site to the downstream SC01 site.

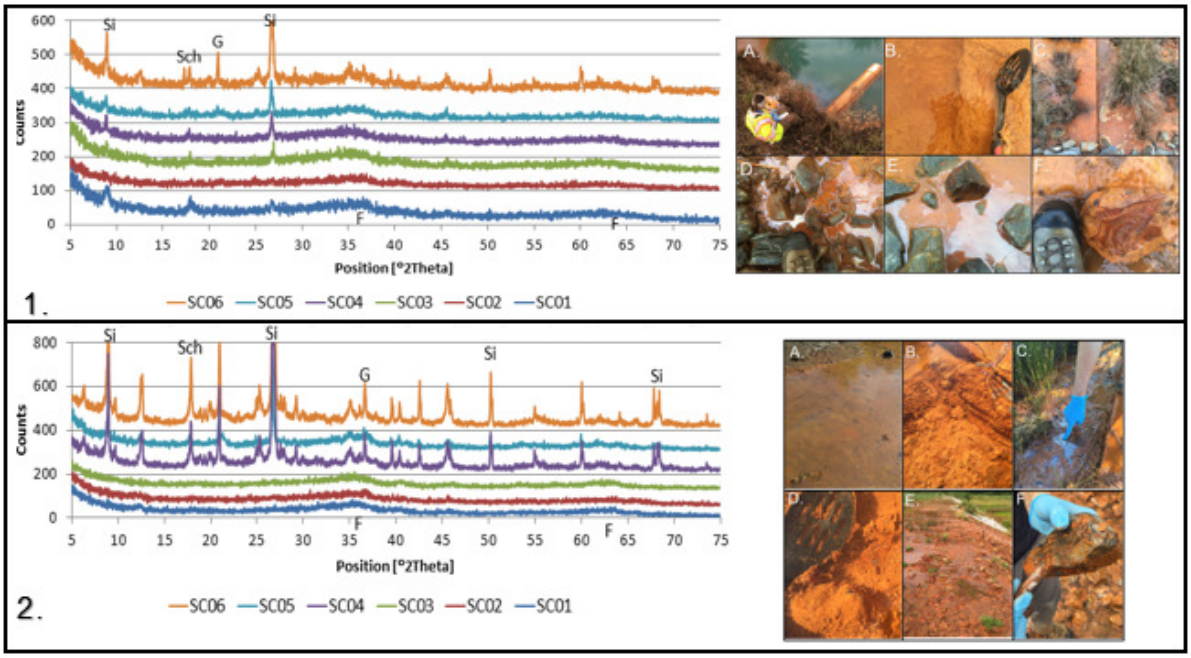

NOTE:

1. BIOGENIC MINERAL PRECIPITATES SAMPLED WITHIN THE SILVER CREEK PASSIVE TREATMENT SYSTEM IN DECEMBER 2015, FROM UPSTREAM TO DOWNSTREAM: (A) PASSIVE TREATMENT INFLOW PIPE AT SC06; (B) FLUFFY PRECIPITATES AT SC05; (C) PRECIPITATES AND VEGETATION INTEGRATED AT SCO4; (D) PRECIPITATES AND IRRIDESCENT BIOFILM AT SC03; (E) PRECIITATES AND IRRIDESCENT BIOFIM AT SC02; (D) HARD PRECIPITATES AT SC01.

Figure 14 X-Ray Diffraction Results and photos of Silver Creek sampling site

3.2.2.2 Energy Dispersive Spectrometry

Energy dispersive spectrometry (EDS) was completed to determine if sufficient quantities of REYs could be observed together, which would indicate formation of REY-minerals vs. REY sorption to organic materials or metal hydroxides (Table 21). The sites with the greatest REY accumulations, SC05-Dec and SC04-Aug were selected for this analysis. Three replicates at different location on each sample were completed, together with twelve to thirteen different sampling locations.

REYs were not observed in sufficient quantities for detection; however, it is possible that REYs exist in concentrated areas via mineralization. The EDS results were able to confirm the abundance of solid-phase iron, composing a range of ~42% to ~68% of the sample. Oxygen, aluminum and silica were the next most abundant elements.

Table 21 Results of Energy Dispersive Spectrometry (EDS)

Site-replicate	Al	Si	S	Fe	O
SC05-Dec-rep1	2.7 ± 0.69	2.1 ± 0.45	0.7 ± 0.3	42.3 ± 1.76	22.3 ± 0.66
SC05-Dec-rep2	5 ± 1.47	3.3 ± 0.52	1 ± 0.37	63 ± 2.96	27.7 ± 1.04
SC05-Dec-rep3	4.1 ± 2.17	3.4 ± 2.21	0.8 ± 0.56	64.4 ± 7.74	27.2 ± 2.83
SC04-Aug-rep1	3.5 ± 1.64	5 ± 3.22	0.7 ± 0.41	62.9 ± 6.74	27.9 ± 2.52
SC04-Aug-rep2	2 ± 1.77	2.8 ± 1.23	0.7 ± 0.58	68.7 ± 5.15	25.8 ± 1.95
SC04-Aug-rep3	4.5 ± 1.83	4.6 ± 1.56	1.2 ± 0.27	61.2 ± 4.34	28.5 ± 1.59

NOTES:
1. UNITES ARE IN WT.%.

3.2.2.3 Total Aqua Regia Digestions

The completeness of the aqua regia digestions was verified using two different solid standards. TORT-2, provided by the Queen's University Analytical Services unit (free of charge) and REE-1 was provided by Natural Resources Canada to support research activities (Appendix B1, Table B1.9). Two additional standards GXR-3 and TILL-2 were provided by the Canadian Geological Survey; however, the standards were later deemed not representative of data collected. The aqua regia digestion showed good recovery with the TORT-2 standard (major and trace elements); however, Ce, Fe and Zn showed >25% RPD variability between the standard the measured values. To understand the recovery of REYs, Natural Resources Canada's REE-1 standard was utilized. Results indicated high precision for REYS, but very high variability for aluminum. Other parameters were also elevated >40% RPD, including: arsenic, cobalt, chromium, copper, nickel and strontium. Normative oxides were also completed as a quality check (Appendix B1, Table B1.10). Results show that there is a difference in the representative nature of the extraction depending on the site. Regularly, site SC06, and oSC05 and SC04 during August show poor representation of total element fractions. It is not known exactly what component are missing from this solid fraction. One hypothesis is organic matter, which is notoriously difficult to measure when it is intermixed with oxide materials. The second hypothesis is that the aqua regia digestion is failing to digest refractory materials, such as silicates or potentially there is an issue with the extraction completely isolating aluminum, as was observed when comparing to the REE-1 standard. In any case, these caveats should be kept in mind when viewing the data below.

Biogenic precipitates at the Silver Creek site are dominantly composed of iron (8-45%), with high amounts of aluminum, manganese, phosphorous and sulphur at certain sites (up to 5%). Concentrations of calcium, magnesium and sodium are lower (maximum of 0.17-1.7%) (Figure 15; Table 22). In general, iron concentrations are lowest at the inflow site (SC06), and gradually increase downstream. Iron concentrations, however, fluctuate during the August afternoon sampling event, with SC04 showing similar iron concentrations to SC06. Solid aluminum concentrations show an inverse pattern to iron. Aluminum concentrations are elevated at sites closest to the groundwater inflow (SC06, SC05 and SC04), and are reduced at sites further downstream (SC03, SC02, SC01). Silica and sulphur concentrations are generally constant throughout the treatment facility, with the exception that samples collected during the morning August sampling event show some variation. Manganese concentrations are close to zero at sites closest to the inflow site, and increase downstream, with maximum concentrations recorded at SC02. Calcium values show a similar trend, with lowest calcium concentrations at inflow (SC06), with slightly increased concentrations downstream, and a large increase noted at SC01 for the August afternoon sampling event. Phosphorous concentrations are extremely elevated at sites SC03, SC02 and SC01 during December. During August, there is marked absence of these elevated phosphorous values.

To determine if the 'sum of REY' proxy was a useful indicator to represent the behaviour of the majority of REYs within the heterogeneous biogenic precipitates, a scatterplot and correlation matrix was completed with major ions and REYs. Results of the correlation matrix (Appendix B2, Figure B2.1, Figure B2.2) indicate that the sum of REY parameter is highly correlated (0.96-1.0) with all REYs except La (0.77), Y (0.80), Lu (0.42) and Sc (0.52). As a result, the Sum of REY parameters was used for a general representation of REY behaviour and association of La, Y, Lu and Sc with other major ions was investigated. In general the sum of REY in the solid phase is elevated at the inflow sites (SC06), and reaches a maximum slightly downstream at either the SC05 or SC04 sites, depending on the season. The sum of REYs in the solid phase then decreases downstream. The sum of REYs + Sc range from a maximum of 724 mg/L (SC05-Dec) to a minimum of 170 mg/L (SC01-Aug-PM). It is noted that solid concentrations of REY tend to decrease, as pH increases, which would generally be opposite of what is expected.

When all sites are grouped together, the sum of REY parameter shows strong correlation with pH and moderate correlation with aluminum (0.68), calcium (0.68) and manganese (0.51) (Appendix B2, Figure B2.3). Iron is strongly correlated with aluminum (0.80); however, the sum of REY parameter is not strongly correlated with iron (0.29). Further investigation of the sites shows that there are two populations of data within the treatment sites (Figure 12). When data from the SC01, SC02 and SC03 sites are plotted against the sum of REYs, a strong positive correlation with aluminum is noted (0.91), in addition to a moderate negative correlation with calcium (0.77). In contrast, when data from SC04, SC05 and SC06 are plotted together, manganese shows a moderate positive correlation (0.70), in addition to iron (0.57). Direct correlations between Sum of REY data from SC04, SC05 and SC06 sites with aluminum are weak (0.32); however, for sites SC04, SC05 and SC06, there is a strong correlation between aluminum and iron (0.87).

To investigate this further, molar ratios were completed for aluminum, manganese, sulphur, calcium silica and iron (Table 24). Sites SC06 through SC04 have the highest Al:Fe, Al:Se, Al:Ca and Al:Si ratios, with the exception of the Al:Si ratio at the SC02 site sampled in the morning, August. Fe: Mn and Fe:Ca ratios are highest at sites SC06 to SC04, with the exception of Fe:Mn ratios at C01, SC02

and SC03 sites sampled in December. Molar ratios for Fe:S, Fe:Si, Mn:Ca, Mn:Si; Mn:S and Ca:S generally increase from the inlet of treatment facility (SC06) to the outlet (SC01).

Saturation indices for REY minerals were calculated using dissolved water data, and the llnl database in PHREEQC (Table 25). Results from this modelling indicate that REY-phosphates are the most commonly formed REY mineral. Pm, Sm, Sc and Y were the only REYs that did not form REY-phosphates at any sites. Cerium formed both a phosphate and an oxide at certain sites. HREYs like Er, Tm and Lu were saturated at fewer sites than LREEs (La, Ce, Pr and Nd) (Table 26, Table 27, Table 28). Certain minerals were at saturation at all sites, during all seasons, such as $MnPO_4$, diaspore, mica, pyrophyllite, maghemite, magnetite, cupric ferrite, cuprous ferrite, $Fe(OH)_3$ and $Fe(OH)_{2.7}Cl_3$. Figure 13 shows the strong pH dependence of aluminum minerals, alunite, basaluminite, boehmite etc. These minerals are above saturation when site pH is below 6, which generally corresponds to the inflow sites (SC06, SC05).

Anomaly calculations were completed for total digestions of the biogenic precipitates (Table 29). All sites have a high Y/Ho ratio ranging from approximately 20 to 43. Non-normalized REY composition of the solid precipitates indicates the majority of solid REYs are LREEs, with lower composition of both MREEs and HREYs; however, comparison of normalized ratios shows the sum of MREEs exceeds both MREEs and HREYs. There are no apparent anomalies recorded for La, Ce, Eu and Gd at any of the Silver Creek sites. A slight positive Y anomaly or increase in Y anomaly occurs at sites SC03, SC02 and SC01, depending on the calculation method.

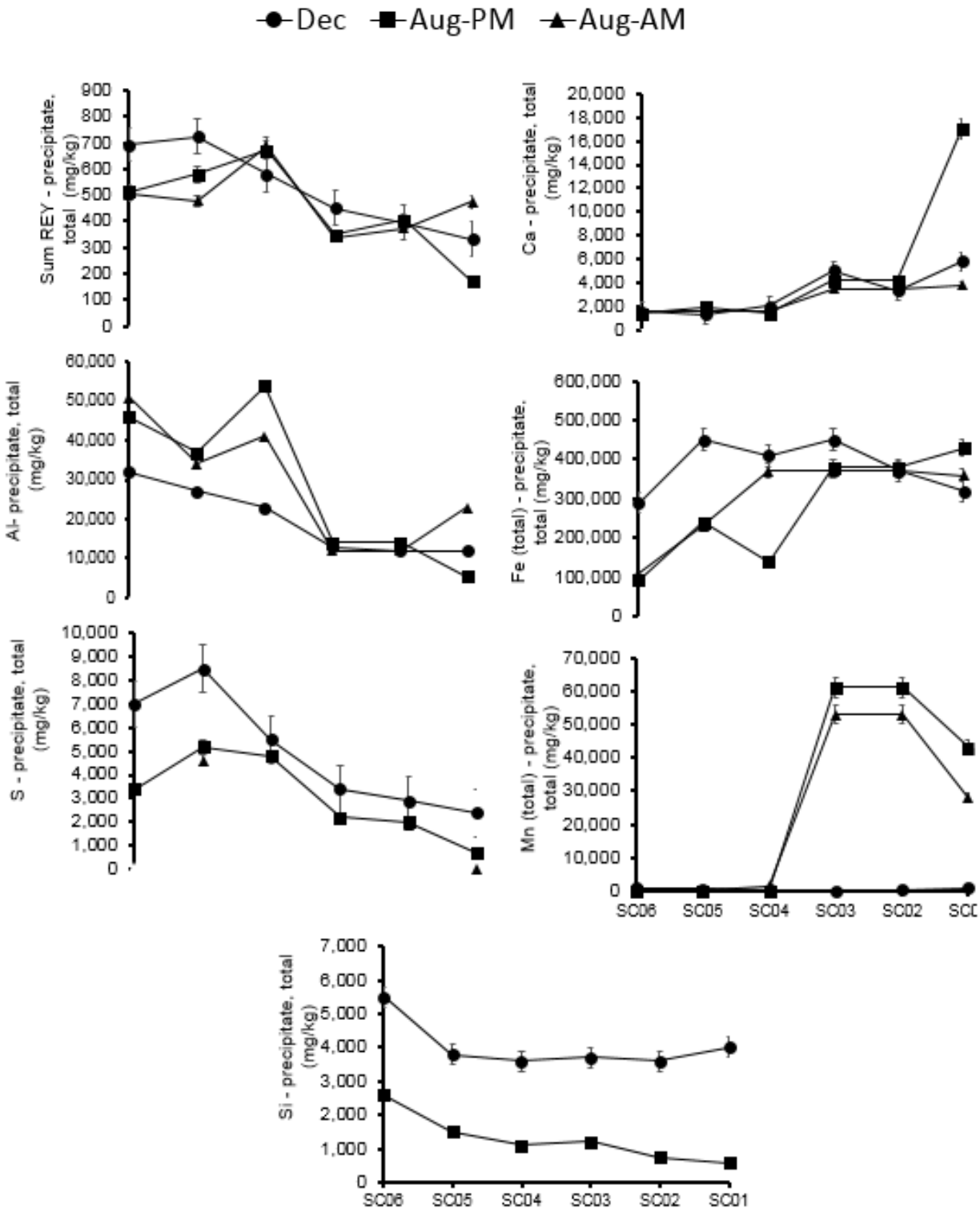

Figure 15 Seasonal and Diurnal Trends of Major Ions and REYs at Silver Creek site

Table 22 Major and Minor Ions – Total Digestion - Silver Creek Precipitate Chemistry (mg/kg)

Sample	LOI	%TC	%OC	Al	Ca	Fe	Mg	Mn	K	Na	P	S	Si
		OI Analytical TIC-TOC Analyzer (Aurora Model 1030)		27 [NoHe] & 396.152	422.673	259.94	279.553	55 [NoHe]	766	589.592	177.434	180.669	251.611
				ICP-ES + ICP-MS	ICP-ES	ICP-ES	ICP-ES	ICP-MS	ICP-ES	ICP-ES	ICP-ES	ICP-ES	ICP-ES
SC06-Dec	13%	4.9	2.7	32,000	1,500	290,000	1,700	1,100	290	290	190	7,000	5,500
SC06-Aug-PM	13%	7.5	7.3	46,000	1,400	93,000	2,200	210	6,800	790	340	3,400	2,600
SC06-Aug-AM	9%	NA	NA	51,000	1,600	110,000	2,800	240	NA	NA	NA	NA	NA
SC05-Dec	11%	1.4	0.7	27,000	1,300	450,000	1,200	670	100	230	160	8,500	3,800
SC05-Aug-PM	12%	2.2	1.2	37,000	1,900	240,000	1,600	250	3,000	460	150	5,200	1,500
SC05-Aug-AM	10%	NA	NA	34,000	1,500	230,000	1,600	230	4,800	540	210	4,600	1,600
SC04-Dec	15%	1.4	0.4	23,000	2,000	410,000	920	600	120	190	1,000	5,500	3,600
SC04-Aug-PM	16%	11.4	11.4	54,000	1,400	140,000	2,100	220	7,300	900	340	4,800	1,100
SC04-Aug-AM	18%	NA	NA	41,000	1,500	370,000	640	1,600	NA	NA	NA	NA	NA
SC03-Dec	12%	1.1	0.4	13,000	5,000	450,000	230	370	58	130	12,000	3,400	3,700
SC03-Aug-PM	14%	0.6	0.2	14,000	4,200	380,000	890	61,000	330	330	NA	2,200	1,200
SC03-Aug-AM	19%	NA	NA	12,000	3,500	370,000	720	53,000	NA	NA	NA	NA	NA
SC02-Dec	15%	2.7	0.8	12,000	3,300	370,000	370	620	91	200	22,000	2,900	3,600
SC02-Aug-PM	16%	1.6	0.2	14,000	4,200	380,000	890	61,000	290	150	NA	2,000	760
SC02-Aug-AM	13%	NA	NA	12,000	3,500	370,000	720	53,000	370	280	NA	1,900	190
SC01-Dec	17%	3.9	2.1	12,000	5,800	320,000	680	1,100	120	190	45,000	2,400	4,000
SC01-Aug-PM	18%	1.0	0.3	5,500	17,000	430,000	1,700	43,000	310	110	NA	NA	NA
SC01-Aug-AM	17%	NA	NA	23,000	3,800	360,000	970	28,000	NA	NA	NA	NA	NA

NOTES:

1. ALL VALUES ARE PROVIDED IN mg/L.

Table 23 Silver Creek Precipitate Data – Total Digestion – Rare Earth Element data (mg/kg dry weight)

Sample	La	Ce	Pr	Nd	Sm	Eu	Gd	Tb	Dy	Y	Er	Ho	Tm	Yb	Lu	Sc	Sum REY + Sc	Avg REY
Analysis Method	ICP-MS	ICP-MS	ICP-MS	ICP-MS	ICP-MS	ICP-MS	ICP-MS	ICP-MS	ICP-MS	ICP-MS	ICP-MS	ICP-MS	ICP-MS	ICP-MS	ICP-MS	ICP-MS		
Mass	139	140	141	146	147	153	157	159	163	172	166	165	169	89	175	45		
SC06-Dec	74	200	25	110	22	5	23	3	15	60	9	3	1	7	130	6	693	570
SC06-Aug-PM	83	180	22	88	17	4	17	3	12	59	6	2	1	5	1	12	512	
SC06-Aug-AM	81	180	22	85	18	4	20	3	12	55	7	2	1	6	1	7	504	
SC05-Dec	77	220	28	110	25	6	24	3	16	60	9	3	1	7	130	5	724	593
SC05-Aug-PM	79	210	27	110	22	5	21	3	15	60	8	3	1	6	1	8	578	
SC05-Aug-AM	70	170	22	87	17	4	17	2	11	51	6	2	1	5	1	11	477	
SC04-Dec	71	170	21	85	18	4	18	3	13	57	7	3	1	6	100	4	580	646
SC04-Aug-PM	96	240	30	120	24	5	24	3	17	78	9	3	1	8	1	12	672	
SC04-Aug-AM	92	260	30	120	26	6	28	4	19	73	10	4	1	9	1	4	687	
SC03-Dec	68	130	15	57	11	3	13	2	9	54	5	2	1	4	75	2	450	380
SC03-Aug-PM	70	120	13	50	9	2	11	2	8	53	4	2	1	3	1	2	350	
SC03-Aug-AM	64	120	13	48	10	2	12	2	8	48	4	2	1	3	1	1	339	
SC02-Dec	60	110	13	50	10	2	12	2	8	49	5	2	1	4	66	3	395	391
SC02-Aug-PM	76	140	15	60	11	3	13	2	10	59	5	2	1	4	1	3	404	
SC02-Aug-AM	70	130	14	55	10	2	12	2	9	55	5	2	1	4	1	3	373	
SC01-Dec	50	94	11	41	8	2	10	2	7	44	4	2	1	3	53	2	333	326
SC01-Aug-PM	38	52	5	21	3	1	5	1	4	33	2	1	0	1	0	2	170	
SC01-Aug-AM	87	160	18	73	15	4	18	2	12	68	7	3	1	5	1	2	475	

NOTES:

1. ALL VALUES ARE PROVIDED IN mg/L; VALUES HIGHLIGHTED IN GREY REPRESENT MAXIMUM RECORDED VALUE AT THAT SITE.

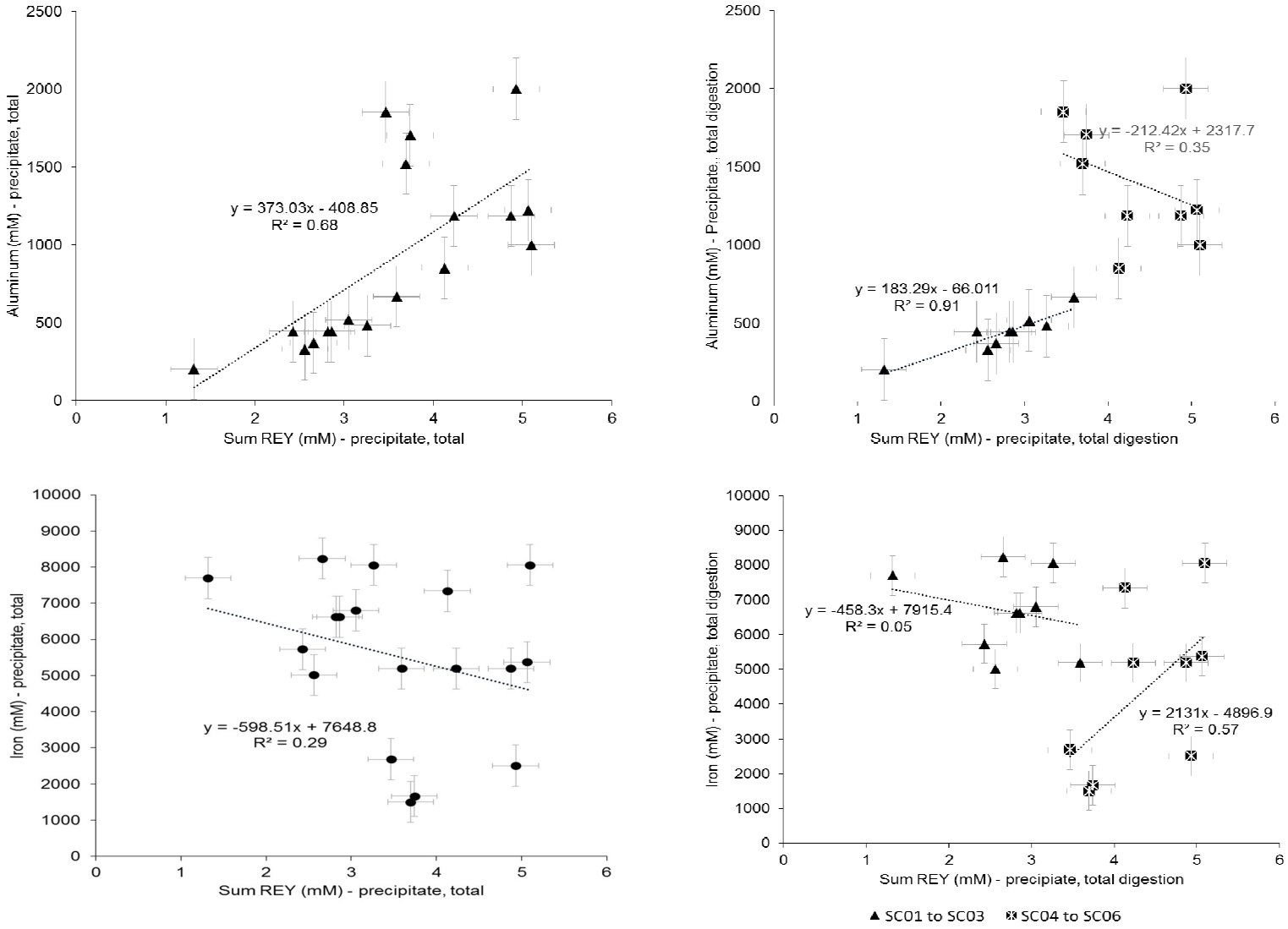

Figure 16 Plots of Aluminum and iron (mM/g) vs. Sum REY (mM/g), indicating divergent behaviour between groups of sites

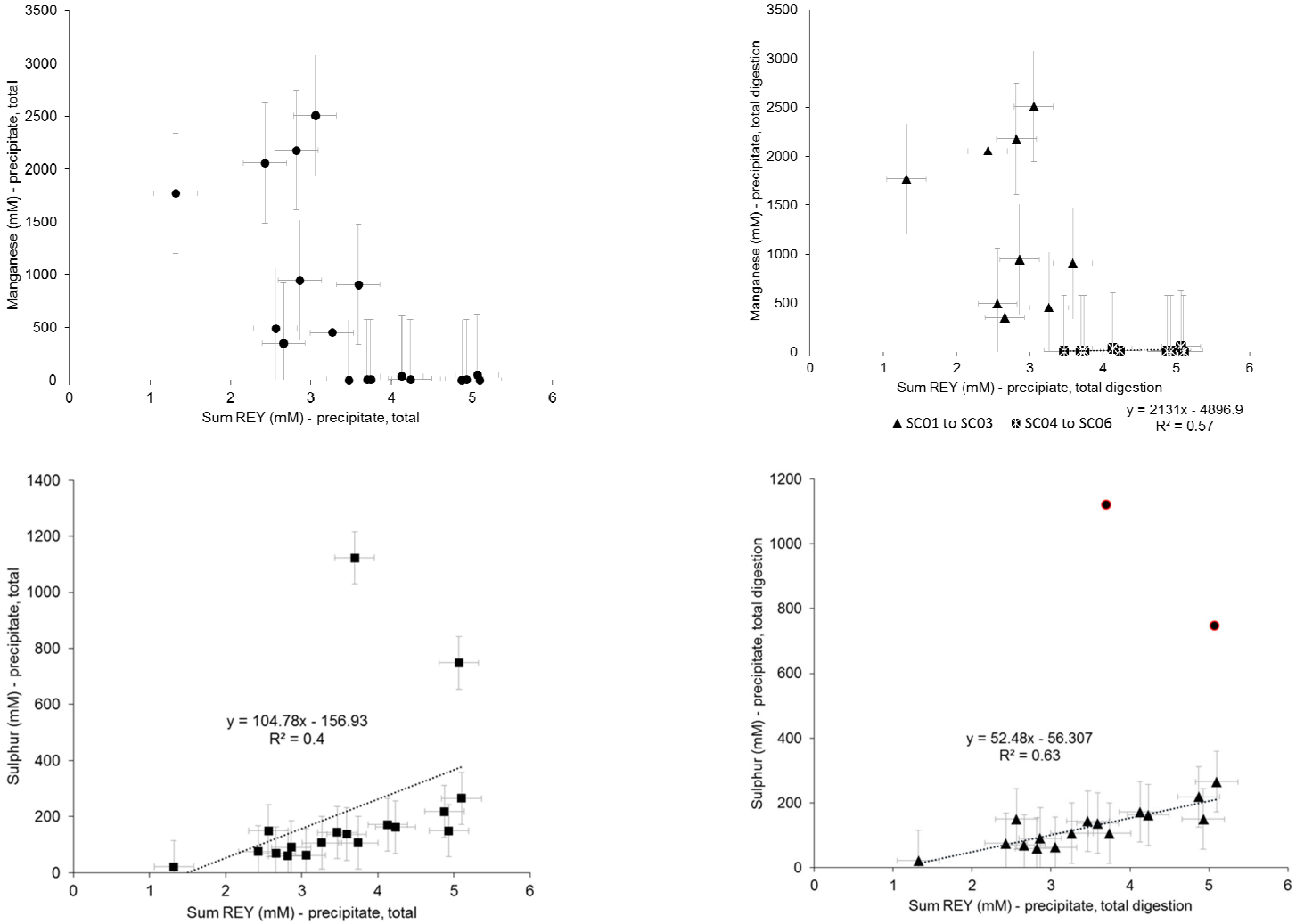

Figure 17 Plots of manganese (mM) and sulphur (mM) vs. Sum REY (mM)

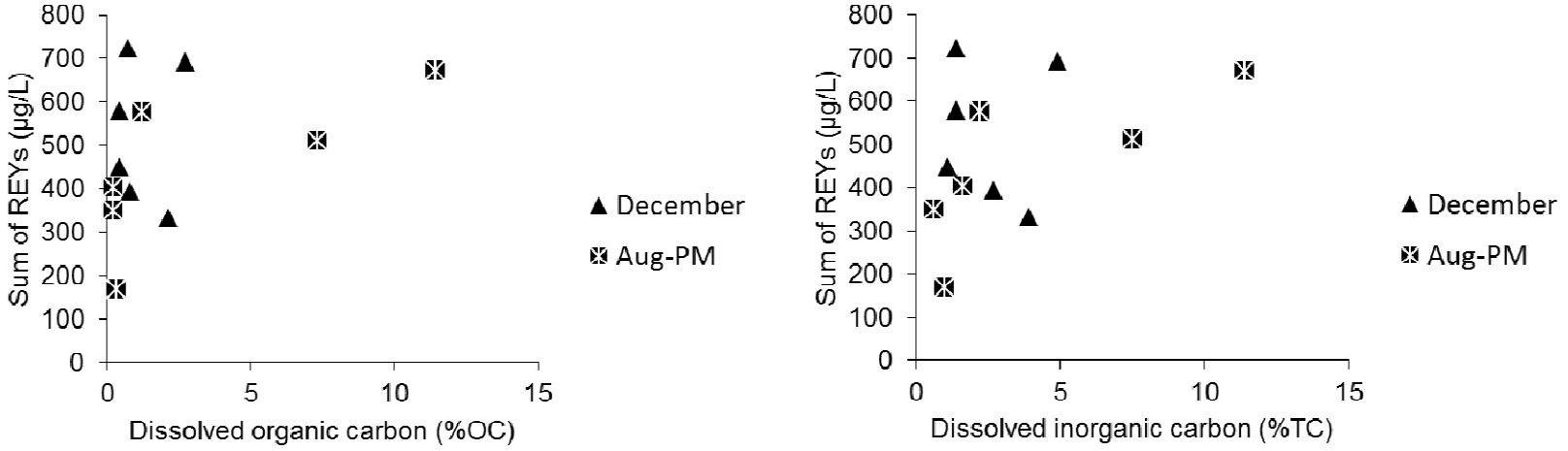

Figure 18 Plots of dissolved organic carbon (%OC) and inorganic carbon (%TC) vs. sum of REYs (µg/L)

Table 24 Molar Ratios at for solids at the Silver Creek site

Sample	Al:Fe	Al:S	Al:Ca	Al:Si	Fe:Mn	Fe:Ca	Fe:Si	Fe:S	S:Fe	SO4:Fe	Mn:Ca	Mn:Si	Mn:S	Ca:S
SC06-Dec	0.2	5	32	6	902	139	27	24	0.04	0.13	0.2	0.0	0.0	0.2
SC06-Aug-PM	1.0	16	49	18	193	48	18	16	0.06	0.19	0.2	0.1	0.1	0.3
SC05-Dec	0.1	4	31	7	1780	248	60	30	0.03	0.10	0.1	0.0	0.0	0.1
SC05-Aug-PM	0.2	7	22	22	451	95	97	32	0.03	0.09	0.2	0.2	0.1	0.3
SC04-Dec	0.1	5	17	7	196	147	57	43	0.02	0.07	0.8	0.3	0.2	0.3
SC04-Aug-PM	0.8	13	57	51	277	72	64	17	0.06	0.18	0.3	0.2	0.1	0.2
SC03-Dec	0.1	5	4	4	18	65	61	76	0.01	0.04	3.6	3.4	4.3	1.2
SC03-Aug-PM	0.08	8	5	12	3	65	159	99	0.01	0.03	24.0	58.7	36.6	1.5
SC02-Dec	0.07	5	5	3	7	80	52	73	0.01	0.04	11.5	7.4	10.5	0.9
SC02-Aug-PM	0.07	8	5	66	3	76	979	112	0.01	0.03	25	322	37	1
SC01-Dec	0.08	6	3	3	3	40	40	77	0.01	0.04	14.2	14.4	27.5	1.9
SC01-Aug-PM	0.03	9	0	10	4	18	367	358	0.00	0.01	4	84	82	20

NOTE:

1. MOLAR RATIO FOR ALL MAJOR IONS RECORDED.

Table 25 Thermodynamic saturation indices for REY Minerals Formed within the Silver Creek Site

Sample	$LaPO4:10H_2O$	$CePO_4:10H_2O$	CeO_2	$PrPO_4:10H_2O$	$NdPO_4:10H_2O$	$EuPO_4:10H_2O$	$GdPO_4:10H_2O$	$TbPO_4:10H_2O$	$DyPO_4:10H_2O$	$HoPO_4:10H_2O$	$ErPO_4:10H_2O$	$TmPO_4:10H_2O$	$YbPO_4:10H_2O$	$LuPO_4:10H_2O$
SC06-Dec	2.4	3.0	-2.1	2.0	2.1	0.5	1.4	0.3	0.9	0.5	0.0	-0.5	0.1	1.3
SC06-Aug-PM	1.6	2.2	-0.9	1.2	1.3	-0.3	0.6	-0.5	0.1	-0.7	-0.3	-1.2	-0.6	-1.5
SC06-Aug-AM	NA	NA	NA	NA	NA	NA	NA	NA	NA	NA	NA	NA	NA	NA
SC05-Dec	2.4	3.0	-1.2	1.9	2.1	0.4	1.4	0.2	0.8	0.4	0.0	-0.7	0.0	1.2
SC05-Aug-PM	1.6	2.2	-0.7	1.2	1.3	-0.4	0.6	-0.6	0.1	-0.7	-0.3	-1.3	-0.7	-1.6
SC05-Aug-AM	1.5	2.2	0.1	1.2	1.3	-0.3	0.7	-0.5	0.1	-0.7	-0.2	-1.2	-0.5	-1.5
SC04-Dec	1.8	2.1	-2.2	0.8	0.8	-0.5	0.5	-0.6	0.0	-0.7	-0.7	-0.8	-0.4	0.9
SC04-Aug-PM	0.8	1.0	-0.6	-0.2	-0.3	-0.8	-0.9	-2.3	-1.7	-2.2	-1.8	-2.6	-2.0	-2.7
SC04-Aug-AM	NA	NA	NA	NA	NA	NA	NA	NA	NA	NA	NA	NA	NA	NA
SC03-Dec	1.5	1.1	-3.3	0.4	0.5	-0.9	-0.1	-1.2	-0.4	-1.3	-0.7	-1.1	-1.0	-1.3
SC03-Aug-PM	0.6	0.9	-1.3	-0.3	-0.6	-1.7	-0.7	-2.0	-1.4	-1.9	-1.6	-2.4	-2.0	-2.6
SC03-Aug-AM	NA	NA	NA	NA	NA	NA	NA	NA	NA	NA	NA	NA	NA	NA
SC02-Dec	2.1	2.3	0.2	0.8	0.9	-0.6	0.8	0.0	0.4	-0.3	0.0	-0.1	-0.1	-0.4
SC02-Aug-PM	0.9	0.9	2.1	-0.5	0.1	-1.5	-0.8	-1.3	-0.9	-1.5	-1.4	-1.6	-1.7	-1.7
SC02-Aug-AM	1.1	1.0	2.8	-0.5	0.1	-1.3	-0.5	-1.3	-0.8	-1.3	-1.4	-1.6	-1.5	-1.8
SC01-Dec	1.9	2.3	0.2	0.8	0.9	-0.6	0.9	0.0	0.5	-0.2	0.1	-0.1	-0.1	-0.4
SC01-Aug-PM	1.8	1.5	5.7	0.0	0.6	-1.9	-0.2	-0.9	-0.9	-0.8	-1.0	-1.1	-1.1	-1.5
SC01-Aug-AM	NA	NA	NA	NA	NA	NA	NA	NA	NA	NA	NA	NA	NA	NA

NOTES:

1. VALUES HIGHLIGHTED IN RED HAVE SATURATION INDICES ABOVE ZERO.
2. RELEVANT REY OXIDES AND HYDROXIDES WERE QUERIED FOR THE FOLLOWING MINERALS:

Ce Ce(OH)3 Ce(OH)3(am) Ce2(CO3)3:8H2O Ce2O3
Ce3(PO4)4 CeF3:.5H2O CePO4:10H2O CeO2
Dy Dy(OH)3 Dy(OH)3(am) Dy2(CO3)3 Dy2O3 DyF3:.5H2O
DyPO4:10H2O Er(OH)3 Er Er2(CO3)3
Er(OH)3(am) Er2O3 ErF3:.5H2O ErPO4:10H2O
Eu Eu(IO3)3:2H2O Eu(NO3)3:6H2O Eu(OH)2.5Cl.5
Eu(OH)2Cl Eu(OH)3 Eu2(CO3)3:3H2O Eu2(SO4)3:8H2O
Eu2O3(cubic) Eu2O3(monoclinic) Eu3O4 EuBr3
EuCl2 EuCl3 EuCl3:6H2O Eucryptite
EuF3:0.5H2O EuO EuOCl EuOHCO3
EuPO4:10H2O EuS EuSO4
Gd Gd(OH)3 Gd(OH)3(am)
Gd2(CO3)3 Gd2O3 GdF3:.5H2O GdPO4:10H2O
Ho Ho(OH)3 Ho(OH)3(am) Ho2O3 Ho2(CO3)3 HoF3:.5H2O
HoPO4:10H2O Hopeite
La(OH)3 La La(OH)3(am)
La2O3 La2(CO3)3:8H2O LaCl3 LaCl3:7H2O
LaF3:.5H2O Lammerite Lanarkite Lansfordite
LaPO4:10H2O Magnesite Magnetite Pr(OH)3(am)
Pr2(CO3)3 Pr2O3 Prehnite PrF3:.5H2O
PrPO4:10H2O Sm Sm(OH)3 Sm(OH)3(am)
Sm2(CO3)3 Sm2(SO4)3 Sm2O3 Yb
Yb(OH)3 Yb(OH)3(am) Yb2(CO3)3 Yb2O3
YbF3:.5H2O YbPO4:10H2O Nd(OH)3 Nd(OH)3(am)
Nd(OH)3(c) Nd Nd2(CO3)3 Nd2O3
NdF3:.5H2O NdOHCO3 NdPO4:10H2O Pm
Pm(OH)3 Pm(OH)3(am) Pm2(CO3)3 Pm2O3
PmF3:.5H2O PmPO4:10H2O Pr(OH)3 Pr
Tb Tb(OH)3 Tb(OH)3(am) Tb2(CO3)3
Tb2O3 TbF3:.5H2O TbPO4:10H2O Tm
Tm(OH)3 Tm(OH)3(am) Tm2(CO3)3 Tm2O3
TmF3:.5H2O TmPO4:10H2O Lu Lu(OH)3
Lu(OH)3(am) Lu2(CO3)3 LuF3:.5H2O Lu2O3
LuPO4:10H2O

Table 26 Thermodynamic saturation Indices for Manganese and Silica minerals formed at the Silver Creek Site

Sample	pH	$MnHPO_4$	Rhodochrosite ($MnCO_3$)	Bixbyite (Mn2O3)	Hausman (Mn3O4	ZnSiO3
SC06-Dec	5.86	0.9	-1.2	-17.9	-22.2	-1.7
SC06-Aug-PM	6.03	0.0	-1.1	-15.6	-19.9	-1.5
SC06-Aug-AM	5.94	NA	NA	NA	NA	NA
SC05-Dec	5.84	1.0	-1.2	-15.8	-20.2	-1.7
SC05-Aug-PM	6.02	0.0	-1.1	-15.4	-19.5	-1.2
SC05-Aug-AM	5.97	0.0	-1.3	-13.6	-17.9	-1.5
SC04-Dec	6.15	1.0	-1.3	-16.2	-20.8	-1.8
SC04-Aug-PM	5.81	0.1	-1.3	-12.6	-16.2	-0.8
SC04-Aug-AM	5.86	NA	NA	NA	NA	NA
SC03-Dec	6.44	1.0	-1.4	-16.4	-21.1	-1.9
SC03-Aug-PM	6.47	0.1	-1.3	-13.4	-16.5	-1.0
SC03-Aug-AM	6.27	NA	NA	NA	NA	NA
SC02-Dec	6.65	1.7	-0.5	-10.5	-13.1	0.0
SC02-Aug-PM	7.18	0.5	-0.5	-6.0	-7.4	0.4
SC02-Aug-AM	6.67	0.6	-0.5	-4.6	-6.3	0.4
SC01-Dec	6.76	1.7	-0.5	-10.6	-13.4	0.0
SC01-Aug-PM	7.56	0.8	0.5	0.9	1.9	2.7
SC01-Aug-AM	7.13	NA	NA	NA	NA	NA

z

NOTES:

1. VALUES HIGHLIGHTED IN RED HAVE SATURATION INDICES ABOVE ZERO.
2. NOTE THAT THIS IS SIMPLY THERMODYNAMIC MODELLING, AND THIS DOES NOT COSNIDER KINETICS. AS A RESULT, MINERALS THAT ARE NOT ENERGETICALLY FAVORED TO FORM MAY BE LISTED HERE.
3. RELEVANT REY OXIDES AND HYDROXIDES WERE QUERIED FOR THE FOLLOWING MINERALS:

Alunite AlumK Basaluminite Boehmite Manganite Mn3(PO4)2 Mn2(SO4)3 Mn3(AsO4)2:8H2O
MnHPO4 MnSO4 MnS(Green) Fe(OH)2.7Cl.3 Fe(OH)3(a) Fe2(SeO3)3 Fe3(OH)8 FeS(ppt)
Goethite Strengite Maghemite Magnetite Jarosite-K Jarosite-Na Jurbanite Kaolinite
Calcite Dolomite Siderite Rhodochrosite Rhodochrosite(d) MnSO4 CupricFerrite CuprousFerrite
Diaspore Gibbsite Halloysite Illite Kmica Pyrophyllite Montmorillonite-Aberdeen Montmorillonite-Ca
Bixbyite Hausmannite Hematite Talc Tremolite ZnSiO3 Quartz SiO2(a) Chalcedony

Table 27 Thermodynamic saturation Indices for Aluminum minerals formed at the Silver Creek Site

Sample	pH	Alunite ($KAl_3(SO_4)_2$): $12H_2O$	Basaluminite $Al_4(OH)_{10}SO_4$	Boehmite (AlOOH)	Kaolinite ($Al_2Si_2O5(OH)_4$)	Diaspore (AlOOH)	Gibbsite ($Al(OH)_3$)
SC06-Dec	5.86	4.0	7.5	1.8	5.9	3.6	2.4
SC06-Aug-PM	6.03	5.5	8.1	1.9	6.3	3.7	2.6
SC06-Aug-AM	5.94	NA	NA	NA	NA	NA	NA
SC05-Dec	5.84	3.8	7.2	1.7	5.7	3.5	2.3
SC05-Aug-PM	6.02	2.6	3.8	1.0	4.3	2.8	1.6
SC05-Aug-AM	5.97	5.3	7.8	1.8	6.2	3.6	2.5
SC04-Dec	6.15	-2.1	-0.8	-0.5	1.5	1.4	0.2
SC04-Aug-PM	5.81	4.5	5.9	1.8	5.7	3.6	2.4
SC04-Aug-AM	5.86	NA	NA	NA	NA	NA	NA
SC03-Dec	6.44	-2.2	-0.7	-0.5	1.4	1.3	0.2
SC03-Aug-PM	6.47	-1.5	-3.5	-0.1	1.6	1.7	0.4
SC03-Aug-AM	6.27	NA	NA	NA	NA	NA	NA
SC02-Dec	6.65	-3.4	-0.5	0.0	2.5	1.9	0.7
SC02-Aug-PM	7.18	-5.8	-7.3	-0.5	0.5	1.2	0.0
SC02-Aug-AM	6.67	-5.3	-5.8	-0.4	0.9	1.3	0.1
SC01-Dec	6.76	-3.0	-0.1	0.1	2.6	1.9	0.8
SC01-Aug-PM	7.56	-10.0	-11.3	-0.7	-0.1	0.9	-0.3
SC01-Aug-AM	7.13	NA	NA	NA	NA	NA	NA

NOTES:

1. VALUES HIGHLIGHTED IN RED HAVE SATURATION INDICES ABOVE ZERO.
2. NOTE THAT THIS IS SIMPLY THERMODYNAMIC MODELLING, AND THIS DOES NOT COSNIDER KINETICS. AS A RESULT, MINERALS THAT ARE NOT ENERGETICALLY FAVORED TO FORM MAY BE LISTED HERE.

2. RELEVANT REY OXIDES AND HYDROXIDES WERE QUERIED FOR THE FOLLOWING MINERALS:

Alunite AlumK Basaluminite Boehmite
Manganite Mn3(PO4)2 Mn2(SO4)3 Mn3(AsO4)2:8H2O
MnHPO4 MnSO4 MnS(Green) Fe(OH)2.7Cl.3
Fe(OH)3(a) Fe2(SeO3)3 Fe3(OH)8 FeS(ppt)
Goethite Strengite Maghemite Magnetite
Jarosite-K Jarosite-Na Jurbanite Kaolinite
Calcite Dolomite Siderite Rhodochrosite
Rhodochrosite(d) MnSO4 CupricFerrite CuprousFerrite
Diaspore Gibbsite Halloysite Illite
Kmica Pyrophyllite Montmorillonite-Aberdeen Montmorillonite-Ca
Bixbyite Hausmannite Hematite Talc
Tremolite ZnSiO3 Quartz SiO2(a) Chalcedony

Table 28 Thermodynamic saturation Indices for Iron minerals formed at the Silver Creek Site

Sample	pH	Fe(OH)2.7Cl.3	$Fe(OH)_3(a)$	$Fe_3(OH)_8$	Goethite (FeO(OH)	Strengite ($FePO_4:2H_2O$)	Maghemite (Fe_2O_3)	Magnetite (Fe_3O_4)	Jarosite-K ($KeFe_3(OH)_6(SO_4)_2$)	CupricFerrite ($CuFe_2O_4$)	CuprousFerrite ($CuFeO_2$)	Hematite (Fe_2O_3)
SC06-Dec	5.86	5.0	0.0	-2.1	5.4	-0.6	3.5	12.7	-6.6	5.5	9.2	12.8
SC06-Aug-PM	6.03	6.0	1.1	0.1	6.5	-0.5	5.6	14.9	-2.4	8.3	10.0	14.9
SC06-Aug-AM	5.94	NA	NA	NA	NA	NA	NA	NA	NA	NA	NA	NA
SC05-Dec	5.84	6.0	1.0	-0.1	6.4	0.4	5.5	14.7	-3.6	7.5	9.3	14.8
SC05-Aug-PM	6.02	6.1	1.1	0.1	6.6	-0.5	5.6	15.2	-2.1	7.9	9.4	15.2
SC05-Aug-AM	5.97	7.0	2.1	2.1	7.5	0.5	7.6	16.9	0.8	9.7	9.3	17.0
SC04-Dec	6.15	5.7	0.7	-1.0	6.1	0.1	4.8	13.5	-4.3	7.7	9.9	14.0
SC04-Aug-PM	5.81	6.9	2.0	1.7	7.6	0.5	7.4	17.3	0.7	10.2	9.4	17.3
SC04-Aug-AM	5.86	NA	NA	NA	NA	NA	NA	NA	NA	NA	NA	NA
SC03-Dec	6.44	5.4	0.4	-1.8	5.7	-0.2	4.3	12.6	-5.3	6.8	9.3	13.4
SC03-Aug-PM	6.47	4.9	0.0	-3.5	5.9	-1.4	3.4	13.0	-4.6	6.8	8.5	13.8
SC03-Aug-AM	6.27	NA	NA	NA	NA	NA	NA	NA	NA	NA	NA	NA
SC02-Dec	6.65	7.6	3.0	4.8	8.3	1.1	9.3	19.2	-0.6	13.5	12.5	18.4
SC02-Aug-PM	7.18	6.7	2.0	0.6	8.0	-0.6	7.5	17.2	-1.5	12.6	10.1	17.9
SC02-Aug-AM	6.67	7.0	2.3	0.5	8.1	-0.4	8.0	16.5	-1.0	12.7	9.3	18.1
SC01-Dec	6.76	7.4	2.7	4.1	8.0	0.8	8.9	18.3	-1.1	12.6	12.0	17.9
SC01-Aug-PM	7.56	6.4	2.0	-0.5	8.1	-2.4	7.5	16.5	-4.3	13.9	10.2	18.2
SC01-Aug-AM	7.13	NA	NA	NA	NA	NA	NA	NA	NA	NA	NA	NA

NOTES:

1. VALUES HIGHLIGHTED IN RED HAVE SATURATION INDICES ABOVE ZERO.
2. RELEVANT REY OXIDES AND HYDROXIDES WERE QUERIED FOR THE FOLLOWING MINERALS:

Alunite AlumK Basaluminite Boehmite
Manganite Mn3(PO4)2 Mn2(SO4)3 Mn3(AsO4)2:8H2O
MnHPO4 MnSO4 MnS(Green) Fe(OH)2.7Cl.3
Fe(OH)3(a) Fe2(SeO3)3 Fe3(OH)8 FeS(ppt)
Goethite Strengite Maghemite Magnetite
Jarosite-K Jarosite-Na Jurbanite Kaolinite
Calcite Dolomite Siderite Rhodochrosite
Rhodochrosite(d) MnSO4 CupricFerrite CuprousFerrite
Diaspore Gibbsite Halloysite Illite
Kmica Pyrophyllite Montmorillonite-Aberdeen Montmorillonite-Ca
Bixbyite Hausmannite Hematite Talc
Tremolite ZnSiO3 Quartz SiO2(a) Chalcedony

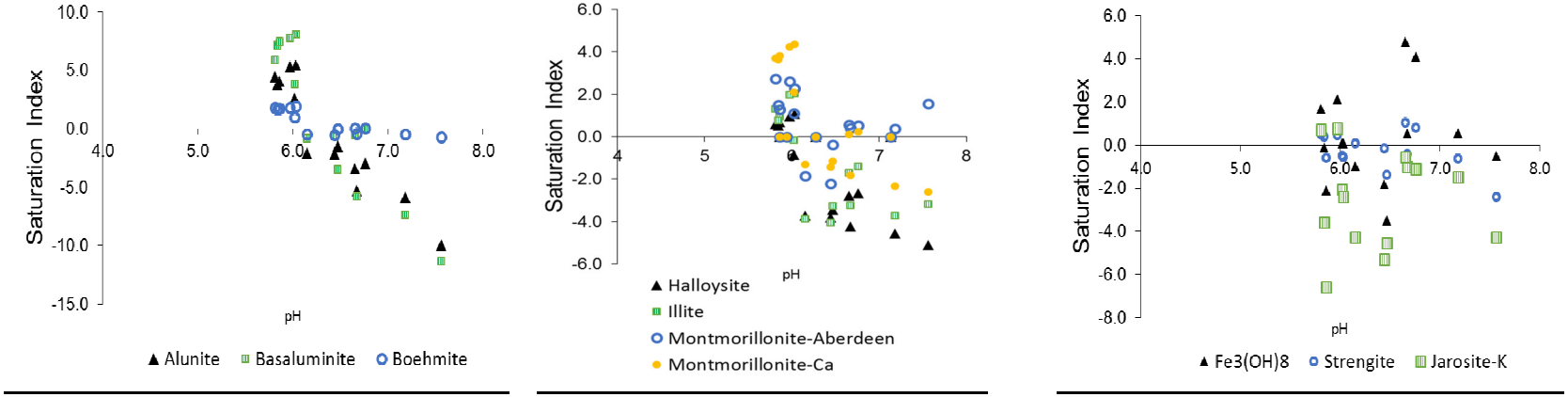

NOTES:

1. SATURATION INDICES FOR ALUMINUM AND IRON MINERALS CALCULATED IN PHREEQC USING THE WATEQ DATABASE.

Figure 19 Correlations of Sum of REY with Al, Fe, and S

Table 29 Solid Phase Rare Earth Element Anomaly Calculations – Complete Digestion

Site	Sum REY + Sc (ug/L)	pH	Y/Ho	LREY/ total	HREY /total	LREY/ HREY	MREY/ HREY	LREYn/ HREYn	LREYn/ MREYn	MREYn/ HREYn	La/La*	Ce/Ce*		Eu/Eu*		Gd/Gd*		Y/Y*	
								Prn/Yb n	Prn/Tb m	Gdn/Ybn	Lan/(Prn* Prn/Ndn)	Ce/SQRT(La*Pr)	Cen/(0.5*Lan + 0.5*Prn)	Eun/(0.67 *Smn + 0.33*Tbn)	Eun/(SQRT(Smn*Gdn))	Gdn/(Tbn*(Tbn/Dyn))	Gdn/(Tbn2 * Smn)1/3	[2/3]*Dyn + [1/3]Hon	[1/3]*Dyn + [2/3]*Hon
SC06-Dec	693.0	5.86	20.7	66%	34%	2.0	0.6	1.4	0.9	2.0	1.1	1.1	1.1	1.1	1.0	1.27	1.25	0.81	1.18
SC06-Aug-PM	512.0	6.03	25.7	80%	20%	4.1	1.2	1.7	1.0	2.0	1.2	1.0	1.0	1.1	1.0	1.15	1.17	1.00	1.46
SC06-Aug-AM	503.8	5.94	22.9	81%	19%	4.4	1.3	1.5	0.9	2.2	1.1	1.0	1.0	1.1	1.0	1.16	1.28	0.93	1.34
SC05-Dec	724.4	5.84	19.4	68%	32%	2.1	0.6	1.6	0.9	2.1	0.8	1.1	1.1	1.1	1.0	1.17	1.18	0.76	1.11
SC05-Aug-PM	578.4	6.02	22.2	82%	18%	4.5	1.3	1.7	1.0	2.0	0.9	1.1	1.0	1.1	1.0	1.24	1.17	0.82	1.21
SC05-Aug-AM	476.9	5.97	25.5	81%	19%	4.3	1.2	1.7	1.0	2.1	1.0	1.0	1.0	1.1	1.0	1.15	1.20	0.95	1.40
SC04-Dec	580.0	6.15	22.8	67%	33%	2.0	0.6	1.4	0.9	1.9	1.1	1.0	1.0	1.0	0.9	1.13	1.15	0.89	1.30
SC04-Aug-PM	671.8	5.81	25.2	80%	20%	4.1	1.2	1.6	1.0	2.0	1.0	1.0	1.0	1.1	1.0	1.25	1.20	0.94	1.38
SC04-Aug-AM	686.5	5.86	20.3	82%	18%	4.5	1.4	1.4	0.8	2.1	1.0	1.1	1.1	1.1	1.0	1.18	1.22	0.78	1.14
SC03-Dec	450.0	6.44	30.0	66%	34%	1.9	0.6	1.5	0.9	2.1	1.3	0.9	0.9	1.1	1.0	1.15	1.24	1.21	1.75
SC03-Aug-PM	350.4	6.47	35.3	79%	21%	3.7	1.2	1.6	0.9	2.1	1.6	0.9	0.9	1.1	1.0	1.19	1.25	1.38	2.01
SC03-Aug-AM	338.6	6.27	30.0	79%	21%	3.9	1.3	1.5	0.9	2.2	1.3	1.0	1.0	1.0	0.9	1.38	1.33	1.17	1.71
SC02-Dec	394.7	6.65	30.6	65%	35%	1.9	0.6	1.5	0.8	2.1	1.3	0.9	0.9	1.1	1.0	1.19	1.28	1.22	1.77
SC02-Aug-PM	404.1	7.18	29.5	79%	21%	3.7	1.2	1.4	0.8	1.9	1.6	1.0	1.0	1.1	1.0	1.10	1.20	1.23	1.77
SC02-Aug-AM	372.9	6.67	32.4	79%	21%	3.7	1.2	1.5	0.9	2.1	1.5	1.0	1.0	1.1	0.9	1.26	1.28	1.29	1.87
SC01-Dec	332.9	6.76	29.3	65%	35%	1.8	0.7	1.3	0.8	1.8	1.2	0.9	0.9	1.0	0.9	1.08	1.23	1.27	1.80
SC01-Aug-PM	170.0	7.56	42.9	74%	26%	2.8	1.1	1.5	0.8	2.2	2.1	0.8	0.8	1.2	1.0	1.13	1.29	1.75	2.52
SC01-Aug-AM	475.4	7.13	27.2	79%	21%	3.7	1.3	1.4	0.8	2.2	1.6	0.9	0.9	1.1	1.0	1.33	1.32	1.14	1.63

NOTES:

1. FRACTIONS OF Y/HO AND LREE/TOTAL; HREY/TOTAL; LREE/HREY AND MREE/HREY WERE COMPLETED WITH DATA THAT WAS NOT NORMALIZED. THE REMAINING CALCUATIONS (LREEn/HREYn etc.) WERE COMPLETED WITH NASC NORMALIZED DATA.

Table 30 Comparison of Nitric Acid vs. Aqua Regia Digestions (December sampling event)

Sample	Al	Fe	Mn	La	Ce	Pr	Nd	Sm	Eu	Gd	Tb	Dy	Y	Er	Ho	Tm	Yb	Lu
Analysis Method	**ICP-MS**	**ICP-MS**	**ICP-MS**	**ICP-MS**	**ICP-MS**	**ICP-MS**	**ICP-MS**	**ICP-MS**	**ICP-MS**	**ICP-MS**	**ICP-MS**	**ICP-MS**	**ICP-MS**	**ICP-MS**	**ICP-MS**	**ICP-MS**	**ICP-MS**	**ICP-MS**
Mass	**27**	**57**	**55**	**139**	**140**	**141**	**146**	**147**	**153**	**157**	**159**	**163**	**172**	**166**	**165**	**169**	**89**	**175**
SC-01 - AR	12,000	320,000	45,000	50.0	94.0	11.0	41.0	8.2	2.0	10.0	1.5	6.9	44.0	4.0	1.5	0.5	3.4	53.0
SC-01 - Nitric	12,000	350,000	51,000	54.0	99.0	11.0	44.0	8.6	2.0	10.0	1.5	7.2	48.0	4.2	1.5	0.6	3.5	58.0
RPD	**0%**	**-9%**	**-13%**	**-8%**	**-5%**	**0%**	**-7%**	**-5%**	**0%**	**0%**	**0%**	**-4%**	**-9%**	**-5%**	**0%**	**-11%**	**-3%**	**-9%**
SC-02 - AR	12,000	370,000	22,000	60.0	110.0	13.0	50.0	9.7	2.3	12.0	1.7	8.1	49.0	4.5	1.6	0.6	3.5	66.0
SC-02 - Nitric	13,000	420,000	25,000	68.0	130.0	15.0	57.0	11.0	2.6	13.0	1.8	9.0	56.0	5.3	1.8	0.6	4.2	74.0
RPD	**-8%**	**-13%**	**-13%**	**-13%**	**-17%**	**-14%**	**-13%**	**-13%**	**-12%**	**-8%**	**-6%**	**-11%**	**-13%**	**-16%**	**-12%**	**-8%**	**-18%**	**-11%**
SC-03 - AR	13,000	450,000	12,000	68.0	130.0	15.0	57.0	11.0	2.6	13.0	1.9	9.0	54.0	5.1	1.8	0.6	3.9	75.0
SC-03 - Nitric	12,000	450,000	12,000	67.0	130.0	14.0	57.0	11.0	2.6	13.0	1.8	8.7	54.0	5.1	1.8	0.7	3.9	71.0
RPD	**8%**	**0%**	**0%**	**1%**	**0%**	**7%**	**0%**	**0%**	**0%**	**0%**	**5%**	**3%**	**0%**	**0%**	**0%**	**-3%**	**0%**	**5%**
SC-04 - AR	23,000	410,000	1,000	71.0	170.0	21.0	85.0	18.0	4.0	18.0	2.7	13.0	57.0	7.0	2.5	0.9	6.0	100.0
SC-04 - Nitric	20,000	400,000	1,100	67.0	160.0	20.0	81.0	17.0	3.8	18.0	2.5	12.0	54.0	7.0	2.3	0.9	6.1	100.0
RPD	**14%**	**2%**	**-10%**	**6%**	**6%**	**5%**	**5%**	**6%**	**5%**	**0%**	**8%**	**8%**	**5%**	**0%**	**8%**	**4%**	**-2%**	**0%**
SC-05 - AR	27,000	450,000	160	77.0	220.0	28.0	110.0	25.0	5.5	24.0	3.4	16.0	60.0	8.8	3.1	1.2	7.1	130.0
SC-05 - Nitric	23,000	390,000	140	65.0	190.0	24.0	98.0	22.0	4.6	21.0	2.8	14.0	51.0	7.5	2.6	1.0	6.6	110.0
RPD	**16%**	**14%**	**13%**	**17%**	**15%**	**15%**	**12%**	**13%**	**18%**	**13%**	**19%**	**13%**	**16%**	**16%**	**18%**	**18%**	**7%**	**17%**
SC-06 - AR	32,000	290,000	190	74.0	200.0	25.0	110.0	22.0	4.9	23.0	3.1	15.0	60.0	8.7	2.9	1.1	7.1	130.0
SC-06 - Nitric	25,000	250,000	160	61.0	170.0	22.0	88.0	19.0	4.1	19.0	2.8	13.0	52.0	6.9	2.5	0.9	6.1	110.0
RPD	**25%**	**15%**	**17%**	**19%**	**16%**	**13%**	**22%**	**15%**	**18%**	**19%**	**10%**	**14%**	**14%**	**23%**	**15%**	**19%**	**15%**	**17%**

NOTE:
GREY HIGHLIGHTING INDICATES SAMPLES WITH RPD GREATER THAN 20%.

3.2.2.4 Nitric-Peroxide Digestions

Nitric-peroxide digestions were completed to compare with results of the aqua regia digestion. Results from both extractions ranged from 0-21% RPD, and were within the range of heterogeneity expected. With the exception of Al, Nd and Er parameters within the SC06 sample, the December samples analyzed using both digestion techniques showed less than 20% RPD for Al, Fe, Mn and rare earth elements. This was consistent with other parameters measured; however, a subset of the most relevant data is shown here.

3.2.2.5 NASC, PAAS and rock Normalized REY Patterns

Aqua regia digestions were completed to quantify the total amount of metals associated with the heterogeneous biogenic precipitates. Results of these digestions were normalized to three standards: Pennsylvania Anthracite-Mammoth No 8 (Schuylkill County), the NASC and the PAAS (Figure 20). These normalizations remove the 'saw-tooth' pattern characteristic of REYs that results from even atomic-numbered elements occurring an order of magnitude greater than odd-numbered elements.

The NAAS and PAAS normalized curves indicate that the biogenic precipitates portray a MREE-enriched pattern, with peak anomalies occurring either at Gd, or Eu, depending on the normalization method. Yttrium is noted to have a consistent positive anomaly at the SC01, SC02 and SC03 sites during both August and December sampling, with both NASC and PAAS normalization, whereas yttrium has a consistent negative anomaly at the SC04, SC05 and SC06 sites throughout sampling events and normalization methods.

The largest seasonal difference between the three sites is the large Lu anomaly that occurred in the December precipitates, but was not plotted. This anomaly is two orders of magnitude greater than the Lu values recorded during August within the precipitates; however, December water samples filtered to 0.45 µm also show two orders of magnitude enrichment, indicating this value may represent field conditions. Other seasonal differences include: sites that record the greatest solid phase enrichment are not consistent between the August and December sampling events. Site SC04 shows greatest solid enrichment of REYs during August, while SC05, closely followed by SC06, shows the greatest solid enrichment in December.

Diurnal differences in REY enrichment within the precipitate at several sites are noted. Site SC01 shows the largest diurnal difference, with almost a three-fold increase in solid phase REY during the morning sampling event when compared to the afternoon sampling event, which would be expected for sites with large differences in temperature. Site SC04 indicates MREE enrichment during the August-AM sampling event, when compared to the August-PM sampling event. Sites SC06, SC05, and SC03 show that solid REY concentrations are actually higher during the December sampling event, which has consistently lower pH.

3.2.3 Quantification of metals associated with iron-bearing fractions

Non-sequential solid extractions were completed to determine whether REYs were associated with the iron oxide fraction of the heterogeneous biogenic precipitates. Dithionite and oxalate extractions are used to determine the total amount of major ions and REYs associated with amorphous iron (III) oxides, crystalline iron (III) oxides and avid volatile sulphides, following the methods of Kostka and Luther[59].

Since there are few studies that have used these extractions to specifically analyze rare earth elements, two sites were digested with both dithionite and oxalate to compare to REY concentrations obtained from complete aqua regia digestion (Table 31). Results indicate that both methods quantify a greater fraction of iron, aluminum, manganese and REYs when compared with the aqua regia digestion. Anomalous results for Lu

were noted. Lu values in the aqua regia extraction were two orders of magnitude greater than Lu values recorded for either the oxalate or dithionite extractions. There was also a two order of magnitude difference between the 0.45 µm and 0.2 µm filtered water samples.

Results using oxalate and dithionite extraction methods were comparable. For that reason, both extraction methods were deemed acceptable and the oxalate extraction method was used to quantitatively assess the association of REYs with the iron fraction. In addition, an organic extraction method was also employed, designed to assess REYs was used to quantify the proportion of the organics portion. Compiled results from these extractions, compared with the complete aqua regia digestion are shown in Table 32 and Table 33. In spite of fairly high standard deviations, these results generally indicate that REYs are almost completely extracted with oxalate and that REY trends follow those of iron and aluminum.

A non-sequential extraction was completed to quantify REYs associated with the organic fraction, but due to uncertainty in results, the data is not provided here.

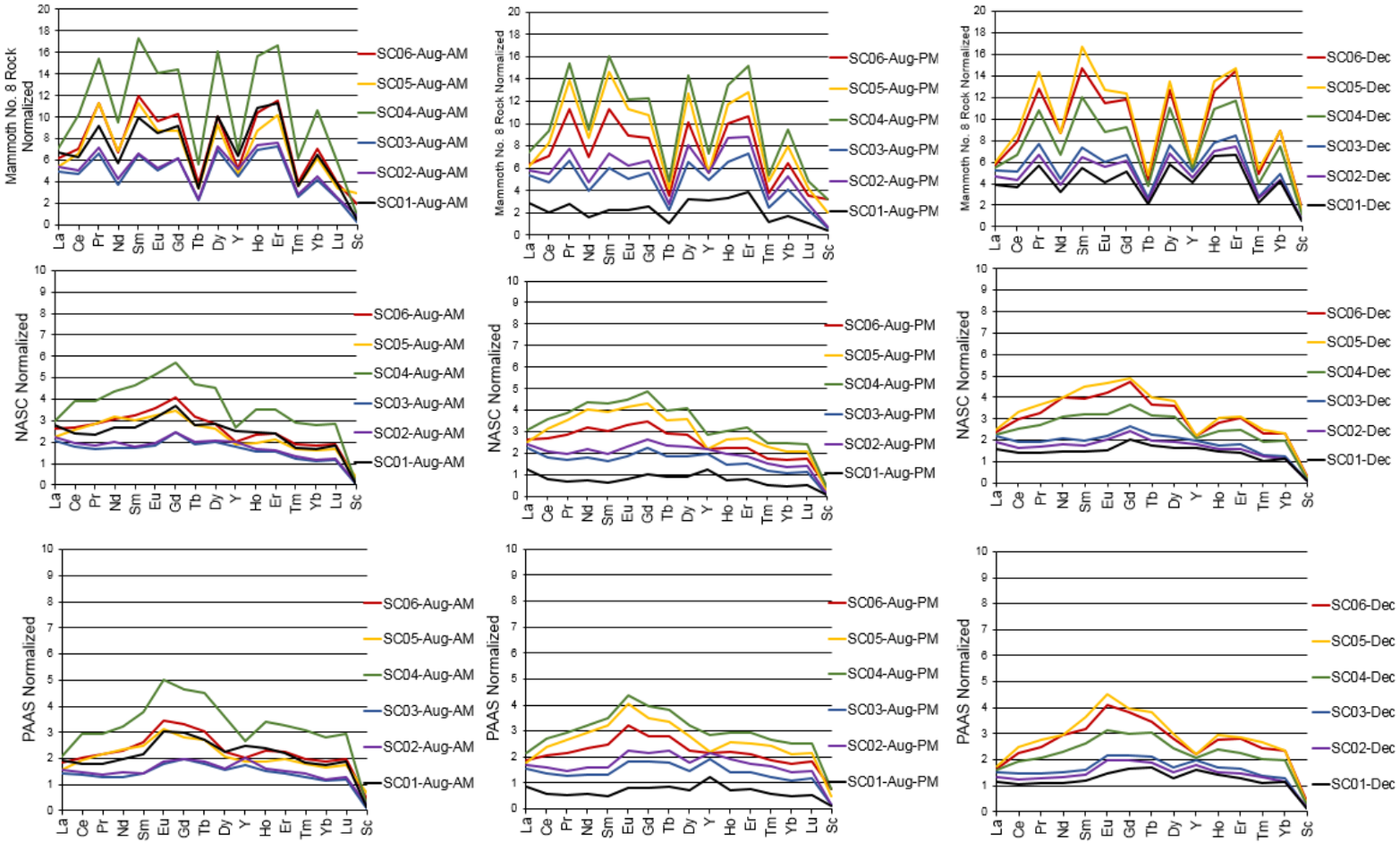

NOTES:

1. LU VALUES ARE NOT PLOTTED FOR DECEMBER.

Figure 20 Mammoth No. 8 Rock, NASC and PAAS Normalized – Aqua Regia Total Digestions of biogenic precipitate – Silver Creek December 2015 and August 2016

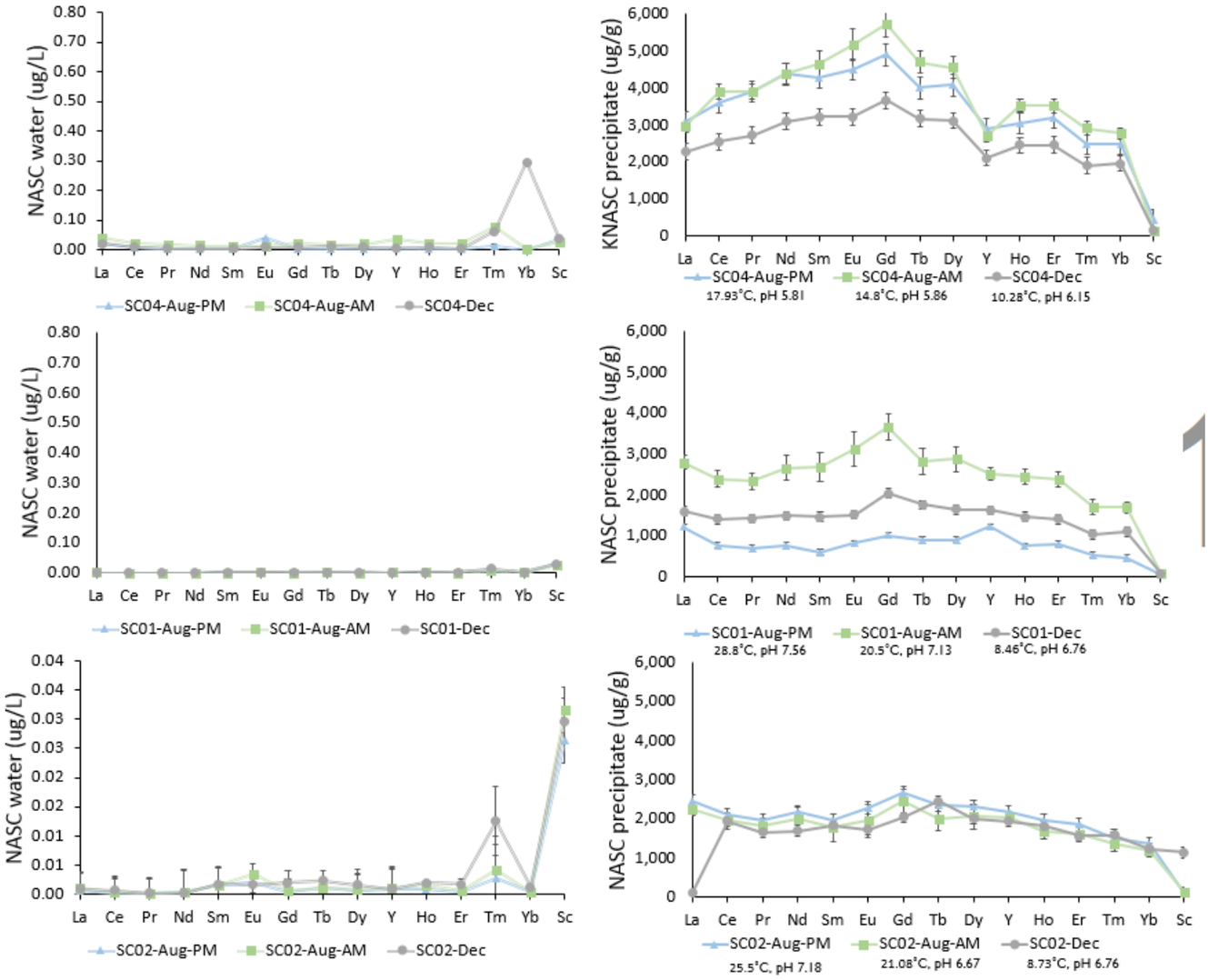

Figure 21 Sites SC04, SC01 and SC02 showing seasonal differences with peak solid concentrations in August (NASC normalized water and precipitate concentrations)

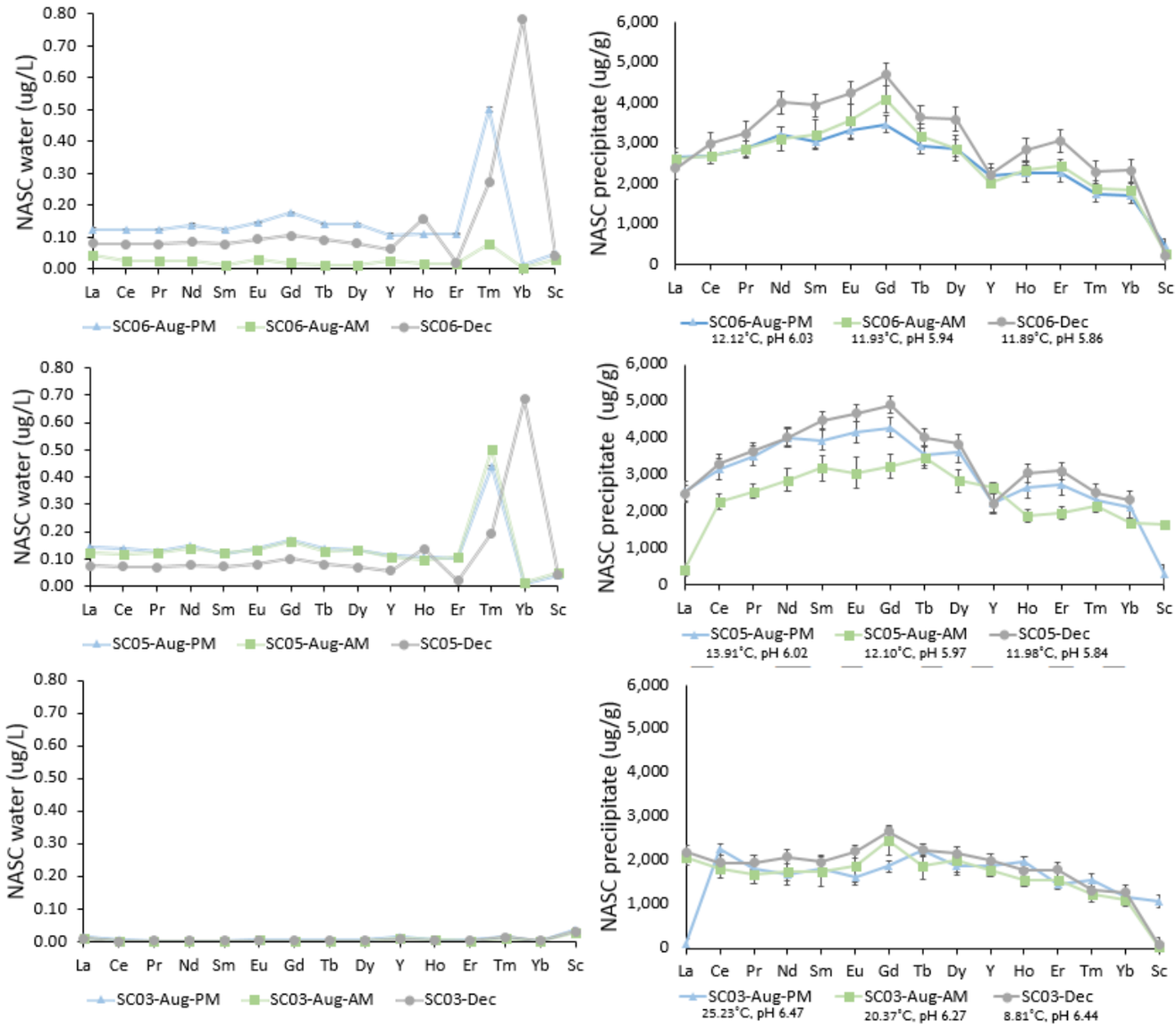

Figure 22 Sites SC06, SC05 and SC03 showing seasonal differences with peak solid concentrations occurring in December (NASC normalized water and precipitate concentrations)

Table 31 Comparison of Aqua Regia, Dithionite and Oxalate non-sequential extractions

	Site	Digestion	La	Ce	Pr	Nd	Sm	Eu	Gd	Tb	Dy	Er	Ho	Tm	Yb	Lu	Y	Sc	Sum REY
Solid phase (mg/gdwt)	SC04-Dec	Aqua Regia	71	170	21	85	18	3.8	18	2.7	13	7	2.5	0.91	6	100	57	4.1	580
	SC04-Dec	Dithionite	80	200	25	97	21	4.7	21	3.1	15	7.6	2.8	1.1	6.4	0.96	59	6.5	551
	SC04-Dec	Oxalate	66	180	19	76	16	3.8	18	2.7	14	7.7	2.7	1.1	6.3	1	61	6	481
	SC05-Dec	Aqua Regia	77	220	28	110	25	5.5	24	3.4	16	8.8	3.1	1.2	7.1	130	60	5.3	724
	SC05-Dec	Dithionite	78	210	29	120	28	5.9	25	3.7	18	8.9	3.2	1.2	7.6	1.1	57	6.8	603
	SC05-Dec	Oxalate	92	270	33	130	29	6.8	30	4.7	23	13	4.4	1.8	11	1.6	88	9.1	747
Fraction (%)	SC04-Dec	Dithionite	113%	118%	119%	114%	117%	124%	117%	115%	115%	109%	112%	121%	107%	1%	104%	159%	95%
	SC04-Dec	Oxalate	93%	106%	90%	89%	89%	100%	100%	100%	108%	110%	108%	121%	105%	1%	107%	146%	83%
	SC05-Dec	Dithionite	101%	95%	104%	109%	112%	107%	104%	109%	113%	101%	103%	100%	107%	1%	95%	128%	83%
	SC05-Dec	Oxalate	119%	123%	118%	118%	116%	124%	125%	138%	144%	148%	142%	150%	155%	1%	147%	172%	103%

Table 32 Comparison of aqua regia complete digestion with non-sequential oxalate and organics extractions – December Silver Creek site samples

	Site	Extraction	Al	Fe	Mn	S	La	Ce	Pr	Nd	Sm	Eu	Gd	Tb	Dy	Er	Ho	Tm	Yb	Lu	Y	Sc
Solid phase (mg/gdwt)	SC06-Dec	Aqua Regia	32,000	290,000	140	7,000	74	200	25	110	22	5	23	3.1	15	8.7	2.9	1.1	7.1	130	60	6.1
	SC05-Dec	Aqua Regia	27,000	450,000	110	8,500	77	220	28	110	25	5.5	24	3.4	16	8.8	3.1	1.2	7.1	130	60	5.3
	SC04-Dec	Aqua Regia	23,000	410,000	910	5,500	71	170	21	85	18	3.8	18	2.7	13	7	2.5	0.91	6	100	57	4.1
	SC03-Dec	Aqua Regia	13,000	450,000	11,000	3,400	68	130	15	57	11	2.6	13	1.9	9	5.1	1.8	0.63	3.9	75	54	2.1
	SC02-Dec	Aqua Regia	12,000	370,000	23,000	2,900	60	110	13	50	9.7	2.4	12	1.7	8.1	4.5	1.6	0.59	3.5	66	49	2.6
	SC01-Dec	Aqua Regia	12,000	320,000	50,000	2,400	50	94	11	41	8.2	1.8	10	1.5	6.9	4	1.5	0.5	3.4	53	44	2.1
		SD	*3,669*	*24,395*	*21*	*495*	*6.4*	*19*	*2.1*	*11*	*2.1*	*0.5*	*1.8*	*0.3*	*1.6*	*0.7*	*0.3*	*0.1*	*0.6*	*0.1*	*5*	*1.1*
	SC06-Dec	Oxalate	43,000	330,000	270	15,000	100	300	34	140	31	7	34	5	25	14	5	2	12	2	98	10
	SC05-Dec	Oxalate	37,000	470,000	190	12,000	92	270	33	130	29	7	30	5	23	13	4	2	11	2	88	9
	SC04-Dec	Oxalate	21,000	310,000	1,000	5,000	66	180	19	76	16	4	18	3	14	8	3	1	6	1	61	6
	SC03-Dec	Oxalate	7,400	200,000	8,200	2,100	32	70	7	25	5	1	7	1	5	3	1	0	2	0	30	4
	SC02-Dec	Oxalate	6,800	160,000	14,000	1,300	31	70	7	26	5	1	7	1	5	3	1	0	2	0	30	4
	SC01-Dec	Oxalate	21,000	470,000	93,000	3,500	52	130	10	37	8	2	11	2	11	7	2	1	5	1	70	NA
		SD	*3,064*	*29,227*	*32*	*495*	*8.7*	*26.6*	*2.5*	*11.1*	*2.5*	*0.6*	*2.4*	*0.4*	*1.8*	*0.9*	*0.3*	*0.1*	*14.1*	*0.1*	*21.0*	*0.9*
Fraction (%)	SC06-Dec	Oxalate	134%	114%	193%	214%	135%	150%	136%	127%	141%	148%	148%	165%	167%	161%	166%	173%	169%	1%	163%	164%
	SC05-Dec	Oxalate	137%	104%	173%	141%	119%	123%	118%	118%	116%	124%	125%	138%	144%	148%	142%	150%	155%	1%	147%	172%
	SC04-Dec	Oxalate	91%	76%	110%	91%	93%	106%	90%	89%	89%	100%	100%	100%	108%	110%	108%	121%	105%	1%	107%	146%
	SC03-Dec	Oxalate	57%	44%	75%	62%	47%	54%	44%	44%	47%	54%	51%	52%	57%	57%	56%	63%	59%	0%	56%	171%
	SC02-Dec	Oxalate	57%	43%	61%	45%	52%	64%	51%	52%	54%	50%	55%	58%	62%	67%	63%	68%	66%	1%	61%	135%
	SC01-Dec	Oxalate	175%	147%	186%	146%	104%	138%	89%	90%	95%	122%	110%	127%	159%	163%	147%	172%	150%	2%	159%	NA

NOTES:

1. PERCENTAGES GREATER THAN 50% ARE HIGHLIGHTED IN RED.

Table 33 Comparison of aqua regia complete digestion with non-sequential oxalate and organics extractions – August Silver Creek site samples

	Site	Extraction	Al	Fe	Mn	S	La	Ce	Pr	Nd	Sm	Eu	Gd	Tb	Dy	Er	Ho	Tm	Yb	Lu	Y	Sc
Solid phase (mg/gdwt)	SC06-Aug-PM	Aqua Regia	46,000	93,000	210	3,400	83	180	22	88	17	3.9	17	2.5	12	6.4	2.3	0.84	5.2	0.81	59	12
	SC05-Aug-PM	Aqua Regia	32,000	290,000	280	5,200	79	210	27	110	22	4.9	21	3	15	7.7	2.7	1.1	6.4	0.94	60	7.7
	SC04-Aug-PM	Aqua Regia	54,000	140,000	220	4,800	96	240	30	120	24	5.3	24	3.4	17	9.1	3.1	1.2	7.6	1.1	78	12
	SC03-Aug-PM	Aqua Regia	14,000	380,000	61,000	2,200	70	120	13	50	9.1	2.2	11	1.6	7.8	4.4	1.5	0.56	3.3	0.51	53	2.4
	SC02-Aug-PM	Aqua Regia	14,000	380,000	61,000	2,000	76	140	15	60	11	2.7	13	2	9.6	5.3	2	0.73	4.2	0.64	59	2.9
	SC01-Aug-PM	Aqua Regia	5,500	430,000	43,000	690	38	52	5.4	21	3.4	0.97	5	0.77	3.8	2.3	0.77	0.26	1.4	0.24	33	1.7
		SD	*3,889*	*24,395*	*21*	*495*	*6.4*	*16*	*2.1*	*11*	*2.1*	*0.5*	*1.8*	*0.3*	*1.6*	*0.7*	*0.3*	*0.1*	*0.6*	*0.1*	*5*	*1.1*
	SC06-Aug-PM	Oxalate	14,000	58,000	92	3,300	43	110	13	54	12	3	13	2	9	5	2	1	4	1	40	3
	SC05-fdup-Aug-PM	Oxalate	25,000	320,000	260	7,200	76	220	26	110	23	5	25	4	17	9	3	1	8	1	66	7
	SC04-Aug-PM	Oxalate	22,000	110,000	130	4,200	61	170	20	84	18	4	20	3	15	8	3	1	7	1	64	6
	SC03-Aug-PM	Oxalate	9,300	410,000	8,000	2,200	67	130	12	48	9	2	12	2	8	5	2	1	4	1	55	7
	SC02-Aug-PM	Oxalate	15,000	440,000	69,000	2,900	48	110	9	35	8	2	10	2	8	5	2	1	4	1	51	9
	SC01-Aug-PM	Oxalate	3,600	290,000	23,000	370	6	14	1	3	1	0	1	0	1	1	0	0	1	0	11	NA
		SD	*3,064*	*29,227*	*32*	*495*	*8.7*	*26.6*	*2.5*	*11.1*	*2.5*	*0.6*	*2.4*	*0.4*	*1.8*	*0.9*	*0.3*	*0.1*	*14.1*	*0.1*	*21.0*	*0.9*
Fraction (%)	SC06-Aug-PM	Oxalate	30%	62%	44%	97%	52%	61%	59%	61%	71%	72%	76%	76%	76%	78%	74%	85%	85%	77%	68%	28%
	SC05-fdup-Aug-PM	Oxalate	78%	110%	93%	138%	96%	105%	96%	100%	105%	108%	119%	120%	113%	119%	122%	118%	125%	128%	110%	95%
	SC04-Aug-PM	Oxalate	41%	79%	59%	88%	64%	71%	67%	70%	75%	81%	83%	88%	88%	92%	97%	100%	96%	100%	82%	48%
	SC03-Aug-PM	Oxalate	66%	108%	13%	100%	96%	108%	92%	96%	100%	100%	109%	106%	108%	109%	113%	111%	115%	114%	104%	292%
	SC02-Aug-PM	Oxalate	107%	116%	113%	145%	63%	79%	62%	58%	69%	70%	76%	75%	85%	91%	85%	90%	95%	95%	86%	300%
	SC01-Aug-PM	Oxalate	65%	67%	53%	54%	15%	27%	15%	14%	16%	21%	20%	27%	29%	37%	38%	54%	49%	50%	33%	NA

NOTES:

1. PERCENTAGES GREATER THAN 50% ARE HIGHLIGHTED IN RED.

3.2.4 Distribution coefficients (Kd)

Distribution coefficients were calculated by dividing measured solid concentrations, digested by aqua regia (ug/g dry weight), with measured water chemistry (0.45 µm filtered; ug/L). Partitioning coefficients in excess of 1E6 were consistently seen at the SC01 and SC02 sites for the majority of REYs. Calculated REY Kd values showed a wide range of values, from a minimum of 2.2E2 ± 58 (Lu, SC06-Aug PM dup) to a maximum of 1.5E7 ± 2.24E3 (Pr, SC02-Aug PM) (Table 34; Figure 25). In general, calculated Kd values at SC01 and SC02 are an order of magnitude above those at SC03 and SC04, which are a magnitude above Kd values at SC05 and SC06. Sites SC01 and SC02 consistently showed greater LREE enrichment when compared to Kd values measured for MREEs or HREYs (Figure 25). REY parameters Sc, Tm and Lu showed the lowest partitioning coefficients, while Yb, another HREY contained consistently elevated partitioning coefficients. Log transformed plots indicate greater variability in calculated Kd values between REYs, with SC06 and SC05 sites indicating less variability. Log transformed plots reveal that sites SC01, SC02, SC03 and SC04 generally have elevated Kd values for both LREEs and MREEs.

For comparison, partitioning coefficients for REYs were compared to major and trace metals. The major and trace metals with the greatest partitioning coefficients are provided in Table 35. Aluminum and iron both showed very high partitioning coefficients that generally exceeded maximum partitioning coefficients observed for REYs. Partitioning coefficients for Pb, V and Cu were within the range of those observed for REYs, but showed lower maximum values. REY partitioning coefficients were greater than Cr, Th, As, Zn, Cd, Mo, Co and Ni (shown in Table 35). REY partitioning coefficients were generally greater than partitioning coefficients observed for Sr, Ti, U, Ca, Mg, Mn, S, Si, B, and Ba.

Review of Figure 23 shows that the variable patterns showed in Kd values across the REY group are a results of non-linear patterns within the water data. Compared to the water data, the biofilm data shows a relatively flat pattern that could represent saturation of all adsorption sites.

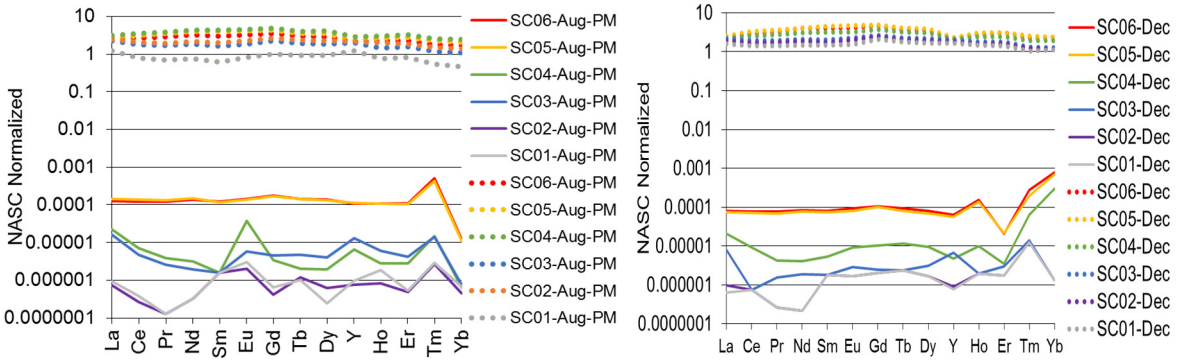

Figure 23 Comparison of water data (solid) and biofilm data (dotted) for the August-PM and December sampling events

Table 34 Partitioning coefficients (unitless) for Silver Creek Rare Earth Element Data

Kd	La	Ce	Pr	Nd	Sm	Eu	Gd	Tb	Dy	Y	Ho	Er	Tm	Yb	Lu	Sc
SD	**2.4E+03**	**2.7E+03**	**2.2E+03**	**3.6E+03**	**5.1E+03**	**3.9E+03**	**3.3E+03**	**3.2E+03**	**3.8E+03**	**2.4E+03**	**3.0E+03**	**3.0E+03**	**2.9E+02**	**1.5E+04**	**5.8E+01**	**7.7E+02**
SC01-Aug-PM	1.31E+06	2.00E+06	5.40E+06	2.33E+06	3.78E+05	2.69E+05	1.56E+06	8.85E+05	3.80E+06	1.27E+06	4.05E+05	1.53E+06	1.86E+05	6.67E+05	1.85E+05	2.07E+03
SC02-Aug-PM	3.30E+06	7.78E+06	1.50E+07	6.67E+06	1.22E+06	1.13E+06	6.50E+06	2.00E+06	3.69E+06	2.81E+06	2.33E+06	3.79E+06	5.62E+05	3.00E+06	3.05E+04	4.08E+03
SC03-Aug-PM	1.40E+05	3.75E+05	6.50E+05	9.43E+05	1.01E+06	3.17E+05	5.00E+05	3.90E+05	4.59E+05	1.51E+05	2.46E+05	3.67E+05	8.12E+04	1.43E+06	1.46E+03	2.40E+03
SC04-Aug-PM	1.41E+05	5.00E+05	1.00E+06	1.38E+06	2.67E+06	1.18E+05	1.41E+06	2.00E+06	2.13E+06	4.33E+05	1.07E+06	1.12E+06	1.69E+05	3.80E+06	6.11E+03	1.20E+04
SC05-Aug-PM	7.18E+04	1.40E+05	1.80E+05	1.93E+05	8.80E+05	1.31E+05	2.66E+05	3.37E+05	3.49E+05	1.18E+05	2.08E+05	1.79E+05	3.93E+04	1.42E+06	1.84E+03	7.70E+03
SC06-Aug-PM	2.13E+04	2.22E+04	2.32E+04	2.32E+04	2.50E+04	2.29E+04	1.98E+04	2.08E+04	2.07E+04	2.03E+04	2.09E+04	2.06E+04	3.50E+03	1.41E+05	2.79E+02	9.23E+03
SC06-fdup-Aug-PM	1.68E+04	1.79E+04	1.90E+04	1.78E+04	1.76E+04	1.77E+04	1.61E+04	1.54E+04	1.57E+04	1.69E+04	1.64E+04	1.63E+04	3.13E+03	1.20E+05	2.21E+02	9.17E+03
SC01-Aug-AM	2.72E+06	8.89E+06	8.18E+06	8.11E+06	7.50E+06	1.95E+06	4.50E+06	1.20E+06	4.00E+06	2.72E+06	6.25E+05	3.40E+06	2.05E+05	1.73E+06	3.32E+04	3.09E+03
SC02-Aug-AM	1.94E+06	5.42E+06	1.40E+07	6.11E+06	1.10E+06	5.68E+05	3.43E+06	1.89E+06	2.61E+06	1.83E+06	1.00E+06	2.88E+06	3.25E+05	2.77E+06	1.87E+04	3.88E+03
SC03-Aug-AM	1.78E+05	6.32E+05	9.29E+05	1.07E+06	1.96E+06	5.71E+05	1.00E+06	8.00E+05	9.54E+05	2.09E+05	4.00E+05	6.11E+05	1.44E+05	1.13E+06	2.30E+03	1.58E+03
SC04-Aug-AM	7.08E+04	1.73E+05	2.31E+05	2.93E+05	4.19E+05	3.49E+05	2.55E+05	2.50E+05	2.32E+05	7.30E+04	1.71E+05	1.61E+05	3.78E+04	1.20E+06	1.30E+03	4.93E+03
SC05-Aug-AM	1.79E+04	2.13E+04	2.34E+04	2.29E+04	2.46E+04	2.38E+04	2.13E+04	2.18E+04	1.96E+04	1.76E+04	2.00E+04	1.97E+04	3.38E+03	1.43E+05	2.66E+02	8.46E+03
SC05-fdup-Aug-AM	2.03E+04	2.47E+04	2.56E+04	2.76E+04	3.17E+04	2.97E+04	2.70E+04	2.55E+04	2.55E+04	2.09E+04	2.40E+04	2.37E+04	3.83E+03	1.66E+05	3.70E+02	6.34E+03
SC06-Aug-AM	5.79E+04	1.00E+05	1.22E+05	1.20E+05	2.57E+05	1.24E+05	2.17E+05	2.70E+05	2.07E+05	8.46E+04	1.50E+05	1.41E+05	2.43E+04	1.00E+06	1.32E+03	9.10E+03
SC01-Dec	2.50E+06	1.88E+06	5.50E+06	6.83E+06	8.20E+05	9.00E+05	1.00E+06	7.50E+05	9.86E+05	2.10E+06	7.50E+05	8.00E+05	8.33E+04	8.50E+05	2.52E+06	2.63E+03
SC02-Dec	2.00E+06	2.20E+06	6.50E+06	8.33E+06	9.70E+05	1.20E+06	1.20E+06	8.50E+05	1.16E+06	2.04E+06	8.00E+05	9.00E+05	9.83E+04	8.75E+05	2.75E+06	3.25E+03
SC03-Dec	2.83E+05	2.60E+06	1.25E+06	1.12E+06	1.10E+06	7.65E+05	1.08E+06	9.50E+05	6.92E+05	3.00E+05	9.00E+05	6.00E+05	9.40E+04	9.75E+05	4.17E+05	2.56E+03
SC04-Dec	1.09E+05	2.74E+05	6.36E+05	7.73E+05	6.00E+05	3.45E+05	3.60E+05	2.70E+05	3.25E+05	4.38E+05	2.50E+05	7.00E+05	3.03E+04	6.67E+03	7.69E+05	4.10E+03
SC05-Dec	3.35E+04	4.58E+04	5.28E+04	5.24E+04	6.10E+04	5.88E+04	4.80E+04	5.00E+04	5.52E+04	4.00E+04	2.21E+04	1.44E+05	1.29E+04	3.38E+03	8.67E+04	4.82E+03
SC06-Dec	2.96E+04	3.85E+04	4.24E+04	4.78E+04	5.00E+04	4.55E+04	4.51E+04	3.97E+04	4.55E+04	3.53E+04	1.81E+04	1.50E+05	8.46E+03	2.96E+03	7.65E+04	5.55E+03
Max	**3.30E+06**	**8.89E+06**	**1.50E+07**	**8.33E+06**	**7.50E+06**	**1.95E+06**	**6.50E+06**	**2.00E+06**	**4.00E+06**	**2.81E+06**	**2.33E+06**	**3.79E+06**	**5.62E+05**	**3.80E+06**	**2.75E+06**	**1.20E+04**
Min	**1.68E+04**	**1.79E+04**	**1.90E+04**	**1.78E+04**	**1.76E+04**	**1.77E+04**	**1.61E+04**	**1.54E+04**	**1.57E+04**	**1.69E+04**	**1.64E+04**	**1.63E+04**	**3.13E+03**	**2.96E+03**	**2.21E+02**	**1.58E+03**

NOTES:

1. DISTRIBUTION COEFFICIENTS WERE CALCULATED BY DIVIDING SOLID CONCENTRATIONS FROM AQUA REGIA DIGESTIONS (ug/g dry weight) BY 0.45 µm FILTERED WATER SAMPLES (ug/L).
2. STANDARD DEVIATION WAS MEASURED BY AVERAGING THE STANDARD DEVIATION BETWEEN DUPLICATE SAMPLES.
3. HIGHLIGHTED CELLS REPRESENT KD VALUES ELEVATED OVER 1E6.

Table 35 Partitioning coefficients (unitless) for select Silver Creek Major and Trace element data

Kd	Al	Fe	Pb	V	Cu	Cr	Th	As	Zn	Cd	Mo	Co	Ni
SD	**1.7E+04**	**2.5E+03**	**1.6E+06**	**1.1E+06**	**2.1E+06**	**1.9E+05**	**9.3E+05**	**9.9E+03**	**4.9E+02**	**4.3E+03**	**5.2E+03**	**1.5E+02**	**1.5E+02**
SC01-Aug-PM	8.87E+05	1.59E+06	2.84E+05	8.24E+03	3.06E+04	1.00E+04	5.42E+05	4.85E+05	9.60E+04	8.00E+04	7.94E+04	4.30E+04	2.61E+04
SC02-Aug-PM	1.40E+07	1.36E+06	1.75E+06	2.91E+04	1.20E+05	1.33E+04	6.25E+05	9.62E+05	6.11E+04	1.09E+05	1.61E+05	1.31E+05	2.94E+04
SC03-Aug-PM	1.08E+07	4.81E+05	1.50E+06	4.62E+04	1.00E+05	1.00E+04	2.05E+05	2.65E+05	1.50E+04	1.43E+04	1.17E+05	8.49E+03	3.13E+03
SC04-Aug-PM	5.40E+05	1.17E+04	6.30E+06	1.39E+06	4.80E+05	5.17E+05	1.14E+05	5.00E+04	1.21E+03	1.29E+04	5.38E+04	2.96E+02	4.93E+02
SC05-Aug-PM	1.07E+07	1.53E+04	6.09E+06	6.22E+05	7.74E+04	8.57E+04	8.30E+04	3.23E+04	1.13E+03	1.50E+04	3.64E+04	4.90E+02	7.42E+02
SC06-Aug-PM	2.71E+05	4.65E+03	4.84E+05	4.50E+06	1.00E+05	3.33E+05	3.25E+04	1.29E+04	2.08E+03	2.33E+03	1.38E+04	2.50E+02	4.02E+02
SC06-fdup-Aug-PM	2.50E+05	3.70E+03	9.31E+05	4.10E+06	4.10E+05	6.34E+05	3.10E+04	1.05E+04	1.83E+03	1.20E+04	1.47E+04	2.06E+02	3.38E+02
SC01-Aug-AM	5.11E+06	3.00E+07	1.32E+06	2.00E+05	8.57E+05	2.20E+05	4.05E+05	1.88E+05	4.81E+04	2.00E+05	1.00E+04	4.83E+04	1.40E+04
SC02-Aug-AM	1.58E+07	1.28E+06	3.19E+05	1.80E+05	9.20E+04	1.00E+04	4.20E+04	1.13E+06	3.85E+04	5.79E+04	8.79E+04	6.84E+04	1.70E+04
SC03-Aug-AM	2.86E+07	1.54E+06	5.60E+05	1.63E+05	9.67E+05	5.00E+04	1.50E+05	1.35E+05	1.78E+04	5.22E+04	7.50E+03	1.70E+04	4.52E+03
SC04-Aug-AM	3.15E+06	1.03E+05	1.96E+06	2.33E+05	2.94E+06	3.00E+05	6.00E+05	1.82E+05	3.37E+03	1.67E+04	7.75E+03	1.96E+03	5.81E+02
SC05-Aug-AM	2.43E+05	1.10E+04	6.11E+05	3.30E+06	3.50E+05	6.67E+05	5.85E+04	1.97E+04	2.17E+03	5.25E+03	2.21E+04	2.73E+02	4.58E+02
SC05-fdup-Aug-AM	2.71E+05	1.71E+04	4.60E+06	6.83E+05	6.00E+06	9.00E+05	2.70E+06	4.55E+04	3.30E+03	7.78E+03	8.25E+03	6.55E+02	8.24E+02
SC06-Aug-AM	1.11E+07	7.86E+03	6.60E+06	1.05E+06	7.11E+06	1.45E+06	3.95E+06	3.06E+04	1.87E+03	9.89E+04	7.50E+03	6.21E+02	7.44E+02
SC01-Dec	1.50E+07	2.67E+05	2.38E+04	2.42E+03	8.28E+04	2.06E+03	2.10E+04	2.67E+04	3.08E+04	2.32E+04	8.50E+02	3.16E+04	1.61E+04
SC02-Dec	1.50E+07	1.85E+05	1.55E+05	2.41E+03	1.66E+04	1.12E+03	8.00E+03	3.76E+04	1.82E+04	1.63E+04	3.33E+03	1.84E+04	6.03E+03
SC03-Dec	1.63E+07	9.00E+04	1.26E+05	3.25E+03	3.00E+04	2.15E+03	7.50E+03	3.45E+04	1.15E+04	6.67E+03	9.20E+03	1.17E+04	3.23E+03
SC04-Dec	2.88E+07	4.41E+04	3.85E+05	1.00E+04	2.14E+04	5.98E+03	4.10E+04	4.07E+04	4.50E+03	2.67E+03	1.30E+04	9.77E+02	6.45E+02
SC05-Dec	2.70E+05	2.65E+04	5.50E+05	3.09E+04	2.30E+05	1.18E+04	6.70E+04	4.48E+03	2.78E+03	3.33E+03	2.80E+04	3.10E+02	5.00E+02
SC06-Dec	2.67E+05	1.71E+04	8.00E+05	5.00E+04	3.20E+05	1.67E+04	1.00E+05	2.17E+04	2.47E+03	6.33E+03	4.50E+04	2.05E+02	3.44E+02
Max	**2.88E+07**	**3.00E+07**	**6.60E+06**	**4.50E+06**	**7.11E+06**	**1.45E+06**	**3.95E+06**	**1.13E+06**	**9.60E+04**	**2.00E+05**	**1.61E+05**	**1.31E+05**	**2.94E+04**
Min	**2.43E+05**	**3.70E+03**	**2.38E+04**	**2.41E+03**	**1.66E+04**	**1.12E+03**	**7.50E+03**	**4.48E+03**	**1.13E+03**	**2.33E+03**	**8.50E+02**	**2.05E+02**	**3.38E+02**

NOTES:

1. DISTRIBUTION COEFFICIENTS WERE CALCULATED BY DIVIDING SOLID CONCENTRATIONS FROM AQUA REGIA DIGESTIONS (ug/g dry weight) BY 0.45 µm FILTERED WATER SAMPLES (ug/L).
2. STANDARD DEVIATION WAS MEASURED BY AVERAGING THE STANDARD DEVIATION BETWEEN DUPLICATE SAMPLES.
3. HIGHLIGHTED CELLS REPRESENT KD VALUES ELEVATED OVER 1E6.

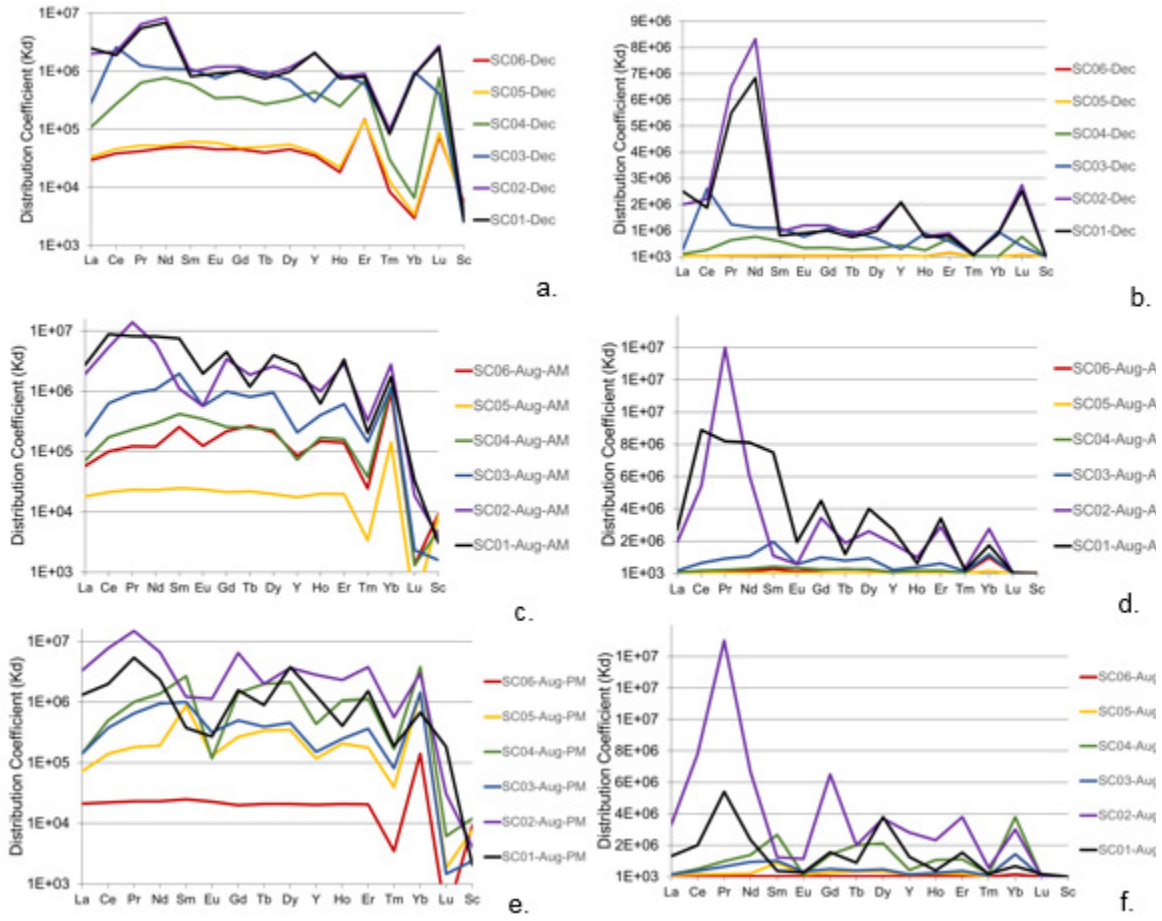

NOTES:

1. REY DISTRIBUTION PATTERNS WERE CALCULATED: [REY IN SOLID (ug/g)]/[REY IN 0.45 µm WATER].

Figure 24 REY distribution patterns between biogenic precipitates and water for Silver Creek Sites (a) December-log scale; (b) December; (c) August-Am-log scale; (d) August-AM; (e) August-PM-log scale; (f) August-PM.

3.2.5 Sorption Isotherms

Linear, Langmuir and Freundlich isotherms were plotted for sample sites SC06 through SC01 at the three sampling events (December, August-PM and August-AM). Relative error was calculated for the predicted solid concentrations, and the measured solid concentrations. Isotherms have been presented together with pH and temperature information, which are key variables affecting sorption, recognizing that a surface assemblage model (presented in Section 3.2.6) is needed to thoroughly understand complex changes in pH, temperature, dissolved oxygen etc.

Relative error for the different isotherms is presented in Table 36. Based on comparing the relative error, the Langmuir isotherm provides the best fit for December data, with the exception of a few HREYs, including: Tb, Dy, Er, Tm, Lu and Sc, which show less error using linear isotherms. In contrast to the expected sorption trend with pH, the sites with indicate greatest sorption (SC05 and SC06), have the lowest pH, but they also have the highest aqueous concentrations of REYs. Temperature differences for the December data are a maximum of 4 degrees, with the warmest sites occurring

closest to the groundwater discharge (SC05 and SC06). Previous authors have found warmest sites to generally exhibit less sorption of REYs than colder sites[22].

The Aug-PM has much higher relative error data than any of the other sampling events. The plots show greater variability than the December data, and particularly anomalous data for the SC04 site, where solid precipitates measured the highest amount of La (96,000 ug/g), with water concentrations much below upstream sites (0.68 ug/L compared to 3.9 ug/L and 4.5 ug/L). Site SC04 in fact, has the lowest pH of all the sites, and would therefore be expected to have the lowest amount of sorption. There are significant temperature differences, almost 20˚C, observed at the August sites. In general, these temperature differences should re-enforce the sorption trend; sites with greatest aqueous REY concentrations (sites SC05 and SC06), also have the lowest temperatures.

The August-AM data shows lowest relative error with the Langmuir isotherm, compared to the other isotherms. Plots of the data show that, compared with aqueous concentrations, the solid concentrations cluster along a horizontal linear line. Based on review of the plots, it is hard to see a discernable Langmuir trend.

Plots for La, Gd, and Ho as representatives of LREE, MREE and HREYs. LREEs generally exhibit trends that more closely match the Langmuir isotherm, while HREYs more closely follow linear trends. There are 10 sites in the August-AM sampling that show calculated relative error between 10% to 50% for the Langmuir isotherm,

Table 36 Summary of the Relative Error (%)

Element	Linear Isotherm			Langmuir Isotherm			Freundlich Isotherm		
	Aug-PM	Aug-AM	Dec	Aug-PM	Aug-AM	Dec	Aug-PM	Aug-AM	Dec
La	35%	10%	5%	32%	10%	1%	>100%	>100%	2%
Ce	77%	40%	15%	61%	40%	7%	>100%	>100%	12%
Pr	96%	44%	22%	64%	55%	12%	>100%	>100%	>100%
Nd	99%	50%	26%	67%	50%	17%	>100%	>100%	>100%
Sm	>100%	64%	34%	>100%	64%	6%	>100%	>100%	>100%
Eu	88%	66%	23%	91%	60%	6%	>100%	71%	>100%
Gd	85%	51%	15%	70%	50%	3%	>100%	>100%	>100%
Tb	78%	56%	16%	48%	36%	30%	>100%	68%	>100%
Dy	81%	49%	18%	48%	49%	51%	>100%	68%	>100%
Er	72%	46%	14%	57%	41%	48%	>100%	>100%	>100%
Ho	70%	47%	15%	72%	30%	2%	>100%	43%	>100%
Tm	78%	56%	16%	75%	36%	30%	>100%	68%	>100%
Yb	92%	56%	4%	92%	50%	3%	>100%	81%	>100%
Lu	80%	50%	18%	47%	51%	58%	>100%	45%	>100%
Sc	>100%	>100%	47%	>1	>1	91%	>100%	>100%	88%
Y	31%	14%	3%	28%	14%	1%	>100%	94%	1%
Sum REY	67%	31%	11%	86%	31%	46%	>100%	37%	17%

NOTE:

1. RELATIVE ERROR HAS BEEN CALCULATED: (PREDICTED-MEASURED/PREDICTED)^2.

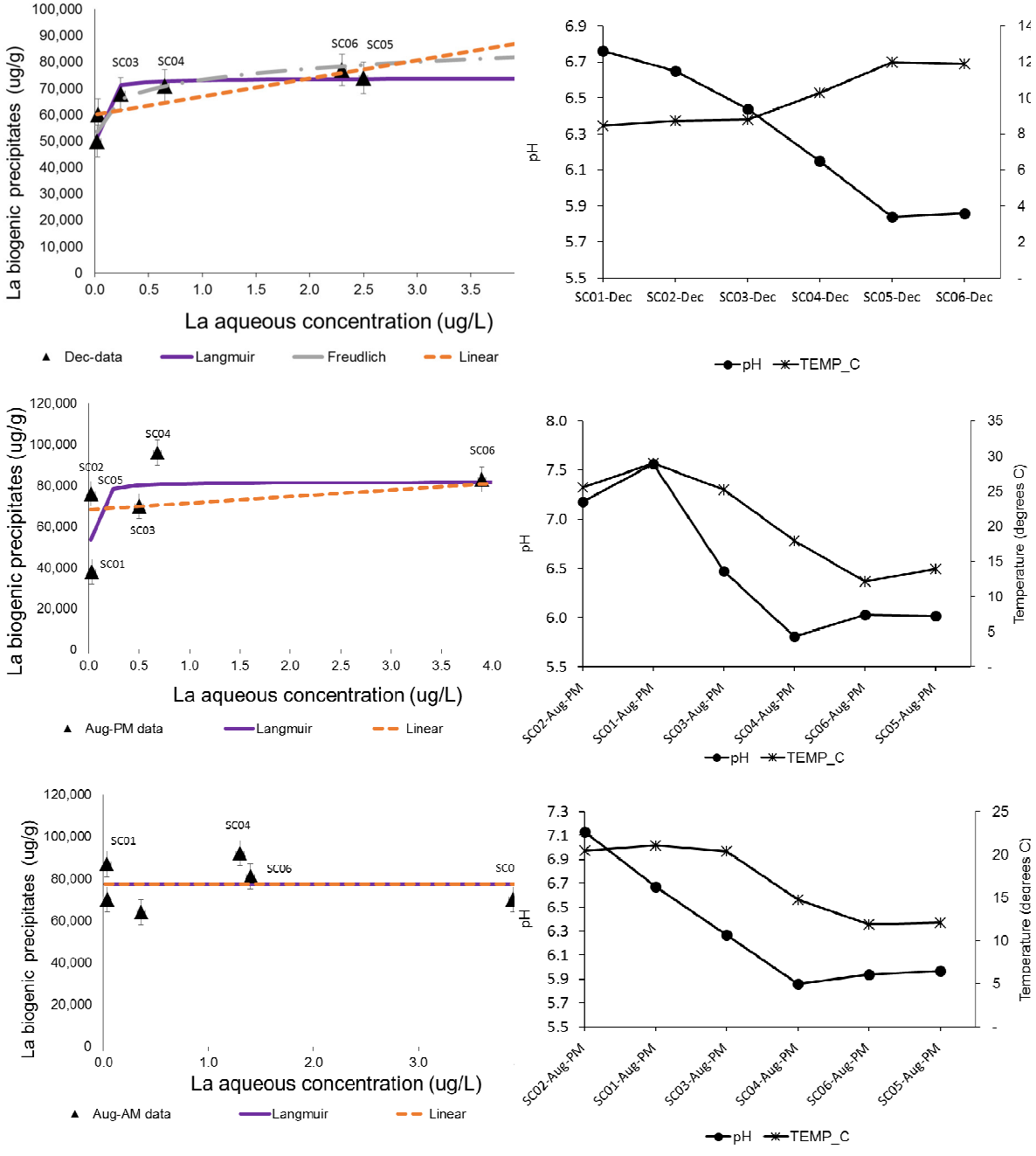

Figure 25 Linear, Freundlich and Langmuir Isotherms – La, December 2015, August-PM 2016 and August-Am 2016

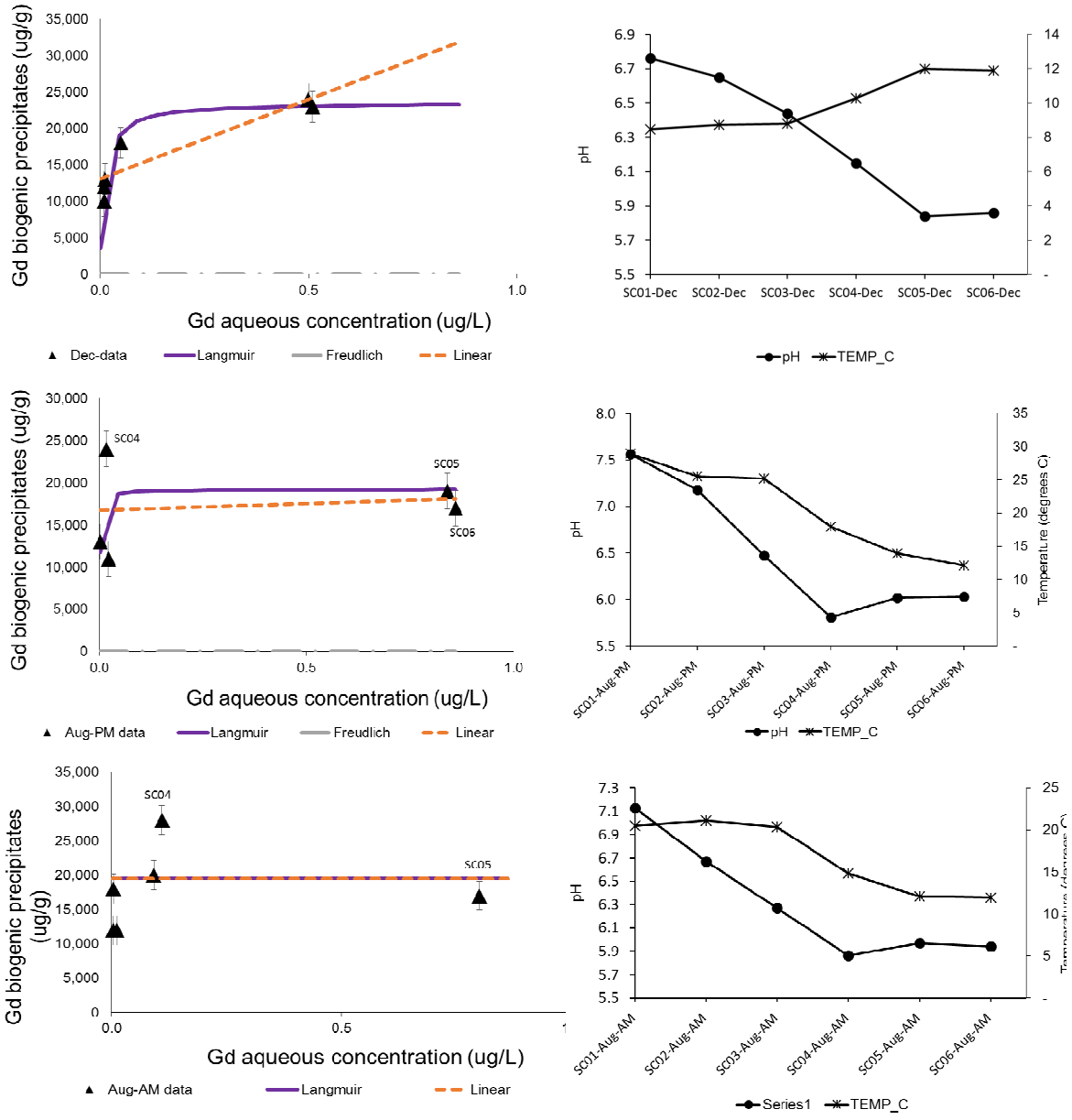

Figure 26 Linear, Freundlich and Langmuir Isotherms – Gd, December 2015, August-PM 2016 and August-Am 2016

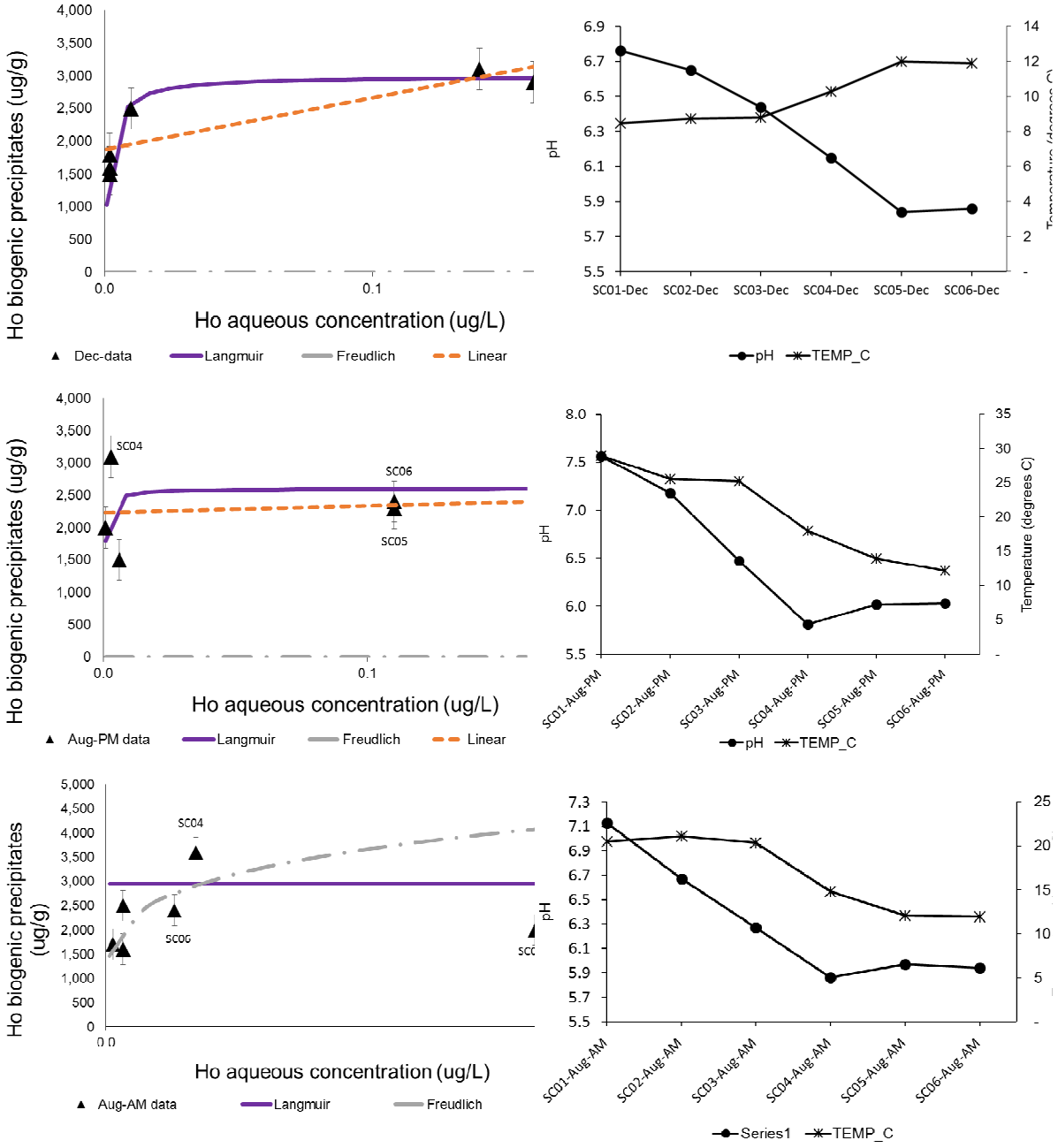

Figure 27 Linear, Freundlich and Langmuir Isotherms – Ho, December 2015, August-PM 2016 and August-Am 2016

3.2.6 Windermere Humic Aqueous Model, version 7 Modelling

3.2.6.1 Model assumption verification

Assumptions mentioned in Section 2.4.5 were verified as much as possible with collected data; however, detailed lab analysis to verify surface area, bulk density and details of the surface acid-base properties were beyond the scope of this analysis. Measuring zeta potential for the SC06 site in December (50% sample and 50% 0.01 M NaCl), the surface of the mixed material was observed to be positive when the pH reached 5.97. This indicates that the pristine point of zero charge (PPZC) is at or less than pH 5.97. Adapting the equation provided by Dzombak and Morel (equation 5.1), we can compare the pH at which the heterogeneous oxide surface is positive with the average PPZC calculated using the pk1 and pk2 values for the three modelled oxides (Equation 13). For the proposed model, we find a PPZCavg to be 6.15, which is fairly close to the measured value.

Equation 13 $PPZC_{avg} = [0.5(pK1_{Mn} + pK2_{Mn}) + 0.5(pK1_{Fe} + pK2_{Fe}) + 0.5(pK1_{Al} + pK2_{Al})]/3$

To ensure the model was working correctly for the oxidation of iron, the model was first run with just the Fe-oxides/HFO component. Redox potential (specifically, pe calculated from Eh using the Nernst equation) was used to calculate the speciation of iron Fe(II)/Fe(III). The ferrozine method was also used to determine Fe(II)/Fe(III) speciation; however, colorimetric data did not yield consistent values for the December sampling events. As a result, ferrozine measured iron Fe(II)/Fe(III) was compared with Fe(II)/Fe(III) modelled with pe.

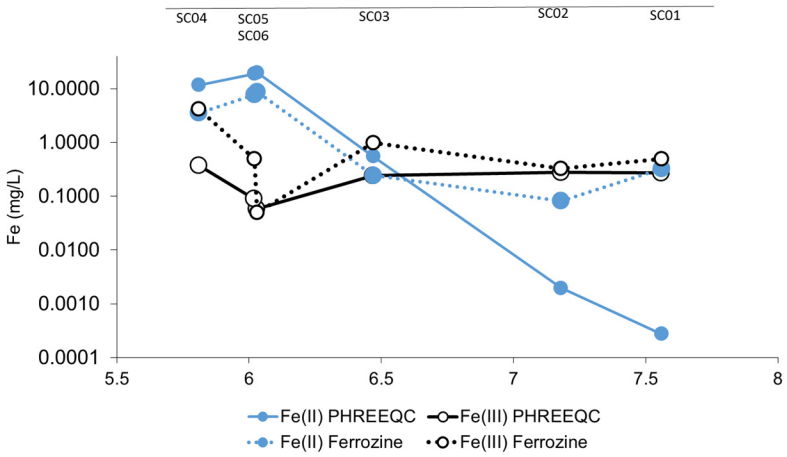

Figure 28 Comparison of ferrozine Fe(II)/Fe(III) and PHREEQC modelled Fe(II)/Fe(III)

The carbonate system with the WHAM model was input using pH and calculated pCO_2 (atm) values. Due to some uncertainty with measured particulate total organic carbon (TOC%) (referred to by Lofts and Tipping as particulate organic carbon [POC]) within the solid phase, two different WHAM models were created: model #1 contained input parameters for DOC, but no TOC and the second model contained inputs for both DOC and TOC. Consistent with the approach of Lofts and Tipping, and based on experimental data, 50% of DOC was measured was input as fulvic acid, with the remainder being inert. For TOC, 50% of measured values were assumed to contain carbon, and of this fraction 50% was input as fulvic acid and 50% as humic acid[71]. Although these are large assumptions regarding the organic phase, these were selected as the simple model equivalent of a complex surface.

The model was run to calculate charge balance and to use the Debye-Huckel activity correction equation. To check equilibrium assumptions, the model was run with the option to allow precipitation

of Fe and aluminum oxides; however, none were precipitated and the model was assumed to represent equilibrium conditions.

3.2.6.2 Summary of Results

Comparison of Kd values

Inputs for WHAM models 1 and 2 are contained within Appendix B1: Table B1.11, Table B1.12. Similar to the approach taken by Lofts and Tipping to verify metal binding observed in a field setting to an earlier version of the WHAM model, observed and modelled $\log_{10}$ partitioning coefficients (Kd) were compared to each other[71]. The equations used for this comparison include:

$$\textbf{Equation 14 Kd,obs} = \frac{[M]\boldsymbol{total\ aqua\ regia,obs}}{[M]\mathbf{0.45}\boldsymbol{\mu m\ filt,obs}}$$

$$\textbf{Equation 15 Kd,pred} = \frac{[M]\boldsymbol{part,pred}}{[M]\boldsymbol{filt,pred}}$$

Using the same definition as Lofts and Tipping, within the "Kd,pred" calculation, [M] 'filt' refers to the sum metal calculated as free/aqua ion, inorganic complexes and DOC-bound metal and [M] 'part' refers to the sum of metal calculated to be bound to TOC, manganese oxides, iron oxides and aluminum oxides[71]. Results from WHAM modelling indicate that there are two distinct populations of data: the SC01 to SC03 sites and the SC04 to SC06 sites (Figure 29). Both groupings of sites show quite similar results between the two models (Model 1 includes DOC but no TOC and Model 2 includes both DOC and TOC). All models show that observed partitioning coefficients at all sites are much greater than the predicted partitioning coefficients. This is not a kinetic model, and it does not take into account rates or duration of sorption. The observed partitioning coefficient represents the total REY sorbed to the mixed mineral biofilm over a long duration of time.

Proportion of solid bound to each phase

The WHAM assemblage model predicts the colloidal and particulate speciation of the metal of interest with respect to organic colloidal ligands, and inorganic and organic particulate phases. Modelled results for sites SC01 to SC03 show manganese oxides are responsible for almost the majority of the REY adsorption, with decreasing proportions of manganese oxides for HREYs and MREEs compared to LREEs (Table 37, Table 38, Table 39). In general, the SC04 to SC06 sites show a greater heterogeneity of binding sites, and specifically REY sorption to iron oxides, manganese oxides and colloidal and particulate organic matter. Consistently, SC05 seems to be the site with the greatest proportion of iron oxidation. HREYs and MREEs show greater partitioning to organic phases than LREEs. SC06, during all sampling events, and for all REYs shows the greatest association organic matter (both colloidal and particulate) out of all sites sampled.

When the model is allowed to precipitate aluminum and iron oxides, iron oxides can be observed to form throughout the system, decreasing from the inlet (SC06) to outlet (SC01). Aluminum oxides can only be observed to form at sites SC04 to SC06. Again, since the amount of sorption/precipitation is dependent on the rate of precipitation and duration of time allowed for this precipitation, numbers provided should be viewed in terms of their magnitude relative to each other, and not for their abosulte magnitude (Table 40).

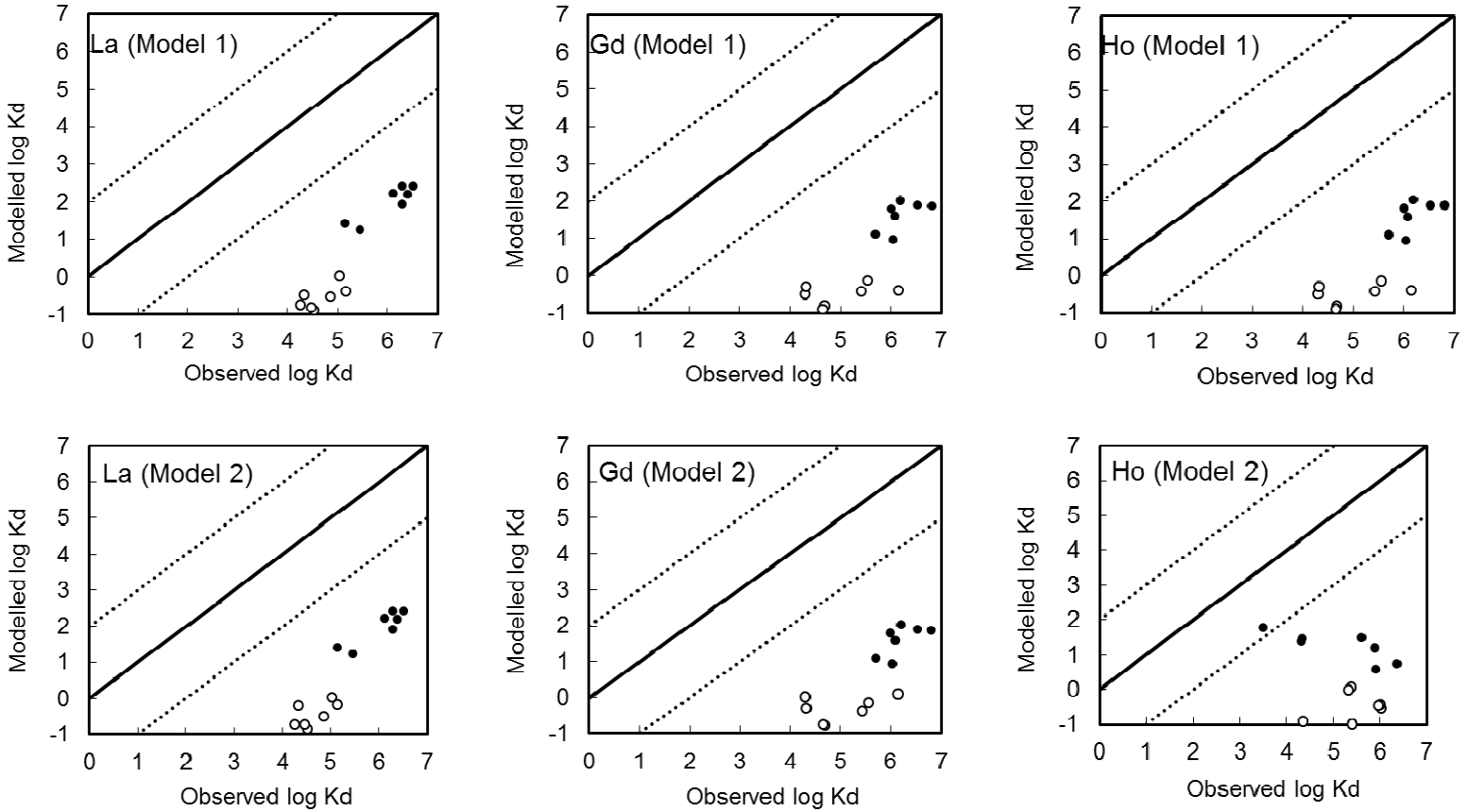

Figure 29 Comparison of observed log Kd value vs. WHAM Modelled log Kd value (solid black dots represent sites SC01-SC03 and hallow dots represent sites SC04-SC06)

Table 37 WHAM Model 2: proportion of binding to solid phase - La

Sites	pH	Colloidal FA : La	Part. HA : La	Part. FA : La	Part. FeOx : La	Part. MnOx : La	Part. AlOx : La
SC01-Aug-PM	7.6	0%	0%	0%	22%	78%	0%
SC01-Dec	6.8	0%	0%	0%	3%	97%	0%
SC02-Aug-PM	7.2	0%	0%	0%	6%	94%	0%
SC02-Aug-AM	6.7	0%	0%	0%	2%	98%	0%
SC02-Dec	6.7	0%	0%	0%	4%	96%	0%
SC03-Aug-PM	6.5	0%	0%	0%	7%	92%	0%
SC03-Dec	6.4	0%	0%	0%	7%	93%	0%
SC04-Aug-PM	5.8	6%	14%	18%	9%	40%	0%
SC04-Dec	6.2	3%	0%	0%	29%	65%	0%
SC05-Aug-PM	6.0	7%	2%	2%	30%	42%	0%
SC05-Aug-AM	6.0	4%	0%	0%	32%	32%	1%
SC05-Dec	5.8	14%	1%	2%	42%	25%	0%
SC06-Aug-PM	6.0	9%	14%	21%	12%	28%	1%
SC06-Dec	5.9	19%	5%	6%	27%	29%	0%

Table 38 WHAM Model 2: proportion of binding to solid phase - Gd

Sites	pH	Colloidal FA : Gd	Part. HA : Gd	Part. FA : Gd	Part. FeOx : Gd	Part. MnOx : Gd	Part. AlOx : Gd
SC01-Aug-PM	7.6	0%	0%	0%	68%	30%	1%
SC01-Dec	6.8	0%	0%	0%	9%	91%	0%
SC02-Aug-PM	7.2	0%	0%	0%	24%	75%	1%
SC02-Aug-AM	6.7	0%	0%	0%	6%	94%	0%
SC02-Dec	6.7	0%	0%	0%	11%	88%	0%
SC03-Aug-PM	6.5	1%	0%	0%	23%	76%	0%
SC03-Dec	6.4	1%	0%	0%	17%	82%	0%
SC04-Aug-PM	5.8	12%	24%	37%	10%	17%	1%
SC04-Dec	6.2	8%	1%	1%	51%	40%	0%
SC05-Aug-PM	6.0	18%	4%	6%	48%	23%	1%
SC05-Aug-AM	6.0	12%	0%	0%	59%	21%	3%
SC05-Dec	5.8	30%	2%	3%	55%	12%	0%
SC06-Aug-PM	6.0	16%	22%	37%	13%	11%	1%
SC06-Dec	5.9	39%	8%	13%	32%	13%	0%

Table 39 WHAM Model 2: proportion of binding to solid phase - Ho

Sites	pH	Colloidal FA : Ho	Part. HA : Ho	Part. FA : Ho	Part. FeOx : Ho	Part. MnOx : Ho	Part. AlOx : Ho
SC01-Aug-PM	7.6	0%	0%	0%	80%	18%	2%
SC01-Dec	6.8	0%	0%	0%	13%	86%	0%
SC02-Aug-PM	7.2	0%	0%	0%	36%	62%	2%
SC02-Aug-AM	6.7	0%	0%	0%	10%	90%	0%
SC02-Dec	6.7	0%	0%	0%	16%	83%	0%
SC03-Aug-PM	6.5	1%	0%	0%	33%	66%	0%
SC03-Dec	6.4	2%	0%	0%	23%	74%	0%
SC04-Aug-PM	5.8	14%	29%	44%	7%	8%	1%
SC04-Dec	6.2	17%	1%	2%	53%	29%	1%
SC05-Aug-PM	6.0	30%	6%	10%	42%	14%	2%
SC05-Aug-AM	6.0	22%	0%	0%	59%	15%	5%
SC05-Dec	5.8	46%	3%	5%	46%	7%	0%
SC06-Aug-PM	6.0	19%	26%	43%	8%	5%	1%
SC06-Dec	5.9	52%	11%	17%	23%	6%	0%

Table 40 WHAM Model 2: formation of aluminum and iron oxide

Site	Al(OH)3 precipitate (M)	Fe(III)(OH)3 precipitate (M)
SC01-Aug-PM	0	9.7E-07
SC01-Dec	0	4.3E-06
SC02-Aug-PM	0	1.0E-06
SC02-Aug-AM	0	1.0E-06
SC02-Dec	0	7.2E-06
SC03-Aug-PM	0	2.8E-06
SC03-Dec	0	1.8E-05
SC04-Aug-PM	3.5E-06	4.3E-05
SC04-Dec	0	3.3E-05
SC05-Aug-PM	5.6E-07	6.8E-05
SC05-Aug-AM	5.1E-06	7.5E-05
SC05-Dec	3.3E-06	6.1E-05
SC06-Aug-PM	6.2E-06	7.2E-05
SC06-Dec	4.0E-06	6.1E-05

4 – DISCUSSION

The focus of this section is to discuss the water and biofilm chemistry analyzed in comparison to modelled results, to understand the major geochemical processes taking place, and REY speciation within the aqueous and solid phase. Screening level review of a variety of water and biofilm sites in North and South America indicated that coal mine drainage sites contained the greatest accumulations of REYs. Subsequently, detailed study was completed of a passive mine treatment site.

4.1 BULK WATER SAMPLE CHEMICAL ANALYSIS AND MODELLING

Water chemistry plays a key role to indicate and determine what geochemical processes are occurring within the system, such as: oxidation and reduction, mineral dissolution and precipitation, aqueous-complexation and surface-complexation. Major trends within the water sample chemical analysis include:

- Elevated concentrations of SO_4, Fe, Mn and Al, and changes in aqueous Fe and Al by three orders of magnitude within the system
- Elevated trace metals including: Sr, Zn, Ni, Co and Cu
- Decreasing gradient from high pCO_2 values at the mine discharge point, to pCO_2 values close to atmospheric levels at the exit of treatment system
- Increasing gradient from low DO levels (0.57 – 0.87 mg/L) at the mine discharge point, to saturated or almost saturated DO levels at exit of treatment system
- Increasing gradient from low to high pe levels
- A general gradient of increasing pH values; however, the lowest pH values observed at SC05 and SC04, depending on sampling season
- Aqueous sum of REY (including Sc) concentrations are elevated (26 µg/L to 0.8 µg/L) and generally decrease by two orders of magnitude within the treatment system
- Aqueous water content of REYs is strongly influenced by pH, with greatest amounts of aqueous REYs during acidic conditions.
- Unlike the majority of samples analyzed in the site overview, pH does not seem to be a large predictor for quantities of solid-phase REY enrichment. In fact, the greatest REY concentrations occur at lowest pH.
- General HREY enrichment over LREE enrichment was observed, and upstream sites show little to no LREE fractionation, whereas, downstream sites show greater LREE fractionation
- Positive La, Eu, Y and Y/Ho fractionation calculated at all sites, in addition to potential positive Tm and Lu anomalies and negative Er anomalies observed in NASC plots.
- Positive Gd anomalies noted at upper sites (SC06, SC05, SC04) and a negative Gd anomaly was noted at the lower sites (SC01, SC02, and SC03)

4.1.1 Major Processes: oxidation of pyritic minerals and carbon dioxide degassing

In 2008, Cravotta completed a comprehensive review of the quantities, correlations and geochemical controls of dissolved metals in bituminous and anthracite coal-mine discharges[72]. Cravotta's work provides an important baseline to understand the major geochemical processes at work in bituminous and anthracite CMD-affected systems and provides a direct comparison to samples collected in a similar location. Stewart and colleagues recently examined REY concentrations within CMD and predominately bituminous coal sites[4]. In general, both bituminous and anthracite CMD is characterized by high amounts of sulphate, iron, manganese, aluminum and other trace metals, such as As, Cd, Pb, Se, and Zn, that results from dissolution of carbonate, silicate and oxide minerals by hydrogen sulphide (H_2SO_4), generated by the oxidation of pyritic and sulfidic minerals[72]. At the Silver Creek site, dissolved

concentrations of SO_4, Fe, Mn and Al are elevated, but within the lower range of samples collected by Cravotta and Stewart[4,72]. The most abundant trace metals in the Silver Creek system were: strontium (67-880 µg/L), zinc (0.8 - 780 µg/L), nickel (6.6 to 230 µg/L), cobalt (5.4 to 150 µg/L) and copper (0.009 to 18 mg/L). With the exception of strontium, this follows closely the most abundant trace elements noted by Cravotta[72]. In comparison to pH values sampled by Cravotta (pH 2.7 to 7.3), the Silver Creek site samples slightly exceed, and are on the higher pH range (pH 5.81 to 7.56) when compared with the pH[72].

During all sampling events, pH generally increased from slightly acidic (pH 5.86-6.03) at the inflow of the passive treatment system to circumneutral at the outlet (pH 6.76-7.56). During the December sampling event, sites SC06 and SC05 measured the lowest pH. In August, the lowest pH during both the morning and afternoon sampling events was recorded at SC04, with sites SC06 and SC05 showing very similar pH values. During all sampling events, DIC decreased from approximately 40 mg/L at the inflow to approximately 6 mg/L at the outflow, while changes in DOC showed smaller or non-existent trends. Diurnal and seasonal changes in pH were noted. Trends in pH and DIC can be partially explained by the degassing of CO_2. During sampling of 140 abandoned, discharging coal mines, Cravotta found $pC0_2$ values in CMD samples were elevated, and ranged between $10^{-2.45}$ to $10^{-0.54}$ atm[72]. The $pC0_2$ values measured at the Silver Creek sampling site are very similar, and fall just below, and within the lower end of this range ($10^{-1.1}$ to $10^{-3.3}$ atm)[72]. Measured pCO_2 values are highest at the mine discharge point and increase as water flows downstream as water equilibrates with pCO_2 in the atmosphere. Dissolved oxygen levels show an inverse pattern to pCO_2, with lowest DO concentrations recorded at the mine discharge point (0.57 to 0.87 mg/L or ~5% to 7%) and highest dissolved oxygen levels recorded at the outflow point as anoxic groundwater equilibrate with oxygen in the atmosphere, and reach close to, or above saturation (termed "O_2 ingassing"). With the exception of SC04, $pC0_2$ values are slightly lower than during the August afternoon sampling event. At sites SC06 and SC05, pCO_2 values are reduced approximately 65%. Further downstream, pCO_2 values are reduced by 52%, 27% and 11% between the December and August sampling events at sites SC03, SC02 and SC01, respectively. This reduction in CO_2 could be a result of biologically mediated photosynthesis that consumes CO_2 and would be expected to have increased rates during summer months. Temperatures were observed to show the greatest difference between August and December sampling events at sites SC01, SC02 and SC03. These sites showed high to supersaturation of oxygen.

4.1.2 Measured REY aqueous chemistry

Major ion chemistry at the site fell within the top quadrant of the trilinear piper plot, which indicates enrichment of calcium, magnesium and sulphate, characteristic of waters associated with mine drainage. Sum of aqueous REY concentrations ranged from ~24 µg/L at the passive treatment inflow, to ~0.8 µg/L at the treatment system outflow, with strong correlations between the sum of REYs and all LREEs, MREEs and HREYs except Ho, Er, Sc and Lu. These aqueous concentrations of REYs are two orders of magnitude lower than those observed by Ayora and colleagues within the Iberian Pyrite Belt (3,500 µg/L or 3.5 mg/L to 7,900 µg/L to 7.9 mg/L)[1]. In addition, there were many differences between *in situ* chemistry and major ion chemistry at this site: the pH measured at Ayora's Monte Romera and Almagrera sites were much lower (pH 2.6-2.7 vs. 5.86-7.56 at Silver Creek), sulphate concentrations were much higher (3,500 mgL to 1,700 mg/L vs. 180-200 mg/L at Silver Creek), aqueous iron concentrations were higher (161 mg/L and 744 mg/L vs. 0.012-17 mg/ Fe at Silver Creek) and aqueous aluminum was also much higher (128 – 251 mg/L vs. 0.12 to 0.0045 mg/L at Silver Creek). Major ion chemistry at the Silver Creek site was more similar to results observed by Stewart and colleagues. Most sites sampled by Stewart and colleagues had a pH range between 4.4 to 6.6,

with aluminum concentrations ranging from 0.1 mg/L to 1.3 mg/L, although Fe(II) and sulphate concentrations were higher in the sites sampled by Stewart, when compared to Silver Creek. Stewart and colleagues measured the sum of REY at most sites to equal between 0.29 µg/L to 32 µg/L; however, certain sites had measured aqueous concentrations up to 505 µg/L and 1,134 µg/L sum of REY. Based on this comparison to other sites where aqueous REYs have been identified as an alternative source of REYs, it is unlikely that aqueous REYs at Silver Creek represent an economic source of REYs.

Diurnal variation in REY concentration was noted to occur within the Silver Creek passive treatment system; however, inconsistent diurnal differences were noted. Site SC06 showed increases in the August afternoon sampling event that ranged from 127% to 169% above concentrations measured in the morning sampling event. These results were consistent with results obtained during field studies completed by Vesper and Smilley and Gammons[22,23]. Vesper and Smilley found that concentrations of REY increased up to 863% during the night, and decreased during the day[22]. They found these cycles had an inverse relationship with temperature, and no discernable cycle was noted for pH. The hypothesized mechanism was increased scavenging of iron oxides during the day, due to the increased rate of Fe(II) oxidation in warmer water. Gammons and colleagues also found that concentrations of dissolved REE were 2.9 to 9.4 fold greater in the early morning compared to the late afternoon[23]. In this study, these observations were also hypothesized to occur as a result of increased daytime temperature and scavenging of iron and aluminum oxides. At Silver Creek, SC04 and SC01 showed an opposite trend to that observed at SC06, indicating a different mechanism may be at work sequestering REYs. In addition, sites SC03 and SC02 showed litte diurnal variability, possibly indicating less of an influence on REY concentrations from iron oxides.

4.1.3 Aqueous REY speciation

PHREEQC modelling completed for water within the Silver Creek drainage indicated sulphate complexes are generally the most abundant inorganic REY complex; however, as pH becomes circumneutral (pH 6.8-7.2), carbonate-REY complexes play a dominant role. Modelling for Gd and Ce indicate these metals are more often found as aqua/free ions, which may provide an explanation for these anomalies. When organic matter was introduced and aqueous speciation was determined in WHAM, colloidal organic complexes were determined to play a key role. To consider the sorption of REYs to humic substances (fulvic and humic acids), linear free energy relationships are used to determine metal-humic acid binding parameters. Colloidal organics are predicted to have an inverse relationship with sulphate complexes and are expected to almost completely control availability of HREYs (significant, but less influence on LREYs).

The theory of hard and soft acids and bases is used to determine REY aqueous speciation; this well-established theory predicts that hard ions, such as trivalent REYs, prefer to bind with other hard ligands containing electronegative donor atoms (e.g., hydroxide, sulphate, phosphate, fluoride etc.)[29,73]. As a result, bonds formed by REYs are predominately electrostatic instead of covalent. Stability constants differ for REYs, and are dependent on the ligand. Noteably, the stability constant for both carbonate, phosphate and hydroxide increase with atomic number, while the stability constant of sulphate complexes decrease with atomic number (Figure 30).

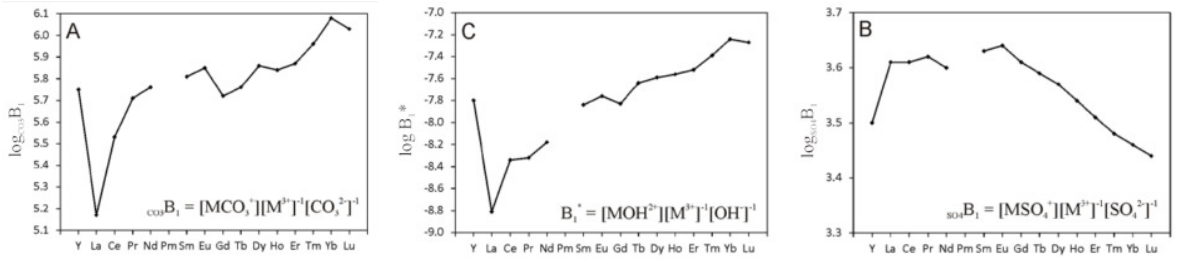

Figure 30 Relevant stability constants that influence aqueous speciation of REYs (source: Purdy and Jamieson)[29]

The Silver Creek sites are complicated because a number of different gradients that affect aqueous REY speciation occur at once, for example: a gradient of high pCO2 and high DIC to low pCO2 and DIC (affects binding to CO_3). A gradient of low pH to high pH (affects biding to OH^-), fairly constant sulphate levels and during the winter, there seems to be a gradient of organic carbon concentrations from inflow to outflow. The dominance of REY-sulphate complexes is consistent with the site water chemistry, as sulphate is by far the dominant anion. In addition, dominance of REY-sulphate complexes is consistent with observation of REY aqueous speciation at other low pH mining-affected areas[5,51]. The important role of organics in aqueous REY speciation has been observed in many natural waters, and several pH neutral mine sites[48,74].

4.2 BIOFILM SAMPLE CHEMICAL ANALYSIS AND MODELLING

REY concentrations within the heterogeneous biogenic precipitates does not follow the pattern expected by pH-dependent adsorption. For sites with a distinct pH gradient, pH has been found to the controlling factor of solid REY concentrations[4,11,19,75]. Within the aqueous phase, peak aqueous REY concentrations are noted at the most upstream sampling site, closest to the discharge with the lowest pH (SC06). This is consistent with previous literature and expectations of enhanced solubility of REYs at low pH. The concentration decrease for aqueous REYs cannot be explained exclusively by dilution, and is likely explained by concentration-dependent adsorption. For example, individual REY concentrations decrease from SC04 to SC03 anywhere from 4 to 10X, while the volume in SC03 is less than twice the volume of SC04. From aqueous data alone, adsorption or precipitation there is evidence that adsorption and participating play important roles in determining aqueous REY concentrations. Within the precipitates, peak REY concentrations occur at either SC05 or SC04, which supports the hypothesis that adsorption or precipitation may be occurring. Sum of REY values for the biogenic precipitates ranges from 339 mg/L to 724 mg/L, with Ce, Lu, La, and Y, as the most abundant REYs (in that order).

When compared to the recent paper by Stewart and colleagues, in a similar area, REY values at the Silver Creek treatment pond are within the range of values presented, but remain on the low end of precipitates sampled[4]. Note that comparison of all collected REYs with the Stewart paper is not possible because not all REYs are presented. When Silver Creek values were compared to the computed REY_2O_3 oxides completed by Ayora and colleagues (0.23% ReY_2O_3, 2,300 mg/L), however, the Silver Creek biogenic precipitates were substantially lower[1]. Ayora and colleagues reported that the 50th percentile of REY grades for working REY mines and prospects is 0.61% REY_2O_3. When maximum values in Silver Creek biofilm (~725 mg/kg dry weight) are compared to grades of ionic clay deposits (0.05-0.3% %wt), Silver Creek precipitates remain a 'borderline' economic.

Early laboratory and field experiments identified REY partitioning to iron oxides as the predominant mechanism of solid-phase enrichment in iron-rich precipitates[11,18,19]. Specifically, schwertmannite was

commonly identified as the predominant iron mineral present in these iron-rich systems that showed greatest REY solid accumulations[11,19]. Recently, Ayora and colleagues examined REY aqueous chemistry within an iron and aluminum-rich acid mine passive treatment system with schwertmannite present as the most common iron mineral[1]. Results from Ayora's field and laboratory work indicated that REYs accumulated exclusively within the aluminum-sulphate mineral present (basaluminite) and did not accumulate in the schwertmannite[1]. In addition, there is come debate on the role of organic matter in both aqueous and solid REY speciation. Previous studies have indicate REY-organic aqueous complexes form the majority of REY colloidal material; however, there is also debate that current modelling programs overestimate the proportion of REY-organic complexes[24,25]. The following sections will examine chemical and modelling data to determine REY speciation.

4.2.1 Normative Oxides

Normative oxides were calculated for the aqua regia digestion, and normative oxides at certain sites do not sum to 100%. Complete digestions with aqua regia and nitric peroxide digestion were compared and found to be identical; however, both methods are known to have difficulty extracting silicates. REYs are known to co-precipitate with silicates, and therefore, the aqua regia digestion method may underestimate both total silicates, and total REYs. Hydrofluoric (HF) acid is often the digestion method of choice for silicates; however, HF cannot be used to determine total REY content, due to its high affinity for REYs. A fusion technique to digest biogenic precipitates is recommended to determine the total amount of REYs. Alternately, it is possible that the organic fraction has not been properly extracted due to its close association with biogenic iron and manganese oxides.

4.2.2 Non-sequential Iron Digestion

Non-sequential iron digestions were completed using both dithionate and oxalate. Both digestions overestimated the amount of iron, manganese and rare earth elements within their respective digestion. There are two primary hypothesis for this occurrence: 1) organic ions amplified the ICP-MS and ICP-ES signal when compared to the aqua regia sample, and 2) chlorides present in the aqua regia sample may have suppressed the REY signal. Chloride concentrations are very low within the samples, and the aqua regia digestion results were found to be very similar to results for the nitric acid and peroxide digestions. As a result, it is unlikely that chlorides present in the aqua regia sample suppressed the REY signal. It is possible that organic ions amplified the ICP-MS and ICP-ES signal. Prior to further use of the oxalate data, it is suggested that this data be re-run in comparison to internal standards.

4.2.3 REY solid speciation: precipitation as REY mineral/ REY co-precipitation?

Results from X-Ray Spectroscopy (EDX) found precipitates were composed primarily of iron (~42% to 68%) and oxygen (22%-28%), with small amounts of aluminum and silica (2% to 5%). Rare earth elements were not observed in large enough quantities for detection. Aqua regia and nitric-peroxide digetsions indicate similar proportions of iron. EDS results could be interpreted that REYs were present in concentrated amounts below detection, or these results could indicate that REY sequestration within the iron-rich biofilms is more likely to occur via a spatially disparate process like sorption vs. precipitation.

Thermodynamic modelling was completed in PHREEQC-i to determine if precipitation of REY minerals would be expected to occur, given the aqueous chemistry. Saturation indices for a variety of REY-minerals were calculated (see Table 23), and REY-phosphate minerals (1:1 molar ratio) were the only minerals expected to precipitate. Due to the low concentration of phosphate (8.0E-4 mmol to 1.3E-2

mmol), it is expected that REY precipitation with phosphate minerals composes a small amount of REY in the solid phase. Based on the above chemical and modelling results, it is hypothesized that enriched REY concentrations within the mineral-rich biofilm are not a result of precipitation.

4.2.4 REY solid speciation: association with organic material?

Organic matter plays a key role in rare earth element speciation within aqueous environments and within solid environments. Davranche and colleagues examined soil phases with Fe(III)-oxyhydroxides, organic matter or mixed Fe-OM particles[76]. Their research determined that REYs and other trace elements preferentially bound to organic matter and was the main source of REEs during wetland soil reduction. In addition, previous studies have indicated REY-organic aqueous complexes form the majority of REY colloidal material; however, there is also debate that current modelling programs overestimate the proportion of REY-organic complexes[24,25]. Work completed by Tosiani and colleagues identified organic carbon as key player in the sequestration of REYs to the particulate phase and identified a negative linear relationship between the partitioning of dissolved REYs to suspended REYs vs. dissolved organic carbon (DOC)[16]. Tang and Johannesson found that in natural waters with high molecular weight dissolved organic matter (e.g., humic acid), MREE-enriched water predominates. In contrast, water dominated by low molecular weight organic matter (e.g., fulvic acids), HREY-enriched water dominates[38]. Water within the Silver Creek treatment facility tends to be enriched both MREYs and HREYs and therefore, from the REY fractionation alone, it is difficult to discern further information about the organic content.

<u>REY patterns with solid OC and DC:</u>

The percentage of OC and TC (%) within the mineralized biofilm were plotted vs. the sum of REY content. Results indicate that sites with TC and OC less than 5% show a wide range of REY concentrations, with no discernable trends. Two samples from the afternoon August sampling event show elevated concentrations of TC, which was calculated to be almost exclusively OC (SC06 and SC04). These samples show an increase in REY concentration with increased organics. Two other samples fall within the linear regression line associated with the two organic enriched sites. Additional samples, however, are required to determine if/when an association between REYs and organic materials does occur.

<u>Organic non-sequential extractions:</u>

There remains debate on the role of organics on the speciation of REYs within both the aqueous and solid phases. A non-sequential extraction that isolated the portion of REYs associated with the organic fraction was completed; however, results were too variable to be presented here or further discussed. It is hypothesized that the extremely tight associated of organics with iron minerals limit efficacy of the non-sequential organic extractions.

<u>REY fractionation:</u>

Normalized REY patterns for the biogenic precipitates show a conserved MREE enrichment, which can be confirmed visually and reinforced through calculation of the Gdn/Ybn ratio (all sites >1.8). MREE enrichment within sites downstream of acid rock drainage has been observed by a number of different authors[18,37,77]. There currently exists no definitive explanation of MREE enrichment. Calculated anomalies for the biogenic precipitate are muted compared to the water samples. For example, the La, Ce, and Eu anomaly calculations all hover around 1.0 and 1.1. Gd and Y anomaly calculations are more positive.

WHAM model:

Results of the WHAM model indicate that sorption with colloidal and particulate organic matter occurs at the most upstream sites (SC05-SC04). In addition, HREYs and MREEs tend to have greater association with organic matter than LREEs. Specifically, colloidal fulvic acid shows the greatest affinity for REYs. The large differences in observed and predicted Kd values for sites SC04 to SC06 that contained the most organics indicates that the WHAM model may be over predicting the amount of REYs associated with colloidal organic complexes. It is difficult to understand the role of organics, however, because this model is not kinetic, and also because there is particularly high uncertainty associated with the measurements of TOC within the biofilm sampled.

4.2.5 REY solid speciation: association with manganese oxides?

Aqua Regia digestion and Correlations:

Although aqueous manganese concentrations were not elevated within the Silver Creek system like iron and aluminum, aqua regia digestions completed at the Silver Creek site revealed large increases in manganese concentrations at site SC01-SC03, closest to the discharge. Solid concentrations of manganese increased from ~200-1000 mg/kd dry weight to a maximum of 61,000 mg/kd dry weight. In addition, binding affinities for manganese oxides are greater than for both iron and aluminum oxides. Sorption to manganese is not only preferred over these oxides, but it occurs at a lower pH[78]. Manganese oxides are frequently associated with iron oxides, and the rates of Mn(II) oxidation are catalyzed in the presence of various amorphous iron oxides[79]. In addition, microbes are key catalysts of manganese oxidation. Strong correlations between manganese and REY concentration in solid phase were not observed. Recent previous studies that have focused on enrichment of REYs within oxide phases have focused primarily on iron and aluminum, not manganese[1,4].

WHAM Modelling:

WHAM modelling was completed at Silver Creek for the August and December sampling events. This surface assemblage model predicted manganese oxides would be responsible for a majority of the sorption to solid phase at sites SC01 to SC03. At sites upstream, the WHAM model predicted manganese would remain an important player in REY adsorption, together with iron and the particulate and colloidal organics. Again this model is expected to be augmented by a kinetic model, which will provide further information. Manganese and ferromanganese oxides within the ocean have been observed to accumulate REYs at extremely large quantities and are also considered potentially mine-able sources of REYs[80]. Freshwater manganese nodules have also been identified and studies for a significant period of time[81].

4.2.6 REY solid speciation: association with aluminum oxides / sulphates?

Correlation data and molar ratios:

Correlation plots completed for the Silver Creek site indicate that there are two sup-populations of precipitate data: (1) SC01, SC02 and SC03 and (2) SC04, SC05 and SC06. The SC01, SC02, SC03 sites are highly positively correlated with aluminum, whereas there is a negative correlation of the SC04 to SC06 sites with aluminum (one outlier). The SC04 to SC06 sites are modestly positively correlated with iron, whereas the SC01 to SC03 sites have a slight negative correlation.

Molar ratios were calculated to provide an indication of the role of co-precipitation in the sequestration of REY minerals to the solid phase. Sites SC06, SC05 and SC04 showed the greatest solid phase enrichments of REYs and also are the sites with the highest Al:S. Al:Ca and Al:Si ratios. It is also

important to note that since aluminum is a trivalent metal, there is also some possibility that aluminum is simply behaving similarly to REYs, which explains its correlation.

Activity data:

To determine at what sites aluminum minerals may form, a solubility plot of Al^{3+} was created. Unlike the iron plots, pe does not need to be plotted, just pH and aluminum activity. Solubility charts are used to determine the least stable minerals, which are the first to form and also to solubilize. The solubility of aluminum is lowest at lowest temperature. Based on plotting the water chemistry data, measured aqueous concentrations are aluminum are slightly below the concentration they would be expected to precipitate. It is possible that aluminum concentrations reach their maximum at times of the day not sampled, or that there is another mechanisms for solubility control for aluminum.

Site	pH	Al^{+3} (log activity)	Temp (˚C)
SC06-Aug-PM	6.03	-6.58	11.93
SC05-Aug-AM	5.97	-6.67	12.1
SC06-Dec	5.86	-6.72	11.89
SC05-Dec	5.84	-6.80	11.98
SC04-Aug-PM	5.81	-7.13	17.93
SC05-Aug-PM	6.02	-7.66	13.91
SC04-Aug-AM	5.86	-7.85	14.79
SC06-Aug-AM	5.94	-8.15	11.93
SC03-Dec	6.44	-8.76	8.81
SC04-Dec	6.15	-8.80	10.28
SC03-Aug-PM	6.47	-9.47	25.23
SC03-Aug-AM	6.27	-9.64	20.37
SC01-Dec	6.76	-11.11	8.46
SC02-Dec	6.65	-11.22	8.73
SC01-Aug-AM	7.13	-11.67	20.47
SC02-Aug-AM	6.67	-12.55	21.08
SC02-Aug-PM	7.18	-12.94	25.55
SC01-Aug-PM	7.56	-16.43	28.97

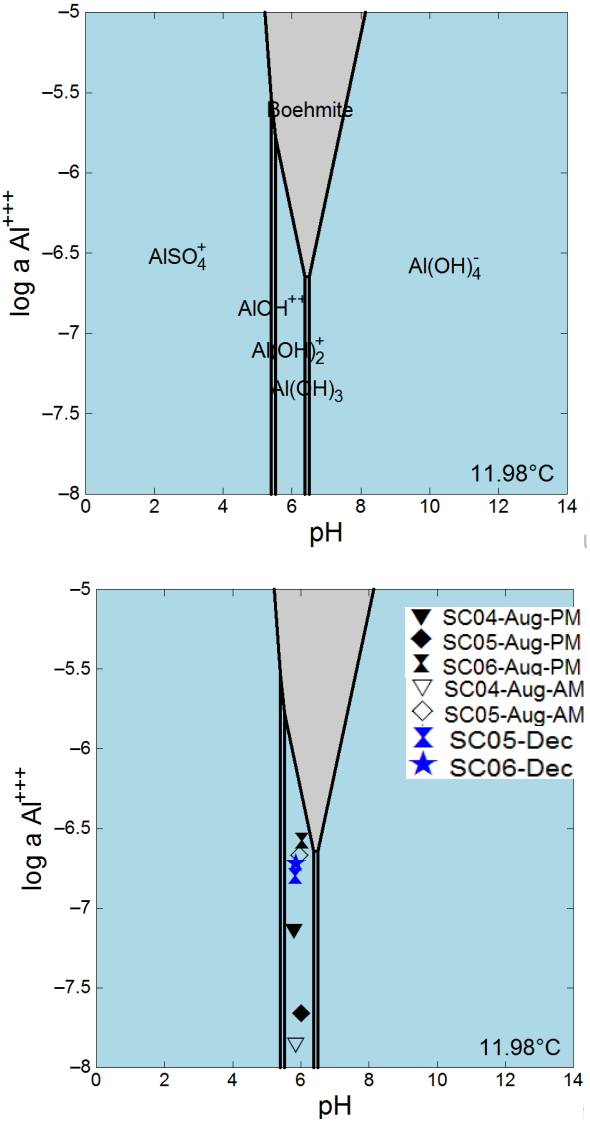

NOTES:

1. FIGURE WERE MADE IN GEOCHEMISTS WORKBENCH.
2. INPUTS FOR SOLUBILIT DIAGRAM: -2.88 LOG ACTIVITY SO_4^{2-}; TEMP=10.28˚C; LOG ACTIVITY O2=-28

Figure 31 Solubility plot for Al^{3+} minerals

Thermodynamic Modelling:

Chemical speciation modelling for a variety of Mn, Fe, and Al minerals indicated that several aluminum and iron minerals were thermodynamically favoured. Al minerals that may be expected to form thermodynamically include: alunite, basaluminite, diapsore and gibbsite. Basaluminite is of particular interest, since another research group (Ayora and colleagues) found that REYs were associated with the basaluminite mineral, while in the presence of iron oxides[1,82].

WHAM Modelling:

The WHAM program assigns a relatively low binding affinity of REYs to aluminum hydroxides. In fact, colloidal and particulate organic matter, manganese and iron all have greater affinities for REY. As a result the WHAM model does not predict sorption to aluminum oxides to be important for REY sequestration. It is important to note that this does not mean that precipitation of aluminum minerals may be involved.

4.2.7 REY solid speciation: association with iron minerals / oxides?

Non-sequential iron digestion:

Oxalate and dithionite extractions were completed to quantify the amount of REYs associated with the iron phase. Oxalate and dithionite are expected to extract iron from both crystalline and amorphous iron phases. Prior to work completed by Kostka and Luther, oxalate extractions were expected to extract only amorphous iron; however, Kostka and Luther (and subsequent authors) found no significant difference between extractions completed with oxalate and dithionite[59,83]. Results in this study matched those found by Kostka and Luther: both dithionite and oxalate extractions are effective at extracting both crystalline and iron minerals and were similar in value. Although the dithionite extraction is expected to be more effective at extracting goethite and hematite, our results indicate that either extraction does equally well extracting crystalline iron oxides. The average relative percent difference (RPD) for REYs extracted using the two techniques was 6% (two different samples; 32 different sampling sites); however, RPD for a number of heavy rare earth elements ranged from 29% to 40% for one set of samples.

Both dithionite and oxalate extractions completed in this study were observed to extract a greater proportion of rare earth elements than the aqua regia digestion. In addition, oxalate extractions completed at all sites during the December and August sampling events show greater amounts of aluminum, iron, manganese and sulphur may be extracted at higher quantities using the oxalate extraction when compared with the aqua regia digestion. Kostka and Luther determined that Fe(II) may be released by extracting Fe-containing silicates with oxalate, without any additional Fe(II), and that Fe(II) may be present in sediments even after air drying[59]. Aqua regia digestions are known to be partial in their digestion and not able to break down refractory compounds (e.g., SiO_2, TiO_2, Al_2O_3), but provide a good representation of elements that would be mobile in aqueous systems. Therefore, it is expected that the greater concentrations of Al, Fe, M, S and REYs within the oxalate digestions may result from incomplete digestion of refractory compounds within the aqua regia digestions, in addition to laboratory extraction variability.

Results of oxalate and dithionite extractions indicate that a majority of the iron, aluminum, manganese, sulphur and REYs are contained within the oxalate-extractable phase. Unfortunately, these results do not allow differentiation between REY to aluminum, manganese or iron-bearing fractions.

Thermodynamic modelling:

Aqueous aluminum and iron concentrations were observed to change by two to three orders of magnitude within the treatment system. Results of the thermodynamic modelling indicate that aluminum oxide minerals preferentially form within sites SC06, SC05 and SC04, while iron minerals are shown to reach saturation throughout the treatment system. Modelling indicates a variety of iron minerals are expected to form throughout the treatment system. Schwertmannite and ferrihydrite have been identified by previous studies of streamwater that receives acid and coal mine drainage as the most frequently observed precipitating iron minerals[72,82,84,85]. In addition, goethite may also be expected to simultaneously precipitate with schwertmannite when sulphate concentrations are low (SO_4/Fe molar ratio < 1.5), or goethite may occur within these samples by alteration from schwertmannite[84]. Both schwertmannite and ferrihydrite are poorly crystalline iron minerals that can have variable chemical composition, which affects their solubility. For example, schwertmannite, has the chemical formula: $Fe_8O_8(OH)_{8-2x}(SO4)_x * nH_2O$ (where $1 < x < \sim 1.86$; and $8.1 < n < 8.6$)[84] and goethite has the chemical formula: $Fe_2O_3 * nH_2O$ ($1.6 < n < 3$). Yu and colleagues determined that the stability boundary between schwertmannite and ferrihydrite depends on both the activity of SO_4 and the pH. Generally, the stability boundary can assume to occur between pH 5.3 and 5.9; however, with uncertainty, the range of this stability boundary is a wide as from pH 5 to 6.5[84]. Dissolution reactions for both schwertmannite and ferrihydrite are included below.

Equation 16 $$Fe_8O_8(OH)_{8-2x}(SO_4)_x + (24-2x)H+ \rightarrow 8\ Fe^{3+} + x\ SO_4^{2-} + (16-2x)H_2O$$

Equation 17 $$0.5\ Fe_2O_3 + 3H^+ \rightarrow Fe^{3+} + 1.5H_2O$$

pH-Eh diagrams:

To determine which iron and iron-hydroxy-sulphate minerals would be expected to form at the sites examined, activities of iron and sulphate were determined in phreeqc-i. There was a wide range of Fe(II) activities, from a minimum of $10^{-10.14}$ to $10^{-3.65}$, as well as a range of temperatures, from 8.46˚C to 25.23˚C. Four groups were created with the data, based first on the amount of Fe^{2+}, and secondarily on temperature. Average measured activities for each grouping were used as input parameters for pH-Eh diagrams (activity of Fe^{2+}, activity of SO_4^{2-} and temperature were specified), which were overlaid with measured Eh and pH values for the samples in that group (

Table 41). Eh-pH plots of iron indicate the Eh and pH conditions at each site are favorable for the formation of ferrihydrite ($Fe(OH)_3$ or more correctly, $Fe_2O_3 * nH_2O$). Exceptions are the SC01 and SC02 sites during August, which have such low amounts of aqueous Fe2+, that iron minerals are not expected to form. In addition, sites SC03-Aug and SC04-Aug have measured water quality parameters conducive to forming schwertmannite instead of ferrihydrite.

REY-anomalies:

In 1999, Bau examined normalized REY concentrations during iron oxide precipitation in laboratory experiments with waters between pH 3.6 to 6.2. Precipitation of HFOs increased with increasing pH, and Y, La, and Gd showed low affinity for iron oxides and a commensurate enrichment in associated waters; whereas, Ce depletion in waters indicated that oxidative scavenging of cerium was occurring on the iron oxide[19]. In addition, Bau's experiments indicated that a smaller Y_n/Ho_n ratio was associated with more iron oxidation. Within the Silver Creek drainage, Gd and Y anomalies were observed, which may be indicative of iron oxidation. Anomalies for La and Ce were not observed; however, and decrease in Y_n/Ho_n ratio was not observed at sites further downstream in the treatment facility.

4.2.8 REY Sorption

Sorption is a pH and temperature-dependent process that shows maximum rates at high pH and high temperature. Sorption was observed at sites within the Silver Creek passive treatment that had low pH and low temperature. Linear, Freundlich and Langmuir isotherms were plotted for the data. December data closely followed the Langmuir isotherm, while August data showed more linear trends, not representative of concentration dependent sorption. Even though the December data followed Langmuir isotherm curves, sites with the lowest pH actually had the greatest solid phase enrichment.

The two most likely explanations for this trend is that the apparent sorption patterns we are observing are in fact, not related to sorption, but mineral co-precipiation. Certain minerals, such as aluminum-sulphates precipitate at low pH and may be sequestering REYs. An alternate explanation is that the high concentration of REYs, which equals a high sorbate density, is in fact the most important parameter that dictates sorption. As Dzombak and Morel indicate, when the concentration of the sorbate is so large that it affects the surface charge of the oxide in a major way, the coulombric interactions are quite complex. In standard sorption, the surface charge on the oxide are largely determined by surface protonation (i.e., pH). In brief, if the concentration of REYs in solution is equal to, or greater than available sorption sites, the shear amount of positively charged REYs sorbed the oxide surface will alter the surface charge. As can be noticed from the fractionation plots, there is hardly any REY fractionation at sites with greatest REYs, indicating saturation of sorption sites.

There may be yet one additional factor that may have results in the December data adhering to a Langmuir-esque trend, while the August data did not. Within the August data, site SC01 to SC03 exhibit high relative loading when compared to upstream sites that showed much greater enrichment to downstream sites in December. Based on WHAM modelling, the data indicates that the majority of REY sorption at sites SC01 to SC03 is occurring via manganese oxides. For an unknown reason,

Table 41 Temperature and log activity of Fe^{2+}, Fe^{3+} and SO_4^{2-} at the Silver Creek sites

Group	Site	Fe^{+2}	Fe^{+3}	SO_4^{-2}	Temperature
Group 1	SC04-Dec	-3.99	-12.39	-2.93	10.28
	SC04-Aug-PM	-3.91	-11.10	-2.89	10.28
	SC06-Aug-AM	-3.81	-12.15	-2.86	11.93
	SC06-Dec	-3.73	-13.08	-2.95	11.89
	SC05-Dec	-3.73	-12.08	-2.95	11.98
	SC05-Aug-PM	-3.70	-11.99	-2.86	13.91
	SC06-Aug-PM	-3.67	-12.01	-2.90	12.12
	SC05-Aug-AM	-3.65	-11.00	-2.88	13.91
	Avg	**-3.77**	**-11.97**	**-2.90**	**12.04**
Group 2	SC01-Aug-PM	-10.14	-17.07	-2.90	28.90
	SC01-Aug-AM	-9.97	-15.11	-2.78	20.47
	SC02-Aug-AM	-7.67	-13.79	-2.90	25.55
	SC02-Aug-PM	-7.08	-14.07	-2.87	21.08
	Avg	**-8.72**	**-15.01**	**-2.86**	**24.00**
Group 3-High Temperature	SC03-Aug-AM	-5.82	-11.96	-2.81	20.37
	SC03-Aug-PM	-5.08	-13.10	-2.89	25.23
	Avg	**-5.45**	**-12.53**	**-2.85**	**22.80**
Group 3-Low temperature	SC01-Dec	-4.93	-13.38	-2.92	8.46
	SC02-Dec	-4.72	-13.14	-2.92	8.73
	SC04-Aug-AM	-4.52	-10.79	-2.83	14.79
	SC03-Dec	-4.25	-12.68	-2.93	8.81
	Avg	**-4.61**	**-12.50**	**-2.90**	**10.20**
	Group Avg	**-5.25**	**-12.81**	**-2.88**	**15.87**

NOTES:

1. REDOX COUPLED CALCULATD FROM pe.
2. TEMPERATURE PROVIDED IN DEGREES CELCIUS AND OTHER PARAMETERS ARE PROVIDED IN LOG ACTIVITIES.

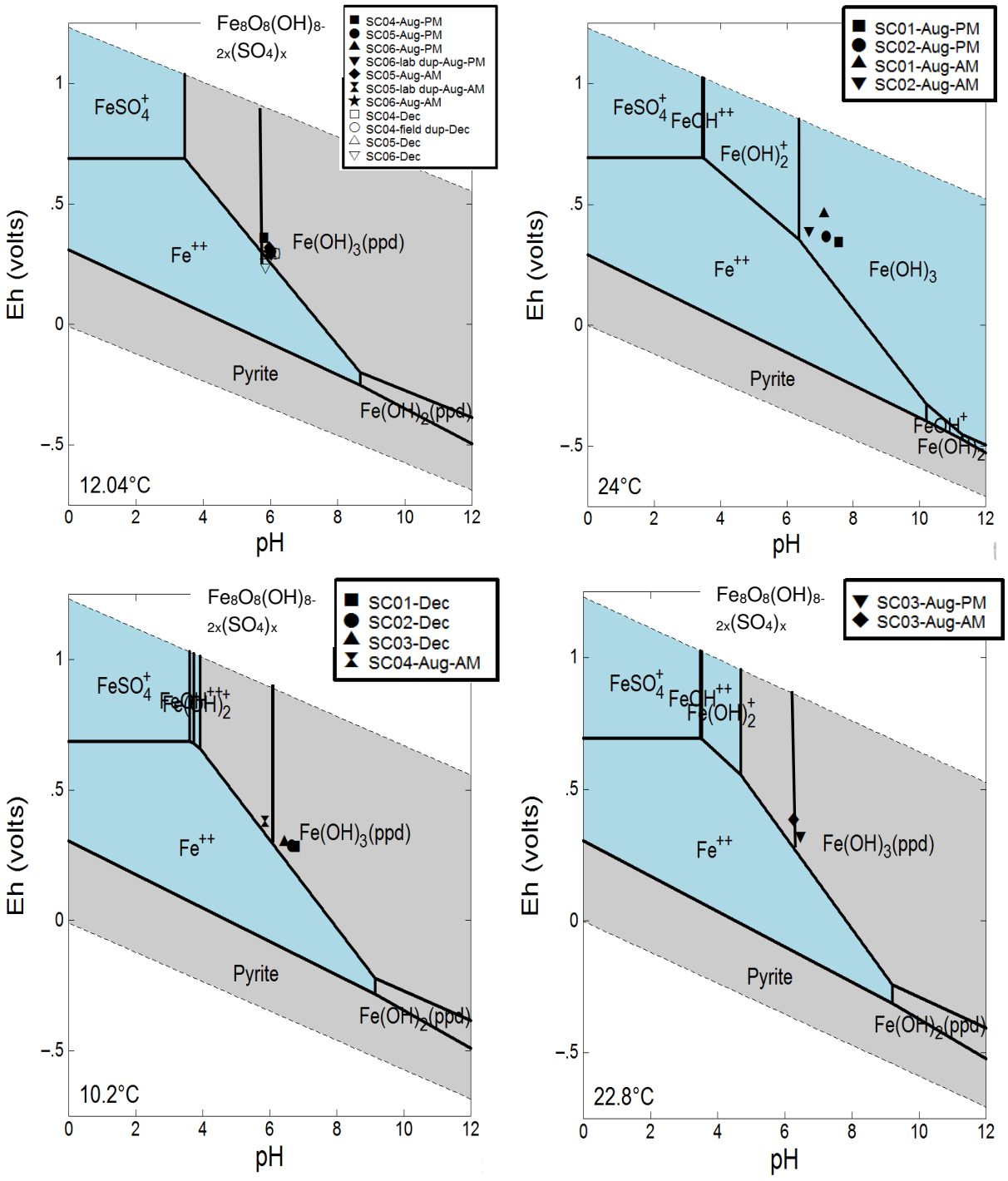

NOTES:

1. FIGURE WERE MADE IN GEOCHEMISTS WORKBENCH.
2. AVERAGE DATA FROM EACH GROUPING (TABLE 23) USED AS INPUT PARAMETERS FOR EH-pH DIAGRAMS.

Figure 32 Eh-pH Diagram for Fe and SO_4^{2-} minerals at the Silver Creek site

there is much less manganese contained within the biofilm in December and it is likely that the increased amount of manganese drastically affects the rate and number of REY binding sites.

4.2.9 Diurnal trends - sorption isotherms

Temperature is the *in situ* parameter that shows the greatest variability, which may affect REY sorption. Temperature may also affect REY aqueous speciation as sulfate compexes are more prevalent at increasing temperature[75]. Ferric oxides have been known to exhibit temperature-dependent sorption[23].

Temperature changes were large between the December and August sampling events, and most magnified at the SC03, SC02 and SC01 sites, that generally had large surface area to volume ratios. Direct comparison of the diurnal patterns of REY concentration were examined for the August morning and afternoon events. Again, the SC03, SC02 and SC01 sites showed the greatest temperature difference (up to 8˚C); however, these sites also showed differences in pH, pe and dissolved oxygen. In spite of large reduction of temperature at the SC03, SC02, and SC01 sites during the August morning sampling event, which should favour REY desorption into the aqueous phase, and lower pH values measured during the morning sampling event, only SC01 and SC04 show generally increased REY concentrations within the morning sampling event. The largest diurnal differences (maximum of 164%) are noted at SC06 and SC04. Unlike SC04, however, SC06 shows the greatest water concentrations within the afternoon. This indicates that REY solid accumulation at SC06 occurs independent of pH or temperature; whereas, solid accumulations at SC04 may be affected by pH and temperature. The lower magnitude of diurnal change at the further downstream sites may simply be a result of the lower overall REY concentrations, or an indication that REY within solid phase is relatively more immobile at these lower sites.

With the exception of site SC06, the Silver Creek seasonal and diurnal pH trend followed the pattern expected for biologically-induced changed in pH as a result of precipitation. The December sampling event has the lowest pH; the August afternoon sampling event has the highest pH, when photosynthetic activity is at its peak, and August morning sampling event pH occurs between the previous two. Seasonal differences in pH range between 0.03 to 0.8 pH points, and diurnal differences in pH range between 0.05 to 0.51 pH points. Field trials completed by Nimick found that pH played the largest role in determining sorption, and the pH change at this sites ranged from 0.22 to 0.79 (Nimick 2003). Both Gammons and Smilley found that temperature played the greatest role in REY sorption, because of smaller diel pH changes (0.06 unit change and 0.1-0.22 unit change, respectively)[22,23]. Since temperature and pH change by different amounts, each node was assessed for the significance of temperature and pH on sorption. Enthalpies were calculated for each site during August, and all sites had positive enthalpy values, with the exception of SC06, which had negative enthalpy values.

4.2.10 REY Concentrations and Anomalies

Elevated aqueous REY concentrations were observed within the Silver Creek treatment system, in addition to an approximately two order of magnitude decrease in aqueous REY concentration with increasing pH as water moves through the treatment system. Verplanck was one of the first to measure REY concentrations in areas with significant iron oxidation, and found aqueous REYs remain dissolved in acid, sulphate water below pH 5.1[11]. Above pH 5.1, Verplanck and colleagues observed REYs behaved non-conservatively and partitioned to solid phase. Sum of REY concentrations (including Sc) ranged from a maximum of 26 µg/L (SC05-Aug-AM) to a minimum of 0.8 µg/L (SC01-Aug-AM and SC02-Aug-PM). The most abundant REY was cerium (maximum 9.2 µg/L), followed by lanthanum (maximum 4.5 µg/L), neodymium (4.1 µg/L), yttrium (3 µg/L) and lutenium (2.4 µg/L). These aqueous concentrations of REYs are well above natural water. For example, the sum of REEs (excluding Y

and Sc) is measured to be 0.08 µg/L within the Mississippi River and 0.52 µg/L within the Amazon River[30]. Various authors have reported on the sum of REEs (excluding Y and Sc) downstream of AMD environments, and these concentrations range from 30 µg/L to 85 µg/L[5,6,16]. Within AMD treatment ponds themselves, aqueous sum of REEs (excluding Y and Sc) ranges from 31 µg/L to 3,091 µg/L[5,6,16,86]. In comparison to AMD sites worldwide, aqueous REY concentrations for Silver Creek remain on the low side. Within the Iberian pyrite belt, Ayora and colleagues determined that REYs range from 0.3 to 11.7mg/L, with a flow weighted average of 1.02 mg/L of total REY[1]. This average is similar to some of the highest concentrations measured in the Pennsylvania coal mine discharges[72].

When comparing REY concentrations measured in Silver Creek to datasets from within the Pennsylvania anthracite and bituminous coal region, REY concentrations at Silver Creek are within the range of previously collected samples, but do not exceed these samples. Aqueous REY concentrations reported in Cravotta showed much greater maximum concentrations for REYs than observed within the Silver Creek system[72]. Y and Sc concentrations measured in Silver Creek are well below those reported in Cravotta. In comparison to data reported by Stewart, the Silver Creek data fit well within the average range, but maximum data at Silver Creek was well below maximum data reported by Stewart[4]. In addition, our REY data is witin the range of grade for ionic clay deposits.

In brief, water exhibited a HREY-enriched pattern when normalized to NASC or adjacent host rock. Minealized biofilm exhibited an MREY-enriched pattern when normalized to NASC, and the partitioning coefficients calculated between the water and biofilm exhibited LREY enrichment. Due to the complicated nature of the biofilm and the multiple potential REY sorption factors: sorption to organics, sorption to mangeanse oxides, sorption to iron oxides and potentially precipitation with aluminum-sulphate minerals, these enrichment patterns are not particularly useful in determining patterns of sorption. For example, iron oxides, aluminum oxides and organic materials are all thought to preferentially absorb HREYs. As a result, HREY enrichment is not particularly useful in determining what mechanism is employed to finish work.

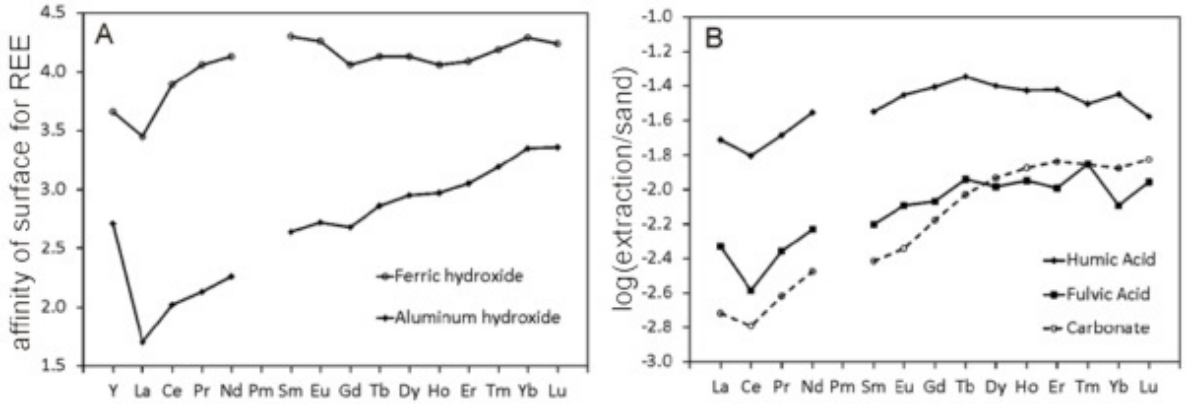

Figure 33 The affinity of surfaces for REYs (source: Purdy and Jamieson)[24]

Although not immediately apparent in NASC normalized plots, anomaly calculations identified the following positive anomalies: La, Eu, Y, and positive Y/Ho fractionation. A positive Gd anomaly was calculated for sites closed to the dsischarge (SC06, SC05, and SC04) and a negative Gd anomaly was calculated for sites further downstream (SC01 and SC02). Investigations of diel cycling of REYs within other high iron environments identified positive Ce, La, Gd, and Y anomalies[22]. This study partially agrees with these results. Similar to findings of others, this study hypothesizes that positive La and Y anomalies originate from the relics of preferential sorption to HFO since La and Y have the lowest HFO affinity of the group[19,87]. Vesper and Smilley hypothesized that the Ce and Gd anomalies

also arise from lower HFO affinity, but these claims have not been supported in other literature[22]. Further investigation is required into the HREY anomalies observed at all sites, regardless of season or sampling time: negative Er anomaly, positive Tm anomaly and positive Lu anomaly.

5 – CONCLUSION

Main conclusions:

- Screening level review of co-occurring mineralized biofilm and water samples at neutral mine drainage, acid rock drainage and coal mine drainage sites within North America and South America indicate, similar to observations by other authors, that aqueous REY concentrations are greater in low pH water and low in high pH water.
- Aqueous REY concentrations in measured sites did not reach levels other authors have considered mineable. This is likely due to a combination of source factors (e.g., source of REYs) and acidity of drainage. Mineable sources of REY seem to occur in areas with high amounts of sulphides in host rock, and elevated REYs within host rock.
- Coal mine drainage sites exhibited the greatest solid phase enrichment of REYs (~1,000 mg/kg dry weight), which are close to REY concentrations observed within ionic clay REY deposits and are at the low-end of concentrations considered mineable. The caveat of this observation is that our control site, located within the Canadian Shield, contained solid REY concentrations within mineralized biofilms equal to coal mine drainage. This indicates that enriched solid accumulations of REYs in freshwater environments are not limited to mining-affected areas.
- REY speciation in water was observed to be dominated by organic colloids and sulphate complexes.
- REY speciation within heterogeneous biofilm is complex, and in spite of the small relative concentration of manganese, the role of manganese oxides in REY sorption should not be overlooked.
- Aqueous samples exhibited strong HREY enrichment and slight MREE enrichment, which differs from previous studies that have consistently observed a strong MREE enrichment.
- The oxalate extraction was at least as effective and possibly more effective than aqua regia digestion for isolating REYs.
- Sequential extractions are not the best tool to isolate amorphous mineral fractions that are extremely close physically and have similar chemical properties. For example, biogenic iron and manganese oxides are so closely associated with organics that sequential extractions to identify one or the other portion are not feasible. Alternate techniques, such as Mossbauer should be considered.
- The Silver Creek system provided an example of sorption at high sorbate density. Due to the high aqueous concentrations of REYs (~10^{-5} M sum of REYs), sorption patterns occurred in opposition to the pH and temperature gradients.

Future work:

- Kinetic modelling should be completed to understand the relative importance of iron oxides, manganese oxides and organics on the sequestration of REYs within the solid phase.

- Additional organic extractions to determine if it possible to differentiate REYs associated with the organic phase.
- Additional investigations on the speciation of REYs within the solid phase should be completed. As determined by this thesis, methods besides from sequential digestion should be employed to target these highly heterogeneous phases. Although, less favourable, there do remain additional sequential digestion techniques that were not completed and may be useful:
    - Although unlikely, a sequential extraction targeting basaluminite, calcite and aluminum oxides should be completed to confirm absence of REYs within the aluminum phase. An extraction approach similar to that used by Ayora and colleagues: extraction with 1M ammonium acetate at pH 4.5 and 20˚C is suggested[1].
    - In addition, additional sequential extractions to determine whether REYs are hosted within the crystalline or amorphous iron oxide fraction may be interesting. Approaches indicated by Tessier or Ayora could be useful[1,88]. The use of synchrotron-based µ-X-ray fluorescence (µXRF) would be useful to provide evidence on the physical association of REYs with iron minerals.

6 – REFERENCES

(1) Ayora, C.; Macías, F.; Torres, E.; Lozano, A.; Carrero, S.; Nieto, J. M.; Pérez-López, R.; Fernández-Martínez, A.; Castillo-Michel, H. Recovery of Rare Earth Elements and Yttrium from Passive-Remediation Systems of Acid Mine Drainage. *Environ. Sci. Technol.* **2016**, *50* (15), 8255–8262.

(2) USGS. Coal-Mine-Draiange Projects in Pennsylvania https://pa.water.usgs.gov/projects/energy/amd/ (accessed Mar 3, 2017).

(3) Cravotta, C. A.; Brady, K. B. C. Priority pollutants and associated constituents in untreated and treated discharges from coal mining or processing facilities in Pennsylvania, USA. *Appl. Geochemistry* **2015**, *62* (March), 108–130.

(4) Stewart, B. W.; Capo, R. C.; Hedin, B. C.; Hedin, R. S. Rare earth element resources in coal mine drainage and treatment precipitates in the Appalachian Basin, USA. *Int. J. Coal Geol.* **2017**, *169*, 28–39.

(5) Sharifi, R.; Moore, F.; Behname, K. Geochemical behavior and speciation modeling of rare earth elements in acid drainages at Sarcheshmeh porphyry copper deposit, Kerman Province, Iran. *Chemie der Erde* **2013**, *Article in* (Article in Press), 1–11.

(6) Ferreira da Silva, E.; Bobos, I.; Xavier Matos, J.; Patinha, C.; Reis, A. P.; Cardoso Fonseca, E. Mineralogy and geochemistry of trace metals and REE in volcanic massive sulfide host rocks, stream sediments, stream waters and acid mine drainage from the Lousal mine area (Iberian Pyrite Belt, Portugal). *Appl. Geochemistry* **2009**, *24* (3), 383–401.

(7) Ayora, C.; Macías, F.; Torres, E.; Nieto, J. M. Rare Earth Elements in Acid Mine Drainage. **2015**, *2016* (1), 1–22.

(8) Sneller, F. E. C.; Kalf, D. F.; L., W.; Van Wezel, a. P. Maximum Permissible Concentrations and Negligible Concentrations for Rare Earth Elements. **2000**, No. 601501, 66.

(9) Haxel, G. B.; Hedrick, J. B.; Orris, G. J.; Sound, S.; Of, M.; Mineral, O. U. R. Rare Earth Elements — Critical Resources for High Technology. *United States Geol. Surv. Fact Sheet* **2002**, *87*, 4.

(10) U.S. Geological Survey. 2016 Mineral Commodities Summaries. *Miner. Commod. Summ.* **2016**, 202.

(11) Verplanck, P. L.; Nordstrom, D. K.; Taylor, H. E.; Kimball, B. a. Rare earth element partitioning between hydrous ferric oxides and acid mine water during iron oxidation. *Appl. Geochemistry* **2004**, *19*, 1339–1354.

(12) Merten, D.; Geletneky, J.; Bergmann, H.; Haferburg, G.; Kothe, E.; Büchel, G. Rare earth element patterns: A tool for understanding processes in remediation of acid mine drainage. *Chemie der Erde - Geochemistry* **2005**, *65*, 97–114.

(13) Grawunder, A.; Lonschinski, M.; Merten, D.; Büchel, G. Rare earth elements as a tool for studying the formation of cemented layers in an area affected by acid mine drainage. *Appl. Geochemistry* **2015**, *54*, 100–110.

(14) Olías, M.; Cerón, J. C.; Fernández, I.; De La Rosa, J. Distribution of rare earth elements in an alluvial aquifer affected by acid mine drainage: The Guadiamar aquifer (SW Spain). *Environ. Pollut.* **2005**, *135*, 53–64.

(15) Protano, G.; Riccobono, F. High contents of rare earth elements (REEs) in stream waters of a Cu-Pb-Zn mining area. *Environ. Pollut.* **2002**, *117*, 499–514.

(16) Romero, F. M.; Prol-Ledesma, R. M.; Canet, C.; Alvares, L. N.; Pérez-Vázquez, R. Acid drainage at the inactive Santa Lucia mine, western Cuba: Natural attenuation of arsenic, barium

and lead, and geochemical behavior of rare earth elements. *Appl. Geochemistry* **2010**, *25* (5), 716–727.

(17) Verplanck, P. L.; Nordstrom, D. K.; Taylor, H. E. Overview of rare earth element investigations in acid waters of the U.S. Geological Survey's abandoned mine lands watersheds. *U.S. Geol. Surv. Toxic Subst. Hydrol. Progr. Proc. Tech. Meet.* **1999**, 83.

(18) Leybourne, M. I.; Johannesson, K. H. Rare earth elements (REE) and yttrium in stream waters, stream sediments, and Fe-Mn oxyhydroxides: Fractionation, speciation, and controls over REE + Y patterns in the surface environment. *Geochim. Cosmochim. Acta* **2008**, *72* (24), 5962–5983.

(19) Bau, M. Scavenging of dissolved yttrium and rare earths by precipitating iron oxyhydroxide: Experimental evidence for Ce oxidation, Y-Ho fractionation, and lanthanide tetrad effect. *Geochim. Cosmochim. Acta* **1999**, *63* (1), 67–77.

(20) Ohta, A.; Kawabe, I. REE(III) adsorption onto Mn dioxide (??-Mn02) and Fe oxyhydroxide: Ce(III) oxidation by ??-MnO2. *Geochim. Cosmochim. Acta* **2001**, *65* (5), 695–703.

(21) Prudêncio, M. I.; Valente, T.; Marques, R.; Sequeira Braga, M. A.; Pamplona, J. Geochemistry of rare earth elements in a passive treatment system built for acid mine drainage remediation. *Chemosphere* **2015**, *138*, 691–700.

(22) Vesper, D. J.; Smilley, M. J. Attenuation and diel cycling of coal-mine drainage constituents in a passive treatment wetland: A case study from Lambert Run, West Virginia, USA. *Appl. Geochemistry* **2010**, *25* (6), 795–808.

(23) Gammons, C. H.; Wood, S. A.; Nimick, D. A. Diel behavior of rare earth elements in a mountain stream with acidic to neutral pH. *Geochim. Cosmochim. Acta* **2005**, *69* (15), 3747–3758.

(24) Purdy, C. J. K.; Jamieson, H. Review of the Factors Controlling the Environmental Moibility of Rare Earth Elements. *Pending Publ.* **2014**.

(25) Zhao, C. M.; Wilkinson, K. J. Biotic ligand model does not predict the bioavailability of rare earth elements in the presence of organic ligands. *Environ. Sci. Technol.* **2015**, *49* (4), 2207–2214.

(26) Connelly, N. G.; Hartshorn, R. M.; Damhus, T.; Hutton, A. T. Nomenclature of Inorganic Chemistry IUPAC Recommendations 2005 IUPAC Periodic Table of the Elements Fm No. *R. Soc. Chem.* **2005**, *128* (21), 50.

(27) Migaszewski, Z. M.; Gałuszka, A. The characteristics, occurrence and geochemical behavior of rare earth elements in the environment: a review. *Crit. Rev. Environ. Sci. Technol.* **2014**, 00–00.

(28) Lewis, A. J.; Palmer, M. R.; Sturchio, N. C.; Kemp, A. J. The rare earth element geochemistry of acid-sulphate and acid-sulphate-chloride geothermal systems from Yellowstone National Park, Wyoming, USA. *Geochim. Cosmochim. Acta* **1997**, *61* (4), 695–706.

(29) Purdy, C. The geochemical and mineralogical controls on the environmental mobility of rare earth elements from Tailings, Nechalacho Deposit. *M.Sc. Thesis* **2014**.

(30) Gonzalez, V.; Vignati, D. a L.; Leyval, C.; Giamberini, L. Environmental fate and ecotoxicity of lanthanides: Are they a uniform group beyond chemistry? *Environ. Int.* **2014**, *71*, 148–157.

(31) Taylor, S. R.; McLennan, S. M. Chapter 79 The significance of the rare earths in geochemistry and cosmochemistry. *Handb. Phys. Chem. Rare Earths* **1988**, *11*, 485–578.

(32) Gromet, L. P.; Dymek, R. F.; Haskin, L. a.; Korotev, R. L. The "North American shale composite" - Its compilation, major and trace element characteristics. **1984**, *48*, 2469–2482.

(33) Piper, D. Z.; Bau, M. Normalized Rare Earth Elements in Water , Sediments , and Wine : Identifying Sources and Environmental Redox Conditions. *Am. J. Anal. Chem.* **2013**, *2013* (October), 69–83.

(34) Piper, D. Z.; Bau, M. Normalized Rare Earth Elements in Water, Sediments, and Wine: Identifying Sources and Environmental Redox Conditions. *Am. J. Anal. Chem.* **2013**, *4* (October), 69–83.

(35) Pokrovsky, O. S.; Dupré, B.; Schott, J. *Fe-Al-organic colloids control of trace elements in peat soil solutions: Results of ultrafiltration and dialysis*; 2005; Vol. 11.

(36) Luo, Y. R.; Byrne, R. H. Carbonate complexation of yttrium and the rare earth elements in natural waters. *Geochim. Cosmochim. Acta* **2004**, *68* (4), 691–699.

(37) Johannesson, K. H.; Zhou, X. Origin of middle rare earth element enrichments in acid waters of a Canadian High Arctic lake. *Geochim. Cosmochim. Acta* **1999**, *63* (1), 153–165.

(38) Tang, J.; Johannesson, K. H. Ligand extraction of rare earth elements from aquifer sediments: Implications for rare earth element complexation with organic matter in natural waters. *Geochim. Cosmochim. Acta* **2010**, *74* (23), 6690–6705.

(39) Martin, S. T. Precipitation and Dissolution of Iron and Manganese Oxides. In *Environmental Catalysis*; Grassian, V. H., Ed.; CRC Press, 2005; pp 61–81.

(40) Cornell, R M and Schwertmann, U. *Iron Oxides in the Laboratory: Preparation and Characterization*, Second edi.; Wiley-VCH: Weinheim, 2000.

(41) Davison, W.; Seed, G. The kinetics of the oxidation of ferrous iron in synthetic and natural waters. *Geochim. Cosmochim. Acta* **1983**, *47* (1), 67–79.

(42) Stumm, W.; Lee, F. G. Oxygenation of Ferrous Iron. *Ind. Eng. Chem* **1961**, *53* (2), 143–146.

(43) Pesic, B.; Olivier, D. J. An electrochemical method of measuring the oxidation rate of ferrous to ferric iron with oxygen in the presence of \textit{Thiobacillus ferrooxidans}. *Biotechnol. Bioeng.* **1989**, *33*, 428–439.

(44) Kirby, C. S.; Thomas, H. M.; Southam, G.; Donald, R. Relative contributions of abiotic and biological factors in Fe(II) oxidation in mine drainage. *Appl. Geochemistry* **1999**, *14* (4), 511–530.

(45) Johannesson, K. H.; Lyons, W. B.; Yelken, M. a.; Gaudette, H. E.; Stetzenbach, K. J. Geochemistry of the rare-earth elements in hypersaline and dilute acidic natural terrestrial waters: Complexation behavior and middle rare-earth element enrichments. *Chem. Geol.* **1996**, *133* (96), 125–144.

(46) Zhao, F.; Cong, Z.; Sun, H.; Ren, D. The geochemistry of rare earth elements (REE) in acid mine drainage from the Sitai coal mine, Shanxi Province, North China. *Int. J. Coal Geol.* **2007**, *70*, 184–192.

(47) Ingri, J.; Widerlund, A.; Land, M.; Gustafsson, Ö.; Andersson, P.; Öhlander, B. Temporal variations in the fractionation of the rare earth elements in a Boreal river; the role of colloidal particles. *Chem. Geol.* **2000**, *166* (1–2), 23–45.

(48) Purdy, C. J. K.; Gault, A.; Bryn, K.; Jamieson, H. Speciation of REE in mine tailings from the Nechalacho. Queens: Kingston 2014, p 18.

(49) Morris, J. M.; Nimick, D. A.; Farag, A. M.; Meyer, J. S. Does biofilm contribute to diel cycling of Zn in High Ore Creek, Montana? *Biogeochemistry* **2005**, *76* (2), 233–259.

(50) Koeppenkastrop, D.; De Carlo, E. H. Sorption of rare-earth elements from seawater onto synthetic mineral particles: An experimental approach. *Chem. Geol.* **1992**, *95* (3–4), 251–263.

(51) Feige Gault, K. B.; Gammon, P.; Fortin, D. A geochemical characterization of cold-water natural acid rock drainage at the Zn-Pb XY deposit, Yukon, Canada. *Appl. Geochemistry* **2015**, *62*, 35–47.

(52) Praharaj, T.; Fortin, D. Seasonal variations of microbial sulfate and iron reduction in alkaline Pb-Zn mine tailings (Ontario, Canada). *Appl. Geochemistry* **2008**, *23* (12), 3728–3740.

(53) Cravotta, C. A. Dissolved metals and associated constituents in abandoned coal-mine discharges, Pennsylvania, USA. Part 1: Constituent quantities and correlations. *Appl. Geochemistry* **2008**, *23* (2), 166–202.

(54) Schuylkill Headwaters Association. Watershed Restoration Projects http://schuylkillheadwaters.org/projects/watershed-restoration-projects/ (accessed Mar 27, 2017).

(55) Nordstrom, D. K. Thermochemical redox equilibria of ZoBell's solution. *Geochim. Cosmochim. Acta* **1977**, *41* (12), 1835–1841.

(56) Stookey, L. L. Ferrozine---a new spectrophotometric reagent for iron. *Anal. Chem.* **1970**, *42* (7), 779–781.

(57) USGS. U.S. GEOLOGICAL SURVEY COAL QUALITY (COALQUAL) DATABASE : VERSION 2 . **1989**.

(58) Freslon, N.; Bayon, G.; Toucanne, S.; Bermell, S.; Bollinger, C.; Chéron, S.; Etoubleau, J.; Germain, Y.; Khripounoff, A.; Ponzevera, E.; et al. Rare earth elements and neodymium isotopes in sedimentary organic matter. *Geochim. Cosmochim. Acta* **2014**, *140*, 177–198.

(59) Kostka, J. E.; Luther, G. W. Partitioning and speciation of solid-phase iron in salt- marsh sediments. *Geochim. Cosmochim. Acta* **1994**, *58* (7), 1701–1710.

(60) Lawrence, M. G.; Greig, A.; Collerson, K. D.; Kamber, B. S. Rare earth element and yttrium variability in South East Queensland waterways. *Aquat. Geochemistry* **2006**, *12* (1), 39–72.

(61) Worrall, F.; Pearson, D. G. Water-rock interaction in an acidic mine discharge as indicated by rare earth element patterns. *Geochim. Cosmochim. Acta* **2001**, *65* (18), 3027–3040.

(62) Bau, M. and D. P. Distribution of yttrium and rare-earth elements in the Penge and Kuruman iron-formations, Transvaal Supergroup, South Africa. *Precambrian Res.* **1996**, *79*, 37–55.

(63) Appelo, C.A.J. and Postma, D. Geochemistry, Groundwater and Pollution. A.A. Balkema Publishers: Leiden, The Netherlands 2013, p 649.

(64) Parkhurst, D. L.; Appelo, C. A. J. Description of Input and Examples for PHREEQC Version 3 — A Computer Program for Speciation , Batch-Reaction , One-Dimensional Transport , and Inverse Geochemical Calculations. U.S. Geological Survey Techniques and Methods, book 6, chapter A43, 497 p. *U.S. Geol. Surv. Tech. Methods, B. 6, chapter A43* **2013**, 6–43A.

(65) Ball, J. W.; Nordstrom, D. K. User's Manual for WATEQ4F, with revised thermodynamic data base and test cases for calculating speciation of major, trace, and redox elements in natural waters. *U.S. Geol. Surv. Water-Resources Investig. Rep.* **1991**, *91–183*, 1–188.

(66) Delany, J. M.; Lundeen, S. R. *The LLNL thermochemical database*; 1990.

(67) Tipping, E.; Lofts, S.; Sonke, J. E. Humic Ion-Binding Model VII: a revised parameterisation of cation-binding by humic substances. *Environ. Chem.* **2011**, *8* (3), 225–235.

(68) Lofts, S.; Tipping, E. An assemblage model for cation binding by natural particulate matter. *Geochim. Cosmochim. Acta* **1998**, *62* (15), 2609–2625.

(69) Dzombak, D. A.; Morel, F. M. . *Surface Complexation Modeling - Hydrous Ferric Oxide*; John Wiley and Sons: Toronto, 1990.

(70) Cornell, R. M. and; Schwertmann, U. *Iron Oxides in the Laboratory*, 2nd Editio.; Wiley-VCH, 2000.

(71) Lofts, S.; Tipping, E. Solid-solution metal partitioning in the Humber rivers: Application of WHAM and SCAMP. *Sci. Total Environ.* **2000**, *251–252*, 381–399.

(72) Cravotta, C. A. Dissolved metals and associated constituents in abandoned coal-mine discharges, Pennsylvania, USA. Part 2: Geochemical controls on constituent concentrations.

Appl. Geochemistry **2008**, *23* (2), 203–226.

(73) Pearson, R. G. Hard and soft acids and bases. *J. Am. Chem. Soc.* **1963**, *85* (22), 3533–3539.

(74) Johannesson, K. H.; Stetzenbach, K. J.; Hodge, V. F.; Lyons, W. B. groundwaters : Assessing the role of carbonate and phosphate ions. *Earth Planet. Sci. Lett.* **1996**, *139* (96), 305–319.

(75) Kevin H. Johannesson, W.Berry Lyons, Klaus J. Stetzenbach, and R. H. B. The Solubility Control of Rare Earth Elements in Natural Terrestrial Waters and the Significance of PO43 - and CO32- in Limiting Dissolved Rare Earth Concentrations : A Review of Recent Information. **1995**, 157–173.

(76) Marsac, R.; Davranche, M.; Gruau, G.; Bouhnik-Le Coz, M.; Dia, A. An improved description of the interactions between rare earth elements and humic acids by modeling: PHREEQC-Model VI coupling. *Geochim. Cosmochim. Acta* **2011**, *75* (19), 5625–5637.

(77) Grawunder, A.; Merten, D.; Büchel, G. Origin of middle rare earth element enrichment in acid mine drainage-impacted areas. *Environ. Sci. Pollut. Res.* **2014**, *21*, 6812–6823.

(78) Pourret, O.; Davranche, M. Rare earth element sorption onto hydrous manganese oxide: A modeling study. *J. Colloid Interface Sci.* **2013**, *395* (1), 18–23.

(79) Davies, S. H. R.; Morgan, J. J. Manganese (II) Oxidation Kinetics on Metal Oxide Surfaces. *J. Colloid Interface Sci.* **1989**, *129* (1), 63–77.

(80) Kasten, S.; Glasby, G. .; Schulz, H. .; Friedrich, G.; Andreev, S. . Rare earth elements in manganese nodules from the South Atlantic Ocean as indicators of oceanic bottom water flow. *Mar. Geol.* **1998**, *146*, 33–52.

(81) Schoettle, M. Friedman, G. M. Fresh Water Iron-Manganese Nodules in Lake George, New York. *Geol. Soc. Am.* **1971**, *82* (1).

(82) Ayora, C.; Caraballo, M. A.; Macias, F.; R??tting, T. S.; Carrera, J.; Nieto, J. M. Acid mine drainage in the Iberian Pyrite Belt: 2. Lessons learned from recent passive remediation experiences. *Environ. Sci. Pollut. Res.* **2013**, *20* (11), 7837–7853.

(83) Najem, T.; Langley, S.; Fortin, D. A comparison of Fe(III) reduction rates between fresh and aged biogenic iron oxides (BIOS) by Shewanella putrefaciens CN32. *Chem. Geol.* **2016**, *439*, 1–12.

(84) Yu, J. Y.; Heo, B.; Choi, I. K.; Cho, J. P.; Chang, H. W. Apparent solubilities of schwertmannite and ferrihydrite in natural stream waters polluted by mine drainage. *Geochim. Cosmochim. Acta* **1999**, *63* (19–20), 3407–3416.

(85) French, R. A.; Caraballo, M.; Kim, B.; Rimstidt, J. D.; Murayama, M.; Hochella, M. F. The enigmatic iron oxyhydroxysulfate nanomineral schwertmannite: Morphology, structure, and composition. *Am. Mineral.* **2012**, *97* (8–9), 1469–1482.

(86) Verplanck, P. L.; Antweiler, R. C.; Nordstrom, D. K.; Taylor, H. E. Standard reference water samples for rare earth element determinations. *Appl. Geochemistry* **2001**, *16*, 231–244.

(87) Smilley, M. J. Determination of diel chemical cycle presense within abandoned coal mine drainage stream in Harrison County, WV. **2007**.

(88) Tessier, A.; Campbell, P. G. C.; Bisson, M. Sequential Extraction Procedure for the Speciation of Particulate Trace Metals. **1979**, *51* (7), 844–851.

CHAPTER 2: REY TOXICITY, BIOACCUMULATION AND LINKAGES TO MICROBIAL COMMUNITY COMPOSITION

1 – BACKGROUND

Recent studies have indicated that rare earth element concentrations are increasing in the biosphere[1,2]. Historically, rare earth elements and yttrium (REYs) were thought to pose little environmental or health hazard as a result of their low natural abundance, low solubility and relatively low toxicity when compared to other compounds. Increased use of REY-containing technology, however, is expanding anthropogenic effect on REY biogeochemistry cycles. Acid Rock Drainage (ARD) environments have recently been identified as having the potential to have high aqueous REY concentrations.

Review of published geochemical literature on acid mine drainage (ARD) sites revealed that mine affected effluent from mine sites can have extremely elevated REY concentrations (range 31 ug/L to 3091 µg/L)[3–5]. REY concentrations quickly decrease at downstream surface water sites, due to REY complexation with organic and inorganic ligands and potentially as a result of sorption with sediments. As a result, REYs may occur at very elevated levels in both water and sediments within and downstream of ARD-affected areas. Low pH conditions that characterize ARD are expected to create conditions with a large amount of aqueous REY (via dissolution). Under these low pH conditions, REY may occur as free aqua complexed ions; however, complexation with sulphate is expected to dominate in high sulphate environments. Based on geochemical speciation modelling, at low pH, solutions with high amounts of sulphate found in ARD environments would be expected to have <10% aqua ion REY[3,4,6].

Although the bioassay data for REYs is limited and of variable quality, the concentrations at which REY begin to have adverse effects are relatively high when compared to the average background REY concentration (i.e., exposure in ng/L range and guidelines in µg/L). The largest toxicological threat regarding REYs exposure are elevated bio-concentration factors (BCF) that have been observed within aquatic plants/algae, arthropods/crustaceans, bacteria and water/sediment. For example, field-collected marine algae have been recorded to have BCF relative to water that range from 10 to 3,000,000 L/kg dry weight[7,8]. In addition, BCF for REYs and bacteria are so elevated that they have been investigated for use in REY-mining separation technology[9]. Such elevated BCF and water-sediment partitioning levels are particularly concerning if they occur at elevated water concentrations observed in ARD environments. BCF are generally inversely related to metal exposure concentrations[10]. This assumption is not supported by the available REY data. Based on current exposure concentrations and the BCFs observed, large enrichments of REY occur in biota within ARD-affected aquatic environments.

Previous work has shown an extremely close linkage between REYs with iron and manganese that may limit the REYs that are available for uptake by biota[6,11]. In real-world environments, however, iron, manganese, and organic matter, including organic acids and other eukaryotic and prokaryotic biota such as bacteria and algae co-exist[12]. Separately, all of these compounds have a high affinity for REYs, and together, these complex biotic-abiotic mixtures are expected to have even greater BCFs or partitioning coefficients. In addition, some authors have indicated that different REY patterns can be used to differentiate between biotic and abiotic iron oxidation processes due to differences in REY

fractionation[12–14]. In addition, other investigators have examined the role of naturally occurring bacteria in REY fractionation and sequestration, as a potential method for greener separation technology[9,15,16], as a possible tool to identify biosignatures[12–14] and as a mechanism of bioconcentration into the bottom of the food chain[2,17]. Few studies have examined the biogeochemical processes of REY enrichment at a field site with enriched REY concentrations and strong geochemical gradients, with sampling occuring during multiple seasons, and times of day.

1.1 OBJECTIVES

The main objectives of this chapter include:

- Examining the potential toxicological threat of REYs, considering their high BCF, the high concentrations of REYs observed in the aqueous environment downstream of ARD sites and results of geochemical characterization completed in **Chapter 1: REY Geochemistry in Mining-Affected Aqueous Environments**.
- Examination of REY partitioning coefficients between water and biofilm, under a variety of aqueous REY concentrations. Are REY partitioning coefficients greater than partitioning coefficients for other metals? What is the relationship between REY concentration and partitioning coefficient?
- Examining any linkages between microbial population composition and abundance on REY fractionation.

1.2 HYPOTHESES

This research tests the following alternate hypotheses:

- REYs pose a toxicological threat to aquatic life in areas downstream of mining environments.
- REY partitioning coefficients are greater than partitioning coefficients observed for other metals, regardless of aqueous REY concentration.
- Bacterial presence alters REY fractionation and may be used as a biosignature.

1.3 EXPOSURE CHARACTERIZATION

1.3.1 Natural and anthropogenic sources

Rare earth elements are naturally occurring elements that have moderate crustal abundance but few economic deposits. The principal REE ores include bastnasite, xenotime and monazite , where LREEs are formed at lower crystallization temperature and pressures compared to HREEs[18]. REEs also co-occur with other metal deposits, and have been found in a range of mineral ores including: halides, carbonates, oxides, phosphates and silicates[19]. Recent research by Emsbo and colleagues indicate that previously overlooked ore materials, such as sedimentary phosphate deposits, may provide unrecognized sources of HREEs at levels similar or higher than traditional REE deposits[20]. Natural sources of REE in the environment are derived exclusively from weathering and generally occur at low concentrations.

Elevated REE concentrations are generally associated with anthropogenic activities. The main sources of anthropogenic REEs include: the mining and refining processes, agricultural phosphate fertilizer, use or production of catalysts, leachate from landfills containing discarded technology and

medical imaging / diagnosis[21]. Generally, concentrations of emitted REE are low. REEs have the unique ability to easily gain and lose electrons, which makes them very useful for a variety of technologies. In addition to use in catalysts, REEs are used within magnets (laptops, wind turbines and headphones), liquid crystal displays (cell phones, flat screens), fluorescent materials and batteries (vehicular, industrial)[22]. Cerium compounds are also currently used as a fuel additive[23].

Within the mining and processing industry, recent research has identified elevated REE concentrations in acidic coal and metal mine drainage[3,4,6,24]. Acid mine affected stream water and mine effluent have REE concentrations that range from 3 to 5 orders of magnitude greater than background or baseline stream concentrations[4]. REEs occur naturally in phosphate fertilizers, which are derived from monazite materials. In addition, some phosphate fertilizers have been amended with REEs after they were reported to increase plant yields.

REEs have been used as a proxy for radionucleotides in the medical industry. For example, lanthanum carbonate (Fosrenol) is used in the medical industry to treat chronic renal failure.

1.3.2 Environmental concentrations

REYs are commonly found in such low concentrations (ng/L or ng/kg) that their environmental and geochemical fate has previously been difficult to determine. Advances in mass spectrometry techniques (inductively coupled plasma optical emission spectroscopy (ICP-OES), mass spectroscopy (ICP-MS), laser ablation IPC-MS and secondary ion mass spectrometry (SIMS)) have enabled quantification of REYs within a variety of media at low concentrations.

The Upper Continental Crust and the whole Continental Crust are characterized by distinct Eu anomalies and have REY abundance that range from 144.3 mg/kg to 146.4 mg/kg. Total REY abundance is much lower in CI chondrite (2,480 ug/kg), and is characterized by positive HREY anomalies [2]. REY in bedrock is soluble during low-temperature weathering and REY fractionation depends on secondary and tertiary mineral phases and climatic variables[25]. Quickly after low-temperature weathering, REYs are normally sequestered back into the solid phase through precipitation or sorption and as a result, REY concentrations in naturally occurring freshwater are low and range from 0.04 µg/L (Sum of REE, excluding Y from Mississippi River, 1988 to 2001)[2] to 1.90 µg/L (sum of REE concentrations within Color Lake, Canada)[26].

REY levels in marine, freshwater and soil mediums have been noted by many authors to be increasing during recent years[27,28]. Everyday use of REYs in a variety of products, including as a fuel additive, is the primary reason cited for the increase in anthropogenic sources of REYs. Often overlooked are the elevated concentrations of REYs in an increasing number of Acid Mine Drainage (ARD) systems, which are usually of concern due to other metal contamination. While geochemical research has examined REY patterns and concentrations in ARD systems, few toxicological studies have examined REY concentrations in acidic environments[27].

Similar to +II oxidation state trace metals, speciation of REYs is very important when considering exposure levels. Similar to other metals, it is hypothesized that aqua ion (or “free ions”) represent the most bioavailable form of REY. In low pH settings, REY dissolution increases dissolved REY levels and low pH conditions favour the aqua ion form. In addition to pH, sulphate plays a key role in controlling the amount of REY aqua ion. Speciation modelling in low pH environments indicates that as the concentration of sulphate increases, the proportion of REY aqua ion decreases[3,29,30].

1.3.3 Exposure pathways

Elevated concentration of REYs in the aquatic environment as a result of ARD may have effects via sediment, surface water and groundwater environmental exposure pathways. Aquatic receptors include algae and aquatic plants, bacteria/periphyton, arthropods/crustaceans (e.g., *Daphnia magna*) and fish. The expected route of exposure to aquatic organisms is via direct dermal contact and absorption. Determining exposure to bioavailable REYs may be quite difficult, due to REY affinity for other organic acids and iron oxides.

1.3.4 Absorption, disruption, metabolism and excretion

REYs are xenobiotics that have no known role in living organisms. REY absorption, disruption, metabolism and excretion activities are based on REY's ability to mimic essential elements used by the body. REY bioaccumulation has been observed to occur at a variety of trophic levels. BCF are greatest in aquatic plants, then arthropods/crustaceans, shellfish and fish[31]. Depending on water chemistry, REYs tend to complex with other organic and inorganic ligands. REY form insoluble complexes with carbonate, phosphate and hydroxides have particularly low solubility. It is expected that a large portion of REYs will be excreted in their insoluble complexed form. This possibility is even more likely if the pH of the organism is higher than the pH of the surrounding water. The exact adsorption, disruption, metabolism and excretion pathway is not completely figured out for REYs.

1.4 EFFECT CHARACTERIZATION

1.4.1 Aquatic Toxicity Data

Review of REE bioassay and bioconcentration data revealed that data collected to date is quite variable[27]. Previous research has struggled to accurately characterize REYs in light of their complex chemistry and tendency to precipitate in solution. A lack of representative bioassays that consider all REEs, a wider variety of biological test species and water chemistry conditions was also noted.

Considering the caveats above and based on the available data, the concentrations at which REY begin to have adverse effects are relatively high, especially compared to the average background REY concentration (i.e., exposure in ng/L range and guidelines in µg/L). The largest toxicological threat regarding exposure REEs are the high BCF that have been observed within aquatic plants/algae, arthropods/crustaceans and bacteria[7,8]. Investigation into BCF of other metals indicates that BCF are inversely related to exposure concentrations. This assumption, however is not supported by the available REE data. Based on current exposure concentrations and assuming the BCFs observed, large enrichments of REE could occur in certain domains of the aquatic environment.

1.4.2 Bioaccumulation and Bioconcentration

Bioconcentration, bioaccumulation, and biomagnification are distinct processes for which the definitions used by Arnot and Gobas (2006) are utilized in this paper[32]. Bioconcentration, measured via BCFs, is the "process by which a chemical substance is absorbed by an organism from the ambient environment only through its respiratory and dermal surfaces", excluding diet. In contrast, bioaccumulation factors (BAFs) are the amount of chemical absorbed "by all routes of exposure in the natural environment", including dietary sources. Biomagnification is the "process in which the thermodynamic activity of the chemical in an organism exceeds that of its diet".

The largest toxicological threat regarding exposure REYs are the high BCF that have been observed[27,33]. Early work by Hou and Yan investigating BCFs in aquatic systems identified that calculated BCFs for REYs are among the highest recorded for metals[7]. Yin and colleagues determined REE bioaccumulation to be greatest in aquatic plants, then arthopods/crustaceans, shellfish and fish[31]. Despite these high rates of bioaccumulation at lower trophic levels, biomagnificaiton seems unlikely[34]. For the purposes of examining the potential toxic threat of REYs in aqueous environments downstream of mining-affected areas, bioaccumulation factors previously recorded in the literature for aquatic plants, arthropods and bacteria have been compiled.

There is no consensus on whether a universally predictable BCF pattern exists for REY based on their chemical and physical properties. There have been studies that show a decrease in bioaccumulation with increasing atomic number, other studies that show increasing bioaccumulation with increasing atomic number and studies in marine environments that show no pattern whatsoever[31,34,35]. There is little recognition in the existing literature that metal BCFs have been shown to be concentration dependent for many metals. DeForest and colleagues showed that metal concentration tends to have a linear relationship with BCFs and metals with low exposure concentrations have higher BCFs[10].

1.4.2.1 Aquatic Plants

As stated above, aquatic plants are expected to be among the greatest concentrators of REYs in the aquatic environment. Differences between salt water and freshwater have not been observed, and as a result BCTs for both freshwater and marine plants have been provided below[34]. The following range of BCFs have been observed for the range of lanthanide elements:

- 1,000 to 300,000 L/kg dry weight range: freshwater plants, *Potamogeton pectinatus* and *Lemna minor*, Weltje et al. 2002[34]
- 3,000,000 L/kg dry weight average: marine algae, Hou and Yan 1998[7]. Concentrations of rare earth elements were higher in green and red algae species when compared to brown algae species. In addition, dry weight concentrations of La, Ce and Nd were found to be an order of magnitude higher than Tb, Yb and Lu, and partitioning coefficients are greatest for Ce, then Nd and La, with a general decrease with increasing atomic number
- 10 to 1,000,000 L/kg dry weight range: unknown algae species, Van Dijk Looyaard and Montziann[1] 1986 in Sneller et al., 2000[34]

Recent investigations by Tai and colleagues found that biological toxicity of 13 lanthanides on marine monocellular algae was not influenced by the variable abundance of lanthanides in marine systems[31]. As a result, it is hypothesized that BCFs for aquatic plants are not expected to vary appreciably within the REY grouping.

1.4.2.2 Arthropods

Field measurements of BCF in amphipods by Stronkhorst and Yland, reported by Sneller and colleagues, indicated that BCF in amphipods ranged from 4,800 to 48,000 L/kg[34]. This is one of the few studies that examined concentrations and BCFs for the entire grouping of REYs. A noticeable trend of greater bioaccumulation within LREYs when compared to HREYs was observed.

[1] Original reference in dutch; unable to confirm test species.

1.4.2.3 Microbes / bacteria

Bacterial cell walls and extracellular polymeric substances (EPS) are known to effectively adsorb a variety of cationic metals[36,37]. Microbes belonging to the prokaryote domain and the archaea domain may have cell walls that are either gram-positive or gram-negative, and all of which are anionic in charge. Generally, prokaryotic gram-positive bacteria are rich in carboxylic groups whereas prokaryotic gram-negative bacteria are rich in phosphate groups[38]. In the environment, microbes often form microbial mats or biofilm, and are associated with iron oxides. Extracellular polymeric substances are extruded by microbes and are a mixture of biopolymers including polysaccharides, proteins, nucleic acids, uronic acids, humic acids and lipids[37]. These polyanionic mixtures of high molecular weight organic macromolecues may be generated by both prokaryotic (Bacteria, Archaea) and eukaryotic microorganisms (algae and fungi). The term “biofilm” generally refers to aggregated microorganisms that are embedded within a matrix of EPS and that may or may not be attached to a solid surface[39]. Biofilms are often extremely heterogeneous mixtures that are composed of accumulations of microorganisms, EPS, multivalent cations, biogenic and inorganic particles as well as colloidal and dissolved compounds[39].

One of the first papers to examine the fractionation of the complete set of REYs between bacterial and aqueous phases was written by Takahashi and colleagues (2005)[23]. They examined *Bacillus subtilis* (gram positive) and *Escherichia coli* (gram negative), which have well characterized cell wall properties and are commonly found in nature. All partitioning coefficients calculated in the laboratory experiments with the above species showed a strong enrichment in HREY, especially for Tm, Yb and Lu, and a moderate enrichment in the MREYs. The M-type tetrad effect was observed for La-Ce-Pr-Nd and Sm-Eu-Gd, which is present when a REY is sorbed to inner sphere complexes and absent when a REY forms outer sphere complexes. In addition, partitioning values were observed to increase with increasing temperature, and resulting in the enrichment of HREY. These results support the mechanism that there are two main biding sites for REYs on bacterial cell walls: carboxylate site (MREY) and phosphate site (HREY).

In a subsequent paper (2007), Takahashi and colleagues proposed the occurrence of a similar REY pattern to that described above for five different bacterial species[14]. The pattern observed was elevated MREY concentrations, with an increase in HREY within the solid biofilm samples. A similar pattern was noted within the Fe oxyhydroxide precipitates formed below the biofilm. Bacterial enrichments of REY were noted for Sm and Eu. In addition, there were steep enrichments of REYs in the biofilm between Tm to Lu within the HREY. It should be noted, however, that certain samples had to be corrected for the role of aqueous carbonate complexes (they preferentially bind HREY). Partitioning coefficients calculated between the biofilm and dissolved water did not reveal the HREY enrichment; however, when sterilized river water was allowed to oxidize, the abiotic precipitates did not include REYs. These results were similar to the 2005 investigations by Takahashi[15]. Adsorption to bacterial cells were noted at pH values as low as 2; however, when pH was shifted from pH 2 to pH 3, the partitioning coefficient increased by an order of magnitude. This was also noted between pH 3 to pH 4; however, after pH 4, order of magnitude increases in partitioning coefficients were not noted.

Tsuruta (2007) examined the accumulation of REYs from solution using various microorganisms[17]. Previous work by Tsuruta found that gram-positive bacteria accumulated more REYs than gram-negative bacteria, fungi or yeasts[40]. His work in 2005 indicated that bioaccumulation

to REYs increased with increasing atomic number, and that Sm was accumulated by *Arthrobacter nicotianae* well over six times the accumulation of other divalent metals.

Gallionella ferruginea biofilms were examined by Anderson and Pederson (2003) to differentiate partitioning of REYs and actinides between biological material and ferric oxyhydroxides at circumneutral pH (7.2 -7.6). Primary findings included: *G. ferruginea* biofilms could concentrate metals more than 10^6 times the levels found in groundwater and no preferential uptake of HREYs over LREYs was observed. *Gallionella sp.* stalks are not expected to fractionate REYs. Controlled field sites within the Aspö HRL were selected to test the hypothesis that a combination of biological and inorganic system had a greater capacity to adsorb trace metals. Iron oxyhydroxide precipitation was seen to be directly related to the stalk length and the proportion of lanthanides adsorbed. The authors found that the optimum conditions for stalk growth included oxygen saturation between 0.1 mg/L to 1.5 mg/L (up to 3.2 mg/L) and Eh between 130 mV to 170 mV, with an upper limit of 250 mV. Age was also identified as a key factor in surface reactivity, with younger iron oxides providing more binding sites and remaining highly amorphous. In addition, the addition of iron had negative effects on REY sorption, because soluble ionic Fe competes for binding sites with REYs. The conclusion of Anderson and Pederson's work hypothesized that *Gallionella*-dominated BIOS have the capacity to adsorb 30-15,000 times more lanthanides than abiotic and synthetic iron oxides at neutral pH[12]. In addition, the bacterial catalysis of the Fe(II) oxidation may increase the adsorption of BIOS by 60 times over abiotic.

In 2015, Heim and colleagues completed long-term reactor flow studies in the Tunnel of Aspo in the Aspö Hard Rock Laboratory, Sweden to test the hypothesis that trace and REY signatures could help distinguish between whether iron oxides were biogenic or abiotic[13]. The dominant iron oxidizing bacteria in the long-term reactor studies were *Gallionella sp.* and *Mariprofunds sp.* With the exception of the Eu anomaly, they found that REY patterns of microbially formed iron oxyhydroxides were similar to those of the Archaen Banded Iron Formations (BIFs). Takahashi and colleagues came to a similar conclusion in 2007[14]. When the biogenic iron oxides were compared to the abiotic iron oxides formed from precipitation from the same feeder fluid, there were few differences in the observed patterns. Ni and Tl, however, were only found to accumulate in microbially mediated iron oxides.

Kirby et al., examined the relative contributions of abiotic and biological factors in Fe(II) oxidation within mine drainage[41]. They determined that from pH 2.8 to 5, Fe(II) oxidation rates are negatively correlated with pH and catalyzed biologically by a range of acidiphilic iron oxidizers (*such as Acidithiobacillus ferrooxidans*); between pH 5 to 6.4, Fe(II) oxidation appears negatively correlated with pH and oxidized by abiotic, chemical mechanisms and above pH of 6.4, Fe(II) oxidation appears independent of pH.

1.4.3 Microbial iron oxidation

Biological iron oxidation is one of the most common examples of biologically induced mineralization, whereby interactions between biological activity and the environment lead to the secondary precipitation of minerals[42]. In fact, iron biominerals are expected to comprise 40% of all minerals formed by organisms, and the capacity to oxidize iron is found throughout the evolutationary trees of bacteria and archaea[42,43]. There are three general mechanisms of biologically induced mineralization that are observed: (1) microorganisms gain energy by direct redox conversion of specific ions; (2) indirect mineral precipitation resulting from release of metabolic products from the microbial community; (3) passive mineralization induced by non-living organic matter (such as extracellular polymeric substances or cell debris)[38].

Iron oxidizing bacteria have been well studied in both acidic and neutral systems. *Acidithiobacillus sp.* is most well-studied species of the iron oxidizing bacteria. Many iron oxidizers that occur at low pH are within the Gammaproteobacteria class (such as *Acdiferrobacter thiooxydans*); however, recently *Ferrovum myxofaciens*, has been placed within the Betaproteobacteria class[44]. A great diversity of Fe-oxidizing bacteria in neutral waters, however, currently all known oxygen-dependent, neutrophilic, lithotrophic iron oxidizers are proteobacteria[45]. Further, all freshwater species are within the Betaproteobacteria class, while marine species are affiliated with the Zetaproteobacteria class. Common iron oxidizing bacteri include: *Gallionella sp.*[46], *Leptothrix sp.*[47], and *Sphaerotilus sp.* [41,48].

In more neutral pH waters, neutrophilic, aerobic iron-oxidizing bacteria play a key role in iron oxidation and iron oxide formation. Since abiotic oxidation is very fast in pH-neutral waters, aerobic, neutrophilic iron oxidizers frequently colonize the interface between aerobic and anoxic zones in sediments and groundwaters. Key freshwater neutrolphilic iron oxidizing bacteria include:

- *Gallionella sp. are* both autotrophic and mixotrophic, and represent the most well studied neutrophilic iron oxidizing genera. The dissimilatory iron oxidation mechanism for *Gallionella sp.* is well supported, and all species in this genera are microaerophilic, with optimal oxygen concentrations ranging from 0.1 to 1 mg/L[45]. Mixotrophic organisms can obtain energy (electrons), carbon or both from inorganic and organic substrates and CO_2[49]. Its characteristic signature is the formation of twisted stalks of ferrihydrite-like precipitates, also known as extracellular polymeric substances (EPS). It has been found that the twisted stalks are only present when ferric hydroxide is available[41]. It is hypothesized that these twisted stalks protect *Gallionella sp.* from oxygen free radicals formed during iron metabolism[49]. The tolerated pH range for *Gallionella sp.* ranges from pH 5 to pH 6.5, with the optimum ranging from 6.3 to 6.6 and the observed absence of twisted stalk growth below pH 6[50]. In 2013, Fabish and colleagues (2013) identified *Gallionella ferrunginea* as the most abundant iron-oxidizing bacteria at three iron-rich, metal-contaminated creeks (ranging in pH from 4.4 through 6.3), indicating a wider pH tolerance for *Gallionella ferrunginea* than previously thought[51].

- *Leptothrix sp. and Sphaerotilus natans*: *Leptrothrix sp.* are heterotrophic, facultative iron oxidizers. All four species of *Leptothrix* and *S. natans* are able to accumulate ferric iron and/or manganese (IV) on their sheaths, yet definitive evidence that these bacteria utilize energy from iron oxidation is not available. There is little and conflicting evidence regarding the optimal oxygen range for the *Leptothrix* genus growth. Zhang and colleagues[52] found *Leptothrix discophora* able to oxidize manganese in waters between 0 to 8.05 mg/L of oxygen, while other authors[53] found low-oxygen environments provided optimal growth conditions for *Leptothrix*.

- *Sideroyxdans sp.*: This includes *Sideroxydans* strain ES-1, *Sideroxydans paludicola*, and *Ferritophicum radicicola* (although this novel genus may be acidic). Sideroxydans sp. are closely related to Gallionella sp., and together with *Gallionella sp.* form order Gallionellales within Betaproteobacteria[43]. Sideroxydans are physically associated very closely with iron oxides, but unlike *Gallionella sp.* or *Leptothrix sp.*, they do not produce recognizable EPS.

- Strain TW-2: This is a newly identified strain is a mixotroph that grows lithoautotrophically on Fe(II) with carbon dioxide as the carbon source, and grows on acetate alone[43]. TW-2 do not produce EPS, but may produce chelaters to protect themselves from iron encrustation[43]. Other less known iron oxidizing bacteria include the *Siderocapsa sp.*, and *Crentothrix sp.*[43].

Table 1 Bioconcentration factors observed for biofilm and bacteria under field conditions

	Takahashi et al., 2005	Takahashi et al., 2005	Takahashi et al., 2007	Takahashi et al., 2007
	Sulphate reducing bacteria (BCF)	Phototrophic bacteria (BCF)	Biofilm A (BCF)	Biofilm B (BCF)
La	4.5E+05	7.5E+05	1.0E+04	1.1E+05
Ce	8.8E+05	1.4E+06	3.3E+04	1.2E+05
Pr	7.7E+05	1.1E+06	1.1E+04	1.1E+05
Nd	9.3E+05	1.5E+06	1.1E+04	1.1E+05
Sm	9.1E+05	1.4E+06	1.3E+04	1.0E+05
Eu	8.2E+05	1.2E+06	NA	NA
Gd	7.1E+05	9.7E+05	1.0E+04	1.0E+05
Tb	7.6E+05	1.1E+06	1.2E+04	1.1E+05
Dy	6.2E+05	9.3E+05	1.1E+04	1.6E+05
Ho	5.3E+05	7.9E+05	1.0E+04	2.0E+05
Er	4.8E+05	7.1E+05	9.9E+03	3.2E+05
Tm	5.0E+05	7.4E+05	1.2E+04	2.8E+05
Yb	5.3E+05	7.7E+05	1.9E+04	6.8E+05
Lu	5.8E+05	8.5E+05	3.1E+04	5.2E+05
Y	6.7E+05	9.8E+05	NA	NA
pH	8-8.5	8-8.5	6.1-6.5	6.1-6.5

NOTES:
1. BCF PROVIDED IN L/Kg.

1.4.4 REY sorption and complexation with organic acids

In addition to strong affinity to aquatic plants, arthropods and bacteria, REY show strong affinity to organic acids and ligands. Work completed by Tosiani and colleagues identified organic carbon as key player in the sequestration of REYs to the particulate phase and identified a negative linear relationship between the partitioning of dissolved REYs to suspended REYs vs. dissolved organic carbon (DOC)[5]. Other studies found strong linkages between REY concentration, organic carbon, aluminum and iron, and evidence of temporal and seasonal variability[54–56]. These and other studies demonstrate that within tropical and boreal rivers, with high amounts of organic carbon, iron-rich and/or organic colloids play an important role in REY distribution. Within streams characterized by lower amounts of organics, Leybourne and Johannesson found selective iron extractions indicated that approximately 21-29% of REYs were associated with iron[57]. They also found waters to be LREY depleted, with strong negative Ce anomalies and positive Eu anomalies, compared with the sediment which had flatter distribution patterns when compared to the North American Shale Composite (NASC)[57].

1.5 APPLICABLE REGULATIONS

There are currently no existing regulations or guidelines for REE themselves in Canada, the USA or Australia. Pre-feasibility investigations of potential REE mines in Canada is prompting regulatory

review of these elements. The Molycorp Mountain Pass Project, which recommenced operations in 2010, is the largest operating REY mine outside of China. CanMIN laboratory, in association with Natural Resources Canada and the Canadian Research Network, is examining the toxicity of REEs to *Daphnia pulex*, a freshwater aquatic invertebrate, and *Daphnia middendoffiana*, a northern freshwater aquatic invertebrate[43].

In 2000, the Netherlands' National Institute of Public Health and the Environment government completed a literature review on REY exposure and toxicity and created Maximum Permissible Concentration values for La, Ce, Pr, Nd, Sm, Gd, Dy and Y for soil[2], surface water and sediment[34] (Table 2). Guidelines for both freshwater and saltwater environments were provided, but for the purposes of this assessment of effects to aquatic freshwater environments, the saltwater values have not been reported here. In January 2015, Canada's Nuclear Waste Management Organization produced Non-Radiological Interim Acceptance Criteria for the Protection of Persons and the Environment values for surface water, groundwater, sediment and soil. Values from Sneller et al. were used for the interim freshwater surface water and sediment guidelines for rare earth elements.

Table 2 Netherlands' National Institute of Public Health and the Environment Maximum Permissible Concentration (MPC) for select Rare Earth Elements

REE	MPC - Freshwater Surface Water (ug/L)	MPC - Freshwater Sediment (mg/kg)
La	10.1	4,700
Ce	22.1	19,000
Pr	9.1	5,800
Nd	1.8	7,500
Sm	8.2	2,500
Gd	7.1	1,800
Dy	9.3	2,200
Y	6.4	1,400

NOTES:

1. MPC FOR NATURALLY OCCURING SUBSTANCES IS DEFINED AS THE SUM OF THE MAXIMUM PERMISSABLE ADDITION (MPA) AND THE BACKGROUND CONCENTRATION.
2. SNELLER ET AL., 2000.
3. THE MPC FOR FRESHWATER SEDIMENT IS BASED ON THE SEDIMENT-PORE WATER PARTITION COEFFICIENT AND IS CONSISTENT WITH MINIMUM VALUES REPORTED BY ODEQ (2001).

2 – METHODS

2.1.1 Site selection

To gain an understanding of the quantity and pattern of enrichment accumulation of REYs within heterogeneous biofilm commonly found downstream of mining-affected environments, the Silver Creek passive treatment was selected as a model field site. This site was selected due to its high levels of ferrous iron, and its strong chemical gradients. Preliminary investigations indicated that the

[2] Cerium was the only Maximum Permissible Concentration value provided for soil.

pH and Eh conditions at the inflow of the passive remediation system would be conducive to biogenic iron oxidation, while sites near the outflow would be dominated by chemical iron oxidation.

Six sites at the Silver Creek passive treatment system (40.718749; -70.17662), located near New Philadelphia, Pennsylvania, were sampled during low-flow conditions in both December 2015 and August 2016. Water and solid chemistry samples were collected together with samples for subsequent DNA extraction, where DNA was isolated and used for 16S and 18S gene sequencing, and droplet digital polymerase chain reaction (ddPCR). In addition, solid BIOS samples were collected at each site for subsequent scanning electron microscopy (SEM) and x-ray spectroscopy (EDX). Samples were placed directly into 5 mL Nalgene cryogenic vials at field sampling sites and freeze dried with dry ice at the sampling location, immediately after collection, which is the preferred method to preserve sample nucleic acid content[58]. Samples were kept frozen, if possible, and upon reception at the laboratory, immediately stored at -20°C. One litre of unfiltered water was collected at all sites for the abiotic oxidation experiment. Due to study limitations, only the inflow and outflow sites (SC06 and SC01) were analyzed for microbial 16S rRNA gene and 18S rRNA gene sequencing. In addition, ddPCR was completed at sites SC06, SC05 and SC01. Water was collected for the abiotic iron oxidation experiment at all sites; however, due to low amounts of ferrous iron at sites SC01, SC02 and SC03, results from these sites could not be used for further analysis.

Gene sequencing was completed to provide an understanding of exactly which prokaryotes and eukaryotes were present at the site, and their relative abundance. Droplet digital PCR, was completed to provide additional data on the relative abundance of the key bacteria: *Gallionella* sp. and *Leptothrix* sp. Droplet digital PCR is a high-throughput approach to absolute quantification of DNA copy number that is similar to quantitative PCR, and provides the number of reads of a given sequence per µL of solution of DNA extract.

The Silver Creek passive treatment system represents a combination of treatment ponds and aerobic wetlands, located at the anoxic mine discharge outflow (~pH 5.8). At the discharge point, mine water contains elevated ferrous iron (14-17 ppm) and slightly acidic pH conditions (5.94 to 5.86), which rise to circumneutral pH at the terminus of the treatment system (7.13 to 6.76). The treatment site is composed of three ponds and two wetlands: water first passes through mine discharge and scour pool (Pond 1), then it enters the aeration pond which facilities CO_2 outgassing, raising pH (Pond 2). Subsequently water enters Pond 3, designed to precipitate aqueous iron to into solid phase; this pool has the longest retention time (see Figure 1). Water then flows through the two wetlands and is discharged. The facility is designed to discharge 4.5 L/min over the 20 year life of the facility[59]. Samples at this site were collected during the afternoon in December 2015 and then sampled twice in August 2016, during the afternoon and early in the morning.

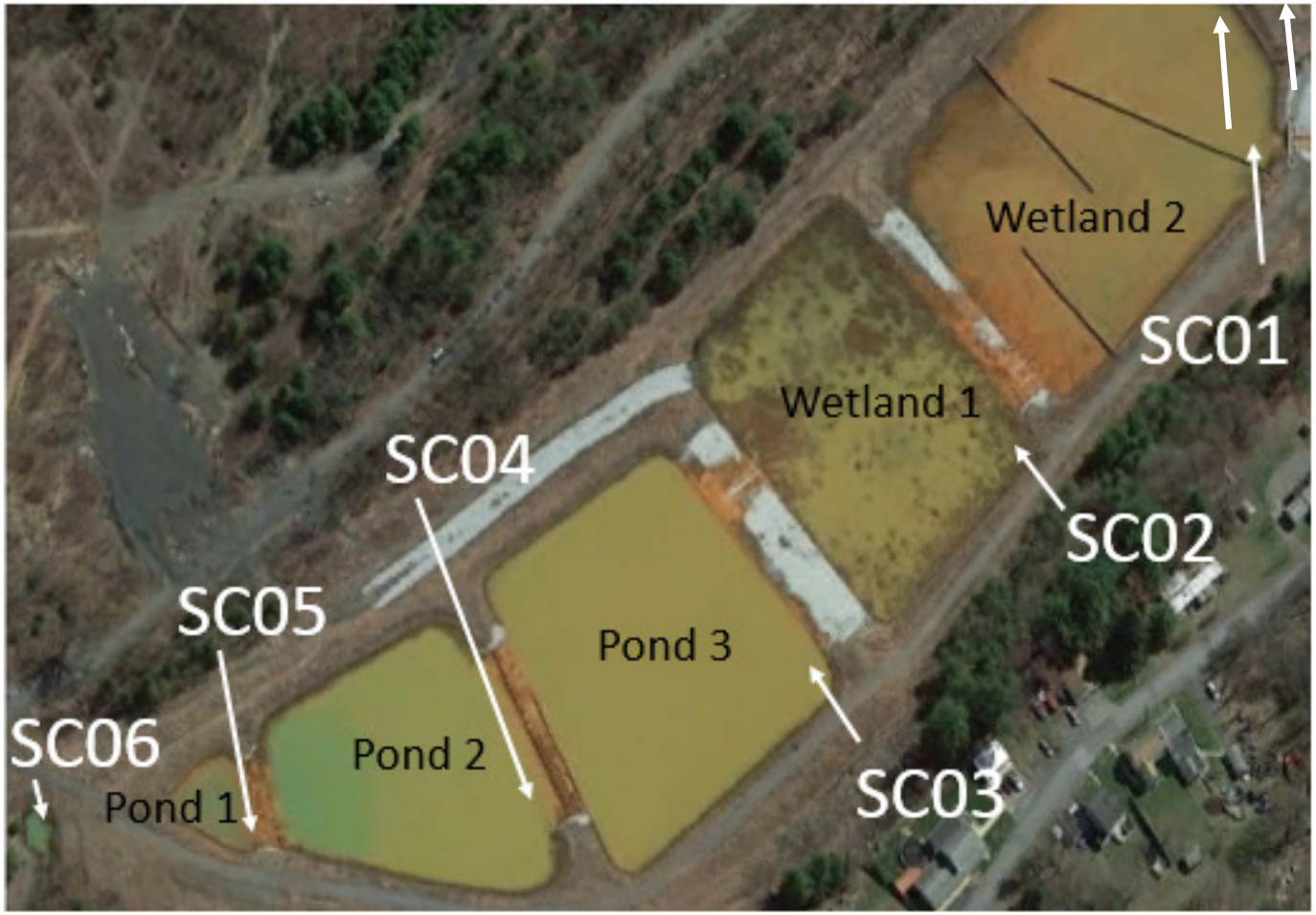

NOTES:

1. POND 1 IS THE MINE DISCHARGE AND SCOUR POOL.
2. POND 2 IS THE AERATION POND.
3. POND 3 IS THE SETTLING POND, WITH THE LONGEST RETENTION TIME OF ALL OF THE POOLS.

Figure 1 Silver Creek Site Passive Remediation Site (image from Google earth©)

Table 3 Silver Creek Site Details and Sampling Sites

Feature	Description of Feature	Sampling Sites	Area of water at surface (m^2)	Design Depth (m)	Geometric Design volume (m^3)
Pond 1	Mine discharge and scour pool	Inflow: SC05A Outflow: SC05	551	0.93	117
Pond 2	Aeration basin	Inflow: SC04A Outflow: SC04A	5,962	3.21	14,182
Pond 3	Settling basin	Inflow: SC03A Outflow: SC03	7,892	3.97	24,239
Wetland 1	Wetland cell	Inflow: SC02A Outflow: SC02	6,972	0.62	3,233
Wetland 2	Variable level pond	Inflow: SC01A Outflow: SC01	8,954	0.61	4,082

NOTES:

1. REFERENCE: PERSONAL COMMUNICATION WITH C. CRAVOTTA, 2017.
2. A LIMESTONE SPILLWAY (NOW COATED IN HFO) CONNECTS PONDS AND WETLAND CELLS TO EACHOTHER.
3. SAMPLING SITE SC5 IS THE MOST UPSTREAM OF THE SAMPLING SITES AND DISCHARGES AT A NATURAL SEEP THAT IS NOT MODELLED. ALL INFLUENT FROM THIS POND REPORTS TO POND 1.

2.1.2 Water chemistry and chemistry of biofilms

Water and biofilm sampling methods and chemical analysis methods are described in detail in **Chapter 1: REY Geochemistry in Mining-Affected Aqueous Environments**. Please refer to Sections 2.2 and 2.3.

2.1.3 Scanning Electron Microscopy (SEM)

Biofilm samples collected from sites in Pennsylvania were air dried for visualization with a JEOL 6610LV Scanning Electron Microscope (SEM) at the University of Ottawa-Canadian Museum of Nature Micro Analysis Laboratory. The SEM was set in secondary electron imaging (SEI) mode, using high vacuum mode, with a spot size of 25 µm, and an electron beam accelerated at 15kV to obtain photos of organic material associated with iron oxides.

2.1.4 Light Microscopy

Analysis of cover slips and slides exposed for several days, singly, in multiple and in both horizontal and vertical alignment, by light microscopy, scanning and transmission electron microscopy has been used by other authors to identify iron bacteria by morphology, as well as estimate rates of *Gallionella sp.* stalk development[60]. Duplicate glass microscope slides were submerged at a subset of sampling sites in Pennsylvania (Silver Creek and Pine Forest sites) to provide information regarding epilithic bacteria (bacteria attached to solid surfaces) and flocculate bacteria (bacteria associated with loose

flocculate) as per Robbins and colleagues[61]. Two microscope slides were submerged at each site sampled (one horizontally into biofilm and one vertically into biofilm) for one week prior to removal. Slides were air dried at room temperature after retrieval and examined using a 100X magnification on a BX51P Olympus light microscope with a DP71 peltier cooled camera.

2.1.5 Abiotic Iron Oxidation Experiment

To test the influence of bacterial samples on REY fractionation, inorganic Fe oxyhydroxide samples formed without bacterial influence were collected from a subset of sites in Pennsylvania (n=8). The methods used for this experiment followed those used to create "Fe_{inorg}" data used by Takahashi and colleagues[14]. This method involved collecting a volume of water (500 mL to 1 L), filtering the water in the laboratory (0.20 µm) to remove any existing bacteria, and allowing the Fe^{2+} water to slowly oxidize over a period of weeks in stoppered glass bottles. Sterilized one litre microcosm bottles were used to provide adequate aerobic headspace and the bottles were left to oxidize for a month in sterile, autoclaved glass bottles. To ensure complete oxidation, autoclaved stirbars were added under sterile conditions to complete remaining oxidation. After the oxidation was complete, samples were filtered through a 0.2 µm filter and residual Fe(III) was digested with aqua regia digestion (Section 2.3.3 in **Chapter 1: REY Geochemistry in Mining-Affected Aqueous Environments**).

2.1.6 DNA extraction, rRNA amplification and sequencing

Total DNA content of algae-microbial communities at each site was extracted using the MO BIO Laboratories Inc. Powersoil® DNA Isolation Kit (catalogue no. 12888-50) at the Centre for Advanced Research in Environmental Genomics, at the University of Ottawa. Approximately 0.25 g of wet sample was used for the nucleic acid digestion. Upon completion of the DNA extraction, nanodrop analysis was completed to determine nucleic acid concentration after extraction, and the 260/280 and 260/230 ratios. As a quality assurance and control check, a PCR was run using 16S universal primers (27F, 5`-AGAGTTTGATCMTGGCTCAG-3`;907R, 5`CCGTCAATTCMTTTRAGTTT-3`) targeting 16S rRNA gene and 18S universal primers (EUK60F, 5'-GAAACTGCGAATGGCTCATT-3'; EUK515R, 5'-ACCAGACTTGCCCTCC-3') to confirm presence of DNA. Extracted DNA samples were sent to Molecular Research LP for 16S rRNAs and 18S rRNA genes amplification and sequencing.

2.1.6.1 16S data processing

Illumina 16S rRNA gene sequencing data was provided by Molecular Research LP for further processing and manipulation. Data was processed in QIIME script and library version 1.9.1 (full system specifications included in Appendix C.1). Raw outputs from Mr. DNA, including: the mapping file (_mapping.txt), raw sequences file (.fasta) and the raw sequences quality file (.qual), where used as inputs to a computational pipeline. Data from 16S rRNA is sequenced to determine diversity of organisms within the domains Bacteria and Archaea. The computational pipeline was based on preliminary pipeline set out by Caporaso and collaborators[62], and drawing on the 18S tutorial from the Werner Lab[63], with steps outlined below (Figure 2). OTU picking was completed using the uclust method, which generates OTU clusters based on percent identity[64].

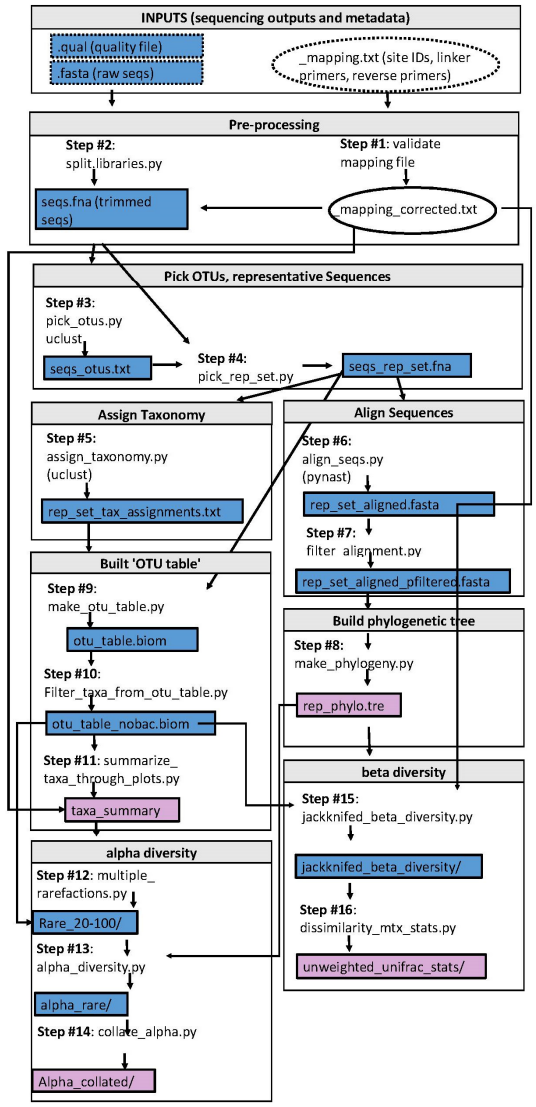

NOTES:

1. COMPUTATIONAL PIPELINE FOR USE IN QIIME SOFTWARE. NAMES OF OUTPUTS ARE ARBITRARY; HOWEVER, ANYTHING ENDING IN .PY IS A PREDEFINED FUNCTION.
2. ITEMS WITH DOTTED EXTERIOR REPRESENT INPUTS AND ITEMS IN PURPLE INDICATE OUTPUTS.

Figure 2 16S data processing pipeline

2.1.6.2 18S data processing

Illumina 18S rRNA data was provided by Molecular Research LP for further processing and manipulation. Data was processed in QIIME script and library version 1.9.1 (full system specifications included in Appendix C.1). Raw outputs from Mr. DNA, including: the mapping file (_mapping.txt), raw sequences file (.fasta) and the raw sequences quality file (.qual), where used as inputs to a computational pipeline. In addition, the SILVA data database was used as a reference when picking Operational taxonomic units (OTUs)[65,66]. The SILVA database contains aligned ribosomal RNA gene sequence from the three major domains that compose microbial life on earth: Bacteria, Archaea and Eukaryota (e.g., protists). Recent advances in sequencing technology enable the rapid computation of

The computational pipeline was based on preliminary pipeline set out by Caporaso and collaborators[62], and specific steps from the Werner Lab[67], with steps outlined below (Figure 3).

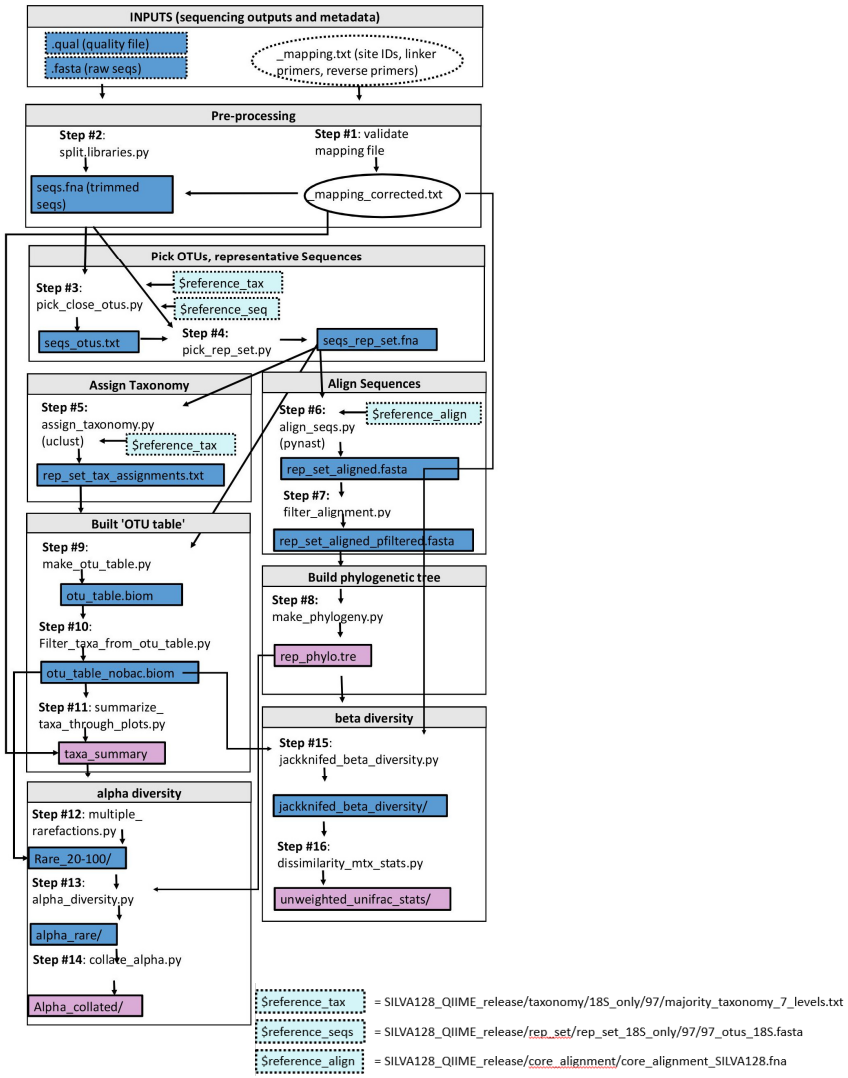

NOTES:

1. COMPUTATIONAL PIPELINE FOR USE IN QIIME SOFTWARE. NAMES OF OUTPUTS ARE ARBITRARY; HOWEVER, ANYTHING ENDING IN .PY IS A PREDEFINED FUNCTION.
2. ITEMS WITH DOTTED EXTERIOR REPRESENT INPUTS AND ITEMS IN PURPLE INDICATE OUTPUTS.

Figure 3 18S data processing pipeline

2.1.7 Droplet Digital PCR

2.1.7.1 Conserved Sequences and Positive Controls

In contrast to quantitative PCR, ddPCR has improved accuracy as a result of large sample sizes and the use of Poisson statistics. The accuracy of ddPCR is dependent on the number of droplets read for each sample. For a theoretical sample that reads 20,000 droplets, the system can estimate original copy levels that range from 1-100,000 target reads[68]. It is important to not exceed 5,000 copies of target/µL of the final ddPCR reaction mix or to have less than 10,000 droplet read per sample[68]. During transfer steps and cutoffs applied by the QuantaSoft software, samples generally read from 12,000 to 16,000 droplets. Variation in this number does not affect the ultimate results, since all quantities are

relative; however, samples below 10,000 droplets are not recommended. All samples analyzed by ddPCR for this study contained between 14,188 and 18,067 droplets, which is well within and exceeding the acceptable range. For the purposes of reporting, average droplets utilized for each analysis (e.g., Lep228F/Lep518R, Gal122f/Gal283R, and ClaP45f/ClaP47R) were pooled to provide an average droplet number.

Within the domains Bacteria and Archaea, the *glnA* gene encodes glutamine synthetase, which functions in ammonia assimilation and glutamine synthesis[69]. The *glnA* gene is perfectly conserved in alpha, beta, gamma-Proteobacteria, Enterobacteria, Thermotoagles, low GC gram positive bacteria and cyanobacteria (except weak conservation in *Trichodesmium thiebautii)* [69]. As a result, *glnA* was selected as the housekeeping gene, to provide an indication of the total bacteria abundance at each site.

Positive controls were unavailable for *Gallionella sp.* and *Leptothrix sp.*, which would need to be run prior to any publication. A positive control was run for cyanobacteria: *Microcystis aeruginosa* strain (CPCC633). This strain is registered in the Canadian Phycological Culture Centre (CPCC), and was received Mar-2005 from UTEX as UTEX LB 2386. It was originally collected Sep-1954 by A. Zehnder at Little Rideau Lake, ON, Canada and isolated by W. Carmichael. It was deposited Apr-1984 by P. Gorham as NRC-1(SS-17). DNA was extracted following a modified protocol, with the help of Nathalie Fortin, Biotechnology Research Institute, National Research Council of Canada, from Hisbergues and colleagues[70].

2.1.7.2 Primer Selection

Droplet digital PCR (ddPCR) was completed to quantify the 16SrRNA gene copy numbers associated with *Leptothrix sp.* (Lep228F, 5`-TCCTACGGGAGGCAGCAGT-3`; Lep518R, 5`-ATTACCGCGGCTGCTGG-3`)[71], *Gallionella ferruginea* (Gal122f, 5`-ATATCGGAACATATCCGGAAGT-3`; Gal 283R, GGTATGGCTGGATCAGGC-3`)[72] and green algae (ClaP45f, 5`-ACCTGGTTGATCCTGCCAG-3`; ClaP47R, 5`-TCTCAGGCTCCCTCTCCGGA-3`)[73]. Primer selection was based on primers previously used for quantitative PCR, and due to limited availability, these primers do not meet all recommendations of BIORAD including: GC content of 50-60% and avoid repeats of Gs and Cs longer than 3 bases. Genomes have not been sequences for *Gallionella ferrunginea*, or any *Leptothrix* species (e.g., *Leptothrix cholondii, Leptothrix discophora, Leptothrix mobilis,* and *Leptothrix vaginalis*). As a result, quantitative PCR and digital droplet PCR (ddPCR) techniques must use conserved 16S rDNA sequences to quantify the amounts of these species. Since bacteria are known to have more than one copy of 16S rDNA, the abundance of iron oxidizers cannot be inferred directly from ddPCR results. For final quantification, ddPCR must be completed to probe for total 16S copy numbers. Ideally, this step would be completed in ddPCR; however, this step would require completion prior to publication.

To complete this analysis, genomic DNA was extracted from sites SC06, SC05 and SC01 during both August and December as per above. Samples were stored at -20˚C until analyzed.

2.1.7.3 Equipment and Method

Droplet digital PCR, termed “third generation PCR”, was utilized, as an alternative to quantitative PCR or the most probable number method, to quantify the relative amounts of *Gallionella ferrunginea* and *Leptothrix sp.* present in samples collected. Droplet digital PCR is an extremely precise and accurate absolute measure of target sequences, and is a trademarked version of the digital PCR method. Digital PCR methods calculate absolute quantification of the number of target DNA molecules present in a

sample by determining the fraction of positive end-point reactions, out of the total and fittng data to a Poisson distribution[68]. Droplet digital PCR technology utilizes microfluidic circuits and surfactant chemistries to divide a 20 µL mixed sample into ~20,000 droplets, or partitions. This division of nucleic acid into small droplets then utilizes amplication technology consistent with original PCR technology.

Digital droplet PCR was completed with the BIO-RAD QX200 Digital Droplet system. The ddPCR workflow involved (1) Completion of ddPCR for *glnA* housekeeping gene at all sites (previously determined concentration and thermal gradient); (2) Concentration optimization for different primers pairs: Lep228F/Lep518R, Gal122f/Gal283R, and ClaP45f/ClaP47R; (3) Thermal optimization for different primer pairs; and (4) final run with optimized concentration and temperature. For each of these stages, assembly of PCR reactions was required, which necessitated creation of three separate master mixes, which combined water, taq and forward and reverse primers: Lep228F/Lep518R, Gal122f/Gal283R, and ClaP45f/ClaP47R. Template DNA is combined with each of the respective master mixes and loaded into individual wells of single-use molded cartridge. Samples were prepared for PCR using the recipe indicated in Table 4. Droplet generation oil, containing stabilizing surfactants, was loaded into the wells next to the samples, and the cartridge is loaded into the BIO-RAD QX200™ Droplet Generator[68]. Within the droplet generator, vacuum is applied to the outlet wells, which partitions ddPCR into approximately 20,000 nanoliter-sized droplets that contain DNA fragments. Droplets were transferred via pipette to 96-well PCR plate to complete thermal cycling (C100 TouchTM Thermal Cycler) within a 96-deep well reaction mode, and read individually by fluorescence on the QX200™ Droplet Reader. Droplet digital PCR enables quantification of nucleic acids without using standard curves and independent reaction efficiency. Samples run with the *Gallionella sp.* primers used the following PCR cycling method: initial denaturing at 94◦C for 2 minutes, 35 cycles of denaturing at 94◦C for 20 s, annealing at 51◦C for 20 s, and extension at 72◦C for 30 s, and followed by a final extension at 72◦C for 5 minutes. Samples run with *Leptothrix* and green algae primers used the following PCR cycling method: initial denaturing at 94◦C for 2 minutes, 35 cycles of denaturing at 94◦C for 20 s, annealing at 56◦C for 20 s, and extension at 72◦C for 30 s, and followed by final extension at 72◦C for 5 minutes. Positive controls for the primers were run, using *Microcystis aeruginosa* strain CPCC633 for the green algae control.

The number of positive, negative and total droplets in each sample was quantified using QuantaSoftTM software. The fraction of positive targets to total targets is corrected using the Poisson algorithim to determine the starting concentration of target DNA (copies/uL).

Table 4 Droplet Digital PCR Recipe

Input	n=1 (µL)
Sample	2.0
Forward primer	0.33
Reverse primer	0.33
EconoTaq	11.00
H_20	8.34

3 – RESULTS

3.1 SCANNING ELECTRON MICROSCOPY

Completely dried microbial mats were observed at high voltage (15 kV) with a Scanning Electron Microscope (Figure 4). Images of surficial BIOS revealed a heterogeneous mineral surface at the SC06 site, in addition a number of helical stalk structures, characteristic of certain iron oxidizers such as *Gallionella ferruginea* and *Mariprofundus ferrooxydans*. Helical stalk structures were observed by SEM at the SC06 site during both August and December, with different levels of mineral encrustation. In addition, straight stalks were also observed within the SC06-dec sample, which are characteristic *Leptothrix sp.*, and several other iron oxidizing species. SEM imagining of the SC05-dec and SC04-dec sites was also completed. Results of this imaging are not shown here; however, straight stalks were observed within the SC04-dec and SC05-dec samples, in additional a helical stalk was observed at the SC05-dec site. X-Ray Spectroscopy (EDX) was completed to determine if REY concentrations were detectable, indicating formation of REY minerals. Please refer to Section 3.2.2.2 in **Chapter 1: REY Geochemistry in Mining-Affected Aqueous Environments**.

3.2 LIGHT MICROSCOPY

Microscope slides that were inserted vertically and horizontally in August 2016 were analyzed by light microscopy (Figure 5). Sites SC01 and SC02 showed presence of several different diatoms, indicating silica levels are likely near or at saturation at these sites. Diatoms were not noted at upstream sites; however, at the SC06 sites, organic matter was observed to be integrated with darkly coloured masses, indicative of oxidized metals.

3.3 16S AND 18S rRNA GENE SEQUENCING

3.3.1 16S and 18S alpha diversity and rarefaction analysis

Analysis of 16S and 18S rRNA follows a number of steps that are commonly referred to as an “analysis pipeline”. The series of steps used to analyze the sequenced data is provided in the above Methods section (Sections 2.1.6). To make it possible to analyze large quantities of sequences, sequences are separated into operational taxonomic units

(OTUs), and further parsed into representative OTUs, that are then assigned taxonomies and can be further quantified. Total and relative abundance of different taxonomic units, used to estimate alpha diversity, can be obtained from an OTU table. Alpha diversity indicates species richness, as the number of species in a given sample size or, in this case, OTU[74]. Analyzing alpha diversity in genomics has added challenges when compared to a simple terrestrial or aquatic taxonomic species inventory. Greater genomic species diversity is always observed with an increased number of base pairs analyzed, or “sample depth”. To understand the influence of sample depth on a specific dataset, rarefaction analysis can be completed. This is a method of random subsampling OTUs that assesses subsampling variability, and more importantly, shows where an increase in sequence length sampled does not equal a large increase in species diversity. Ideally, rarefaction analysis can optimize the OTU read length that best approximates total sample diversity.

Rarefaction curves were completed up to 100 or 200 sequences per sample, using the chao1 index to estimate alpha diversity (Figure 6). Generally, these graphs indicate that alpha diversity increases with sampling depth, as expected. For 18S data, sites seem to reach a diversity maxima between 80 to 100 sequences per sample, indicating this sample depth is representative of total sample diversity.

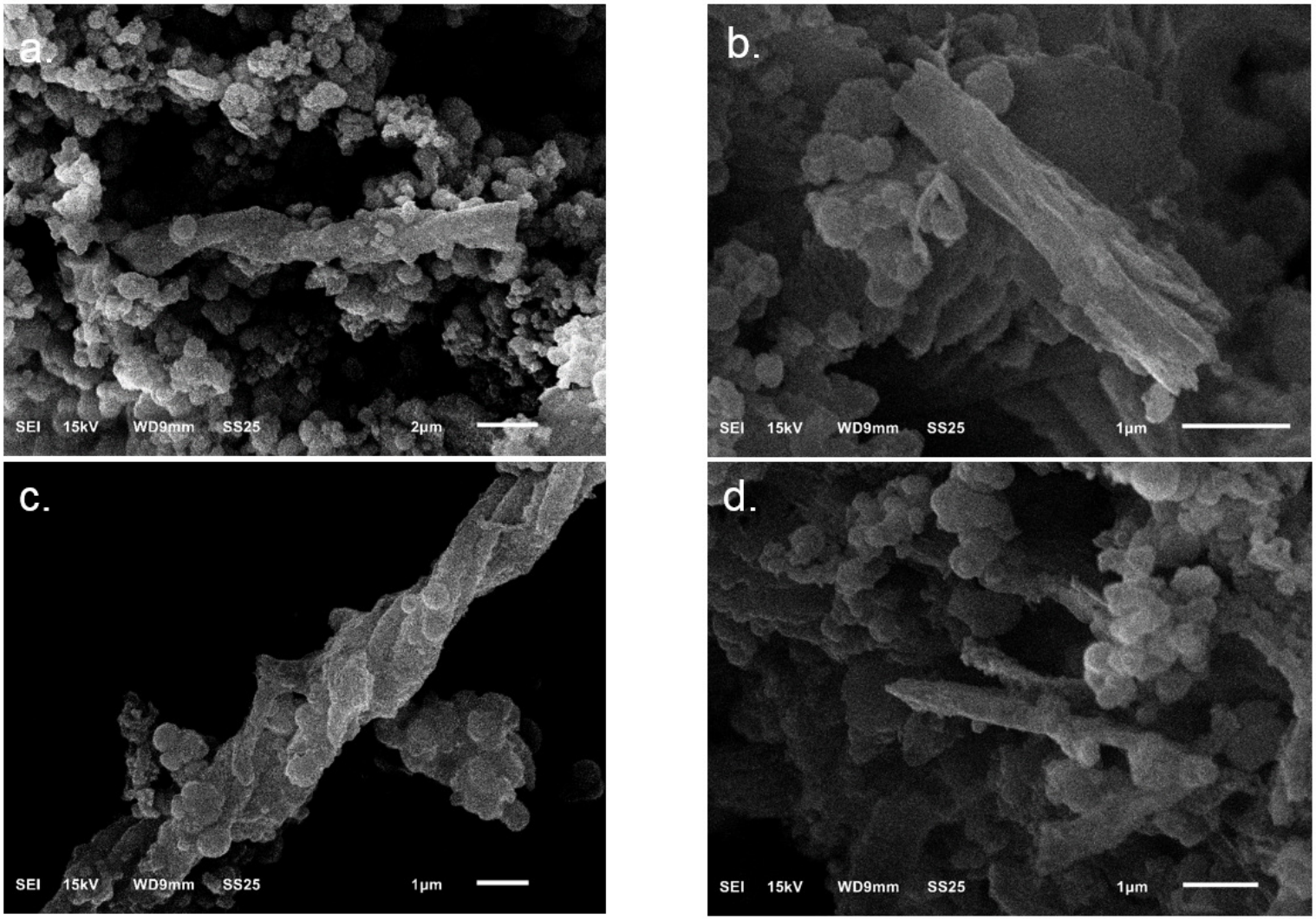

Figure 4 Scanning Electron Microscopy Images a. SC06-Aug twisted stalk; b. SC06-Dec straight stalk; c. SC06-Dec straight stalk; d. SC06-dec twisted stalk.

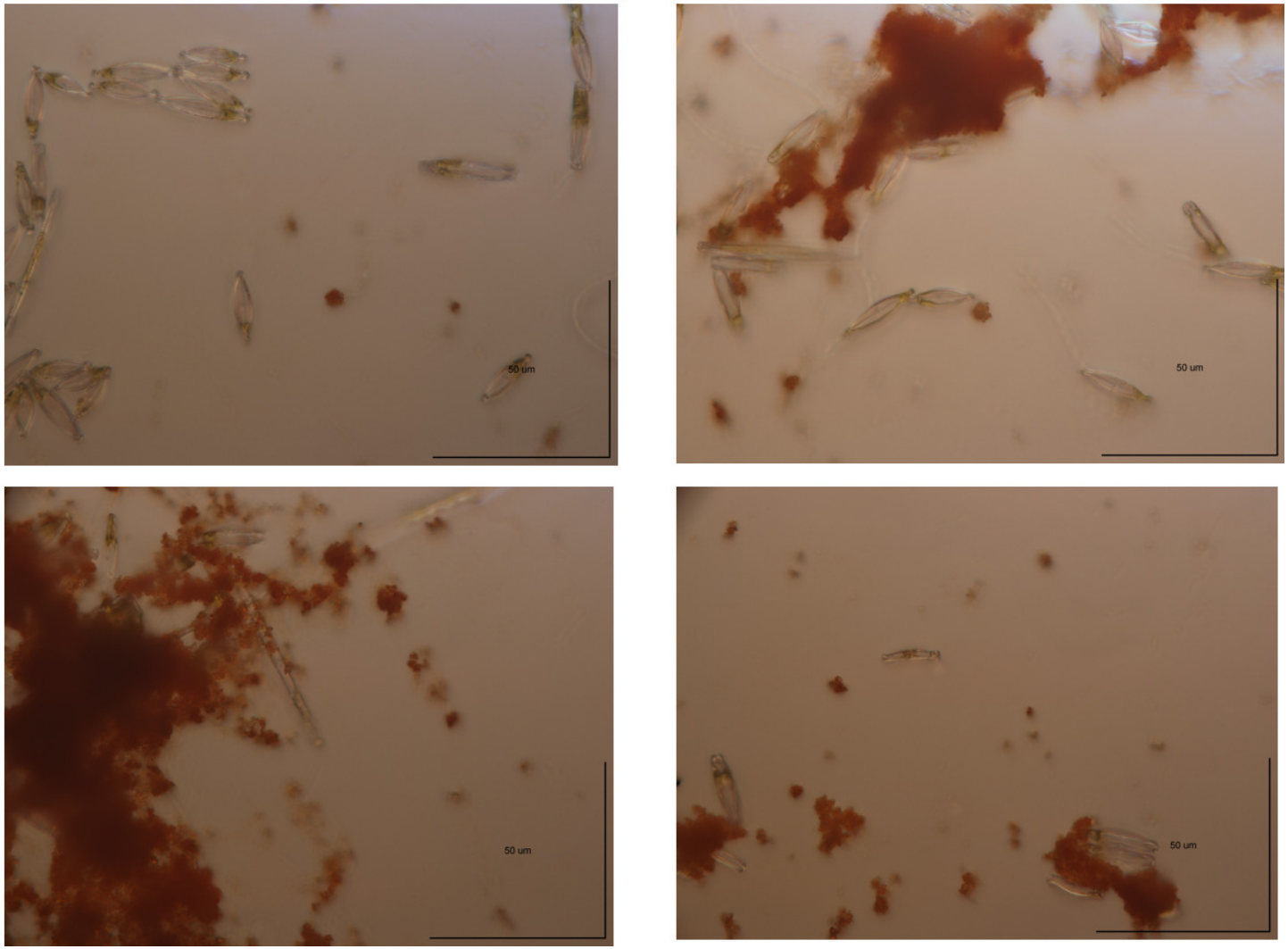

Figure 5 Diatoms observed at SC01 and SC02 sites, Silver Creek (August 2016)

In contrast, rarefaction curves for 16S data do not indicate that sample depth maxima has been reached at any sites, despite analyzing 200 sequences per sample. This means we should be cautious when extrapolating 16S diversity data to estimate total diversity, even at 200 sequences per sample.

The rarefaction curves also show interesting differences between the 16S and 18S data. For 16S data, SC01-Dec has the greatest alpha diversity, and SC06-dec has the lowest alpha diversity, whereas SC01-Aug and SC06-aug show very similar average alpha diversity (n=10). The 18S data shows an inverse trend: SC06-aug shows the greatest average eukaryotic diversity and SC01-Dec shows the lowest eukaryotic diversity. In contrast, average eukaryotic alpha diversity for sites SC01-Dec and SC06-dec are very similar, yet elevated compared to the SC01-Aug site.

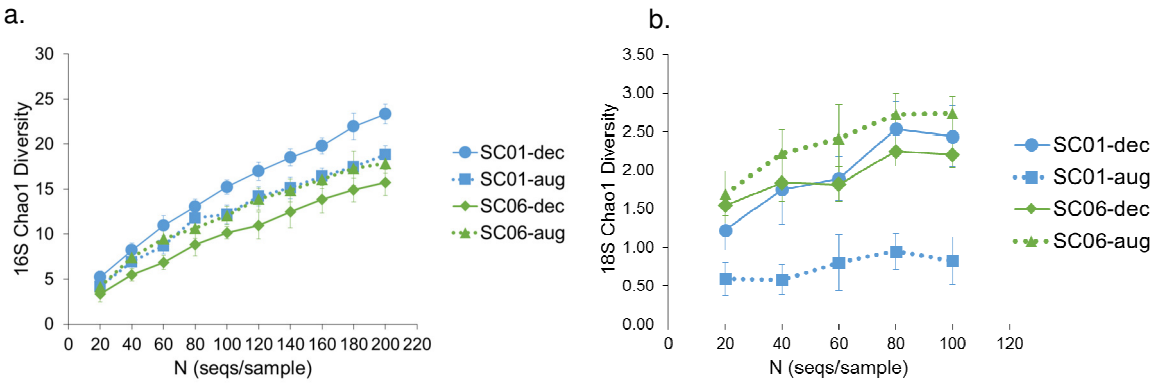

NOTES:

1. ALPHA DIVERSITY CALCULATED USING THE CHAO1 INDEX; ERROR BARS = STANDARD DEVIATION FOR n=10.

Figure 6 Rarefaction Curves for 16S analysis (a) and 18S analysis (b)

3.3.2 16S taxonomic diversity

Relative abundance of different taxa has been estimated using the summarize_taxa_through_plots.py script that runs the summarize_taxa.py function in QIIME. This script outputs taxonomy strings for different phylogenetic classifications. A general overview plot (Figure 7) is provided to confirm results of the rarefaction plot. Consistent with the rarefaction data, site SC01-Dec shows must greater diversity than SC06-dec. Comparisons between the December and August data are difficult to make; however, differences between class composition at sites SC01 and SC06 in August are smaller when compared to class composition at sites SC01 and SC06 during December. To visualize differences in major class comparison, the top ten classes were plotted in subsequent Figure 8.

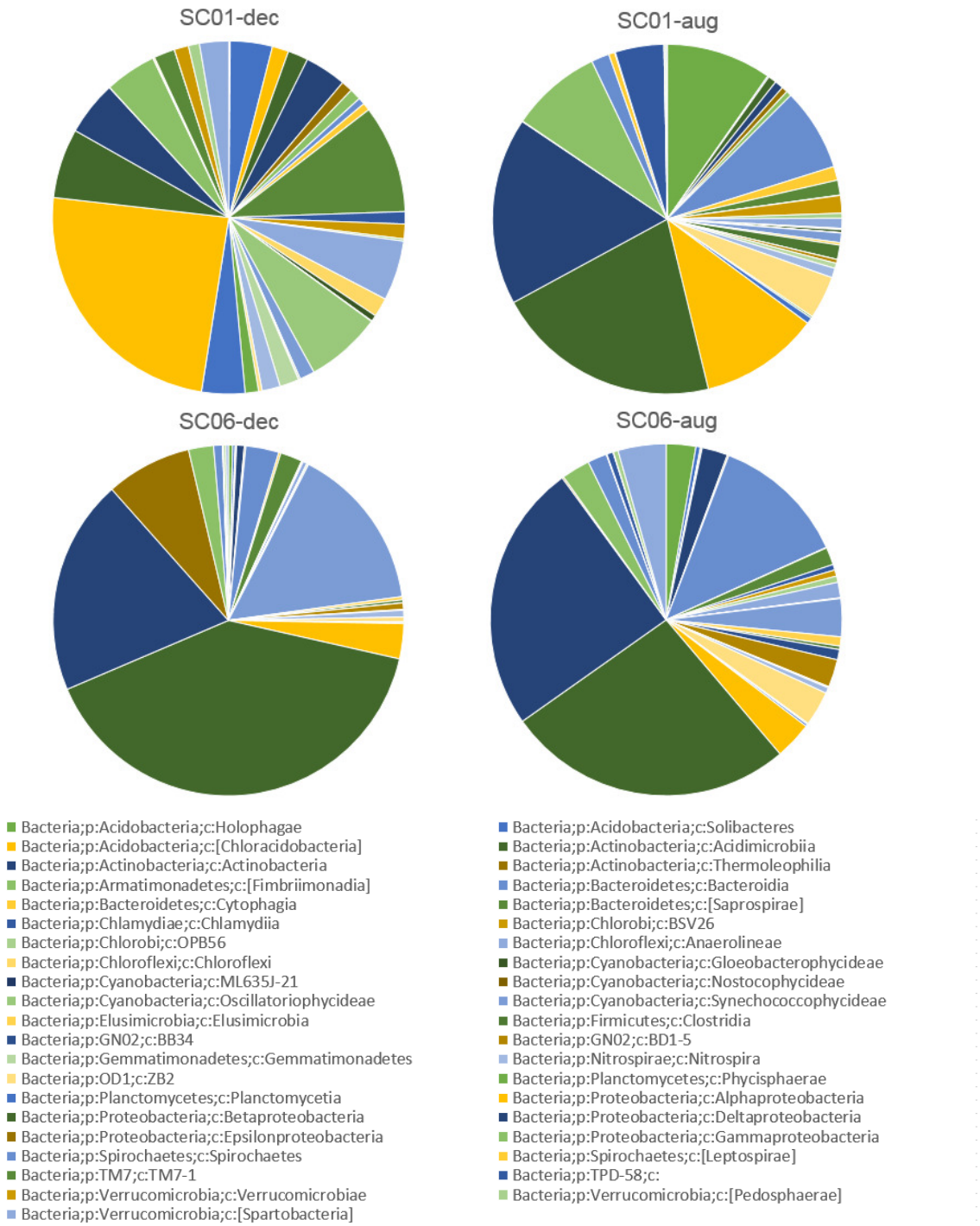

NOTES:

1. ALL PHYLUMS AND CLASSES IDENTIFIED FOR KINGDOM BACTERIAL AND ARCHAEA ARE INCLUDED.
2. SUMMARY OF RELATIVE ABUNDANCE EQUAL CLOSE TO 100%: SC01-DEC (94%); SC06-DEC (97%); SC01-AUG (95%) AND SC06-AUG (96%).

Figure 7 Total relative abundance of 16S bacterial and archaea classes identified within Silver Creek samples

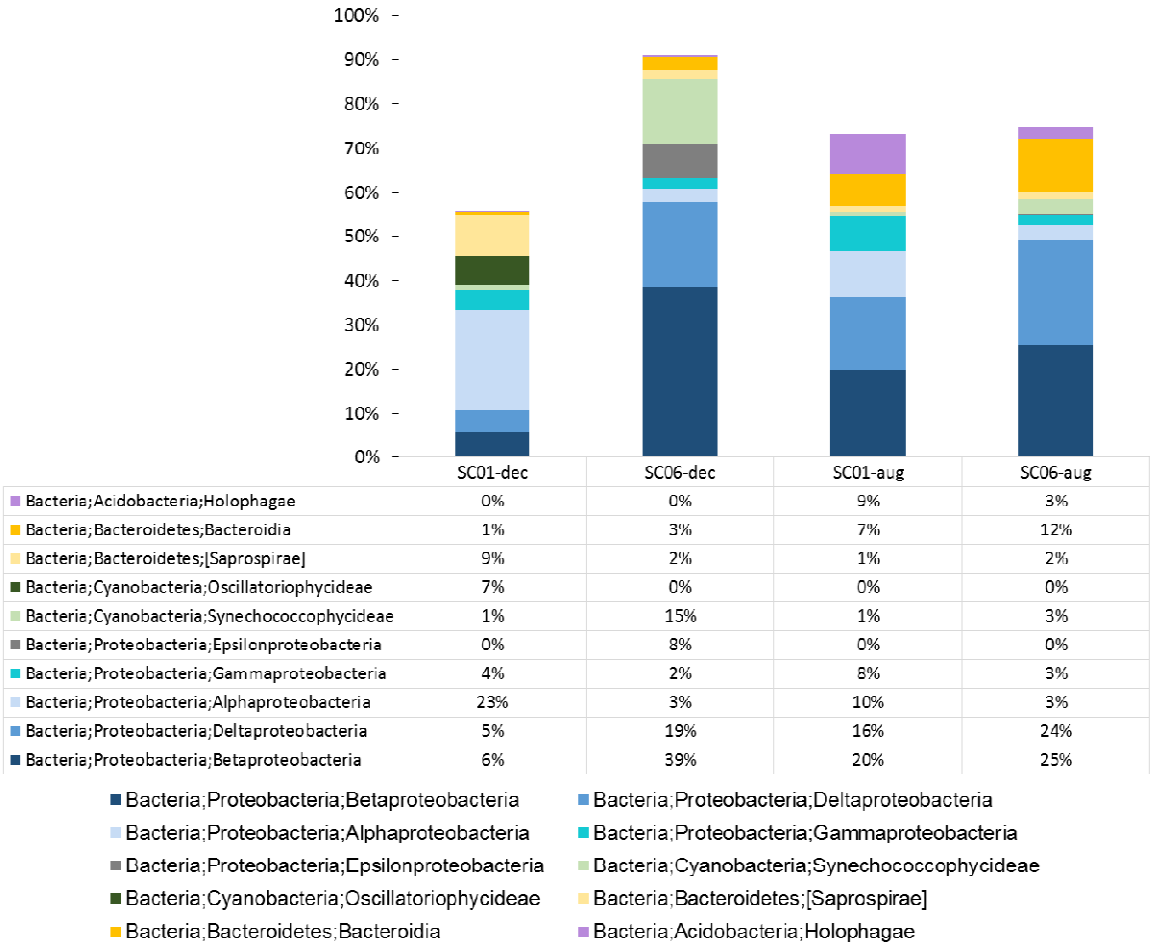

	SC01-dec	SC06-dec	SC01-aug	SC06-aug
Bacteria;Acidobacteria;Holophagae	0%	0%	9%	3%
Bacteria;Bacteroidetes;Bacteroidia	1%	3%	7%	12%
Bacteria;Bacteroidetes;[Saprospirae]	9%	2%	1%	2%
Bacteria;Cyanobacteria;Oscillatoriophycideae	7%	0%	0%	0%
Bacteria;Cyanobacteria;Synechococcophycideae	1%	15%	1%	3%
Bacteria;Proteobacteria;Epsilonproteobacteria	0%	8%	0%	0%
Bacteria;Proteobacteria;Gammaproteobacteria	4%	2%	8%	3%
Bacteria;Proteobacteria;Alphaproteobacteria	23%	3%	10%	3%
Bacteria;Proteobacteria;Deltaproteobacteria	5%	19%	16%	24%
Bacteria;Proteobacteria;Betaproteobacteria	6%	39%	20%	25%

Figure 8 Total relative abundance of ten most abundant classes for 16S bacterial and within Silver Creek samples

Although both the archaea and bacteria kingdom were sampled using a universal primer targeting both bacteria and archaea, the top ten most abundant classes were all bacteria. The most abundant classes observed at the sampled Silver Creek site include: betaproteobacteria, deltaproteobacteria and alphaproteobacteria. With the exception of SC01-Dec, betaproteobacteria is the most dominant class, followed by deltaproteobacteria. At site SC01-Dec, alphaproteobacteria comprises the dominant class, followed by a nearly even split between betaproteobacteria and deltaproteobacteria classes.

Breaking down the taxonomic classification one level further, to order (Table 5), the majority of the deltaproteobacteria class can be accounted for by order desulfuromadales. In addition, the majority of the betaproteobacteria class are accounted for by either order burkholderiales or order gallionellales. The composition of the alphaproteobacteria is split between a number of orders, including rhizobiales, rhodobacterales and sphingomonadales. At the lowest taxonomic level generated in QIIME, there are

four groupings of organisms that remain the most abundant: genus Gallionella, genus Geobacter, family Comamonadaceae and order Bacteroidales. These four classes are observed at all sites, except SC01-Dec. In addition, Genus Gallionella and Genus Geobacter are better represented at the site SC06-dec, while class Commonodecaea and Order Bacteroides are better represented at sites SC01-sug and SC06-aug.

Table 5 Total relative abundance of 16S data, to taxonomic order

Taxonomic Classification (Kingdom; Phylum; Class; Order)	SC01-Dec	SC06-dec	SC01-Aug	SC06-aug
Bacteria;Proteobacteria;Betaproteobacteria;Burkholderiales	3%	7%	13%	14%
Bacteria;Proteobacteria;Betaproteobacteria;Gallionellales	0%	20%	2%	4%
Bacteria;Proteobacteria;Betaproteobacteria;SBla14	0%	6%	1%	2%
Bacteria;Proteobacteria;Deltaproteobacteria;Desulfuromonadales	0%	17%	9%	13%
Bacteria;Proteobacteria;Deltaproteobacteria;Bdellovibrionales	0%	1%	0%	3%
Bacteria;Proteobacteria;Deltaproteobacteria;Myxococcales	2%	0%	2%	4%
Bacteria;Proteobacteria;Alphaproteobacteria;	2%	0%	1%	1%
Bacteria;Proteobacteria;Alphaproteobacteria;Rhizobiales	9%	1%	5%	1%
Bacteria;Proteobacteria;Alphaproteobacteria;Rhodobacterales	3%	0%	0%	0%
Bacteria;Proteobacteria;Alphaproteobacteria;Sphingomonadales	6%	1%	3%	0%
Bacteria;Proteobacteria;Gammaproteobacteria;Legionellales	2%	0%	3%	1%
Bacteria;Proteobacteria;Epsilonproteobacteria;Campylobacterales	0%	8%	0%	0%
Bacteria;Cyanobacteria;Oscillatoriophycideae;Oscillatoriales	6%	0%	0%	0%
Bacteria;Cyanobacteria;Synechococcophycideae;Pseudanabaenales	1%	14%	1%	3%
Bacteria;Bacteroidetes;Bacteroidia;Bacteroidales	1%	3%	7%	12%
Bacteria;Bacteroidetes;[Saprospirae];[Saprospirales]	9%	2%	1%	2%
Bacteria;Acidobacteria;Holophagae;Holophagales	0%	0%	9%	3%

NOTES:

1. THIS TABLE INCLUDES FRACTIOSN OF CLONE SEQUENCES WITH > 97% SEQUENCE IDENTITIY TO 16S rRNA CLONE LIBRARIES.
2. CALCULATIONS WERE BASED ON THE TOTAL NUMBER OF CLONES ASSOCIATED WITH PHYLOTYPES OF SEQUENCED REPRESENTATIVES AT THE ORDER LEVEL.

Table 6 Most abundant genus/family/order of lowest taxonomic grouping

Lowest Taxonomic Classification	SC01-Dec	SC06-dec	SC01-Aug	SC06-aug
Class: Betaproteobacteria; Order: Gallionellales; Family: Gallionellaceae; Genus: Gallionella	0%	20%	2%	4%
Class: Betaproteobacteria; Order: Burkholderiales; Family Comamonadaceae	1%	4%	11%	8%
Class: Deltaproteobacteria; Order; Desulfuromonadales; Family: Geobacteraceae; Genus: Geobacter	0%	17%	9%	13%
Class: Bacteroidia; Order: Bacteroidales	0%	2%	4%	11%

3.3.3 18S taxonomic diversity:

Four phyla comprise 99%-100% of the eukaryotic diversity: Archaeoplastida, Opisthokonta, SAR, and Excavata (Table 7). Relative abundance of classes observed at sites SC01 and SC06 during August and December supports the results obtained for the 18S rarefaction plots: the SC01-Aug sample showed the least diversity, since 98% of the sample was identified as class Alveolata. Similarly, the majority of the taxonomic abundance (75%) at the SC01-Dec could be attributed to one class (Chloroplastida); however, the presence of a number of other classes in low abundance, led to its relatively higher alpha diversity compared with the SC01-Aug site.

In contrast to the SC01 site, the SC06 site during both sampling events has more even taxonomic distribution. In particular, sample SC06-Aug has almost even abundance in four different taxonomic classes (Chloroplastida, Holozoa, Nucletmycea, and Stramenopiles). The taxonomic distribution at SC06-Dec is slightly less even, with 58% of the sample abundance comprised of class Holozoa. Further analysis reveals that *Petricichia sp.* consititute the entirety of the Alveolata class. Similarly, *Chromadorea monhysterida* makes up close to the entirety of Class Holozoan.

Table 7 Taxonomic Orders that comprise domain Eukaryota

Taxonomic Diversity (Eukaryota)	SC01-Dec	SC06-dec	SC01-Aug	SC06-aug
Phylum: Archaeplastida; Class: Chloroplastida	75%	6%	1%	20%
Phylum: Opisthokonta; Class: Holozoa	8%	58%	1%	20%
Phylum: Opisthokonta; Class: Nucletmycea	11%	6%	0%	16%
Phylum: SAR; Class: Alveolata	2%	10%	98%	2%
Phylum: SAR; Class: Rhizaria	2%	0%	0%	7%
Phylum: SAR; Class: Stramenopiles	1%	16%	0%	32%
Phylum: Excavata; Class: Discoba	0%	4%	0%	2%
total	100%	100%	100%	99%

Table 8 Lowest taxonomic grouping that represents majority of domain Eukaryota

Taxonomic Diversity (Eukaryota)	SC01-Dec	SC06-dec	SC01-Aug	SC06-aug
Phylum: Archaeplastida; Class:Chloroplastida; Order:Chlorophyta; Family: Trebouxiophyceae; Other	0%	5%	0%	17%
Phylum: Archaeplastida; Class:Chloroplastida; Other; Other; Other	72%	0%	0%	1%
Phylum: Opisthokonta; Class:Holozoa; Order:Metazoa (Animalia); Genus: Chromadorea; Species: Monhysterida	4%	57%	1%	20%
Phylum: SAR; Class:Alveolata; Order:Ciliophora; Genus: Peritrichia; Other	1%	0%	98%	0%
Phylum: SAR; Class:Stramenopiles; Order:Ochrophyta; Other; Other	0%	7%	0%	25%
Fraction of total alpha diversity	**77%**	**70%**	**99%**	**62%**

3.4 DROPLET DIGITAL PCR

Droplet digital PCR (ddPCR) was completed to quantify the number of bacteria present at the Silver Creek site. Droplet digital PCR is similar to quantitative PCR, and provides the number of reads of a given sequence per µL of solution of DNA extract. In contrast to quantitative PCR, ddPCR has improved accuracy as a result of large sample sizes and the use of Poisson statistics. The accuracy of ddPCR is dependent on the number of droplets read for each sample. For a theoretical sample that reads 20,000 droplets, the system can estimate original copy levels that range from 1-100,000 target reads[68]. It is important to not exceed 5,000 copies of target/µL of the final ddPCR reaction mix or to have less than 10,000 droplet read per sample[68]. During transfer steps and cutoffs applied by the QuantaSoft software, samples generally read from 12,000 to 16,000 droplets. Variation in this number does not affect the ultimate results, since all quantities are relative; however, samples below 10,000 droplets are not recommended. All samples analyzed by ddPCR for this study contained between 14,188 and 18,067 droplets, which is well within and exceeding the acceptable range. For the purposes of reporting, average droplets utilized for each analysis (e.g., Lep228F/Lep518R, Gal122f/Gal283R, and ClaP45f/ClaP47R) were pooled to provide an average droplet number.

The negative control indicated that false overexpression was generally not an issue for the primers tested; however, results for the negative control, and for the CPCC633 positive control for *Leptothrix sp.* indicate the primer is slightly nonspecific, and values under approximately 6,000 copies/µL should be considered equal to zero. Results for the positive control, CPCC633, indicate that the positive control was unsuccessful.

Results from the *glnA* assay showed large seasonal and spatial differences in bacterial composition. First, the SC01-Aug sample showed an extremely reduced bacterial population, compared with its December population. In addition, there were distinct seasonal differences observed between the SC06-Aug and SC06-Dec samples. The SC06-Aug sample shows more than 3x greater abundance of bacteria when compared with the SC06-Dec sample. Although the *glnA* results do not indicate abundance of a particular species, these numbers are assumed to be a good estimate of the total number of bacteria. In addition, by applying the relative abundance rations observed during 16S sequencing, general estimate of species abundance can be completed.

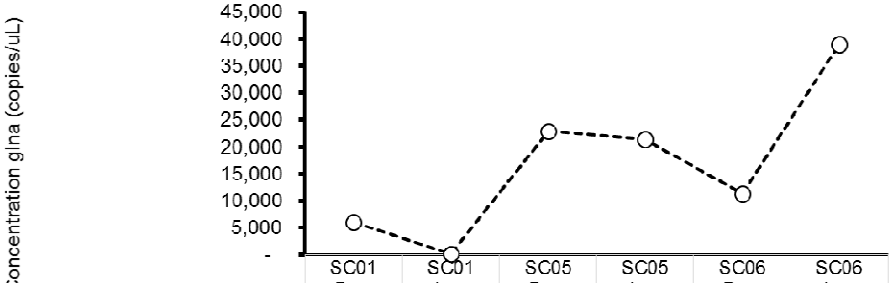

	SC01 Dec	SC01 Aug	SC05 Dec	SC05 Aug	SC06 Dec	SC06 Aug
glnA (copies/uL)	6,025	100	22,950	21,350	11,300	39,050
PoissonConfMax (copies/uL)	126	3	471	439	234	799
PoissonConfMin (copies/uL)	118	2	453	421	222	772

NOTES:
1. NEGATIVE CONTROL FOR THE gnlA ASSAY WERE 21 copies/uL.

Figure 9 Results of *glnA* assay (ClaP45f/ClaP47R)

Results from the *Gallionella sp.* and *Leptothrix sp.* assays show slightly different spatial trends when compared to the *glnA* assay. Relative abundance of all sites except SC06-Dec follow the results of the *glnA* assay; however, in contrast to the *glnA* assay, the species-specific ddPCR assay shows that SC06-Dec has the greatest concentrations of *Gallionella sp.* and *Leptothrix sp.* Results of the 16S sequencing indicate that the SC06-Dec having the greatest relative proportion of *Gallionella sp.* when compared to other sites.

Gallionella sp. and *Leptothrix sp.* concentrations with the species-specific ddPCR assays are very elevated when compared to the *glnA* assay. In contrast to the *glnA* assay, the species-specific assays are based on 16S rDNA primers. Since there is more than one copy of 16S rDNA in a given bacteria, it is expected that the concentrations in the species-specific assay would be higher and could only be interpreted in relative terms. The extremely elevated nature of the *Leptothrix sp.* over the *Gallionella sp.* is difficult to explain; however, these results indicate that the results of each assay are only useful in reference to each particular species. In other words, the relative abundance of *Leptothrix sp.* 16S can be compared between geographic sites; however, comparison of this species abundance to *Gallionella sp.* is not valid.

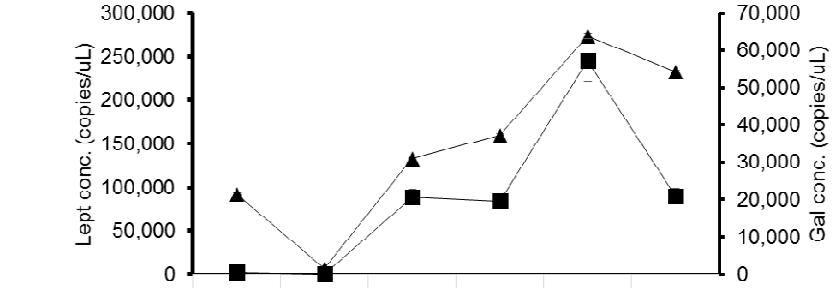

	SC01 Dec	SC01 Aug	SC05 Dec	SC05 Aug	SC06 Dec	SC06 Aug
lept (copies/uL)	91,900	6,330	132,50	159,40	273,30	232,60
gal (copies/uL)	561	28	20,620	19,580	57,200	21,000

NOTES:

1. NEGATIVE CONTROL FOR THE gnlA ASSAY WERE 21 copies/uL.
2. ERROR BARS ARE CALCUALTED BASED ON TECHNICAL ERRORS ESTIMATED WITH A POISSON DISTRUBTION AT 95% CONFIDENCE INTERVAL.

Figure 10 Results of the gal, lept and cla assays

Table 9 Summary of key and solid chemistry results

Site	Date	Water									Biofilm			
		Temp (◦C)	DO (mg/L)	Eh	pH	DIC	DOC	Dissolved total iron (Fe(II) and Fe(III))	Calculated Hardness	Sum Aqueous REYs + Sc (µg/L)	%TC	%OC	Total Fe (mg/kg)	Sum Solid REYs + Sc (mg/kg)
SC06-Dec	12/12/2015	11.89	0.57	236.8	5.86	40.14	4.16	17	200.9	17.6	4.9	2.7	290,000	693
SC06-Aug-PM	08/08/2016	12.12	0.56	291.3	6.03	29.8	2.3	20	202.5	24.1	7.5	7.3	93,000	512
SC06-Aug-AM	09/08/2016	11.93	0.83	294	5.94	NA	NA	14	187.7	5.9	NA	NA	110,000	504
SC05-Dec	12/12/2015	11.98	1.86	281.3	5.84	37.53	2.89	17	200.9	16.1	1.4	0.7	450,000	724
SC05-Aug-PM	08/08/2016	13.91	1.18	299.3	6.02	27.5	1.8	19	198.4	26	2.2	1.2	240,000	578
SC05-Aug-AM	09/08/2016	12.1	2.12	319	5.97	22.6	0.8	21	216.6	23.9	NA	NA	230,000	477
SC04-Dec	12/12/2015	10.28	8.34	293.2	6.15	17.07	1.58	9.3	210	3.6	1.4	0.4	410,000	580
SC04-Aug-PM	08/08/2016	17.93	3.4	358.5	5.81	17.8	1.8	12	211.6	5.5	11.4	11.4	140,000	672
SC04-Aug-AM	09/08/2016	14.79	5.56	378.9	5.86	NA	NA	3.6	189.3	2.6	NA	NA	370,000	687
SC03-Dec	12/12/2015	8.81	10.49	297.8	6.44	9.92	1	5	205.9	1.4	1.1	0.4	450,000	450
SC03-Aug-PM	08/08/2016	25.23	7.89	322.1	6.47	5.4	1.7	0.79	216.6	2.3	0.6	0.2	380,000	350
SC03-Aug-AM	09/08/2016	20.37	7.78	384.1	6.27	NA	NA	0.24	198.4	1.7	NA	NA	370,000	339
SC02-Dec	12/12/2015	8.73	11.34	286.1	6.65	7.68	0.88	2	210	1	2.7	0.8	370,000	395
SC02-Aug-PM	08/08/2016	25.55	10.21	367.1	7.18	5.5	2.3	0.28	196.8	0.8	1.6	0.2	380,000	404
SC02-Aug-AM	09/08/2016	21.08	6.74	391.8	6.67	7.1	1.8	0.29	224.1	1	NA	NA	370,000	373
SC01-Dec	12/12/2015	8.46	12.01	283.1	6.76	6.28	1	1.2	210	1	3.9	2.1	320,000	333
SC01-Aug-PM	08/08/2016	28.97	9.64	342.2	7.56	3.4	2.3	0.27	212.5	0.9	1	0.3	430,000	170
SC01-Aug-AM	09/08/2016	20.47	7.7	460.2	7.13	NA	NA	0.012	207.5	0.8	NA	NA	360,000	475

3.5 IN SITU WATER CHEMISTRY, MAJOR AND TRACE ION COMPOSITION

Concentrations of cations and anions are provided in **Chapter 1: REY Geochemistry in Mining-Affected Aqueous Environments.** Table 9 provides a summary of key water and solid chemistry parameters. Iron is the main element that makes up the biofilm, ranging from <14% to 46%. Al is next most common element within the biofilm. Dissolved oxygen, pH and the amount of dissolved ferrous iron are key parameters to determine which species of circumneutral iron-oxidizing bacteria would be expected to dominate.

In general, dissolved oxygen is observed to occur at very low levels at the inflow site (SC06), ranging from 0.57 to 0.83 mg/L. Likely as a result of an increase in oxygen resulting from turbulent mixing of water, and potentially photosynthetic activities by eukaryotes or prokaryotes, oxygen levels increase downstream. At the discharge of the passive treatment facility, dissolved oxygen levels range from 7.7 mg/L to 12.01 mg/L. These data indicate that each site may potentially have different microbial populations, as result of widely different levels of dissolved oxygen. Measured pH values also occur on a gradient, from lowest (SC06/SC05/SC04) to highest (SC01). As expected from an iron rich groundwater source, water at the inflow to the passive treatment system has high amounts of ferrous iron, which subsequently oxidizes into solid solution downstream.

In order to complete screening of REYs against guidelines proposed by Sneller et al., water and biofilm concentrations for La, Ce, Pr, Nd, Sm, Gd, Dy, and are provided in Table X. Biofilm concentrations remain orders of magnitude below the preliminary guidelines for sediment. Similarly, water chemistry concentrations are well below guidelines proposed by Sneller et al[34].

Table 10 Comparison of REY biofilm and water concentrations to guidelines proposed by Sneller et al.

	Biofilm Concentrations (mg/kg)								Water Concentrations (ug/L)							
Sample	**La**	**Ce**	**Pr**	**Nd**	**Sm**	**Gd**	**Dy**	**Y**	**La**	**Ce**	**Pr**	**Nd**	**Sm**	**Gd**	**Dy**	**Y**
	4,700	19,000	5,800	7,500	2,500	1,800	2,200	1,400	10.1	22.1	9.1	1.8	8.2	7.1	9.3	6.4
SC06-Dec	74	200	25	110	22	23	15	60	2.5	5.2	0.59	2.3	0.44	0.51	0.33	1.7
SC06-Aug-PM	83	180	22	88	17	17	12	59	3.9	8.1	0.95	3.8	0.68	0.86	0.58	2.9
SC06-Aug-AM	81	180	22	85	18	20	12	55	1.4	1.8	0.18	0.71	0.07	0.092	0.058	0.65
SC05-Dec	77	220	28	110	25	24	16	60	2.3	4.8	0.53	2.1	0.41	0.5	0.29	1.5
SC05-Aug-PM	79	210	27	110	22	21	15	60	4.5	9.2	1.00	4.1	0.66	0.84	0.55	3.1
SC05-Aug-AM	70	170	22	87	17	17	11	51	3.9	8.0	0.94	3.8	0.69	0.8	0.56	2.9
SC04-Dec	71	170	21	85	18	18	13	57	0.65	0.62	0.033	0.11	<0.03	<0.05	<0.04	0.13
SC04-Aug-PM	96	240	30	120	24	24	17	78	0.68	0.48	0.03	0.087	<0.009	0.017	0.008	0.0020
SC04-Aug-AM	92	260	30	120	26	28	19	73	1.3	1.5	0.13	0.41	0.062	0.11	0.0820	0.0071
SC03-Dec	68	130	15	57	11	13	9	54	0.24	<0.05	0.012	0.051	<0.01	0.012	0.013	0.18
SC03-Aug-PM	70	120	13	50	9	11	8	53	0.50	0.32	0.02	0.053	<0.009	0.022	0.017	0.35
SC03-Aug-AM	64	120	13	48	10	12	8	48	0.36	0.19	0.014	0.045	0.005	0.012	0.009	0.23
SC02-Dec	60	110	13	50	10	12	8	49	0.030	<0.05	<0.002	<0.006	<0.01	<0.01	<0.007	0.024
SC02-Aug-PM	76	140	15	60	11	13	10	59	0.023	0.018	<0.001	<0.009	<0.009	0.002	0.00260	0.021
SC02-Aug-AM	70	130	14	55	10	12	9	55	0.036	0.024	<0.001	<0.009	<0.009	0.0035	0.00330	0.03
SC01-Dec	50	94	11	41	8	10	7	44	0.020	<0.05	<0.002	<0.006	<0.01	<0.01	<0.007	0.021
SC01-Aug-PM	38	52	5	21	3	5	4	33	0.029	0.026	<0.001	<0.009	<0.009	0.0032	<0.001	0.026
SC01-Aug-AM	87	160	18	73	15	18	12	68	0.032	0.018	0.0022	0.009	<0.002	<0.004	<0.003	0.025

NOTES:

1. COMPLETE CHEMICAL SUITE CAN BE FOUND IN CHAPTER 1: REY GEOCHEMISTRY IN MINING-AFFECTED AQUEOUS ENVIRONMENTS.

3.6 REY ACCUMULATION AND FRACTIONATION WITHIN BIOFILM

3.6.1 Magnitudes of REY Partitioning Coefficients

To determine magnitudes of REY accumulations, similar to Takahashi, Heim and Verplank and colleagues, the concentration of various parameters in the microbial mat (mg/kg), obtained through total aqua regia digestions, were divided by the measured concentration in co-occurring water (mg/L), also called a partitioning coefficient[6,13–15]. To determine the magnitude of REY accumulations relative to other cations and anions, the following parameter suite was examined: REYs, Sc, Al, Ca, Fe, Mg, Mn, K, Na, P, S, Si, Ho, Tm, Tb, Lu, As, B, Ba, Co, Cr, Mo, Ni, Sr, Th, Tl, U and Zn. Cd, Cu and Pb were also analyzed, but large variability in the calculated partitioning coefficient prohibited further examination. In depth discussion of REY concentration and associated geochemical processes within the solids/biofilms and co-occurring water can be found in **Chapter 1: REY Geochemistry in Mining-Affected Aqueous Environments.**

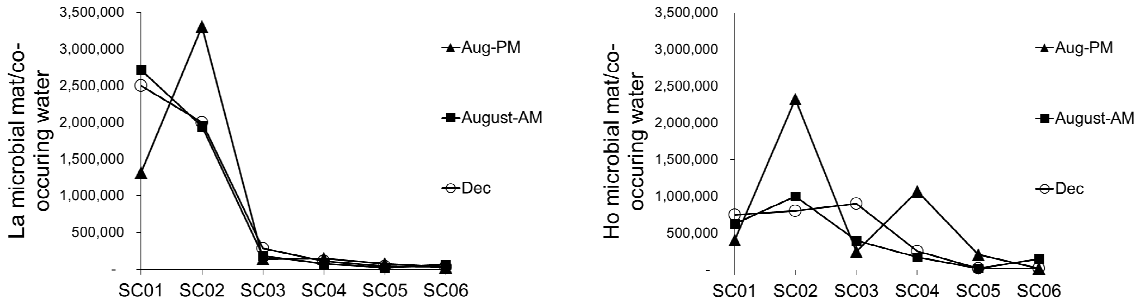

Figure 11 Spatial Trends in REY portioning coefficient (L/kg) between biofilms (total aqua regia digestion) and co-occurring water

Magnitudes of REY accumulations can vary substantially, particularly for maximum accumulations. For example, the partitioning coefficient between the biofilms and co-occurring water ranges from a minimum of ~20,000 to a maximum that ranged from ~1,000,000 (Tm) to ~15,000,000 (Pr). Sc shows substantially lower partitioning coefficients that range from a minimum of 1,579 to a maximum of 12,000. Partitioning coefficients showed large variability between different rare earth elements (e.g., La vs. Ho vs. Gd), but also spatially within the passive treatment system, seasonally between summer and winter sampling events, and diurnally. Figure 11 indicates the general spatial trend for partitioning coefficients: an increase from upstream (SC06) to downstream (SC01). Most LREYs show a trend similar to La, while most HREYs show a slightly more variable trend, consistent with Ho. An increase in portioning coefficient is noted for Ho and other HREYs at sites SC02 and SC05 during the August-PM sampling event.

To understand if the trend of increasing partitioning coefficients further downstream in the treatment facility is simply due to decreased aqueous water concentrations that result from increased pH, La water concentration was plotted vs. La partitioning coefficient between microbial mat and co-occurring water. The results indicate that a log-linear inverse relationship best describes the relationship between water and biofilm concentrations.

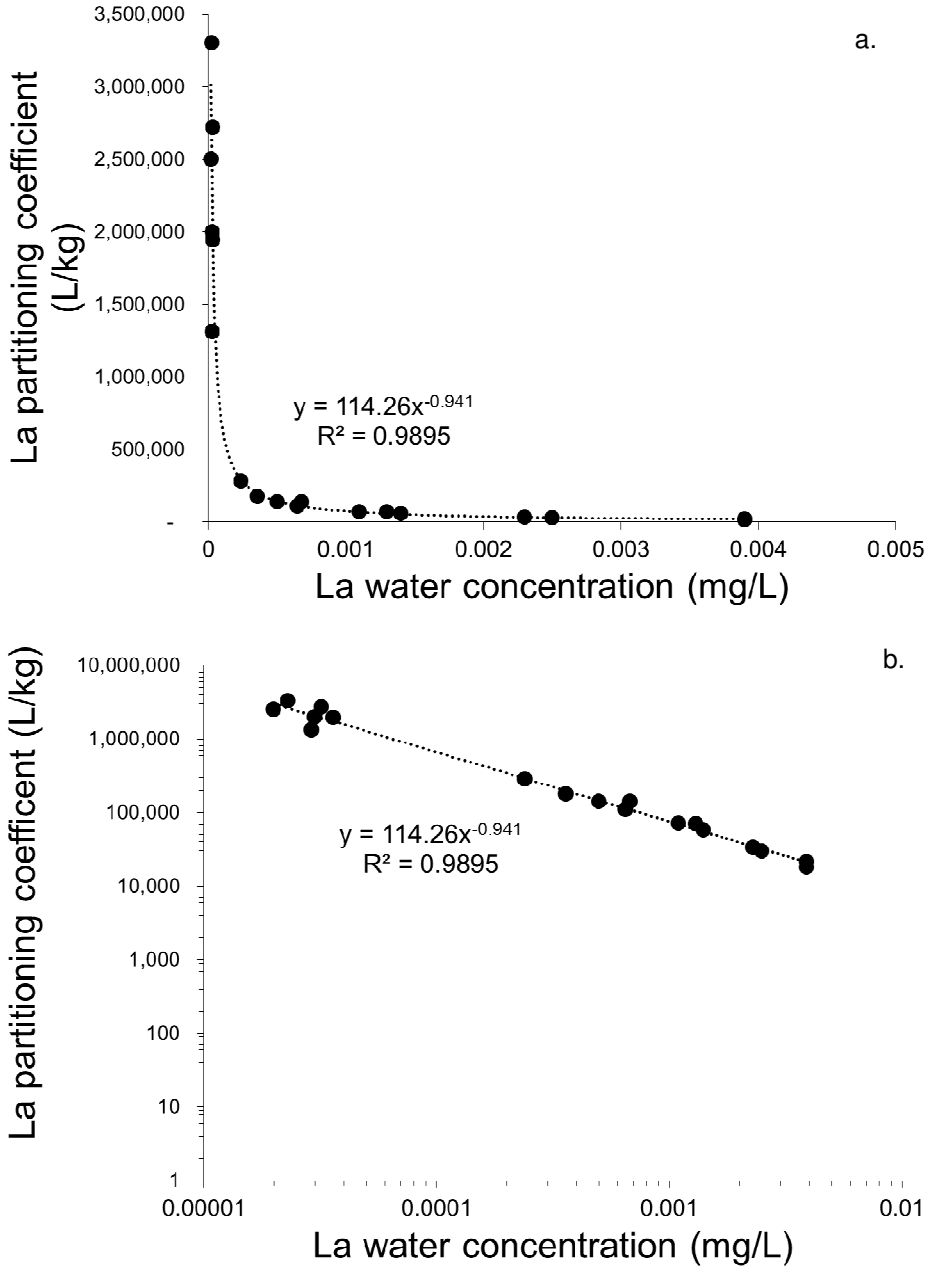

Figure 12 Comparison of La partitioning coefficient (L/kg) with aqueous water concentration (a) normal scale, (b) log-log scale

Detailed spatial, seasonal and diurnal comparison of partitioning coefficients for REY and a variety of other anions and cations are presented in Figure 13 and Figure 14. Sites SC01, SC02, and SC03 all show that Al, REYs and occasionally Fe are the elements that have the greatest portioning coefficients. Comparison of partitioning coefficients between the August sampling event indicates that there is an excellent correlation between August sampling events at sites SC02 and SC03 (R^2=0.95 and R^2=0.99, respectively). In comparison, the SC01 sampling site shows are poorer correlation between sampling events (R^2=0.3). The SC02 site indicates very similar partitioning coefficients were calculated during the August morning and afternoon sampling events. In contrast, the partitioning coefficients for the

August morning sampling event are greater than those of the August afternoon sampling event at sites SC01 and SC03.

In contrast to the further downstream sites, SC06, SC05 and SC04 generally show poor correlations between partitioning coefficients calculated for different sampling events. The only pair of samples that shows any kind of correlation is the partitioning coefficient calculated at the December afternoon and August afternoon sampling event at SC05 (R^2=0.4). Despite a lack of correlation between the plots, it is clear that during August, the greatest partitioning coefficients are observed during the August afternoon sampling event. At the SC04 site, with the exception of Al, all parameters have a great calculated partitioning coefficient during the August morning sampling event when compared to the August afternoon sampling event. Excluding Al and Lu, the calculated partitioning coefficients between the December and August afternoon sampling event are quite similar. At site SC05, with the exception of V, the August afternoon sampling event shows the greatest partitioning coefficient when compared to both the August morning sampling event and the December sampling event. Unlike other sites, at SC06, there are a number of elements outside of Al, and REYs that have significantly elevated partitioning coefficients, including: Th, V, Cr, U, Th and Tl. REY partitioning coefficient at the SC06 site, however, remain above other cations such as Zn, Ba and K. Although the magnitude of the partitioning coefficients at SC06 is not highly variable between sampling events, the portioning coefficients for REYs show more variability in the August morning and December sampling events, when compared to the August afternoon sampling event.

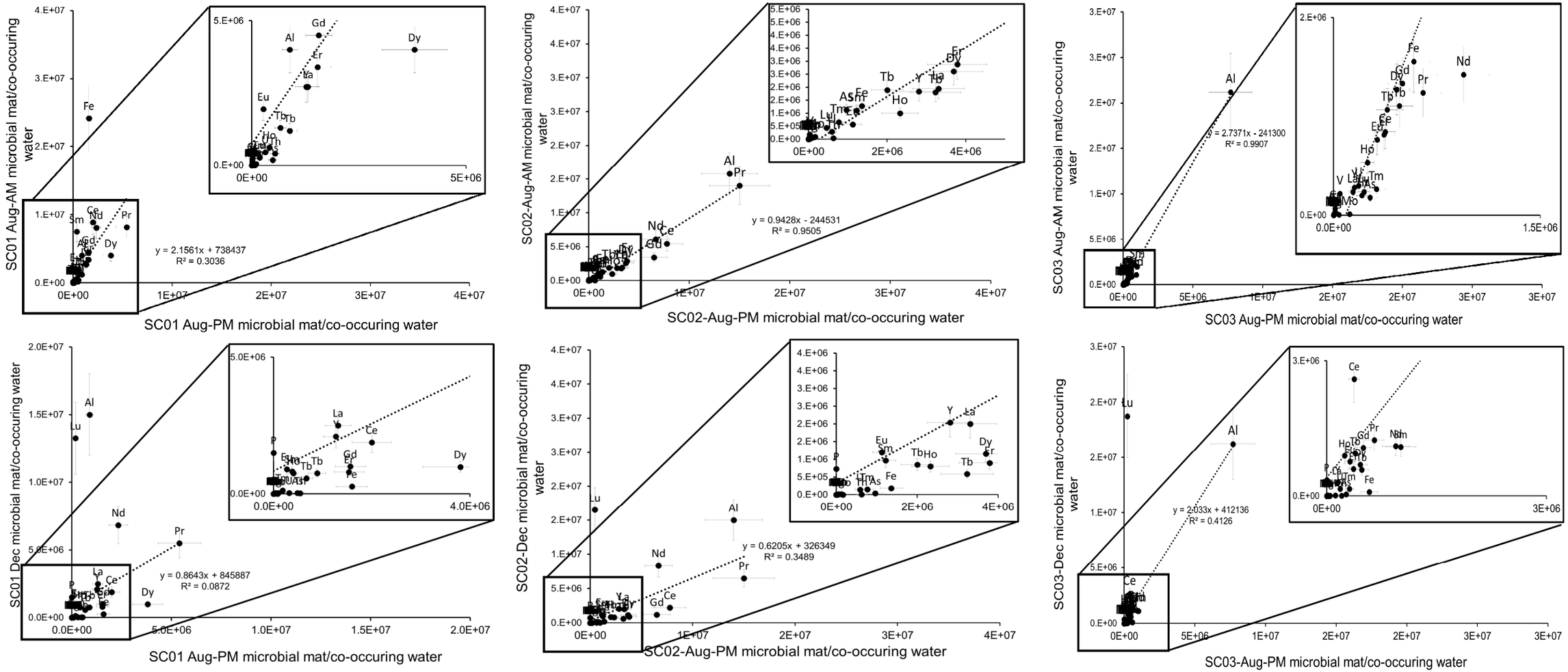

Figure 13 Detailed partitioning coefficient comparison: spatial, seasonal and diurnal comparison (SC01, SC02, SC03) (error bars represent average RPD of lab duplicates)

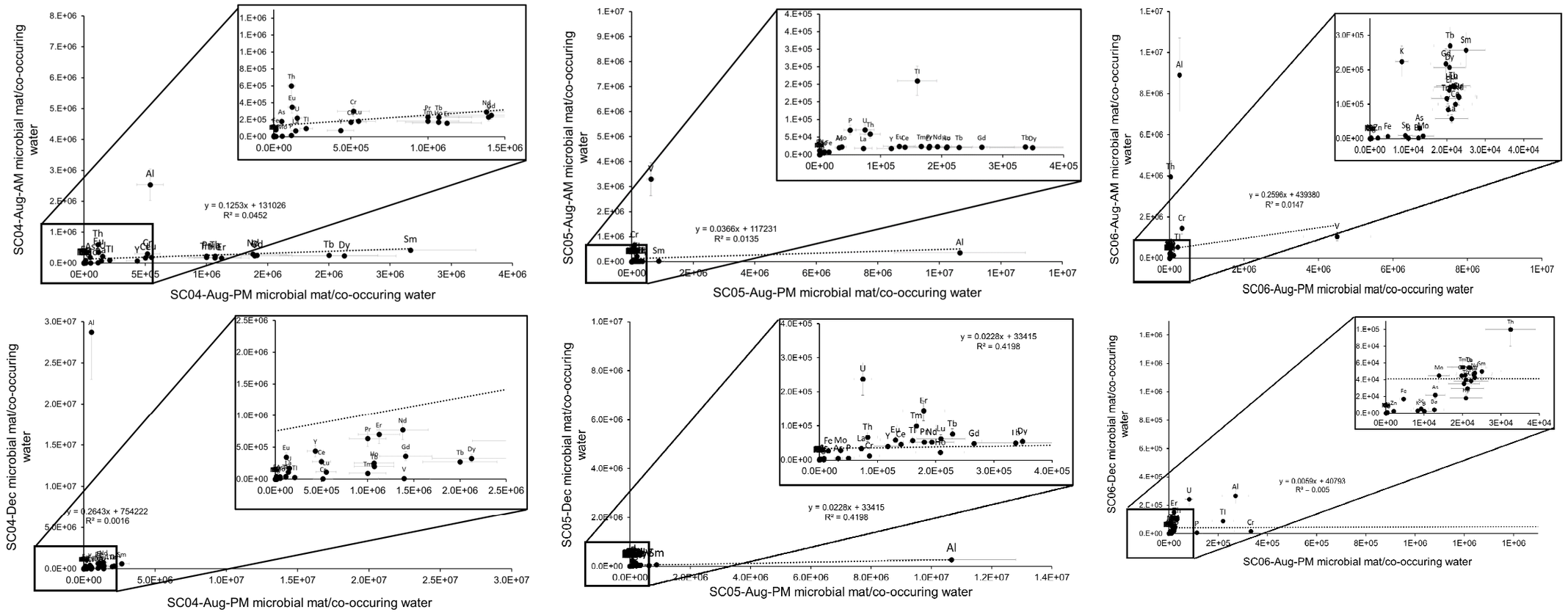

Figure 14 Detailed partitioning coefficient comparison: spatial, seasonal and diurnal comparison (SC04, SC05, SC06) (error bars represent average RPD of lab duplicates)

3.6.2 Patterns of REY Accumulations

Comparison of fractionation between REYs as a result of partitioning from aqueous phase to solid phase can be deduced by observing by plotting partitioning coefficients at each site from La (lowest atomic number) to Lutetium (highest atomic number). Nearly uniform REY partitioning can only be observed at the SC06 and SC05 sites. For some reason, site SC06 shows uniform partitioning during the August afternoon sampling event, yet shows variable portioning during the August morning event. In contrast, the SC05 site shows uniform partitioning during the August morning sampling event, but variability within the August afternoon sampling event.

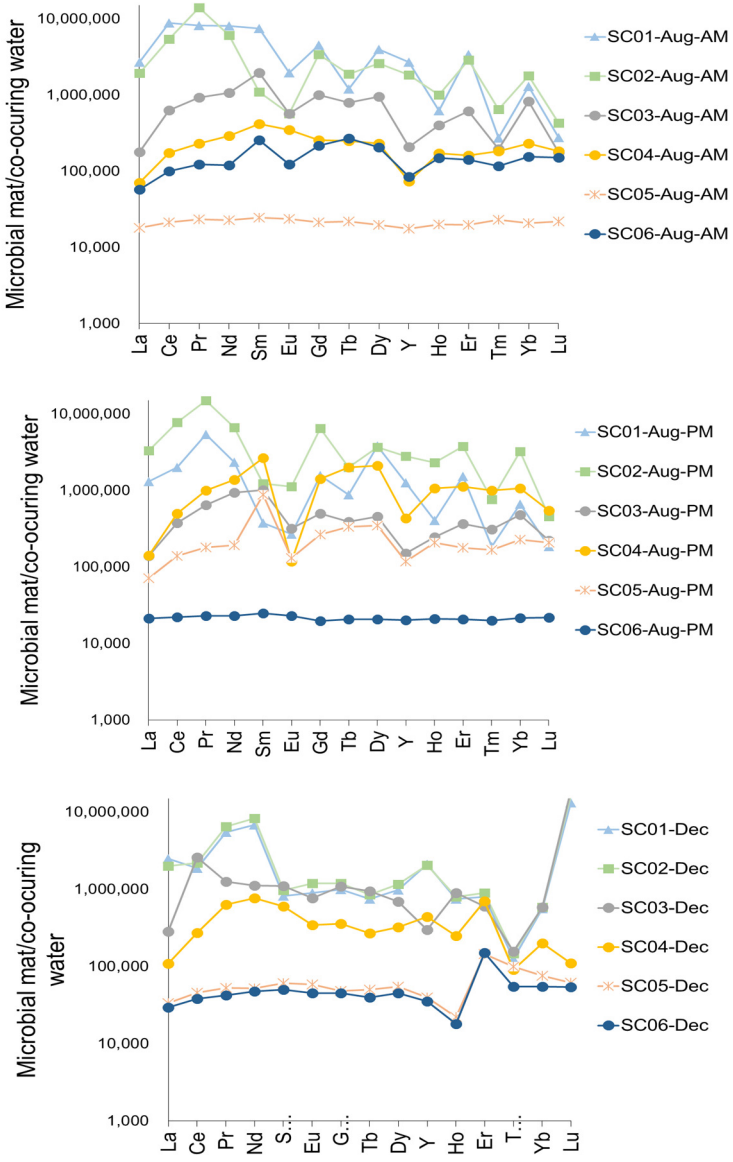

Figure 15 Comparison of REY fraction patterns of partitioning coefficients (L/kg) calculated for each sampling event

3.6.3 Presence of HREY, MREY or LREY enrichment

The greatest accumulation of REY within the biofilm occurred at sites SC06, SC05 and SC04. In particular, during the December sampling event, the greatest REY accumulations occurred at SC05. During both the August sampling events, greatest REY accumulations occurred at SC04. The percentage of organic carbon at SC04-Aug (~11%) is by far the highest of all sites and sampling events; however, the percentage of organic carbon at SC05-Dec is very low (0.7%). Sites SC06, SC05 and SC04 also contained the highest amounts of aqueous REY. Aqueous REY concentrations at the discharge location, SC06, start high (17.6 µg/L) and decrease further downstream sites, likely as a result of increasing pH, sorption, precipitation and dilution. Partitioning coefficients were calculated as per the procedure above, and summed for comparison between sites. Partitioning coefficients were summed to represent the total partitioning coefficients, the LREY partitioning coefficients (La-Gd), the HREY partitioning coefficients (Tb-Lu) and the MREY partitioning coefficients (Sm-Ho).

Summed partitioning coefficients for LREYs, HREYs and MREYs are very similar and range between ~3E5 to ~1E7 L/kg. These data again show a clear trend of lower total partitioning coefficients at the inflow sites (SC05 and SC06), compared to discharge sites and sites further downstream (SC01, SC02, SC03, SC04). For each sampling event, the summed LREY, HREY and MREY partitioning coefficients are generally all the same order of magnitude except for certain sampling events at SC01 and SC02. Comparison between the coefficients by calculating a simple fraction, shows that sites SC06, SC05 and SC04 have elevated HREY partitioning coefficients compared to LREY partitioning coefficients (>1). At the downstream sites (SC01, SC02 and SC03), partitioning coefficients for LREY sorption are greater than for HREY sorption. Results comparing MREY partitioning coefficient with LREY partitioning coefficients are not as clear. Calculated fractions of MREY partitioning coefficient to LREY partitioning coefficient for upstream sites SC06, SC05 and SC04 range from 0.84 to 1.36, with an average value of 1.06. At the further downstream sites, SC03, SC02 and SC01, calculated fractions of MREY partitioning coefficient to LREY partitioning coefficient range from 0.38 to 0.71, with an average value of 0.58.

Table 11 Comparison of summed partitioning coefficients

Site	Sum Aqueous REYs + Sc (µg/L)	Sum Solid REYs + Sc (mg/kg)	Sum of Partitioning Coefficients - total REY + Sc	Sum of Partitioning Coefficients - LREY (L/kg)	Sum of Partitioning Coefficients – HREY (L/kg)	Sum of Partitioning Coefficients – MREY (L/kg)	HREY Kd / LREY Kd	MREY Kd / LREY Kd
SC06-Dec	17.6	693	6.8E+05	3.0E+05	3.8E+05	2.8E+05	1.26	0.93
SC06-Aug-PM	24.1	512	4.1E+05	1.6E+05	2.5E+05	1.5E+05	1.57	0.96
SC06-Aug-AM	5.9	504	2.9E+06	1.0E+06	1.9E+06	1.3E+06	1.88	1.31
SC05-Dec	16.1	724	7.7E+05	3.5E+05	4.1E+05	3.4E+05	1.18	0.95
SC05-Aug-PM	26	578	4.5E+06	1.9E+06	2.7E+06	2.3E+06	1.43	1.23
SC05-Aug-AM	23.9	477	4.1E+05	1.6E+05	2.5E+05	1.5E+05	1.58	0.96
SC04-Dec	3.6	580	5.9E+06	3.1E+06	2.8E+06	2.6E+06	0.90	0.84
SC04-Aug-PM	5.5	672	1.8E+07	7.2E+06	1.1E+07	9.8E+06	1.49	1.36
SC04-Aug-AM	2.6	687	3.9E+06	1.8E+06	2.1E+06	1.7E+06	1.19	0.98
SC03-Dec	1.4	450	1.3E+07	8.2E+06	4.9E+06	5.8E+06	0.60	0.71
SC03-Aug-PM	2.3	350	7.1E+06	3.9E+06	3.1E+06	3.1E+06	0.80	0.78
SC03-Aug-AM	1.7	339	1.1E+07	6.3E+06	4.3E+06	5.9E+06	0.67	0.93
SC02-Dec	1	395	3.2E+07	2.2E+07	9.5E+06	8.2E+06	0.42	0.37
SC02-Aug-PM	0.8	404	6.0E+07	4.2E+07	1.8E+07	2.0E+07	0.44	0.47
SC02-Aug-AM	1	373	4.6E+07	3.3E+07	1.3E+07	1.2E+07	0.41	0.38
SC01-Dec	1	333	2.8E+07	1.9E+07	8.8E+06	7.3E+06	0.45	0.38
SC01-Aug-PM	0.9	170	2.2E+07	1.3E+07	8.9E+06	8.6E+06	0.67	0.65
SC01-Aug-AM	0.8	475	5.6E+07	4.2E+07	1.4E+07	2.2E+07	0.33	0.54

NOTES:

1. PARTITIONING COEFFICIENTS ARE CALCULATED SPEARTELY FOR EACH LREY AND SUBSEQUENTLY SUMMED.

3.6.4 Abiotic Oxidation Experiment

Due to low amounts of ferrous iron at the further downstream sites (SC01, SC02, SC03), sufficient abiotic sample was not able to be generated with the volume of water collected. As a result, only results from SC04, SC05, and SC06, which are the sites with the greatest bacterial abundance, are being presented here (Figure 16). NASC normalized results from the abiotic oxidation experiments indicate that abiotic oxidation results have fewer amounts (approximately 50% less) REY than the total biofilm samples that were analyzed by aqua regia digestion. In addition, NASC normalized curves for the abiotic oxidation samples show much less MREY enrichment. In addition, the abiotic samples negative Ce and Pr anomalies and positive Y anomaly. In contrast, the total biofilm samples show positive Ce and Pr anomalies and a negative Y anomaly. Results indicate that abiotic samples tend to have a negative Eu anomaly compared to total samples that have a positive Eu anomaly.

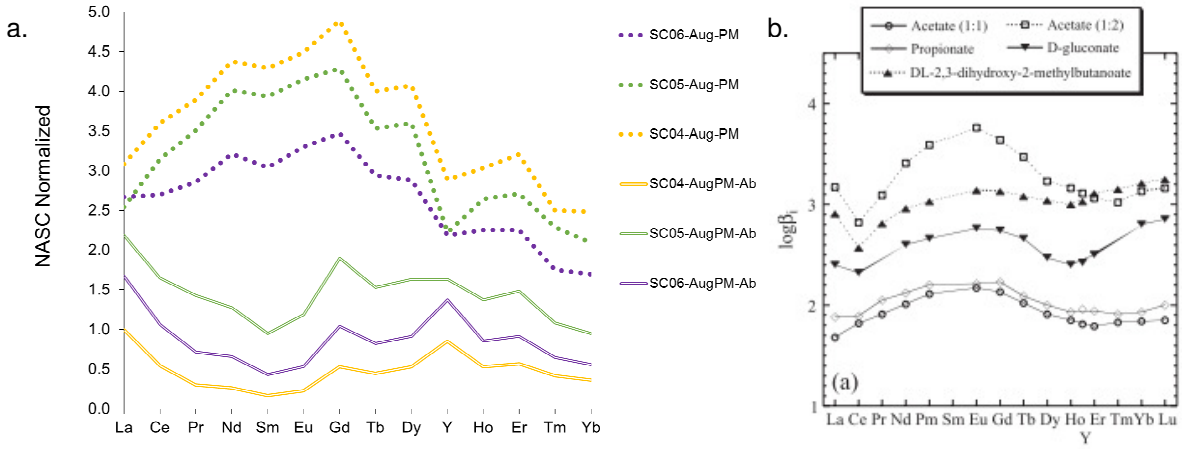

NOTES:

1. FIGURE B REPRESENTS STABILITYCONSTANTS (BETA) OF COMPLEXES FOR REE WITH SIMPLE CARBOXYLIC ACID (PUBLISHED BY TAKAHASHI AND COLLEAGUES[15]).

Figure 16 Results of abiotic iron oxidation experiment (Aqua regia digestion)

4 – DISCUSSION

4.1 MORPHOLOGY AND COMPOSITION (SEM, LIGHT MICROSCOPY)

Can we identify by light microscopy if iron-oxidizing and reducing bacteria present? If so, who are they?

SEM characterization of the solid samples indicates that iron-oxidizing bacteria are present. The occurrence of two different stalk morphologies indicates that at least several species are present, including, but not limited to: *Gallionella ferruginea, Mariprofundus ferrooxydans* and *Leptothrix sp.* At least one of these species was identified within samples from the following sampling events: SC06-Aug, SC06-Dec, SC05-Dec and SC04-Dec. Other samples were not analyzed under SEM, and therefore, assumptions regarding the presence/absence of iron-oxidizing bacteria within these samples cannot be made.

Light microscopy revealed the presence of diatoms at the SC01 and SC02 sites. Presence of diatoms often indicates that silica is at equilibrium, and available for incorporation into biota. This is an important finding, since silica is often found associated with REYs. Silica present in the treatment facility could be a result of silica-containing host rock dissolution and may indicate that silica is present in biofilm in larger quantities than measured. The aqua regia digestion was used to extract REYs and other elements that are likely mobile within the passive treatment facility, but this digestion has poor recovery for silica. As a result, if silica is present in larger quantities than measured via the aqua regia digestion, the solid REY concentrations and partitioning coefficients may be underestimated.

4.2 PROKARYOTIC SPECIES COMPOSITION AND DIVERSITY

4.2.1 Species Composition and Major Chemical Parameters

Are iron-oxidizing and reducing bacteria present? If so, who are they?

Does prokaryotic microbial presence increase REY enrichment within biofilm?

Large taxonomic diversity was observed within the 16S bacteria results. Forty classes of bacteria and archaea were present at two sampling sites, sampled over two different seasons. The most abundant classes observed included: β-proteobacteria, δ-proteobacteria and α-proteobacteria. Total abundance of these classes varied between the sampling events, and sites, with greatest difference in diversity and patterns of major class abundance noted between the SC06-dec and SC01-Dec sampling events. With the exception of the SC01-Dec site, β-proteobacteria was the most dominant class at the sites sampled, followed by δ-proteobacteria. At the SC01-Dec α-proteobacteria is the most dominant class.

β-proteobacteria was the most abundant class sampled, which includes many Fe(II)-oxidizing genera. Specifically, the Burkholderiales and Gallionellales orders were found to dominate composition of the β-proteobacteria class. Further classification identified *Gallionella sp.* (order gallionellales; 0-20% of total abundance per site) and family camamonadaceae (order burkholderiales; 1%-11% of total abundance per site) as the lowest taxonomic orders that could be identified that compose a majority of the most abundant orders. Other β-proteobacteria identified at lower levels include: *Paucibacter sp.* (0-5% per site), *Rhodoferax sp.* (0-1% of total abundance per site), and members of order Methylophilales (0-1% of total abundance per site) and order Rhodocyclales (0-1% of total abundance per site). *Gallionella ferruginea*, one of the most well-known iron oxidizers, and the *Gallionella* strain ES-2, and *Gallionella capsiferriformans* are currently the only members of genus Gallionella.

Gallionella sp. are chemolithoautotrophic bacteria, whose only energy source is ferrous iron oxidation, and therefore these species require high amounts of dissolved ferric iron (5 – 25 mg/L) to form. As obligate Fe(II) chemolithoautotrophs, *Gallionella sp.* exists within a narrow Eh-pH range that overlaps with the range of stability of ferrous iron (Eh>145 mV; tolerated range pH 5.0-6.6 and dissolved oxygen 0.1 – 1.5 mg/L[12]). In addition, *Gallionella sp.* form characteristic twisted stalks composed of extracellular polymeric substances (EPS) and ferric iron. Based purely on *in situ* parameters gathered at the site, sites SC06 and SC05 are the sites that should contain the greatest amounts of Gallionella sp. (dissolved oxygen ranges from 0.57 mg/L to 2.12 mg/L, Eh ranges from 236 mV to 319 mV and pH ranges from 5.84 to 6.03).

Family camonadaceae is the second major group that comprises the majority of the class of β-proteobacteria at the Silver Creek site. The family camonadaceae was formalized as a taxa in 1991, and contains a wide diversity of species[75]. Most members of this family utilize aerobic heterotrophic metabolism; however, certain species denitrify and use nitrates (*Acidovorax, Comamonas* etc.) or Fe(III) (*Albidiferax, Comamonas guangdongensis*) as terminal electron acceptors[45]. *Leptothrix sp.* is an unclassified member of the burkholderiales order. Together with *Gallionella sp.*, *Leptothrix sp.* are often found in large numbers in circumneutral drainages with low pO_2. *Leptothrix sp.* are facultative iron and manganese-oxidizers, and do not require iron or manganese to grow. Although *Leptothrix* is known to promote iron oxidation, little is known about the exact mechanism involved[76]. Members of the *Leptothrix* genus have different, and wide-ranging pH and oxygen optima when compared to *Gallionella sp.* For example, *Leptothroix cholodnii* was found to have optimal growth at 0.78 mg/L + 0.32 m/L O_2, whereas *Leptothrix discophora SS-1* was found to occur throughout the range of 0-8.05 mg/L O_2[76]. A general pH range for the Leptothrix genus has been described as to 6.5 to 8[76]. Based on *in situ* results collected at the Silver Creek site, *Leptothrix sp.* are most likely to be found at sites SC03, SC02 and SC01. Although *Leptothrix sp.* may be found at upstream sites SC06, SC05 and SC04, measured pH at these sites (5.84 to 6.15) is below the optimal range for Leptothrix.

δ-proteobacteria were the second most abundant bacterial class identified. Specifically, the Desulfuromonadales order, and the Geobacter genus comprise the majority of this order. The Geobacter genus has received attention for their potential uses in bioremediation; *Geobacter sp.* using metal ion mediated electron transport to oxidize organic compounds in anaerobic environments to CO_2, which generates energy as adenosine triphosphate[77]. Although species level identification was not provided, it is likely that the Geobacter species within the Silver Creek drainage are associated with Fe(III) reduction, such as *Geobacter metallireducens, Geobacter sulfurreducens*, or *Geobacter psychrophilus,* which reduce iron and sulfur, as their names suggest. *Geobacter metallireducens* and *Geobacter sulfurreducens* have their genomes sequenced[78,77]. *Geobacter metallireducens* can couple oxidation of a variety of organic compounds with the reduction of Fe(III) and Mn(IV) in anaerobic environments. Although previously thought to be strict anaerobes, genome sequencing indicates that *Geobacter sulfurreducens* contains oxidative capacity within its genome that may provide an ability to exist in more oxic environments. The high relative abundance of geobacter *sp.*, especially within the highly oxic water of SC01-Aug was not expected.

Gault and colleagues collected surface samples and samples 5-6 cm deep at a circumneutral seep dominated by BIOS[79]. Gault and colleagues identified members of β-proteobacteria as the dominant identified bacteria phyla at the surface sites. Similar to results at the Silver Creek site, bacteria associated with both Fe(II) oxidizing and reducing species were identified; however, instead of the *Leptothroix sp., Gallionella sp., and Geobacter sp.* identified within Silver Creek, Gault and colleagues observed *Sideroxydans sp., Rhodoferax sp. and Geothrix sp.* Microbial profiling completed by Gault at colleagues at 5-6 cm depth found β-proteobacteria remained the majority of identified phyla;

however, large increases in the presence of δ-proteobacteria occurred. β-proteobacteria at these more anoxic sites included sulfur oxidizers and Fe(II)-oxidizers, including *Lepthtothrix sp.* Similar to the bacterial result at Silver Creek, δ-proteobacteria was predominately composed of members of the order Desulfuromonadales; however, Gault and colleagues found the family Desulfobacteraceae to dominate composition of this order, and this study found the family Geobacteraceae to dominate composition of the Desulfuromonadales order.

Fabisch and colleagues examined the iron-oxidizing bacteria present at three iron-rich creek sites under a variety of pH conditions (pH 2.7, pH 4.4 and pH 6.3)[51]. Unlike our study, geochemical parameters such as dissolved oxygen, and ferrous iron, varied little seasonally during the 1.5 year study (sampled during November, February, May, and August). At these sites, iron-oxidizers and iron-reducers composed anywhere from 18% to 80% of the 16SrRNA clone sequences measured. At two of the sites (pH 2.7 and pH 6.3), iron-oxidizers and iron-reducers composed approximately 50% of total 16S abundance. At another site with the lowest levels of dissolved oxygen (1.7 mg/L DO; pH 4.4) iron-oxidizers composed 73% of total 16SrRNA clone sequences, and *Gallionella ferruginea* specifically composed 69% of total 16SrRNA clone sequences[51]. These results indicate that in the environment, *Gallionella ferruginea* may have a greater tolerance to low pH than originally thought. TOC measurements by Gault and colleagues ranged from 0.7 ± 0.1% to 3.9 ± 0.3%. Values for TOC are within this range, with the exception of very elevated TOC observed at SC06-Aug-PM and SC04-Aug-PM. Low alpha diversity was observed within the moderately acidic site (pH 4.4), that is normally only observed within extremely acidic ARD waters[51].In contrast, data from this study shows the lowest diversity within SC01, with the highest pH, indicating that pH is not the controlling factor for diversity within this system. Likely access to electron donors, such as Fe(II) or organics is the controlling factor for site SC01.

Heim and colleagues examined the formation of microbial iron oxyhydroxides within another set of sites in the Äspö Hard Rock Laboratory in Sweden[80]. Depending on the site, %OC ranged from 3.6% dry weight to 7.0% dry weight. After nine months of iron oxide formation, at one site (1.68 mg/L Fe(II), pH 7.33, 0.28 mg/L O_2), the main iron oxidizers included *Marioprofundus sp.* and uncultivatable members of family Gallionellaceae. At the second site (0.59 mg/L Fe(II), pH 7.41, 0.38 mg/L O_2), Marioprofundus dominated and members of family Gallionellaceae were absent. Both of these sites had substantially greater amounts of sulphate and chloride than the Silver Creek sites.

4.2.2 Species Composition and Seasonal Changes

Are there seasonal changes to prokaryotic abundance and diversity?

Gault examined seasonal changes in neutrophilic BIOS with high amounts of ferrous iron[79]. Enhanced Fe(III) and Mn (IV) was noted to occur during the warmer summer and fall months. These authors hypothesized that enhanced biological productivity, evidenced by elevated DOC concentrations, enabled development of anoxic areas in sediment-water interface that favoured anaerobic microbial processes. Results of the 16SrRNA profiling indicated *Gallionella sp., Sideroxyan sp., Geobacter sp. and Rhodoferax sp.* within the same surficial sediment horizon. These authors also found dominance of Gallionella *sp.* during the winter and suggest a competitive advantage for these organisms in cold, oligotrophic environments with sharp Fe(II)/O_2 redox gradients. At the Silver Creek SC06 site, a greater proportion of β-proteobacteria (predominately iron oxidizers) occurred in December compared to August (33% vs. 20%); and a slightly lesser proportion of δ-proteobacteria (predominately iron reducers) also existed when comparing December with August (18% vs. 20%). In contrast, a greater proportion of β-proteobacteria was observed at the SC01 site during August compared to December.

4.2.3 Abiotic vs. biotic iron oxidation

Are both abiotic and biotic iron oxidation occurring?

Does biogenic iron oxidation alter REY fractionation different from abiotic iron oxidation?

Experiments completed by Anderson and Pederson involved three field sites within the Äspö Laboratory tunnel, and were focused on *Gallionella sp.*-rich biofilms[12]. Results of this experiment focused on determining when stalk development (and hence biofilm formation or "biotic iron oxidation") are optimal. Their results indicate a narrow Eh-pH range for all sites sampled that was within the Fe(OH)3 stability field, but very close to the ferrous iron stability field. In addition, the optimal levels for oxygen saturation for their sites ranged from 0.1 to <1.5 mg/L O_2, with Eh values > 130mV[12]. Stalks were found to form up until 3.2 mg/L of DO, at a slower rate. Using these values to interpret the *in situ* parameters at the Silver Creek site, SC06 Aug and Dec samples, and SC05 Aug-PM samples would have the highest rates of biotic iron oxidation. Sites SC05-Aug-AM, SC05-Dec, SC04-Aug-PM may also have the ability to form biogenic stalks. Results of SEM imaging confirmed abundance of twisted stalks within the SC06-Dec site and SC06-Aug site. Helical stalks were also observed at the SC05-Dec site, although absence of helical stalks at other sites cannot be viewed as definitive evidence of absence of biological iron oxidation mediated by *Gallionella sp.,* since the SC01, SC02 and SC03 sites were not observed under SEM.

Eggerichs and colleagues completed some recent investigations into the influence of pH, oxygen and ferrous iron on growth of both *Gallionella sp.* and *Leptothrix spp*[76]. Results of their investigations indicated that Gallionella oxidation rates increase with increase ferrous iron concentrations, over a range of 1 to 8 mg/L of ferrous iron, and growth rates decrease when more than 2 mg/L of oxygen is present. For *Gallionella sp.,* a pH optimum of 6.5 was identified with 50% of optimum growth observed at pH 5.7 and 7.2, and no stalk growth observed under 5, and little growth observed over 7. *Leptothrix* showed broader pH tolerance, to an optimum pH of 7.52. Oxidation rates of *Leptothrix* cells were observed to exceed *Gallionella sp.* and abiotic iron oxidation, likely as a result of autocatalytic effects. Eggregichs and colleagues created a schematic to indicate abiotic/biotic iron oxidation potentials, which has been shown together with dissolved oxygen and pH data from the Silver Creek site (Figure 17). This figure indicates that sites SC06 and SC05 fall within the borderline conditions for biotic oxidation by *Gallionella sp.*, and that certain SC01 and SC02 sites fall within the range favourable for abiotic and *Leptothrix sp.* oxidation. In general, however, most of the Silver Creek sites fall many sites fall within borderline or 'unfavourable' categories due to their relative acidic pH. The occurrence of observed and prolific helical stalks at SC06 indicates that perhaps the Eggerichs schematic model for *Gallionella sp.* oxidation need to be expanded in the lower pH region.

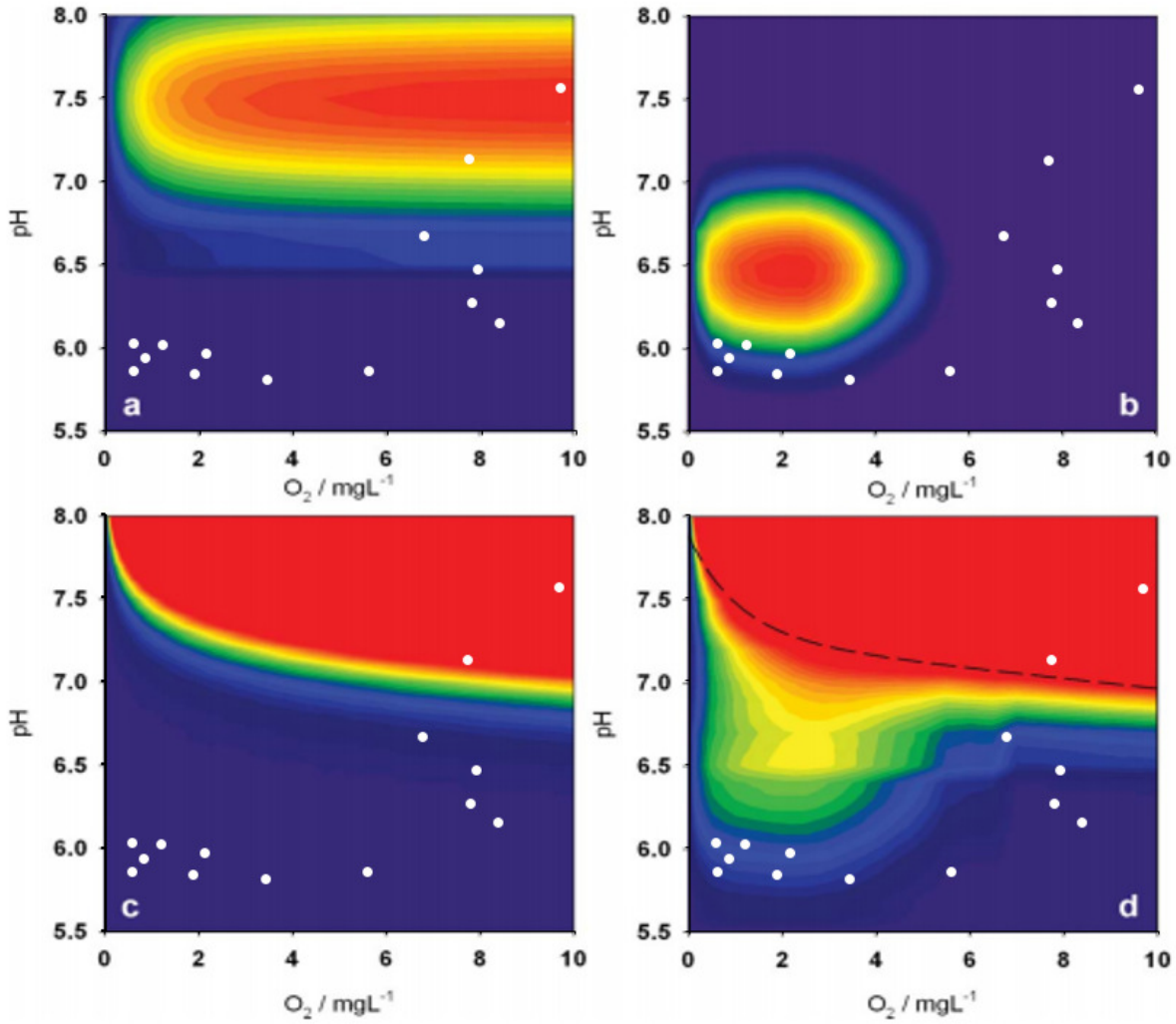

NOTE:

1. PURPLE INDICATES POOR CONDITIONS FOR ABIOTIC AND BIOTIC IRON OXIDATION PROCESSES AND RED INDCATES THE MOST FAVOURABLE CONDITIONS FOR ABIOTIC AND BIOTIC IRON OXIDATION PROCESSES.

Figure 17 Oxygen concentrations vs. pH observed at Silver Creek plotted on base figure representing conditions for biotic and abiotic growth. Base layer from Eggerichs et al.[76], that includes biotic/abiotic iron oxidation potentials for a) *Leptothrix sp.*; b) *Gallionella sp.*; c) abiotic iron oxidation; d) combined potentials.

4.3 EUKARYOTIC DIVERSITY

Does eukaryotic microbial presence increase REY enrichment within biofilm?

How does eukaryotic diversity affect prokaryotic diversity?

There are not many studies that have examined linkages between eukaryotes and Fe(II) oxidizing bacteria. There were several observations that led the project team to examine eukaryotic diversity. First, during field sampling, distinct air or assumed oxygen bubbles, were observed covering the surface of the microbial mats. This had not been observed in December. To analyze the effects of possible photosynthetic processes on iron oxidation, late afternoon samples were collected in August, in addition to early morning samples. At all sites, pH during the morning samples was similar or slightly

lower than evening samples, with larger differences noted at sites with higher temperatures. In other studies with photosynthetic species occurring within heterogeneous microbial mat, a higher pH is often observed during daylight hours rather than during darkness, as a result of CO_2 consumption by photosynthesis[81]. Our results, however, are similar to what was observed by Trouwborst and colleagues at the Chocolate Pots Hot Springs in Yellowstone National Park (temperatures 50-54˚C)[81]. Despite abundant cyanobacteria at the Chocolate Pots Hot Springs, pH remained constant in light and dark studies. Their two-part explanation included: 1) continual flushing of low pH source water, and 2) high rate of oxygen-dependent Fe(II) oxidation, which produces both Fe(III) and protons, which would maintain or potentially lower pH (Figure 15**Error! Reference source not found.**)[81]. Temperature and ionic strength both affect the activities of OH- and Fe(II), and this is expected to play a role within the Silver Creek site[76].

Equation 1 $\mathbf{10H_2O + 4Fe^{2+} + O_2 \rightarrow 4Fe(OH)_3 + 8H^+}$

Trouwborst and colleagues examined the role of microbial photosynthesis on the oxidation of Fe(II), in a hot spring with high amounts of Fe(II), Mn(II) and low sulphide and atmospheric oxygen concentration by completing light and dark *in situ* microelectrode measurements[81]. This study concluded that Fe(II) oxidation seemed to be controlled by oxygen produced by cyanobacteria (*Synechococcus sp.* and *Cyanothece minervae*) despite existence of an anoxygenic photosynthetic iron oxidizing bacteria (*Chloroflexus sp.*). Trouwborst and colleagues found that the rates of Fe(II) oxidation occurring within the microbial mats were consistent with abiotic oxidation of O_2, and did not find evidence of biogenic Fe(II)-oxidation by neutrophilic chemolithotropic iron-oxidizing bacteria[81]. Although cyanobacteria are prokaryotes, not microbes, these findings can be generalized to any biotic oxygenic photosynthesis.

Hegler and colleagues found co-existence of cyanobacteria and *Gallionella sp.* but physical separation of the two species within a bicarbonate and Fe(II)-rich spring in the Swiss Alps[82]. Mori and colleagues recently published research indicating the coexistence of *Gallionella sp.* with oxygen-generating algae *Tribonema sp.* in a heavy metal-rich environment (*Heterokonta superphylum*, Xanthophyceae class)[72]. Photosynthetic green algae and brown algae were identified at the site, however, higher *Gallionella*-related 16SRNA gene copy numbers were observed on the surface of green algae, when compared to brown algae. These are interesting results for *Gallionella sp.*, a strictly microaerophilic iron-oxidizing bacteria. Results of the 18SrRNA sequencing completed for the Silver Creek site did not reveal presence of *Tribonema sp.*; however, members of the SAR supergroup were identified within Silver Creek. Specifically, members of *Peritrichia sp.*, and members of order Ochrophyta, which was observed to be particularly dominant at site SC01 during August sampling. In addition, chloroplast-containing eukaryotes were identified at sites SC01 during December and SC06 during December and August. In addition, a large abundance of *Chromadorea monhysterida*, a type of nematode, were observed at all sampling sites.

4.4 PARTITIONING COEFFICIENTS

- *Do REYs actually have larger partitioning coefficients/BCF than other elements? How do partitioning coefficients relate to solid and aqueous concentrations? Do these elevated partitioning coefficients/BCF of REYs pose a toxicological risk?*

REYs have among the highest partitioning coefficients of the large suite of metals analyzed. There was an unexpected difference in partitioning coefficients between sites, where sites SC01, SC02 and SC03 had very elevated REY partitioning coefficients. In contrast, sites SC04, SC05 and SC06 had

lower REY partitioning coefficients. A strong linear log-linear relationship was observed between partitioning coefficients and concentration. This relationship was observed to occur for lanthanum and the other REYs. This relationship is very similar to the significant inverse relationship observed in both field and lab by DeForest and colleagues for copper, lead, zinc, methyl mercury and Se (freshwater only)[10]. Within their analysis, they found BAFs were 100-1,000 times larger than BCFs for the same metal or species, and they found trophic transfer factors to be inversely related to exposure concentration. Prior to this, McGeer also found an inverse relationship between BAFs and exposure concentrations for Zn, Cd, Cu, Pb and Ni[83]. This finding is consistent with what has been observed for other metals and fills an information gap for REYs at the baes of the food chain[10]. A recent study of 14 Canadian temperate lakes unaffected by mining found that BAFs for REYs ranged from 1.3 to 4.4 L/kg wet weight for fish muscle and trophic transfer of REYs was occurring, with trophic dilution (i.e., benthos showed greatest BAFs, and fish muscle showed lowest BAF)[84]. This study indicates that elevated REYs concentration within sediments may have the potential to enter the food chain. In addition, this study also found very high sum of REY concentrations within sediments (~1,000 mg/L). Background concentrations of REYs are similar to the REY concentrations observed downstream of mining-activities.

Comparison of the water and biofilm concentrations to guideline values proposed by Sneller et al. show that both water and biofilm are well below these proposed guideline concentrations[34]. Recent work completed by Amyot and colleagues indicates that REYs may transfer from sediment to biota, with log1- of median bioaccumulation factors ranging from 1.3 to 4.4 L/kg f or fish muscle and non-predatory invertebrates. The highest levels of REYs occurred within benthic organisms and decreased with trophic dilution[84]. These results combined with the high portioning factors and loading of sediment indicate that REYs in sediment may enter the food chain, and it is unknown if current guidelines are protective of bioaccumulation.

- *Does prokaryotic or eukaryotic microbial presence increase REY enrichment? i.e., Is it possible to determine if naturally-occurring heterogeneous biofilm have higher partitioning coefficients than abiotic iron oxides?*

Heim and colleagues examined trace element and rare earth element signatures within microbial iron oxyhydroxides formed in the Tunnel of Äspö (Äspö Hard Rock Laboratory, Sweden)[13]. They compared feeder fluid and concentrations on biofilms after 2 and 9 months of accumulation. They found concentrations of Be, Zn, Zr, Hf, W, Th, Pb and U within the microbial mats to be 10^3 to 10^5-fold higher than feeder fluids while rare earth elements and Y were found to be 10^4-10^6 enriched. Heim and colleagues identified sorption to iron oxyhydroxides as the method for REY enrichment. They found that sorption to iron oxyhydroxides increased up to 10^4 fold with increasing pH. Results from this study indicated that trace element partitioning coefficients ranged from $10^{2.5}$ to $10^{6.8}$ and REYs ranged from 10^6 to $10^{7.2}$. In addition, REY partitioning coefficients increased with increasing pH. Similar to Heim and colleagues, our study found REYs to have consistently elevated partitioning coefficients that exceeded those observed for trace metals found at the same sites. Laboratory experiments by Bau and colleagues examined the partitioning coefficient of REY to abiotic iron oxides[11]. The partitioning coefficients they identified were very small (0.2-0.5); however, the aqueous concentration of REYs was extremely high (61 µg/L). In addition, very strong positive Ce anomalies and negative Y anomalies were observed. The patterns within our data is much more variable, which suggests a more heterogeneous matrix with different stabilities of surface-complexes and individual REYs.

Detailed analysis of partitioning coefficients of REYs, together with Al and occasionally Fe were consistently elevated at sites SC01, SC02, SC03, SC04 and SC05. Partitioning coefficients for other trace metals were elevated at the SC06 site above partitioning coefficients for REYs: Th, V, Cr, U, Th and Tl. Little fractionation of REYs was noted at the SC06 site, and this indicates the possibility that REYs are adsorbing the microbial mats, and have reached saturation. It is important to note that the largest solid phase concentrations within Silver Creek were noted at sites that had the lowest pH. This finding is different from the solid phase accumulations observed by Heim and colleagues.

The large increase in the partitioning coefficients downstream in the water treatment facility, which has been seen to have relatively less bacteria, preliminarily indicates that key variables such as aqueous REY concentration (dependent on pH), are much more important in determining partitioning levels. In addition, results of 16S and 18S show a huge diversity of prokaryotes and eukaryotes. Results from 18S sampling indicate strong relative increases in photosynthetic eukaryotes at sites SC01 compared to site SC06. Due to high BCF noted for green algae, it is also possible that sites SC01, SC02 and SC03 have elevated water-biofilm partitioning coefficient as a result of the presence of algae (and not simply the absence of bacteria).

- *Does biogenic iron oxidation alter REY fractionation different from abiotic iron oxidation?*

Takahashi and colleagues studied the REE distribution patterns between five different bacterial strains (*Bacillus subtilis, Escherichia coli, Alcaligenes faecalis, Shewanella putrefaciens,* and *Pseudomonas fluorescens*) and water[14]. Takahashi and colleagues calculated the partitioning coefficient for bacteria and water using Equation 2. Their results showed a large increase in heavy rare earth elements, in addition to a weak peak around the middle rare earth elements. Takahashi and colleagues also took environmental samples that showed similar heavy rare earth element enrichment and maxima within the middle rare earth elements. The same authors also demonstrated that abiotic Fe oxyhydroxide precipitates showed the same patterns as the laboratory experiment and the field collected biofilm. Early work by Verplanck also showed that HREYs were preferentially removed from the water column at several field sites when water pH levels rose above 5[6]. Verplanck and colleagues found that all sites sampled within mine-affected, high sulphate waters showed LREY depletion and HREY enrichment. Heim and colleagues completed a similar experiment and found that abiotic, inorganic iron oxyhydroxides showed very similar patterns to biogenic iron oxides. Increases in HREY partitioning coefficient were noted at sites SC06 and SC05, which are confirmed to contain a variety of iron oxidizing bacteria, in addition to some iron-reducing bacteria. Result from our abiotic experiment are slightly different than results obtained by Takahashi and colleagues[14]. Results from our experiment indicate that microbes may be playing a role in MREY sequestration.

Equation 2

$$\frac{[REE\}init - [REE]diss}{[REE]diss}$$

Where:
[REE]diss=REE in aqueous phase (ng/g)
[REE}init=initial concentration of REE in aqueous phase

The following correlation between dissolved oxygen and the fraction of sum of partitioning coefficients for HREY divided by the sum of partitioning coefficients for LREY was observed at the Silver Creek site (Figure 18). This may be explained by the linkages between low dissolved oxygen and ferrous iron stability, which is important for both biotic and abiotic iron oxidation. Recent work by Amyot and colleagues identified dissolved organic carbon, dissolved oxygen and concentration of REYs within

sediment as driver's of water quality[84]. This work suggest that dissolved oxygen may be important for aqueous REY chemistry, which may provide an explanation of the relationship between portioning coefficient and dissolved oxygen.

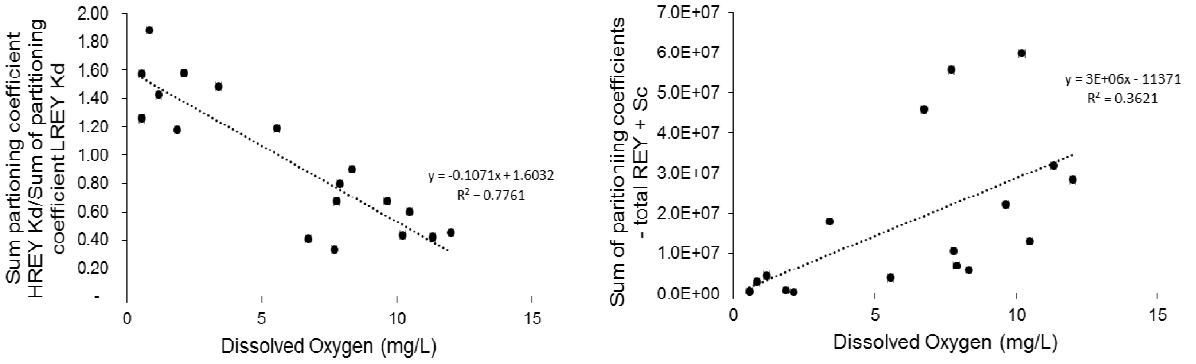

Figure 18 Correlation plots between dissolved oxygen and summed partitioning coefficients

- *Things that didn't work:*

There were several analysis that would have added additional information to this thesis that did not work. The Most Probable Number technique was completed twice to determine the amount of iron-oxidizing bacteria, but did not provide correct results. Organic digestions were completed to separate REYs from their organic substrate; however, results of these digestions were suspect and not presented. Separation of the iron and organic fraction seems to be much more difficult than originally anticipated, and alternate methods, perhaps utilizing iron isotopes or XANES should be considered. In addition, a simple laboratory sorption experiment was completed that did not succeed and data was not presented. Due to time limitations these analysis could not be re-done in time for thesis completion.

5 – CONCLUSION

Iron oxidizing bacteria were identified by morphology through SEM, within 16S rRNA amplification with universal primers for bacteria and archaea and during ddPCR. β-proteobacteria, and δ-proteobacteria were identified by 16S gene sequencing as the most common bacterial classes, with *Gallionella* sp. and the family camamonadaceae comprising the most common β-proteobacteria. *Geobacter* sp. was identified by 16S gene sequencing to make up the majority of the Desulfuromonadales order. A greater relative abundance of β-proteobacteria, and δ-proteobacteria were observed at the SC06 site during December and August when compared to the SC01 site. A wide variety of eukaryotes were also identified at the site. The potential role of photosynthetic eukaryotes in REY sorption at downstream sites has previously been overlooked, and this study suggests the eukaryotic part of the biofilm may play as large a role, or a larger role within the organic fraction sequestering REYs as iron oxides and iron-oxidizing bacteria. The eukaryotes showed particularly uneven distribution, with the vast majority of species at SC01 during December and August composed of one class or genus. Inverse alpha diversity were noted to occur between the eukaryotes and prokaryotes. Results from ddPCR indicate that *Gallionella sp.* and *Leptothrix sp.* are highly abundant, and generally have higher concentrations at the more anoxic sites closest to the outflow (SC05 and SC06) and lower abundance at further downstream sites.

Comparison of *in situ* pH and Eh measured at the site indicates that SC06 and SC05 fall within the borderline conditions for biotic oxidation by *Gallionella sp.*, and sites SC01 and SC02 fall within the range favourable for abiotic or perhaps *Leptothrix sp.* oxidation. The occurrence of observed and prolific helical stalks at SC06 indicates that perhaps the Eggerichs schematic model for *Gallionella sp.* oxidation need to be expanded in the lower pH region. It was not possible, however, to definitively differentiate between sites that were composed exclusively of abiotic iron oxidation, and sites that were formed via biotic iron oxidation.

Partitioning coefficients for REY between water and biofilm were very high within the examined system, but they were strongly influenced by aqueous concentration of REY. Results from this study indicated that trace element partitioning coefficients ranged from $10^{2.5}$ to $10^{6.8}$ and REY partitioning coefficients ranged from 10^{6} to $10^{7.2}$. At the sites with highest aqueous REY, however, the lowest REY partitioning coefficients were observed, which were below those observed for other metals. There was an extremely strong power relationship between aqueous concentration and partitioning coefficients, which indicates that extremely elevated partitioning coefficients observed for REYs are unlikely to occur at elevated aqueous REY concentrations, thereby reducing the potential REY toxic threat. In addition, all aqueous and solid REY concentrations are below proposed target concentrations proposed by Sneller and colleagues[34]. Results from **Chapter 1: Geochemistry of REY in mining-affected environments**, indicates that the majority of aqueous REY are likely present as sulphate and colloidal organic complexes, and REYs in solid phase are predominately bound to the heterogeneous iron-manganese-organic matrix. Based on this preliminary screening of an example site, REYs with the potential to adversely affect organisms are below current thresholds identified. This paper does note that

Increased fractionation to HREYs was noted at the upstream sites that seemed to be characterized by the most elevated iron-oxidizing bacteria. This fractionation is consistent with previous literature that indicates bacteria tend to adsorb HREYs and that algae have a preference with LREYs. However, other studies with abiotic iron oxides have noted a similar pattern of HREY sorption, so HREY sorption can not necessarily be interpreted as a biosignature for biogenic iron oxidation. Results from the abiotic iron oxidation experiment indicate that biota may play a role in MREY fractionation; however, the sample size (n=3) is too small to generalize.

There were strong linkages between iron and REYs, and linkages between iron reducing and oxidizing bacteria and iron. As a result, there were some linkages between REY concentration and certain bacterial populations; however, the association was indirect.

A summary of the results observed:

- Results from this study indicated that maximum partitioning coefficients of REY between water and mineralized biofilm ($10^{7.2}$) were slightly greater than the maximum partitioning coefficients for trace elements ($10^{6.8}$)
- A strong inverse relationship between REY aqueous concentration and water-biofilm partitioning coefficients was observed
- The potential role of photosynthetic eukaryotes in REY sorption at downstream sites has previously been overlooked, and this study suggests the eukaryotic part of the biofilm may play as large a role, or a larger role within the organic fraction sequestering REYs as iron oxides and iron-oxidizing bacteria.
- Inverse alpha diversity between prokaryotic and eukaryotic communities.

- Higher partitioning coefficients for HREY and MREY when compared to LREY at sites with confirmed presence of neutrophilic iron oxidizing bacteria

6 – REFERENCES

(1) González, V.; Vignati, D. a. L.; Pons, M.-N.; Montarges-Pelletier, E.; Bojic, C.; Giamberini, L. Lanthanide ecotoxicity: First attempt to measure environmental risk for aquatic organisms. *Environ. Pollut.* **2015**, *199*, 139–147.

(2) Migaszewski, Z. M.; Gałuszka, A. The characteristics, occurrence and geochemical behavior of rare earth elements in the environment: a review. *Crit. Rev. Environ. Sci. Technol.* **2014**, 00–00.

(3) Sharifi, R.; Moore, F.; Behname, K. Geochemical behavior and speciation modeling of rare earth elements in acid drainages at Sarcheshmeh porphyry copper deposit, Kerman Province, Iran. *Chemie der Erde* **2013**, *Article in* (Article in Press), 1–11.

(4) Ferreira da Silva, E.; Bobos, I.; Xavier Matos, J.; Patinha, C.; Reis, A. P.; Cardoso Fonseca, E. Mineralogy and geochemistry of trace metals and REE in volcanic massive sulfide host rocks, stream sediments, stream waters and acid mine drainage from the Lousal mine area (Iberian Pyrite Belt, Portugal). *Appl. Geochemistry* **2009**, *24* (3), 383–401.

(5) Romero, F. M.; Prol-Ledesma, R. M.; Canet, C.; Alvares, L. N.; Pérez-Vázquez, R. Acid drainage at the inactive Santa Lucia mine, western Cuba: Natural attenuation of arsenic, barium and lead, and geochemical behavior of rare earth elements. *Appl. Geochemistry* **2010**, *25* (5), 716–727.

(6) Verplanck, P. L.; Nordstrom, D. K.; Taylor, H. E.; Kimball, B. a. Rare earth element partitioning between hydrous ferric oxides and acid mine water during iron oxidation. *Appl. Geochemistry* **2004**, *19*, 1339–1354.

(7) Hou, X.; Yan, X. Study on the concentration and seasonal variation of inorganic elements in 35 species of marine algae. *Sci. Total Environ.* **1998**, *222*, 141–156.

(8) Weltje, L.; Heidenreich, H.; Zhu, W.; Wolterbeek, H. T.; Korhammer, S.; Goeij, J. J. M.; Markert, B. Lanthanide concentrations in freshwater plants and molluscs, related to those in surface water, pore water and sediment. A case study in The Netherlands. *Sci. Total Environ.* **2002**, *286*, 191–214.

(9) Moriwaki, H.; Yamamoto, H. Interactions of microorganisms with rare earth ions and their utilization for separation and environmental technology. *Appl. Microbiol. Biotechnol.* **2013**, *97*, 1–8.

(10) DeForest, D. K.; Brix, K. V.; Adams, W. J. Assessing metal bioaccumulation in aquatic environments: The inverse relationship between bioaccumulation factors, trophic transfer factors and exposure concentration. *Aquat. Toxicol.* **2007**, *84*, 236–246.

(11) Bau, M. Scavenging of dissolved yttrium and rare earths by precipitating iron oxyhydroxide: Experimental evidence for Ce oxidation, Y-Ho fractionation, and lanthanide tetrad effect. *Geochim. Cosmochim. Acta* **1999**, *63* (1), 67–77.

(12) Anderson, C. R.; Pedersen, K. In situ growth of Gallionella biofilms and partitioning of lanthanides and actinides between biological material and ferric oxyhydroxides. *Geobiology* **2003**, *1* (2), 169–178.

(13) Heim, C.; Simon, K.; Ionescu, D.; Reimer, A.; De Beer, D.; Quéric, N.-V.; Reitner, J.; Thiel, V. Assessing the utility of trace and rare earth elements as biosignatures in microbial iron oxyhydroxides. *Front. Earth Sci.* **2015**, *3* (February), 1–15.

(14) Takahashi, Y.; Hirata, T.; Shimizu, H.; Ozaki, T.; Fortin, D. A rare earth element signature of bacteria in natural waters? *Chem. Geol.* **2007**, *244*, 569–583.

(15) Takahashi, Y.; Châtellier, X.; Hattori, K. H.; Kato, K.; Fortin, D. Adsorption of rare earth elements onto bacterial cell walls and its implication for REE sorption onto natural microbial mats. *Chem. Geol.* **2005**, *219*, 53–67.

(16) Andrès, Y.; Texier, a C.; Le Cloirec, P. Rare earth elements removal by microbial biosorption: a review. *Environ. Technol.* **2003**, *24* (March 2015), 1367–1375.

(17) Tsuruta, T. Accumulation of Rare Earth Elements in Various Microorganisms. *J. Rare Earths* **2007**, *25* (5), 526–532.

(18) Haxel, G. B.; Hedrick, J. B.; Orris, G. J.; Sound, S.; Of, M.; Mineral, O. U. R. Rare Earth Elements — Critical Resources for High Technology. *United States Geol. Surv. Fact Sheet* **2002**, *87*, 4.

(19) Rim, K. T.; Koo, K. H.; Park, J. S. Toxicological evaluations of rare earths and their health impacts to workers: a literature review. *Saf. Health Work* **2013**, *4* (1), 12–26.

(20) Emsbo, P.; Mclaughlin, P. I.; Breit, G. N.; Edward, a; Koenig, A. E. Rare earth elements in sedimentary phosphate deposits : Solution to the global REE crisis ? *Gondwana Res.* **2014**, *27* (2), 776–785.

(21) Verplanck, P. L.; Nordstrom, D. K.; Taylor, H. E. Overview of rare earth element investigations in acid waters of the U.S. Geological Survey's abandoned mine lands watersheds. *U.S. Geol. Surv. Toxic Subst. Hydrol. Progr. Proc. Tech. Meet.* **1999**, 83.

(22) Humphries, M. (Congressional R. S. Rare Earth Elements: The Global Supply Chain - R41347.pdf http://fas.org/sgp/crs/natsec/R41347.pdf (accessed Feb 17, 2015).

(23) Cassee, F. R.; van Balen, E. C.; Singh, C.; Green, D.; Muijser, H.; Weinstein, J.; Dreher, K. Exposure, health and ecological effects review of engineered nanoscale cerium and cerium oxide associated with its use as a fuel additive. *Crit. Rev. Toxicol.* **2011**, *41* (July 2010), 213–229.

(24) Zhao, F.; Cong, Z.; Sun, H.; Ren, D. The geochemistry of rare earth elements (REE) in acid mine drainage from the Sitai coal mine, Shanxi Province, North China. *Int. J. Coal Geol.* **2007**, *70*, 184–192.

(25) Merten, D.; Geletneky, J.; Bergmann, H.; Haferburg, G.; Kothe, E.; Büchel, G. Rare earth element patterns: A tool for understanding processes in remediation of acid mine drainage. *Chemie der Erde - Geochemistry* **2005**, *65*, 97–114.

(26) Johannesson, K. H.; Lyons, W. B.; Yelken, M. a.; Gaudette, H. E.; Stetzenbach, K. J. Geochemistry of the rare-earth elements in hypersaline and dilute acidic natural terrestrial waters: Complexation behavior and middle rare-earth element enrichments. *Chem. Geol.* **1996**, *133* (96), 125–144.

(27) Pagano, G.; Guida, M.; Tommasi, F.; Oral, R. Health effects and toxicity mechanisms of rare earth elements—Knowledge gaps and research prospects. *Ecotoxicol. Environ. Saf.* **2015**, *115*, 40–48.

(28) Liang, T.; Li, K.; Wang, L. State of rare earth elements in different environmental components in mining areas of China. *Environ. Monit. Assess.* **2014**, *186*, 1499–1513.

(29) Verplanck, P. L.; Antweiler, R. C.; Nordstrom, D. K.; Taylor, H. E. Standard reference water samples for rare earth element determinations. *Appl. Geochemistry* **2001**, *16*, 231–244.

(30) Gimeno Serrano, M. J.; Auqué Sanz, L. F.; Nordstrom, D. K. REE speciation in low-temperature acidic waters and the competitive effects of aluminum. *Chem. Geol.* **2000**, *165*, 167–180.

(31) Tai, P.; Zhao, Q.; Su, D.; Li, P.; Stagnitti, F. Biological toxicity of lanthanide elements on algae. *Chemosphere* **2010**, *80* (9), 1031–1035.

(32) Arnot, J. a; Gobas, F. A. A review of bioconcentration factor (BCF) and bioaccumulation factor

(BAF) assessments for organic chemicals in aquatic organisms. *Environ. Rev.* **2006**, *14*, 257–297.

(33) Gonzalez, V.; Vignati, D. a L.; Leyval, C.; Giamberini, L. Environmental fate and ecotoxicity of lanthanides: Are they a uniform group beyond chemistry? *Environ. Int.* **2014**, *71*, 148–157.

(34) Sneller, F. E. C.; Kalf, D. F.; L., W.; Van Wezel, a. P. Maximum Permissible Concentrations and Negligible Concentrations for Rare Earth Elements. **2000**, No. 601501, 66.

(35) Tsuruta, T. Selective accumulation of light or heavy rare earth elements using gram-positive bacteria. *Colloids Surfaces B Biointerfaces* **2006**, *52*, 117–122.

(36) Mullen, M. D.; Wolf, D. C.; Ferris, F. G.; Beveridge, T. J.; Flemming, C. a; Bailey, G. W. Bacterial Sorption of Heavy-Metals. *Appl. Environ. Microbiol.* **1989**, *55* (12), 3143–3149.

(37) Pal, A.; Paul, A. K. Microbial extracellular polymeric substances: Central elements in heavy metal bioremediation. *Indian J. Microbiol.* **2008**, *48* (1), 49–64.

(38) Frankel, R. B.; Bazylinski, D. A. Biologically Induced Mineralization by Bacteria. **2003**.

(39) Wingender, J.; Thomas, R. .; Flemming, H.-C. *Microbial Extracellular Polymeric Substances: characterization, structure and function*; 1999.

(40) Tsuruta, T. Separation of Rare Earth Elements in Various Microorganisms. *J. Nucl. Radiochem. Sci.* **2005**, *6* (1), 81–84.

(41) Kirby, C. S.; Thomas, H. M.; Southam, G.; Donald, R. Relative contributions of abiotic and biological factors in Fe(II) oxidation in mine drainage. *Appl. Geochemistry* **1999**, *14* (4), 511–530.

(42) Weiner, S. An Overview of Biomineralization Processes and the Problem of the Vital Effect. *Rev. Mineral. Geochemistry* **2003**, *54* (1), 1–29.

(43) Emerson, D.; Fleming, E. J.; McBeth, J. M. Iron-Oxidizing Bacteria: An Environmental and Genomic Perspective. *Annu. Rev. Microbiol.* **2010**, *64* (1), 561–583.

(44) Hedrich, S.; Schlömann, M.; Barrie Johnson, D. The iron-oxidizing proteobacteria. *Microbiology* **2011**, *157* (6), 1551–1564.

(45) Hedrich, S.; Schlomann, M.; Barrie Johnson, D. The iron-oxidizing proteobacteria. *Microbiology* **2011**, *157* (6), 1551–1564.

(46) Ivarson, K. C.; Sojack, M. Microorganims and Ochre Deposits in Field Drains of Ontario. *Can. J. Soil Sci.* **1978**, *58* (1978), 1–16.

(47) Crerar, D. A.; Knox, G. W.; Means, J. L. Biogeochemistry of bog iron in the New Jersey Pine Barrens. *Chem. Geol.* **1979**, *24* (1–2), 111–135.

(48) Stokes, J. L. Studies on the filamentous sheathed iron bacterium Sphaerotilus natans. *J. Bacteriol.* **1954**, *67* (3), 278–291.

(49) Hallbeck, L.; Pedersen, K. Autotrophic and mixotrophic growth of Gallionella ferruginea. *J. Gen. Microbiol.* **1991**, *137* (11), 2657–2661.

(50) Hallbeck, L.; Pedersen, K. Culture parameters regulating stalk formation and growth rate of [i]Gallionella ferruginea/[i]. *J. Gen. Microbiol.* **1990**, *136* (9), 1675–1680.

(51) Fabisch, M.; Beulig, F.; Akob, D. M.; K??sel, K. Surprising abundance of Gallionella-related iron oxidizers in creek sediments at pH 4.4 or at high heavy metal concentrations. *Front. Microbiol.* **2013**, *4* (DEC), 1–12.

(52) Zhang, J.; Lion, L. W.; Nelson, Y. M.; Shuler, M. L.; Ghiorse, W. C. Kinetics of Mn(II) oxidation by Leptothrix discophora SS1. *Geochim. Cosmochim. Acta* **2002**, *66* (5), 773–781.

(53) Emerson, D.; Revsbech, N. P. Investigation of an iron-oxidizing microbial mat community located near Aarhus, Denmark: Field studies. *Appl. Environ. Microbiol.* **1994**, *60* (11), 4022–4031.

(54) Ingri, J.; Widerlund, A.; Land, M.; Gustafsson, Ö.; Andersson, P.; Öhlander, B. Temporal variations in the fractionation of the rare earth elements in a Boreal river; the role of colloidal particles. *Chem. Geol.* **2000**, *166* (1–2), 23–45.

(55) Pokrovsky, O. S.; Dupré, B.; Schott, J. *Fe-Al-organic colloids control of trace elements in peat soil solutions: Results of ultrafiltration and dialysis*; 2005; Vol. 11.

(56) Purdy, C. J. K.; Gault, A.; Bryn, K.; Jamieson, H. Speciation of REE in mine tailings from the Nechalacho. Queens: Kingston 2014, p 18.

(57) Leybourne, M. I.; Johannesson, K. H. Rare earth elements (REE) and yttrium in stream waters, stream sediments, and Fe-Mn oxyhydroxides: Fractionation, speciation, and controls over REE + Y patterns in the surface environment. *Geochim. Cosmochim. Acta* **2008**, *72* (24), 5962–5983.

(58) Rissanen, A. J.; Kurhela, E.; Aho, T.; Oittinen, T.; Tiirola, M. Storage of environmental samples for guaranteeing nucleic acid yields for molecular microbiological studies. *Appl. Microbiol. Biotechnol.* **2010**, *88* (4), 977–984.

(59) Schuylkill Headwaters Association. Watershed Restoration Projects http://schuylkillheadwaters.org/projects/watershed-restoration-projects/ (accessed Mar 27, 2017).

(60) Hanert, H. H. The Genus Gallionella. *Prokaryotes* **2006**, *7*, 990–995.

(61) Robbins, E. I.; CravottaIII, C. A.; Savela, C. E.; NordJr., G. L. Hydrobiogeochemical interactions in “anoxic” limestone drains for neutralization of acidic mine drainage. *Fuel* **1999**, *78* (2), 259–270.

(62) Caporaso, G. J.; Kuczynski, J.; Stombaugh, J.; Bittinger, K.; Bushman, F. D.; Costello, E. K.; Fierer, N.; Pena, A. G.; Goodrich, J. K.; Gordon, J. I.; et al. QIIME allows analysis of high-throughput community sequencing data. *Nat. Methods* **2010**, *7* (5), 335–336.

(63) Werner, J. QIIME Overview Tutorial http://www.wernerlab.org/teaching/qiime/overview (accessed May 23, 2017).

(64) Edgar, R. C. Search and clustering orders of magnitude faster than BLAST. *Bioinformatics* **2010**, *26* (19), 2460–2461.

(65) Yilmaz, P.; Parfrey, L. W.; Yarza, P.; Gerken, J.; Pruesse, E.; Quast, C.; Schweer, T.; Peplies, J.; Ludwig, W.; Glöckner, F. O. The SILVA and “all-species Living Tree Project (LTP)” taxonomic frameworks. *Nucleic Acids Res.* **2014**, *42* (D1), 643–648.

(66) Quast, C.; Pruesse, E.; Yilmaz, P.; Gerken, J.; Schweer, T.; Yarza, P.; Peplies, J.; Glöckner, F. O. The SILVA ribosomal RNA gene database project: Improved data processing and web-based tools. *Nucleic Acids Res.* **2013**, *41* (D1), 590–596.

(67) Werner, J. Processing 18s data http://qiime.org/1.4.0/tutorials/processing_18S_data.html (accessed May 28, 2017).

(68) Hindson, B. J.; Ness, K. D.; Masquelier, D. A.; Belgrader, P.; Heredia, N. J.; Makarewicz, A. J.; Bright, I. J.; Lucero, M. Y.; Hiddessen, A. L.; Legler, T. C.; et al. High-throughput droplet digital PCR system for absolute quantitation of DNA copy number. *Anal. Chem.* **2011**, *83* (22), 8604–8610.

(69) Cohen-Kupiec, R.; Marx, C. J.; Leigh, J. A. Function and regulation of glnA in the methanogenic archaeon Methanococcus maripaludis. *J. Bacteriol.* **1999**, *181* (1), 256–261.

(70) Hisbergues, M.; Christiansen, G.; Rouhiainen, L.; Sivonen, K.; Börner, T. PCR-based

identification of microcystin-producing genotypes of different cyanobacterial genera. *Arch. Microbiol.* **2003**, *180* (6), 402–410.

(71) Johnson, K. W.; Carmichael, M. J.; McDonald, W.; Rose, N.; Pitchford, J.; Windelspecht, M.; Karatan, E.; Bräuer, S. L. Increased Abundance of *Gallionella* spp., *Leptothrix* spp. and Total Bacteria in Response to Enhanced Mn and Fe Concentrations in a Disturbed Southern Appalachian High Elevation Wetland. *Geomicrobiol. J.* **2012**, *29* (2), 124–138.

(72) Mori, J. F.; Neu, T. R.; Lu, S.; H??ndel, M.; Totsche, K. U.; K??sel, K. Iron encrustations on filamentous algae colonized by Gallionella-related bacteria in a metal-polluted freshwater stream. *Biogeosciences* **2015**, *12* (18), 5277–5289.

(73) Dorigo, U.; Bérard, A.; Humbert, J. F. Comparison of eukaryotic phytobenthic community composition in a polluted river by partial 18S rRNA gene cloning and sequencing. *Microb. Ecol.* **2002**, *44* (4), 372–380.

(74) Whittaker, A. R. H. Evolution and Measurement of Species Diversity Published by : International Association for Plant Taxonomy (IAPT) Stable URL : http://www.jstor.org/stable/1218190 REFERENCES Linked references are available on JSTOR for this article : You may need to log. **2016**, *21* (2), 213–251.

(75) Willems, A., De ley, J., Gillis, M.; Kersters, K. Comamonadaceae , a New Family Encompassing the Acidovorans. *Int. jounal Syst. Bacteriol.* **1991**, *41* (3), 445–450.

(76) Eggerichs, T.; Opel, O.; Otte, T.; Ruck, W. Interdependencies between Biotic and Abiotic Ferrous Iron Oxidation and Influence of pH, Oxygen and Ferric Iron Deposits. *Geomicrobiol. J.* **2014**, *316*, 461–472.

(77) Methé, B. A.; K.E., N.; Eisen, J. A.; Paulsen, I. T.; Nelson, W.; Heidelberg, J. F.; Wu, D.; Wu, M.; Ward, N.; Beanan, M. J.; et al. Genome of Geobacter sulfurreducens: Metal Reduction in Subsurface Environments. *Science (80-.).* **2003**, *302*, 1967–1968.

(78) Aklujkar, M.; Krushkal, J.; DiBartolo, G.; Lapidus, A.; Land, M. L.; Lovley, D. R. The genome sequence of Geobacter metallireducens: features of metabolism, physiology and regulation common and dissimilar to Geobacter sulfurreducens. *BMC Microbiol.* **2009**, *9* (1), 109.

(79) Gault, A. G.; Langley, S.; Ibrahim, A.; Renaud, R.; Takahashi, Y.; Boothman, C.; Lloyd, J. R.; Clark, I. D.; Ferris, F. G.; Fortin, D. Seasonal Changes In Mineralogy, Geochemistry and Microbial Community of Bacteriogenic Iron Oxides (BIOS) Deposited in a Circumneutral Wetland. *Geomicrobiol. J.* **2012**, *29* (December 2011), 161–172.

(80) Heim, C.; Simon, K.; Ionescu, D.; Reimer, A.; De Beer, D.; QuÃ©ric, N.-V.; Reitner, J.; Thiel, V. Assessing the utility of trace and rare earth elements as biosignatures in microbial iron oxyhydroxides. *Front. Earth Sci.* **2015**, *3* (February), 1–15.

(81) Trouwborst, R. E.; Johnston, A.; Koch, G.; Luther, G. W.; Pierson, B. K. Biogeochemistry of Fe(II) oxidation in a photosynthetic microbial mat: Implications for Precambrian Fe(II) oxidation. *Geochim. Cosmochim. Acta* **2007**, *71* (19), 4629–4643.

(82) Hegler, F.; Lösekann-Behrens, T.; Hanselmann, K.; Behrens, S.; Kappler, A. Influence of seasonal and geochemical changes on the geomicrobiology of an iron carbonate mineral Water spring. *Appl. Environ. Microbiol.* **2012**, *78* (20), 7185–7196.

(83) McGeer, J. C.; Brix, K. V; Skeaff, J. M.; DeForest, D. K.; Brigham, S. I.; Adams, W. J.; Green, A. Inverse relationship between bioconcentration factor and exposure concentration for metals: implications for hazard assessment of metals in the aquatic environment. *Environ. Toxicol. Chem.* **2003**, *22* (5), 1017–1037.

(84) Amyot, M.; Clayden, M.; MacMillan, G.; Perron, T.; Arscott-Gauvin, A. Fate and Trophic Transfer of Rare Earth Elements in Temperate Lake Food Webs. *Environ. Sci. Technol.* **2017**, *51* (11), 6009–6017.

APPENDIX A

SCREENING LEVEL SITE COMPARISON: WATER VS. BIOFILM DATA

Table A.1 Total Water Samples Analyzed

Site Name	Lab ID	Location	SiteDesc	SampleDesc	Zone	Easting	Northing	Date	Temp	DOmg-L	pH	Eh	pe	DIC (ppm)	DOC (ppm)	SO4_ppm	Al_ppm	Ca_ppm	Fe_ppm	Mg_ppm	Mn_ppm	Na_ppm	Si_ppm	Sum LREE_ppm	Sum HREE_ppm	Total REEs_ppm	Ion balance
IN-RMATR	49,50,51	El Indio, Chile	Upstream of settling pond.	Water	19	404,246	6,704,938	07-05-2014	9.96		3.69	500	9	NA	NA	860	31	177	23	41	5.9	66.7	NA	0.0187	0.0280	0.0467	0.03%
IN-2	52,53,54	El Indio, Chile	Downstream of settling pond.	Water	19	401,358	6,699,644	07-05-2014	3.46		3.38	660	12	NA	NA	1,050	47	207	14	53	7.5	64.7	NA	0.0314	0.0423	0.0737	-0.14%
IN-13	55,56,57	El Indio, Chile	Downstream fo IN-2.	Water	19	365,587	6,760,128	08-05-2014	14.80	0.853	4.68	459	8	NA	NA	995	24	250	4	62	5.2	180.0	NA	0.0246	0.0302	0.0548	1.28%
IN-23 beige	44,45,46	El Indio, Chile	Natural ARD; upstream of mine tailings/affected s	Water	19	407,489	6,709,647	07-05-2014	10.30		7.31	456	8	NA	NA	870	4	100	6	16	0.8	30.8	NA	0.0028	0.0043	0.0072	-0.93%
IN-23 green	44,45,46	El Indio, Chile	Natural ARD; upstream of mine tailings/affected s	Water	19	407,489	6,709,647	07-05-2014	10.30		7.31	456	8	NA	NA	870	4	100	6	16	0.8	30.8	NA	0.0028	0.0043	0.0072	-0.93%
IN-28	47,48	El Indio, Chile	San Pablo closed tunnel; downstream from tailing	Water	19	405,670	6,705,697	07-05-2014	11.03		5.44	579	10	NA	NA	670	15	163	23	28	3.1	69.0	NA	0.0079	0.0125	0.0205	0.27%
LN-VWD	16,17	Lagunas Norte Peru	Waste rock leachate before collection pond (Vizcl	Water	17M	803,623	9,122,653	14-05-2014	12.68	7.21	2.63	766	14	NA	NA	3,600	200	500	495	74	32.5	49.5	NA	0.7430	0.3168	1.0598	-4.03%
LNPW-2B	13,14,15	Lagunas Norte Peru	Pit wall (almost neutral pH).	Water	17M	804,039	9,120,600	14-05-2014	12.99	6.4	6.40	67	1	NA	NA	310	0	153	0	4	0.0	27.7	NA	0.0012	0.0017	0.0029	0.38%
LNPW-2A	13,14,15	Lagunas Norte Peru	Pit wall (almost neutral pH).	Water	17M	804,039	9,120,600	14-05-2014	12.99	6.4	6.40	67	1	NA	NA	310	0	153	0	4	0.0	27.7	NA	0.0012	0.0017	0.0029	0.38%
P-EC	82,83,84	Pierina, Peru	Bedrock stream draining wetland going into mine	Water	18L	216,225	8,955,127	18-05-2014	17.27	6.81	4.27	587	10	NA	NA	1,200	40	360	35	16	34.0	13.0	NA	0.1595	0.1030	0.2625	-0.47%
P-WRD	76,77,78	Pierina, Peru	Waste rock drainage.	Water	18L	215,121	8,952,826	17-05-2014	17.25	5.56	2.75	679	12	NA	NA	2,750	117	383	473	47	146.7	12.0	NA	0.7243	0.3762	1.1006	-3.35%
XY-10-July 19	10 m 19 July	XY Deposit, Yukon	10 m 19 July	Water	NA	NA	NA	19-07-2010	6.40	NA	3.50	459	8	NA	NA	8,120	707	391	211	823	50.6	1.6	28	0.7218	2.5162	3.2380	-8.16%
XY-18-July 19	18 m 19 July	XY Deposit, Yukon	18 m 19 July	Water	NA	NA	NA	19-07-2010	3.60	NA	3.60	490	9	NA	NA	2,492	148	229	61	235	14.9	1.1	12	0.2234	0.6422	0.8656	-2.11%
XY-18-July 21	18 m 21 July	XY Deposit, Yukon	18 m 21 July	Water	NA	NA	NA	21-07-2010	1.90	NA	3.60	488	9	NA	NA	2,808	190	253	74	296	19.1	1.3	12.4	0.2597	0.8129	1.0726	-2.14%
XY-18-July 28	18 m 28 July	XY Deposit, Yukon	18 m 28 July	Water	NA	NA	NA	28-07-2010	2.60	NA	3.50	425	8	NA	NA	3,245	186	249	73	299	19.2	1.3	12.5	0.3098	0.8774	1.1872	-3.04%
XY-40-July 20	40 m 20 July	XY Deposit, Yukon	40 m 20 July	Water	NA	NA	NA	20-07-2010	4.00	NA	4.00	470	9	NA	NA	2,278	130	224	46	209	13.0	1.0	10.5	0.1952	0.5596	0.7548	-1.92%
XY-40-July 21	40 m 21 July	XY Deposit, Yukon	40 m 21 July	Water	NA	NA	NA	21-07-2010	2.60	NA	3.90	481	9	NA	NA	2,346	148	238	51	239	15.0	1.1	11.0	0.2046	0.6320	0.8366	-1.72%
XY-40-July 28	40 m 28 July	XY Deposit, Yukon	40 m 28 July	Water	NA	NA	NA	28-07-2010	12.50	NA	3.80	448	8	NA	NA	2,724	150	241	51	251	15.5	1.1	11.3	0.2490	0.6933	0.9423	-2.40%
XY-100-July 28	100 m 28 July	XY Deposit, Yukon	100 m 28 July	Water	NA	NA	NA	28-07-2010	12.20	NA	4.30	392	7	NA	NA	1,897	96	210	21	176	10.2	0.9	9.3	0.1596	0.4396	0.5992	-1.44%
XY-120-July 28	120 m 28 July	XY Deposit, Yukon	120 m 28 July	Water	NA	NA	NA	28-07-2010	9.80	NA	4.60	385	7	NA	NA	1,549	44	229	12	166	6.9	0.9	7.1	0.1097	0.2989	0.4086	-0.71%
XY-165-Aug 1	165 m 1 Aug	XY Deposit, Yukon	165 m 1 Aug	Water	NA	NA	NA	01-08-2010	10.00	NA	4.60	361	6	NA	NA	1,408	23	235	14	158	6.1	0.8	6.6	0.0886	0.2619	0.3505	-0.45%
XY-165-Aug 3	165 m 3 Aug	XY Deposit, Yukon	165 m 3 Aug	Water	NA	NA	NA	03-08-2010	9.50	NA	5.00	355	6	NA	NA	1,429	22	246	13	165	6.2	0.9	6.5	0.0885	0.2580	0.3465	-0.38%
DU-4-June	Uottawa-June	Duhamel	Control site, Canadian Shield.	Water	43N	500,000	5,094,048	24-06-2015	14.00	NA	6.70	100	2	28	3.0	NA	0.10	53	2	5	0.3	3.7		0.0014	0.0013	0.0027	NA
SC01-Aug	Uottawa - August-16-17-run	Pennsylvania	Wetland 2 outflow	Water	18T	405314	4508995	08-08-2016	28.97	9.64	7.56	342	6	3.4	2.3	140	0.01	44	0	25	2.0	2.3	5.1	0.0009	0.0000	0.0009	0.15%
SC02-Aug	Uottawa - August-16-17-run	Pennsylvania	Wetland 1 outflow	Water	18T	405242	4509077	08-08-2016	25.55	10.21	7.18	367	6	5.5	2.3	180	0.00	41	0	23	1.3	2.1	4.3	0.0008	0.0000	0.0008	0.04%
SC03-Aug	Uottawa - August-16-17-run	Pennsylvania	Pond 3 outflow	Water	18T	405173	4509144	08-08-2016	25.23	7.89	6.47	322	5	5.4	1.7	120	0.00	44	1	26	3.0	2.3	5.9	0.0019	0.0004	0.0023	0.20%
SC04-Aug	Uottawa - August-16-17-2016-run	Pennsylvania	Pond 2 outflow	Water	18T	405118	4509280	08-08-2016	17.93	3.4	5.81	358	6	17.8	1.8	175	0.10	42	12	26	3.0	3.3	6.3	0.0023	0.0002	0.0026	0.09%
SC05-Aug	Uottawa - August-16-17-2016-run	Pennsylvania	Pond1 outflow	Water	18T	405096	4509330	08-08-2016	13.91	1.18	6.02	299	5	27.5	1.8	195	0.00	39	19	24	2.8	5.0	6.5	0.0044	0.0007	0.0051	0.02%
SC05-field dup-Aug	Uottawa - August-16-17-2016-run	Pennsylvania	Pond1 outflow	Water	18T	405096	4509330	08-08-2016	13.91	1.18	6.02	299	5	NA	NA	150	0.02	40	19	24	2.6	2.5	6.6	0.0207	0.0053	0.0260	0.10%
SC06-Aug	Uottawa - August-16-17-2016-run	Pennsylvania	Silver Creek Shaft	Water	18T	405096	4509401	08-08-2016	12.12	0.56	6.03	291	5	29.8	2.3	130	0.17	40	20	25	2.9	2.2	6.4	0.0189	0.0052	0.0241	0.14%
SC06-lab dup-Aug	Uottawa - August-16-17-2016-run	Pennsylvania	Silver Creek Shaft	Water	18T	405096	4509401	08-08-2016	12.12	0.56	6.03	291	5	NA	NA		0.16	40	20	25	2.8	2.1	6.3	0.0195	0.0052	0.0247	0.43%
SC01-Aug AM	Uottawa - Dec-9-13-2016 run	Pennsylvania	Wetland 2 outflow	Water	18T	405314	4508995	09-08-2016	20.47	7.7	7.13	460	8	NA	NA	170	0.00	42	0	25	1.5	3.0	5.9	0.0007	0.0001	0.0008	0.09%
SC02-Aug AM	Uottawa - August-16-17-2016-run	Pennsylvania	Wetland 1 outflow	Water	18T	405242	4509077	09-08-2016	21.08	6.74	6.67	392	7	7.1	1.8	180	0.00	47	0	26	1.6	2.4	4.5	0.0009	0.0000	0.0010	0.09%
SC03-Aug AM	Uottawa - Dec-9-13-2016 run	Pennsylvania	Pond 3 outflow	Water	18T	405173	4509144	09-08-2016	20.37	7.78	6.27	384	7	NA	NA	145	0.00	40	0	24	2.1	2.8	6.2	0.0014	0.0003	0.0017	0.12%
SC04-Aug AM	Uottawa - Dec-9-13-2016 run	Pennsylvania	Pond 2 outflow	Water	18T	405118	4509280	09-08-2016	14.79	5.56	5.86	379	7	NA	NA	145	0.01	38	4	23	2.1	2.6	6.2	0.0042	0.0014	0.0056	0.10%
SC05-Aug AM	Uottawa - August-16-17-2016-run	Pennsylvania	Pond1 outflow	Water	18T	405096	4509330	09-08-2016	12.1	2.12	5.97	319	6	22.6	0.8	165	0.14	44	21	26	2.9	2.4	6.8	0.0188	0.0051	0.0238	0.11%
SC05-lab dup-Aug AM	Uottawa - Dec-9-13-2016 run	Pennsylvania	Silver Creek Shaft	Water	18T	405096	4509330	09-08-2016	11.93	0.83	5.94	294	5	NA	NA	270	0.14	38	14	23	2.1	2.5	6.5	0.0166	0.0046	0.0212	-0.17%
SC06-Aug AM	Uottawa - Dec-9-13-2016 run	Pennsylvania	Wetland2 outflow	Water	18T	405096	4509401	09-08-2016	11.93	0.83	5.94	294	5	NA	NA	165	0.00	39	14	22	2.1	3.6	6.3	0.0050	0.0009	0.0059	0.06%
PF02-Aug	Uottawa - August-16-17-2016-run	Pennsylvania	ALD outflow	Water	18T	400611	4507860	09-08-2016	NA	NA	NA	NA	NA	NA	NA	260	0.10	59	1	44	3.0	8.0	4.7	0.0010	0.0000	0.0010	0.18%
PF05-Aug	Uottawa - August-16-17-2016-run	Pennsylvania	Pine Forest discharge	Water	18T	400661	4508119	09-08-2016	NA	NA	NA	NA	NA	NA	NA	245	0.00	53	4	45	3.7	8.2	5.0	0.0015	0.0002	0.0017	0.19%
PF06-Aug	Uottawa - August-16-17-2016-run	Pennsylvania	Weston mines lost creek	Water	18T	400624	4508202	09-08-2016	NA	NA	NA	NA	NA	NA	NA	225	0.00	50	10	47	4.0	8.1	5.3	0.0014	0.0002	0.0016	0.23%
M07-Dec	Uottawa - Oct-5-2016	Pennsylvania	Weston mines lost creek	Water	18T	394798.3174	4518180.15	11-12-2015	10.73	0.38	5.98	243	4	52.1	4.4	125	0.00	94	12	45	4.2	13.0	5.9	0.0011	0.0001	0.0012	0.69%
M-07 field dup-Dec	Uottawa - Oct-5-2016	Pennsylvania	Girardville seepage	Water	18T	394798.3174	4518180.15	11-12-2015	NA	NA	NA	NA	NA	NA	NA	92	0.00	92	11	45	4.1	13.0	5.8	0.0012	0.0001	0.0012	NA
M11-Dec	Uottawa - Oct-5-2016	Pennsylvania	Packer 5	Water	18T	393049.0462	4518216.407	11-12-2015	10.46	7.32	6.37	249	4	27.1	1.9	100	0.00	40	12	26	2.5	13.0	4.3	0.0009	0.0002	0.0011	0.31%
M14-Dec	Uottawa - June-9-2016-run	Pennsylvania	Centralia mine discharge	Water	18T	392124.7464	4516700.865	11-12-2015	12.68	2.21	6.3	215	4	65.83	4.84	425	0.00	120	14	58	4.8	11.0	5.2	0.0022	0.0011	0.0034	0.28%
M19-Dec	Uottawa - June-9-2016-run	Pennsylvania	Bast mine overflow Pipe discharge	Water	18T	388337.9926	4516642.704	11-12-2015	13.22	6.47	3.72	666	12	10	1.17	425	4.70	63	3	78	4.9	9.2	9.2	0.0656	0.0504	0.1160	0.15%
M20-Dec	Uottawa - June-9-2016-run	Pennsylvania	Bast mine tunnel discharge	Water	18T	388732.5863	4515897.273	11-12-2015	12.44	4.14	6.26	226	4	44.42	3.69	325	0.00	83	8	75	3.2	11.0	5.6	0.0080	0.0032	0.0112	0.45%
M21-Dec	Uottawa - June-9-2016-run	Pennsylvania	Bast mine tunnel discharge	Water	18T	387667.9548	4515743.483	11-12-2015	12.4	4.01	6.19	245	4	44.91	4.25	325	0.03	84	12	58	2.9	9.1	5.7	0.0049	0.0029	0.0078	0.30%
M21-lab dup-Dec	Uottawa - June-9-2016-run	Pennsylvania	Mahanoy Creek d/s Gilberton Pump (not pumping	Water	18T	387667.9548	4515743.483	11-12-2015	NA	NA	NA	NA	0	NA	NA	NA	80	12	57	2.7	8.7	5.5	0.0050	0.0029	0.0078	NA
S13-Dec	Uottawa - Oct-5-2016	Pennsylvania	Shenandoah Creek d/s	Water	18T	394838.9128	4518174.017	11-12-2015	7.33	8.79	6.75	343	6	6.6	5.8	50	0.00	18	0	8	0.5	33.0	2.5	0.0004	0.0001	0.0005	0.36%
S14-Dec	Uottawa - Oct-5-2016	Pennsylvania	Mahanoy Creek at Ashland	Water	18T	392370.136	4516328.679	11-12-2015	10.17	7.5	6.71	216	4	22.96	1.78	310	0.00	110	3	48	2.5	17.0	5.1	0.0009	0.0001	0.0011	0.45%
S16-Dec	Uottawa - June-9-2016-run	Pennsylvania	Mahanoy Creek at Ashland	Water	18T	386976.3717	4514801.332	11-12-2015	11.6	9.28	7.09	133	2	22.02	2.12	275	0.01	92	6	48	3.7	15.0	4.9	0.0009	0.0001	0.0010	0.41%
PF1-Dec	Uottawa - Oct-5-2016	Pennsylvania	Wetland 3 outflow	Water	18T	400610	4507788	12-12-2015	11.88	10.28	6.94	203	4	12.94	1.3	225	0.01	58	2	44	2.1	5.8	4.2	0.0008	0.0001	0.0009	0.23%
PF2-Dec	Uottawa - Oct-5-2016	Pennsylvania	Wetland1 outflow	Water	18T	400611	4507860	12-12-2015	12.04	10.07	6.89	206	4	13.32	1.22	250	0.00	61	2	46	2.0	6.3	4.4	0.0008	0.0001	0.0009	0.21%
PF3-Dec	Uottawa - Oct-5-2016	Pennsylvania	Pond1 outflow	Water	18T	400640	4507960	12-12-2015	12.15	9.86	6.78	196	3	14.44	1.19	225	0.00	61	3	45	2.1	6.3	4.5	0.0009	0.0001	0.0010	0.26%
PF4-Dec	Uottawa - June-9-2016-run	Pennsylvania	Pond1 outflow	Water	18T	400676	4508040	12-12-2015	12.16	8.5	6.4	238	4	21.5	1.73	225	0.00	67	7	49	2.9	7.2	5.1	0.0011	0.0011	0.0022	0.33%
PF4-fdup-Dec	Uottawa - June-9-2016-run	Pennsylvania	ALD outflow	Water	18T	400676	4508040	12-12-2015	NA	NA	NA	NA	NA	21.78	1.76	IP	0.00	67	6	49	2.8	7.2	5.1	0.0011	0.0011	0.0022	NA
PF5-Dec	Uottawa - June-9-2016-run	Pennsylvania	Pine Forest discharge	Water	18T	400661	4508119	12-12-2015	11.6	2.97	6.15	261	5	48.25	4.65	225	0.01	74	10	49	3.0	7.1	5.1	0.0019	0.0011	0.0030	0.36%
PF6-Dec	Uottawa - June-9-2016-run	Pennsylvania	Wetland 2 outflow	Water	18T	400624	4508202	12-12-2015	11.63	0.4	5.79	293	5	42.25	3.67	225	0.09	56	14	51	3.1	7.4	5.4	0.0045	0.0019	0.0063	0.29%
SC01-Dec	Uottawa - Oct-5-2016	Pennsylvania	Wetland 2 outflow	Water	18T	405314	4508995	12-12-2015	8.46	12.01	6.76	283	5	6.28	1	150	0.00	43	1	25	2.1	0.6	4.9	0.0009	0.0001	0.0010	0.11%
SC01-lab dup-Dec	Uottawa - Oct-5-2016	Pennsylvania	Wetland 1 outflow	Water	18T	405314	4508995	12-12-2015					0				0.00	42	1	23	2.0	0.5	4.6	0.0009	0.0001	0.0009	0.40%
SC02-Dec	Uottawa - Oct-5-2016	Pennsylvania	Pond 3 outflow	Water	18T	405242	4509077	12-12-2015	8.73	11.34	6.65	286	5	7.68	0.88	125	0.00	43	2	25	2.0	0.5	4.9	0.0009	0.0001	0.0010	0.16%
SC03-Dec	Uottawa - Oct-5-2016	Pennsylvania	Pond 2 outflow	Water	18T	405173	4509144	12-12-2015	8.81	10.49	6.44	298	5	9.92	1	150	0.00	43	5	24	2.1	0.5	5.1	0.0012	0.0002	0.0014	0.10%
SC04-Dec	Uottawa - June-9-2016-run	Pennsylvania	Pond 2 outflow	Water	18T	405118	4509280	12-12-2015	10.28	8.34	6.15	293	5	17.07	1.58	150	0.00	43	9	25	2.2	0.5	5.5	0.0025	0.0012	0.0036	0.10%
SC04-field dup-Dec	Uottawa - June-9-2016-run	Pennsylvania	Pond1 outflow	Water	18T	405118	4509280	12-12-2015	NA	NA	NA	NA	NA	17.15	1.49	165	0.00	40	10	23	2.3	0.4	5.2	0.0028	0.0013	0.0041	0.05%
SC05-Dec	Uottawa - June-9-2016-run	Pennsylvania	Pond1 outflow	Water	18T	405096	4509330	12-12-2015	11.98	1.86	5.84	281	5	37.53	2.89	125	0.10	41	17	24	2.3	0.4	5.6	0.0113	0.0048	0.0161	0.13%
SC06-Dec	Uottawa - June-9-2016-run	Pennsylvania	Silver Creek Shaft	Water	18T	405096	4509401	12-12-2015	11.89	0.57	5.86	237	4	40.14	4.16	125	0.12	41	17	24	2.2	0.4	5.6	0.0122	0.0054	0.0176	0.13%

NOTES:
1. IF SAMPLE WAS BELOW DETECTION LEVEL -- RECORDED AT DETECTION LEVEL.

APPENDIX B

COAL MINE DRAINAGE SITES – REY SPECIATION IN WATER ENRICHED WITH IRON, ALUMINUM AND ORGANICS

Table B1.1 Manual Water Balance - Silver Creek Water (meq/L)

Sample Id	Cations					Anions					Error
	Ca	Mg	Na	K	sum+	Cl	SO4	NO3	HCO3	sum-	%
SC01-Aug	0.0022	0.0021	0.000100	0.000059	0.0044	0.00011	0.0043	0.000026	0.0002	0.0047	-0.0282
SC02-Aug	0.0020	0.0019	0.000091	0.000054	0.0041	0.00011	0.0046	0.000023	0.0003	0.0050	-0.1031
SC03-Aug	0.0022	0.0021	0.000100	0.000059	0.0045	0.00011	0.0044	0.000032	0.0002	0.0048	-0.0318
SC04-Aug	0.0021	0.0021	0.000144	0.000084	0.0045	0.00011	0.0044	0.000026	0.0003	0.0048	-0.0392
SC05-Aug	0.0019	0.0020	0.000217	0.000128	0.0043	0.00011	0.0048	0.000077	0.0005	0.0055	-0.1299
SC06-Aug	0.0020	0.0021	0.000096	0.000056	0.0042	0.00011	0.0042	0.000123	0.0006	0.0051	-0.0930
SC02-Aug AM	0.0023	0.0021	0.000104	0.000061	0.0047	0.00011	0.0043	0.000029	0.0003	0.0048	-0.0131
SC05-Aug AM	0.0022	0.0021	0.000104	0.000061	0.0045	0.00011	0.0045	0.000074	0.0004	0.0051	-0.0610
SC01-Dec	0.0021	0.0021	0.000025	0.000015	0.0042	0.00011	0.0039	0.000052	0.0003	0.0044	-0.0199
SC02-Dec	0.0021	0.0021	0.000022	0.000013	0.0042	0.00011	0.0039	0.000055	0.0004	0.0045	-0.0252
SC03-Dec	0.0021	0.0020	0.000022	0.000013	0.0042	0.00011	0.0039	0.000087	0.0004	0.0044	-0.0335
SC04-Dec	0.0021	0.0021	0.000022	0.000013	0.0042	0.00011	0.0039	0.000119	0.0004	0.0046	-0.0415
SC05-Dec	0.0020	0.0020	0.000018	0.000010	0.0040	0.00011	0.0037	0.000113	0.0006	0.0046	-0.0588
SC06-Dec	0.0020	0.0020	0.000018	0.000010	0.0040	0.00011	0.0037	0.000148	0.0006	0.0047	-0.0696

NOTE:

1. VALUES IN mg/L WERE NORMALIZED TO THE PENNSYLVANIA ANTHRACITE-MAMMOTH NO. 8 (SCHUYLKILL COUNTY).

LIZ ASHBY-THESIS
TABLE Table B1.2

Table B1.2 Silver Creek Water (0.45µm filtered) Rare Earth Element data detection limits (µg/L)

Sample	La	Ce	Pr	Nd	Sm	Eu	Gd	Tb	Dy	Y	Er	Ho	Tm	Yb	Lu	Sc
Analysis Method	ICP-MS	ICP-MS	ICP-MS	ICP-MS	ICP-MS	ICP-MS	ICP-MS	ICP-MS	ICP-MS	ICP-MS	ICP-MS	ICP-MS	ICP-MS	ICP-MS	ICP-MS	ICP-MS
Mass	139	140	141	146	147	153	157	159	163	172	166	165	169	89	175	45
SC06-Dec	0.06	0.06	0.01	0.05	0.03	0.004	0.05	0.01	0.04	0.06	0.01	0.01	0.01	0.03	0.9	0.04
SC06-Aug-PM	0.0007	0.0008	0.001	0.009	0.009	0.0008	0.002	0.0006	0.001	0.001	0.0009	0.0004	0.0006	0.0004	0.0005	0.02
SC06-Aug-AM	0.003	0.004	0.002	0.001	0.002	0.001	0.004	0.002	0.003	0.002	0.002	0.004	0.003	0.004	0.003	0.01
SC05-Dec	0.06	0.06	0.01	0.05	0.03	0.004	0.05	0.01	0.04	0.06	0.01	0.01	0.01	0.03	0.9	0.04
SC05-Aug-PM	0.0007	0.0008	0.001	0.009	0.009	0.0008	0.002	0.0006	0.001	0.001	0.0009	0.0004	0.0006	0.0004	0.0005	0.02
SC05-Aug-AM	0.0007	0.0008	0.001	0.009	0.009	0.0008	0.002	0.0006	0.001	0.001	0.0009	0.0004	0.0006	0.0004	0.0005	0.02
SC04-Dec	0.06	0.06	0.01	0.05	0.03	0.004	0.05	0.01	0.04	0.06	0.01	0.01	0.01	0.03	0.9	0.04
SC04-Aug-PM	0.0007	0.0008	0.001	0.009	0.009	0.0008	0.002	0.0006	0.001	0.001	0.0009	0.0004	0.0006	0.0004	0.0005	0.02
SC04-Aug-AM	0.003	0.004	0.002	0.001	0.002	0.001	0.004	0.002	0.003	0.002	0.002	0.004	0.003	0.004	0.003	0.01
SC03-Dec	0.003	0.05	0.002	0.006	0.01	0.002	0.01	0.002	0.007	0.006	0.005	0.002	0.004	0.006	0.004	0.04
SC03-Aug-PM	0.0007	0.0008	0.001	0.009	0.009	0.0008	0.002	0.0006	0.001	0.001	0.0009	0.0004	0.0006	0.0004	0.0005	0.02
SC03-Aug-AM	0.003	0.004	0.002	0.001	0.002	0.001	0.004	0.002	0.003	0.002	0.002	0.004	0.003	0.004	0.003	0.01
SC02-Dec	0.003	0.05	0.002	0.006	0.01	0.002	0.01	0.002	0.007	0.006	0.005	0.002	0.004	0.006	0.004	0.04
SC02-Aug-PM	0.0007	0.0008	0.001	0.009	0.009	0.0008	0.002	0.0006	0.001	0.001	0.0009	0.0004	0.0006	0.0004	0.0005	0.02
SC02-Aug-AM	0.0007	0.0008	0.001	0.009	0.009	0.0008	0.002	0.0006	0.001	0.001	0.0009	0.0004	0.0006	0.0004	0.0005	0.02
SC01-Dec	0.003	0.05	0.002	0.006	0.01	0.002	0.01	0.002	0.007	0.006	0.005	0.002	0.004	0.006	0.004	0.04
SC01-Aug-PM	0.0007	0.0008	0.001	0.009	0.009	0.0008	0.002	0.0006	0.001	0.001	0.0009	0.0004	0.0006	0.0004	0.0005	0.02
SC01-Aug-AM	0.003	0.004	0.002	0.001	0.002	0.001	0.004	0.002	0.003	0.002	0.002	0.004	0.003	0.004	0.003	0.01

NOTE:

1. ALL VALUES WERE MEASURED ON THE ICP-MS AND ARE PROVIDED IN µg/L.

2. DETECTION LIMITS WERE CALCULATED BY MULTIPLYING THE DILUTION OF THE SAMPLE BY 3*STANDARD DEVIATION OF 10 BLANK SAMPLES.

Table B1.2 Major and Minor Ions – Silver Creek water chemistry (mMol/L)

Sample	NO_2^-	NO_3^-	PO_4	SO_4^{2-}	SO_4^{2-}	Al	Ca	Fe	Mg	Mn	K	Na	P	S	Si	Sum REY + Sc
	Hach™ SpectroPhotometer DR-2800				Calculated from ICP-ES S	27 [NoHe] & 396.152	422.673	259.9	279.55	55 [NoHe]	766.5	589.592	177.43	180.669	251.61	
							ICP-ES	ICP-ES	ICP-ES	ICP-MS	ICP-ES	ICP-ES	ICP-ES	ICP-ES	ICP-ES	
SC06-Dec	0.15	74	1	1,301	1,874	4.4	1,023	304	614	91	<4	13	<0.55	1,871	199	0.14
SC06-Aug-PM	0.28	61	2	1,353	2,124	6.3	998	358	639	119	36	71	<0.05	2,121	228	0.20
SC06-Aug-AM	0.15	24	2	1,718	2,280	0.2	973	251	563	86	25	116	<0.55	2,277	224	0.06
SC05-Dec	0.15	56	2	1,301	1,874	3.7	1,023	304	614	95	<4	13	<0.55	1,871	199	0.13
SC05-Aug-PM	0.26	40	2	1,562	2,342	0.7	998	340	614	107	37	81	<0.05	2,339	235	0.21
SC05-Aug-AM	0.13	37	13	1,718	2,249	5.2	1,098	376	665	119	42	77	<0.05	2,246	242	0.20
SC04-Dec	0.13	60	3	1,562	1,968	<0.03	1,073	167	639	91	10	16	<0.55	1,965	196	0.04
SC04-Aug-PM	0.11	13	1	1,822	2,217	3.7	1,048	215	665	123	25	107	<0.05	2,215	224	0.05
SC04-Aug-AM	0.11	24	2	1,509	2,405	0.5	948	64	588	86	48	84	<0.55	2,402	221	0.03
SC03-Dec	0.20	44	2	1,562	1,936	<0.03	1,073	90	614	86	9	16	0.61888	1,934	182	0.03
SC03-Aug-PM	0.15	16	2	1,249	2,217	0.05	1,098	14	665	123	38	74	<0.05	2,215	210	0.03
SC03-Aug-AM	0.11	15	2	1,509	2,592	0.02	998	4	614	86	52	90	<0.55	2,589	221	0.02
SC02-Dec	0.13	27	2	1,301	1,968	<0.03	1,073	36	639	82	12	16	<0.55	1,965	174	0.02
SC02-Aug-PM	0.09	11	2	1,874	2,280	<0.04	1,023	5	588	53	30	68	<0.05	2,277	153	0.02
SC02-Aug-AM	0.07	15	1	1,874	2,155	0.03	1,173	5	665	66	34	77	<0.05	2,152	160	0.02
SC01-Dec	0.20	26	1	1,562	1,968	<0.03	1,073	21	639	86	20	19	<0.55	1,965	174	0.02
SC01-Aug-PM	0.04	13	1	1,457	2,155	0.2	1,098	5	639	82	31	74	<0.05	2,152	182	0.02
SC01-Aug-AM	0.04	15	1	1,770	2,780	0.2	1,048	0	639	62	48	97	<0.55	2,776	210	0.02

NOTE:

1. ALL VALUES ARE PROVIDED IN µmol/L.
2. TO CALCULATE SULPHATE VALUES BY ICP-ES, THE MEASURED SULPHATE VALUE WAS MULTIPLED BY THE ATOMIC MASS OF SULPHATE DIVIDED BY SULPHUR (96 g/L/32 g/L).
3. ALL ELEMENTS WERE FILTERED WITH 0.45µm FILTER PRIOR TO ANALYSIS.

LIZ ASHBY-THESIS
TABLE Table B1.4

Table B1.4 Rare earth element data – Silver Creek water chemistry (mMol/L)

Sample	La	Ce	Pr	Nd	Sm	Eu	Gd	Tb	Dy	Y	Er	Ho	Tm	Yb	Lu	Sc	
Analysis Method	ICP-MS	ICP-MS	ICP-MS	ICP-MS	ICP-MS	ICP-MS	ICP-MS	ICP-MS	ICP-MS	ICP-MS	ICP-MS	ICP-MS	ICP-MS	ICP-MS	ICP-MS	ICP-MS	Sum REY + Sc
Mass	139	140	141	146	147	153	157	159	163	172	166	165	169	89	175	45	
SC06-Dec	0.533	1.427	0.1774	0.7626	0.1463	0.0329	0.1463	0.0195	0.0923	0.000019	0.0524	0.0173	0.0065	0.0410	0.743	0.136	4.33
SC06-Aug-PM	0.598	1.285	0.1561	0.6101	0.1131	0.0257	0.1081	0.0157	0.0738	0.000033	0.0386	0.0138	0.0050	0.0300	0.005	0.267	3.34
SC06-Aug-AM	0.583	1.285	0.1561	0.5893	0.1197	0.0276	0.1272	0.0170	0.0738	0.000007	0.0416	0.0143	0.0053	0.0329	0.005	0.158	3.24
SC05-Dec	0.554	1.570	0.1987	0.7626	0.1663	0.0362	0.1526	0.0214	0.0985	0.000017	0.0530	0.0185	0.0071	0.0410	0.743	0.118	4.54
SC05-Aug-PM	0.569	1.499	0.1916	0.7626	0.1463	0.0322	0.1335	0.0189	0.0923	0.000035	0.0464	0.0161	0.0065	0.0370	0.005	0.171	3.73
SC05-Aug-AM	0.504	1.213	0.1561	0.6032	0.1131	0.0250	0.1081	0.0151	0.0677	0.000033	0.0368	0.0120	0.0048	0.0289	0.004	0.245	3.14
SC04-Dec	0.5111	1.2133	0.14903	0.58929	<0.1197	0.02501	<0.114467	<0.016989	<0.08	0.000001	<0.042186	<0.014947	<0.00539	<0.0347	<0.572	0.091	3.579
SC04-Aug-PM	0.6911	1.7129	0.21290	0.83194	<0.1596	0.03488	0.15262	0.02139	0.10462	0.000002	0.05484	0.01853	0.007103	0.04392	0.006287	0.267	4.320
SC04-Aug-AM	0.6623	1.8556	0.21290	0.83194	0.172918	0.04014	0.17806	0.025169	0.116923	0.000011	0.060266	0.021524	0.008287	0.049117	0.007430	0.080	4.323
SC03-Dec	0.4895	<0.9278	0.10645	0.39517	<0.07316	<0.017109	0.082671	<0.011955	0.0553846	0.0000020	0.030736	<0.01076	<0.00373	0.022536	<0.42865	0.047	2.702
SC03-Aug-PM	0.5039	0.8564	0.09226	0.34664	<0.060521	0.014477	0.06995	0.010068	0.04800	0.0000039	0.026517	0.008968	0.003315	0.019069	0.002915	0.053	2.116
SC03-Aug-AM	0.4607	0.8564	0.09226	0.33277	0.065177	0.014477	0.076312	<0.010068	0.05108	0.0000026	0.02652	<0.00957	<0.00349	0.019647	<0.00303	0.027	2.048
SC02-Dec	0.43195	<0.7851	<0.09226	<0.34664	<0.06451	<0.015793	<0.076312	<0.010697	<0.04985	0.0000003	<0.02712	<0.00957	<0.00349	<0.02022	<0.37721	0.058	2.369
SC02-Aug-PM	0.54713	0.99917	<0.106452	<0.41597	<0.073158	0.017767	<0.082671	0.012585	0.059077	0.0000002	0.0319412	0.0119575	0.0043212	0.0242697	0.0036578	0.065	2.455
SC02-Aug-AM	0.50394	0.92780	<0.099356	<0.3813	<0.065842	0.015135	0.076312	0.010697	0.052923	0.0000003	0.0277225	0.010164	0.0038477	0.020803	0.0032006	0.073	2.272
SC01-Dec	0.35996	<0.6709	<0.07807	<0.28424	<0.054536	<0.011845	<0.063593	<0.009438	<0.04246	0.0000002	<0.02411	<0.00897	<0.00296	<0.01965	<0.302914	0.047	1.980
SC01-Aug-PM	0.27357	0.37112	<0.038323	<0.14559	<0.022612	0.006383	0.031797	0.004845	<0.023385	0.0000003	0.0138613	0.004604	0.0015391	0.008090	0.0013717	0.038	0.985
SC01-Aug-AM	0.62633	1.14191	0.12774	<0.50609	<0.099761	<0.024348	<0.114467	<0.015101	<0.07385	0.0000003	<0.04098	<0.01495	<0.00485	<0.03005	<0.00474	0.047	2.872

NOTE:

1. ALL VALUES ARE PROVIDED IN µmol/L.

Table B1.5 Silver Creek Water (0.45µm filtered) Rare Earth Element NASC normalized data

Sample	La	Ce	Pr	Nd	Sm	Eu	Gd	Tb	Dy	Y	Er	Ho	Tm	Yb	Lu	Sc	
Analysis Method	ICP-MS	ICP-MS	ICP-MS	ICP-MS	ICP-MS	ICP-MS	ICP-MS	ICP-MS	ICP-MS	ICP-MS	ICP-MS	ICP-MS	ICP-MS	ICP-MS	ICP-MS	ICP-MS	Sum REY + Sc
Mass	139	140	141	146	147	153	157	159	163	172	166	165	169	89	175	45	
SC06-Dec	8.04E-05	7.80E-05	7.66E-05	8.39E-05	7.87E-05	9.32E-05	1.04E-04	9.18E-05	7.91E-05	6.30E-05	5.69E-05	5.63E-05	4.17E-05	4.25E-05	5.26E-03	4.07E-05	0.006
SC06-Aug-PM	1.25E-04	1.21E-04	1.23E-04	1.39E-04	1.22E-04	1.44E-04	1.76E-04	1.41E-04	1.39E-04	1.07E-04	3.04E-04	3.87E-05	8.75E-05	7.84E-05	8.11E-05	4.81E-05	0.002
SC06-Aug-AM	4.50E-05	2.70E-05	2.34E-05	2.59E-05	1.25E-05	2.88E-05	1.88E-05	1.18E-05	1.39E-05	2.41E-05	4.80E-05	5.63E-06	1.60E-05	1.21E-05	1.25E-05	2.89E-05	0.0004
SC05-Dec	7.40E-05	7.20E-05	6.88E-05	7.66E-05	7.33E-05	7.92E-05	1.02E-04	8.00E-05	6.95E-05	5.56E-05	5.98E-05	4.93E-05	2.50E-05	3.04E-05	4.61E-03	4.07E-05	0.006
SC05-Aug-PM	1.45E-04	1.38E-04	1.30E-04	1.50E-04	1.18E-04	1.40E-04	1.71E-04	1.41E-04	1.32E-04	1.15E-04	2.84E-04	3.87E-05	7.71E-05	6.86E-05	7.46E-05	4.07E-05	0.002
SC05-Aug-AM	1.25E-04	1.20E-04	1.22E-04	1.39E-04	1.23E-04	1.36E-04	1.63E-04	1.29E-04	1.34E-04	1.07E-04	3.04E-04	3.52E-05	7.29E-05	7.84E-05	7.68E-05	4.81E-05	0.002
SC04-Dec	2.09E-05	9.30E-06	4.29E-06	4.01E-06	<0.000005	9.32E-06	<0.00001	<0.000012	<0.00001	4.81E-06	<0.00001	<0.000004	<0.000021	<0.00001	<0.002	3.70E-05	0.0021
SC04-Aug-PM	2.19E-05	7.20E-06	3.90E-06	3.18E-06	<0.000002	3.81E-05	3.47E-06	2.00E-06	1.92E-06	6.67E-06	7.94E-06	1.02E-06	2.50E-06	2.32E-06	4.39E-06	3.70E-05	0.0001
SC04-Aug-AM	4.18E-05	2.25E-05	1.69E-05	1.50E-05	0.0000111	1.48E-05	2.24E-05	1.88E-05	1.97E-05	3.70E-05	6.08E-05	7.39E-06	1.58E-05	1.21E-05	1.56E-05	2.70E-05	0.0004
SC03-Dec	7.72E-06	<0.000001	1.56E-06	1.86E-06	<0.000002	<0.000003	2.45E-06	<0.000002	3.12E-06	6.67E-06	8.33E-06	<0.000001	<0.000008	2.19E-06	8.77E-06	3.70E-05	0.0001
SC03-Aug-PM	1.61E-05	4.80E-06	2.60E-06	1.93E-06	<0.000002	5.89E-06	4.49E-06	4.82E-06	4.08E-06	1.30E-05	1.18E-05	2.15E-06	3.75E-06	2.25E-06	5.04E-06	3.70E-05	0.0001
SC03-Aug-AM	1.16E-05	2.85E-06	1.82E-06	1.64E-06	0.0000009	3.26E-06	2.45E-06	<0.000002	2.09E-06	8.52E-06	7.06E-06	<0.000001	<0.000006	1.34E-06	6.58E-06	2.81E-05	0.0001
SC02-Dec	9.65E-07	<0.000001	<0.0000003	<0.0000002	<0.000002	<0.000002	<0.000002	<0.000002	<0.000002	8.89E-07	<0.000005	<0.000001	<0.000008	<0.000002	<0.000009	3.70E-05	0.0001
SC02-Aug-PM	7.40E-07	2.70E-07	<0.0000001	<0.0000003	<0.000002	2.03E-06	<0.0000004	1.18E-06	6.24E-07	7.78E-07	1.37E-06	3.03E-07	1.98E-06	4.25E-07	3.07E-06	2.63E-05	0.00004
SC02-Aug-AM	1.16E-06	3.60E-07	<0.0000001	<0.0000003	<0.0000016	3.43E-06	7.14E-07	1.06E-06	7.91E-07	1.11E-06	1.57E-06	5.99E-07	2.08E-06	6.54E-07	2.85E-06	3.15E-05	0.0000
SC01-Dec	6.43E-07	<0.000001	<0.0000003	<0.0000002	<0.000002	<0.000002	<0.000002	<0.000002	<0.000002	7.78E-07	<0.000005	<0.000001	<0.000008	<0.000002	<0.000009	3.70E-05	0.0001
SC01-Aug-PM	9.32E-07	3.90E-07	<0.0000001	<0.0000003	<0.000002	3.05E-06	6.53E-07	1.02E-06	<0.0000002	9.63E-07	1.47E-06	6.69E-07	2.92E-06	6.86E-07	2.85E-06	3.04E-05	0.00005
SC01-Aug-AM	1.03E-06	2.70E-07	2.86E-07	<0.0000003	<0.0000004	<0.000002	<0.000001	<0.000002	<0.0000007	9.26E-07	<0.000002	<0.000001	<0.000006	<0.000001	<0.000007	2.52E-05	0.00005

NOTE:

1. VALUES IN mg/L WERE NORMALIZED TO THE NORTH AMERICAN SHALE COMPOSITE.

LIZ ASHBY-THESIS
TABLE Table B1.6

Table B1.6 Silver Creek Water (0.45µm filtered) Rare Earth Element PAAS normalized data

Sample	La	Ce	Pr	Nd	Sm	Eu	Gd	Tb	Dy	Y	Er	Ho	Tm	Yb	Lu	Sc	Sum REY + Sc
Analysis Method	ICP-MS	ICP-MS	ICP-MS	ICP-MS	ICP-MS	ICP-MS	ICP-MS	ICP-MS	ICP-MS	ICP-MS	ICP-MS	ICP-MS	ICP-MS	ICP-MS	ICP-MS	ICP-MS	
Mass	139	140	141	146	147	153	157	159	163	172	166	165	169	89	175	45	
SC06-Dec	5.61E-05	5.89E-05	5.81E-05	6.16E-05	6.39E-05	9.05E-05	8.44E-05	8.75E-05	6.20E-05	6.22E-05	5.51E-05	5.20E-05	4.43E-05	4.32E-05	5.47E-03	6.92E-05	0.006
SC06-Aug-PM	8.75E-05	9.18E-05	9.36E-05	1.02E-04	9.88E-05	1.40E-04	1.42E-04	1.35E-04	1.09E-04	1.06E-04	2.95E-04	3.58E-05	9.31E-05	7.97E-05	8.44E-05	8.18E-05	0.002
SC06-Aug-AM	3.14E-05	2.04E-05	1.77E-05	1.90E-05	1.02E-05	2.80E-05	1.52E-05	1.12E-05	1.09E-05	2.38E-05	4.66E-05	5.20E-06	1.71E-05	1.23E-05	1.30E-05	4.91E-05	0.0003
SC05-Dec	5.16E-05	5.44E-05	5.22E-05	5.63E-05	5.96E-05	7.70E-05	8.27E-05	7.63E-05	5.45E-05	5.49E-05	5.80E-05	4.55E-05	2.66E-05	3.09E-05	4.79E-03	6.92E-05	0.006
SC05-Aug-PM	1.01E-04	1.04E-04	9.85E-05	1.10E-04	9.59E-05	1.36E-04	1.39E-04	1.35E-04	1.03E-04	1.14E-04	2.76E-04	3.58E-05	8.20E-05	6.97E-05	7.75E-05	6.92E-05	0.002
SC05-Aug-AM	8.75E-05	9.07E-05	9.26E-05	1.02E-04	1.00E-04	1.32E-04	1.32E-04	1.23E-04	1.05E-04	1.06E-04	2.95E-04	3.25E-05	7.76E-05	7.97E-05	7.98E-05	8.18E-05	0.002
SC04-Dec	1.46E-05	7.03E-06	3.25E-06	2.95E-06	<0.000004	9.05E-06	<0.000008	<0.000011	<0.000008	0.0000048	<0.00001	<0.000003	<0.000022	<0.00001	<0.002052	0.0000629	0.0022
SC04-Aug-PM	1.53E-05	5.44E-06	2.96E-06	2.33E-06	<0.000001	3.70E-05	2.81E-06	1.91E-06	1.50E-06	6.59E-06	7.70E-06	9.43E-07	2.66E-06	2.36E-06	4.56E-06	6.29E-05	0.0002
SC04-Aug-AM	2.92E-05	1.70E-05	1.28E-05	1.10E-05	9.01E-06	1.44E-05	1.82E-05	1.79E-05	1.54E-05	3.66E-05	5.89E-05	6.83E-06	1.69E-05	1.23E-05	1.62E-05	4.59E-05	0.0003
SC03-Dec	5.39E-06	<0.000001	1.18E-06	1.37E-06	<0.000001	<0.000003	1.99E-06	<0.000002	2.44E-06	6.59E-06	8.08E-06	<0.000001	<0.000009	2.22E-06	9.12E-06	6.29E-05	0.0001
SC03-Aug-PM	1.12E-05	3.63E-06	1.97E-06	1.42E-06	<0.000001	5.72E-06	3.64E-06	4.60E-06	3.19E-06	1.28E-05	1.14E-05	1.98E-06	3.99E-06	2.29E-06	5.24E-06	6.29E-05	0.0001
SC03-Aug-AM	8.08E-06	2.15E-06	1.38E-06	1.21E-06	7.26E-07	3.17E-06	1.99E-06	<0.000002	1.63E-06	8.42E-06	6.84E-06	<0.000001	<0.000007	1.36E-06	6.84E-06	4.78E-05	0.0001
SC02-Dec	6.73E-07	<0.000001	<0.0000002	<0.0000002	<0.000001	<0.000002	<0.000002	<0.000002	<0.000001	0.0000009	<0.000005	<0.000001	<0.000009	<0.000002	<0.000009	6.29327E-05	0.0001
SC02-Aug-PM	5.16E-07	2.04E-07	<0.0000001	<0.0000002	<0.000001	1.98E-06	<0.00000	1.12E-06	4.88E-07	7.69E-07	1.33E-06	2.80E-07	2.11E-06	4.32E-07	3.19E-06	4.47E-05	0.00006
SC02-Aug-AM	8.08E-07	2.72E-07	<0.0000001	<0.0000002	<0.000001	3.33E-06	5.79E-07	1.01E-06	6.20E-07	1.10E-06	1.52E-06	5.53E-07	2.22E-06	6.64E-07	2.96E-06	5.35E-05	0.0001
SC01-Dec	4.49E-07	<0.000001	<0.0000002	<0.0000002	<0.000001	<0.000002	<0.000002	<0.000002	<0.000001	7.69E-07	<0.000005	<0.000001	<0.000009	<0.000002	<0.000009	6.29E-05	0.0001
SC01-Aug-PM	6.51E-07	2.95E-07	<0.0000001	<0.0000002	<0.000001	2.96E-06	5.30E-07	9.76E-07	<0.0000002	9.52E-07	1.43E-06	6.18E-07	3.10E-06	6.97E-07	2.96E-06	5.16E-05	0.00007
SC01-Aug-AM	7.18E-07	2.04E-07	2.17E-07	<0.0000002	<0.0000003	<0.000002	<0.000001	<0.000002	<0.0000006	9.15E-07	<0.000002	<0.000001	<0.000007	<0.000001	<0.000007	4.28E-05	0.00007

NOTE:

1. VALUES IN mg/L WERE NORMALIZED TO THE POST ARCHEAN AVERAGE SHALE.

Table B1.7 Silver Creek Water (0.45µm filtered) Rare Earth Element normalized to Pennsylvania Anthracite-Mammoth No. 8 (Schuylkill County)

Sample	La	Ce	Pr	Nd	Sm	Eu	Gd	Tb	Dy	Y	Er	Ho	Tm	Yb	Lu	Sc	Sum REY + Sc
Analysis Method	ICP-MS	ICP-MS	ICP-MS	ICP-MS	ICP-MS	ICP-MS	ICP-MS	ICP-MS	ICP-MS	ICP-MS	ICP-MS	ICP-MS	ICP-MS	ICP-MS	ICP-MS	ICP-MS	
Mass	139	140	141	146	147	153	157	159	163	172	166	165	169	89	175	45	
SC06-Dec	1.92E-04	2.04E-04	3.03E-04	1.81E-04	2.93E-04	2.53E-04	2.62E-04	1.10E-04	2.78E-04	1.60E-04	9.67E-05	7.11E-04	8.89E-05	1.62E-04	1.07E-02	2.97E-04	0.014
SC06-Aug-PM	3.00E-04	3.18E-04	4.87E-04	3.00E-04	4.53E-04	3.91E-04	4.41E-04	1.69E-04	4.89E-04	2.72E-04	5.17E-04	4.89E-04	1.87E-04	2.99E-04	1.64E-04	3.51E-04	0.006
SC06-Aug-AM	1.08E-04	7.06E-05	9.23E-05	5.60E-05	4.67E-05	7.82E-05	4.72E-05	1.41E-05	4.89E-05	6.10E-05	8.17E-05	7.11E-05	3.42E-05	4.61E-05	2.53E-05	2.11E-04	0.0011
SC05-Dec	1.77E-04	1.88E-04	2.72E-04	1.66E-04	2.73E-04	2.15E-04	2.56E-04	9.58E-05	2.45E-04	1.41E-04	1.02E-04	6.22E-04	5.33E-05	1.16E-04	9.33E-03	2.97E-04	0.013
SC05-Aug-PM	3.46E-04	3.61E-04	5.13E-04	3.23E-04	4.40E-04	3.79E-04	4.31E-04	1.69E-04	4.64E-04	2.91E-04	4.83E-04	4.89E-04	1.64E-04	2.62E-04	1.51E-04	2.97E-04	0.006
SC05-Aug-AM	3.00E-04	3.14E-04	4.82E-04	3.00E-04	4.60E-04	3.68E-04	4.10E-04	1.55E-04	4.73E-04	2.72E-04	5.17E-04	4.44E-04	1.56E-04	2.99E-04	1.56E-04	3.51E-04	0.005
SC04-Dec	5.00E-05	2.43E-05	1.69E-05	8.68E-06	<0.00002	2.53E-05	<0.000026	<0.000014	<0.000034	0.0000122	<0.000017	<0.000044	<0.000044	<0.000037	<0.00400	0.0002703	0.0046
SC04-Aug-PM	5.23E-05	1.88E-05	1.54E-05	6.86E-06	<0.000006	1.03E-04	8.72E-06	2.39E-06	6.75E-06	1.69E-05	1.35E-05	1.29E-05	5.33E-06	8.85E-06	8.89E-06	2.70E-04	0.0006
SC04-Aug-AM	1.00E-04	5.88E-05	6.67E-05	3.23E-05	0.000041	4.02E-05	5.64E-05	2.25E-05	6.92E-05	9.39E-05	1.03E-04	9.33E-05	3.38E-05	4.61E-05	3.16E-05	1.97E-04	0.0011
SC03-Dec	1.85E-05	<0.000002	6.15E-06	4.02E-06	<0.000007	<0.000008	6.15E-06	<0.000003	1.10E-05	1.69E-05	1.42E-05	<0.000009	<0.000018	8.35E-06	1.78E-05	2.70E-04	0.0004
SC03-Aug-PM	3.85E-05	1.25E-05	1.03E-05	4.18E-06	<0.000006	1.60E-05	1.13E-05	5.77E-06	1.43E-05	3.29E-05	2.00E-05	2.71E-05	8.00E-06	8.60E-06	1.02E-05	2.70E-04	0.0005
SC03-Aug-AM	2.77E-05	7.45E-06	7.18E-06	3.55E-06	0.0000033	8.85E-06	6.15E-06	<0.000003	7.34E-06	2.16E-05	1.20E-05	<0.000018	<0.000013	5.11E-06	1.33E-05	2.05E-04	0.0004
SC02-Dec	2.31E-06	<0.000002	<0.000001	<0.0000005	<0.000007	<0.000005	<0.000005	<0.000003	<0.000006	0.0000023	<0.000008	<0.000009	<0.000018	<0.000007	<0.000018	0.00027027	0.0004
SC02-Aug-PM	1.77E-06	7.06E-07	<0.0000005	<0.0000007	<0.000006	5.52E-06	<0.000001	1.41E-06	2.19E-06	1.97E-06	2.33E-06	3.82E-06	4.22E-06	1.62E-06	6.22E-06	1.92E-04	0.00023
SC02-Aug-AM	2.77E-06	9.41E-07	<0.0000005	<0.0000007	<0.000006	9.31E-06	1.79E-06	1.27E-06	2.78E-06	2.82E-06	2.67E-06	7.56E-06	4.44E-06	2.49E-06	5.78E-06	2.30E-04	0.0003
SC01-Dec	1.54E-06	<0.000002	<0.000001	<0.0000005	<0.000007	<0.000005	<0.000005	<0.000003	<0.000006	1.97E-06	<0.000008	<0.000009	<0.000018	<0.000007	<0.000018	2.70E-04	0.0004
SC01-Aug-PM	2.23E-06	1.02E-06	<0.0000005	<0.0000007	<0.000006	8.28E-06	1.64E-06	1.23E-06	<0.0000008	2.44E-06	2.50E-06	8.44E-06	6.22E-06	2.62E-06	5.78E-06	2.22E-04	0.00027
SC01-Aug-AM	2.46E-06	7.06E-07	1.13E-06	<0.0000007	<0.0000013	<0.000004	<0.000002	<0.000003	<0.0000025	2.35E-06	<0.000003	<0.000018	<0.000013	<0.000005	<0.000013	1.84E-04	0.00026

NOTE:

1. VALUES IN mg/L WERE NORMALIZED TO THE PENNSYLVANIA ANTHRACITE-MAMMOTH NO. 8 (SCHUYLKILL COUNTY).

LIZ ASHBY-THESIS
TABLE Table B1.8

Table B1.8 Diurnal Variation of Silver Creek water samples (0.45 μm)

Sample	SC06-Aug-PM	SC06-Aug-AM	Variation (ug/L)	Average (ug/L)	% change
La	**3.9**	1.4	2.5	2.65	94%
Ce	**8.10**	1.8	6.3	4.95	127%
Pr	**0.95**	0.18	0.77	0.565	136%
Nd	**3.8**	0.71	3.09	2.255	137%
Sm	**0.68**	0.07	0.61	0.375	163%
Eu	**0.17**	0.034	0.136	0.102	133%
Gd	**0.86**	0.092	0.768	0.476	161%
Tb	**0.12**	0.01	0.11	0.065	169%
Dy	**0.58**	0.058	0.522	0.319	164%
Er	**0.31**	0.049	0.261	0.1795	145%
Ho	**0.11**	0.016	0.094	0.063	149%
Tm	**0.042**	0.0077	0.0343	0.02485	138%
Yb	**0.24**	0.037	0.203	0.1385	147%
Lu	**0.037**	0.0057	0.0313	0.02135	147%
Y	**2.9**	0.65	2.25	1.775	127%

Sample	SC05-Aug-PM	SC05-Aug-AM	Variation (ug/L)	Average (ug/L)	% change
La	**4.5**	3.9	0.6	4.2	14%
Ce	**9.2**	8	1.2	8.6	14%
Pr	**1**	0.94	0.06	0.97	6%
Nd	**4.1**	3.8	0.3	3.95	8%
Sm	0.66	**0.69**	0.03	0.675	4%
Eu	**0.165**	0.16	0.005	0.1625	3%
Gd	**0.84**	0.8	0.04	0.82	5%
Tb	**0.12**	0.11	0.01	0.115	9%
Dy	0.55	**0.56**	0.01	0.555	2%
Er	0.29	**0.31**	0.02	0.3	7%
Ho	**0.11**	0.1	0.01	0.105	10%
Tm	**0.037**	0.035	0.002	0.036	6%
Yb	0.21	**0.24**	0.03	0.225	13%
Lu	0.034	**0.035**	0.001	0.0345	3%
Y	**3.1**	2.9	0.2	3	7%

Sample	SC04-Aug-PM	SC04-Aug-AM	Variation (ug/L)	Average (ug/L)	% change
La	0.68	**1.3**	0.62	0.99	63%
Ce	0.48	**1.5**	1.02	0.99	103%
Pr	0.03	**0.13**	0.1	0.08	125%
Nd	0.087	**0.41**	0.323	0.2485	130%
Sm	0.009	**0.062**	0.053	0.0355	149%
Eu	**0.045**	0.0175	0.0275	0.03125	88%
Gd	0.017	**0.11**	0.093	0.0635	146%
Tb	0.0017	**0.016**	0.0143	0.00885	162%
Dy	0.008	**0.082**	0.074	0.045	164%
Er	0.0081	**0.062**	0.0539	0.03505	154%
Ho	0.0029	**0.021**	0.0181	0.01195	151%
Tm	0.0012	**0.0076**	0.0064	0.0044	145%
Yb	0.0071	**0.037**	0.0299	0.02205	136%
Lu	0.002	**0.0071**	0.0051	0.00455	112%
Y	0.18	**1**	0.82	0.59	139%

Sample	SC03-Aug-PM	SC03-Aug-AM	Variation (ug/L)	Average (ug/L)	% change
La	**0.5**	0.36	0.14	0.43	33%
Ce	**0.32**	0.19	0.13	0.255	51%
Pr	**0.02**	0.014	0.006	0.017	35%
Nd	<0.053	0.045	0.008	0.049	16%
Sm	**0.009**	0.005	0.004	0.007	57%
Eu	**0.0070**	0.0039	0.0031	0.0054	57%
Gd	**0.0220**	0.0120	0.01	0.017	59%
Tb	**0.0041**	0.002	0.0021	0.00305	69%
Dy	**0.017**	0.0087	0.0083	0.01285	65%
Er	**0.012**	0.0072	0.0048	0.0096	50%
Ho	**0.0061**	0.004	0.0021	0.00505	42%
Tm	0.0018	**0.003**	0.0012	0.0024	50%
Yb	**0.0069**	0.0041	0.0028	0.0055	51%
Lu	0.0023	**0.003**	0.0007	0.00265	26%
Y	**0.35**	0.23	0.12	0.29	41%

Sample	SC02-Aug-PM	SC02-Aug-AM	Variation (ug/L)	Average (ug/L)	% change
La	0.023	**0.036**	0.013	0.0295	44%
Ce	0.018	**0.024**	0.006	0.021	29%
Pr	0.001	0.001	0	0.001	0%
Nd	<0.009	0.009	NA	0.009	NA
Sm	0.009	0.009	0	0.009	0%
Eu	0.0024	**0.0041**	0.00165	0.003225	51%
Gd	0.002	<0.0035	0.0015	0.00275	55%
Tb	**0.001**	0.0009	0.0001	0.00095	11%
Dy	0.0026	**0.0033**	0.0007	0.00295	24%
Er	0.0014	<0.0016	NA	0.0015	NA
Ho	0.00086	<0.0017	NA	0.00128	NA
Tm	0.00095	**0.0010**	0.00005	0.000975	5%
Yb	0.0013	<0.002	NA	0.00165	NA
Lu	**0.0014**	0.0013	0.0001	0.00135	7%
Y	0.021	**0.03**	0.009	0.0255	35%

Sample	SC01-Aug-PM	SC01-Aug-AM	Variation (ug/L)	Average (ug/L)	% change
La	0.029	**0.032**	0.003	0.0305	10%
Ce	<0.026	<0.018	NA	0.022	NA
Pr	<0.001	<0.0022	NA	0.0016	NA
Nd	<0.009	<0.009	NA	0.009	NA
Sm	**0.009**	0.002	0.007	0.0055	127%
Eu	<0.0036	**0.0019**	NA	0.00275	NA
Gd	0.0032	**0.004**	0.0008	0.0036	22%
Tb	0.0009	0.0020	0.0011	0.001435	79%
Dy	0.001	**0.003**	0.002	0.002	100%
Er	0.0015	**0.002**	0.0005	0.00175	29%
Ho	0.0019	**0.004**	0.0021	0.00295	71%
Tm	0.0014	**0.003**	0.0016	0.0022	73%
Yb	0.0021	**0.004**	0.0019	0.00305	62%
Lu	0.0013	**0.003**	0.0017	0.00215	79%
Y	0.026	**0.025**	0.001	0.0255	4%

NOTES;

1. AUG-AM SAMPLES WERE COLLECTED BETWEEN 7:30AM AND 8:30AM; AUG-PM SAMPLES WERE COLLECTED BETWEEN 16:30-18:20.

Table B1.5 Complete Results of Diurnal Investigations at Silver Creek

LIZ ASHBY-THESIS
TABLE Table B1.9

Table B1.9 Solid Standards Used for lab analyses

Sample Labels	Tort-2 Standard	Tort-2 AR	Detection limit	% diff	Tort-2 Nitric	Detection limit	% diff
Al		160.1	35.7		54.1	2.0	
As	18.0	19.6	44.1	8%	15.9	2.4	12%
B		34.6	5.2		377.1	0.3	
Ba		25.6	6.6		1.8	0.4	
Cd	3700.0	3280.8	73.6	12%	3515.9	4.1	5%
Ce	25.0	24.5	5.9	2%	19.1	0.3	27%
Co		DL	9.6		DL	0.5	
Cr	0.8	1.6	6.7	NA	0.6	0.4	23%
Cu	95.0	94.0	5.6	1%	86.0	0.3	10%
Fe	92.0	104.3	15.2	13%	67.6	0.8	31%
K		8032.6	121.9		7146.7	6.7	
Mg	1000.0	1041.4	3.9	4%	928.2	0.2	7%
Mn	13.0	11.5	1.7	12%	9.9	0.1	
Mo		DL	15.5		DL	0.9	
Na		10662.4	33.3		10213.3	1.8	
Ni	2.1	5.4	12.5	N/A	0.7	0.7	N/A
P		10704.3	290.0		9534.3	16.0	
Pb		16.0	67.3		DL	3.7	
S		9166.9	198.6		8208.1	11.0	
Sc		DL	6.0		DL	0.3	
Si		162.8	83.1		997.9	4.6	
Sr	42.0	37.1	6.9	12%	42.2	0.4	0%
Ti		5.8	5.5		1.3	0.3	
V		DL	12.3		1.1	0.7	
Zn	170.0	163.4	6.7	4%	127.3	0.4	29%

NOTES:
1. TORT-2 WAS PROVIDED BY THE QUEENS UNIVERSITY - ANALYTICAL SERVICES UNIT

Parameter	REE-1 Standard	REE-1 - AR	RPD
Al	35,900.00	2,651	172%
As	124.00	77	47%
B		128	
Ba	100.10	111	11%
Cd		9	
Ce	3,960.00	3,532	11%
Co	1.58	1	62%
Cr	277.00	202	31%
Cu	79.70	50	46%
Dy	847.00	791	7%
Er	701.00	597	16%
Eu	23.50	24	1%
Eu	23.50	24	1%
Gd	433.00	460	6%
Ho	208.00	190	9%
La	1,661.00	1,456	13%
Nd	1,456.00	1,455	0%
Ni	24.70	16	41%
Pb	1,137.00	906	23%
Pr	435.00	408	6%
Sm	381.00	397	4%
Sr	129.00	87	39%
Tb	106.20	108	1%
Th	719.00	757	5%
Tm	106.00	91	15%
U	137.00	129	6%
V		9	
Yb	678.00	555	20%

NOTES:
1. STANDARD VALUES ARE FROM NRCAN REE-1 CERTIFICATE OF ANALYSIS.

LIZ ASHBY-THESIS
TABLE Table B1.10

Table B1.10 Normative Oxides

Sample	LOI (%)	%TC	%OC	Fe2O3	Al2O3	MnO2	CaO	K2O	MgO	Na2O	P2O5	SO2	SiO2	LOIH2O	LOICO2	TOTAL (LOI)	TOTAL (%OC)	TOTAL (LOI)
SC01-Aug-PM	18%	1%	0%	61.48	1.04	6.80	2.38	0.04	0.28	0.01	0.14	0.14	0.13	0.94	0.38	74.71	73.76	96.01
SC02-Aug-PM	16.3%	1%	0%	54.33	2.65	9.65	0.59	0.03	0.15	0.02	0.17	0.40	0.16	0.94	0.38	70.19	69.07	89.44
SC03-Aug-PM	13.7%	1%	0%	65.77	1.89	1.35	0.22	0.04	0.06	0.04	0.27	0.44	0.26	0.94	0.38	72.01	70.89	88.00
SC04-Aug-PM	15.7%	11%	11%	20.02	10.20	0.03	0.20	0.88	0.35	0.12	0.25	0.96	0.24	10.20	4.18	47.86	47.34	53.20
SC05-Aug-PM	11.9%	1%	1%	41.46	6.05	0.04	0.31	0.36	0.16	0.06	0.34	1.04	0.32	0.94	0.38	51.66	51.89	65.31
SC05-field dup-Aug-PM	11.9%	1%	1%	34.31	6.99	0.04	0.27	0.59	0.27	0.08	0.32	0.94	0.30	0.94	0.38	45.62	45.81	59.27
SC06-Aug-PM	12.6%	8%	1%	13.30	8.69	0.03	0.20	0.82	0.36	0.11	0.60	0.68	0.56	6.72	2.76	35.02	41.40	41.40
SC06-lab dup-Aug-PM	13.0%	8%	1%	10.58	0.36	0.03	0.90	0.09	0.05	0.34	0.41	0.50	0.39	6.72	2.76	23.34	29.74	30.24
SC01-Dec	17%	4%	2%	45.75	0.13	7.91	0.02	0.02	7.46	0.32	0.92	0.00	0.01	3.51	1.44	63.26	63.26	63.26
SC02-Dec	15%	3%	1%	52.90	0.07	3.64	0.01	0.02	3.65	0.39	0.82	0.00	0.01	2.45	1.00	61.94	61.94	61.94
SC03-Dec	12%	1%	0%	64.34	0.04	1.74	0.01	0.02	1.99	0.46	0.85	0.00	0.01	0.97	0.40	69.80	69.80	69.80
SC04-Dec	15%	1%	0%	58.62	0.17	0.14	0.02	0.02	0.17	0.74	0.82	0.00	0.02	1.25	0.51	60.97	60.97	60.97
SC05-Dec	11%	1%	1%	64.34	0.23	0.02	0.01	0.03	0.03	1.15	0.87	0.00	0.02	0.59	0.24	66.95	66.95	66.95
SC06-Dec	13%	5%	3%	41.46	0.32	0.02	0.04	0.03	0.03	0.94	1.26	0.00	0.02	4.42	1.81	44.40	44.40	44.40

Notes:
1. ALL UNITS IN %.
2. ORIGINAL DATA CALUCATED IN COMPILED DATA FILE.

Table B1.11 Model 1 WHAM inputs

Description	SPM	Temp.	pCO2	pH	Part. Humic Acid	Part. Fulvic Acid	Part. Iron Oxide	Part. Manganese Oxide	Part. Aluminum Oxide	Colloidal Fulvic Acid	Al	K	Ca	Sc	Mn	Fe(II)	Fe(III)	Co	Ni	Cu	Zn	Y	La	Ce	Pr	Nd	Sm	Eu	Gd	Tb	Dy	Ho	Er	Tm	Yb	Lu	Pb	Th	Cl	NO3	SO4
	mg/l	deg C	atm		mg/l	mg/l	mg/l	mg/l	mg/l	mg/l	mg/l	mg/l	mg/l	mg/l	mg/l	mg/l	mg/l	mg/l	mg/l	mg/l	mg/l	mg/l	mg/l	mg/l	mg/l	mg/l	mg/l	mg/l	mg/l	mg/l	mg/l	mg/l	mg/l	mg/l	mg/l	mg/l	mg/l	mg/l	mg/l	mg/l
SC01-Aug-PM	0.00E+00	2.90E+01	5.00E-04	7.56E+00	0.00E+00	0.00E+00	4.30E+05	4.30E+04	5.50E+03	1.15E+00	6.20E-03	7.20E-01	4.40E+01	8.20E-04	2.00E+00	2.16E-01	0.05	2.30E-02	4.60E-02	4.90E-04	5.00E-02	2.60E-05	2.90E-05	2.60E-05	1.00E-06	9.00E-06	9.00E-06	3.60E-06	3.20E-06	8.70E-07	1.00E-06	1.90E-06	1.50E-06	0.00	2.10E-06	1.30E-06	8.10E-06	2.40E-05	4.00E+00	8.00E-01	2.07E+02
SC02-Aug-PM	0.00E+00	2.56E+01	1.70E-03	7.18E+00	0.00E+00	0.00E+00	3.80E+05	6.10E+04	1.40E+04	1.15E+00	1.00E-03	6.80E-01	4.10E+01	7.10E-04	1.30E+00	2.24E-01	0.06	1.30E-02	3.10E-02	1.00E-04	3.60E-02	2.10E-05	2.30E-05	1.80E-05	1.00E-06	9.00E-06	9.00E-06	2.40E-06	2.00E-06	1.00E-06	2.60E-06	8.60E-07	1.40E-06	0.00	1.30E-06	1.40E-06	2.00E-06	1.20E-05	4.00E+00	7.00E-01	2.19E+02
SC03-Aug-PM	0.00E+00	2.52E+01	5.70E-03	6.47E+00	0.00E+00	0.00E+00	4.60E+05	8.50E+03	1.00E+04	8.50E-01	1.30E-03	8.80E-01	4.40E+01	1.00E-03	3.00E+00	6.32E-01	0.158	5.30E-02	6.70E-02	1.00E-04	1.00E-01	3.50E-04	5.00E-04	3.20E-04	2.00E-05	5.30E-05	9.00E-06	6.95E-06	2.20E-05	4.10E-06	1.70E-05	6.10E-06	1.20E-05	1.8E-06	6.90E-06	2.30E-06	2.00E-06	3.70E-05	4.00E+00	1.00E+00	2.13E+02
SC04-Aug-PM	0.00E+00	1.79E+01	3.54E-02	5.81E+00	0.00E+00	0.00E+00	1.40E+05	2.20E+02	5.40E+04	9.00E-01	1.00E-01	5.70E-01	4.20E+01	1.00E-03	3.00E+00	9.60E+00	2.4	5.40E-02	6.70E-02	1.00E-04	2.80E-01	1.80E-04	6.80E-04	4.80E-04	3.00E-05	8.70E-05	9.00E-06	4.50E-05	1.70E-05	1.70E-06	8.00E-06	2.90E-06	8.10E-06	1.2E-06	7.10E-06	2.00E-06	4.60E-06	7.90E-05	4.00E+00	8.00E-01	2.13E+02
SC05-Aug-PM	0.00E+00	1.39E+01	4.75E-02	6.02E+00	0.00E+00	0.00E+00	2.40E+05	2.80E+02	3.20E+04	9.00E-01	1.80E-02	8.60E-01	4.00E+01	1.10E-03	2.60E+00	1.52E+01	3.8	5.90E-02	7.50E-02	1.00E-04	1.70E-01	3.10E-03	4.50E-03	9.20E-03	1.00E-03	4.10E-03	6.60E-04	1.65E-04	8.40E-04	1.20E-04	5.50E-04	1.10E-04	2.90E-04	0.000037	2.10E-04	3.40E-05	1.30E-05	4.20E-04	4.00E+00	2.50E+00	2.25E+02
SC06-Aug-PM	0.00E+00	1.21E+01	5.10E-02	6.03E+00	0.00E+00	0.00E+00	9.30E+04	2.10E+02	4.60E+04	1.15E+00	1.70E-01	8.20E-01	4.00E+01	1.30E-03	2.90E+00	1.60E+01	4.00	6.40E-02	8.20E-02	4.80E-04	1.30E-01	2.90E-03	3.90E-03	8.10E-03	9.50E-04	3.80E-03	6.80E-04	1.70E-04	8.60E-04	1.20E-04	5.80E-04	1.10E-04	3.10E-04	0.00	2.40E-04	3.70E-05	6.40E-05	2.40E-04	4.00E+00	3.80E+00	2.04E+02
SC02-Aug-AM	0.00E+00	2.11E+01	5.60E-03	6.67E+00	0.00E+00	0.00E+00	3.70E+05	5.30E+04	1.20E+04	9.00E-01	7.60E-04	7.80E-01	4.70E+01	8.50E-04	1.60E+00	2.32E-01	0.058	1.90E-02	4.70E-02	1.00E-04	5.20E-02	3.00E-05	3.60E-05	2.40E-05	1.00E-06	9.00E-06	9.00E-06	4.05E-06	3.50E-06	9.00E-07	3.30E-06	1.70E-06	1.60E-06	0.000001	2.00E-06	1.30E-06	9.10E-06	1.00E-04	4.00E+00	9.00E-01	2.07E+02
SC05-Aug-AM	0.00E+00	1.21E+01	4.05E-02	5.97E+00	0.00E+00	0.00E+00	1.90E+05	1.30E+02	5.00E+04	4.00E-01	1.40E-01	9.60E-01	4.40E+01	1.30E-03	2.90E+00	1.68E+01	4.2	6.60E-02	8.30E-02	1.00E-04	1.20E-01	2.90E-03	3.90E-03	8.00E-03	9.40E-04	3.80E-03	6.90E-04	1.60E-04	8.00E-04	1.10E-04	5.60E-04	1.00E-04	3.10E-04	0.000035	2.40E-04	3.50E-05	3.60E-05	1.30E-04	4.00E+00	2.30E+00	2.16E+02
SC01-Dec	0.00E+00	8.46E+00	4.30E-03	6.76E+00	0.00E+00	0.00E+00	3.20E+05	5.00E+04	1.20E+04	5.00E-01	8.00E-04	4.70E-01	4.30E+01	8.00E-04	2.10E+00	9.60E-01	0.24	3.80E-02	6.20E-02	2.90E-04	7.80E-02	2.10E-05	2.00E-05	5.00E-05	2.00E-06	6.00E-06	1.00E-05	2.00E-06	1.00E-05	2.00E-06	7.00E-06	2.00E-06	5.00E-06	0.000004	6.00E-06	4.00E-06	2.10E-04	1.00E-04	4.00E+00	1.60E+00	1.89E+02
SC02-Dec	0.00E+00	8.73E+00	6.20E-03	6.65E+00	0.00E+00	0.00E+00	3.70E+05	2.30E+04	1.20E+04	4.40E-01	8.00E-04	2.70E-01	4.30E+01	8.00E-04	2.00E+00	1.60E+00	0.4	3.70E-02	5.80E-02	5.60E-04	6.60E-02	2.40E-05	3.00E-05	5.00E-05	2.00E-06	6.00E-06	1.00E-05	2.00E-06	1.00E-05	2.00E-06	7.00E-06	2.00E-06	5.00E-06	0.000004	6.00E-06	4.00E-06	2.00E-05	1.00E-04	4.00E+00	1.70E+00	1.89E+02
SC03-Dec	0.00E+00	8.81E+00	1.10E-02	6.44E+00	0.00E+00	0.00E+00	4.50E+05	1.10E+04	1.30E+04	5.00E-01	8.00E-04	2.00E-01	4.30E+01	8.20E-04	2.10E+00	4.00E+00	1	4.20E-02	6.20E-02	5.00E-04	7.90E-02	1.80E-04	2.40E-04	5.00E-05	1.20E-05	5.10E-05	1.00E-05	3.40E-06	1.20E-05	2.00E-06	1.30E-05	2.00E-06	8.50E-06	0.000004	6.70E-06	4.00E-06	2.70E-05	1.00E-04	4.00E+00	2.70E+00	1.86E+02
SC04-Dec	0.00E+00	1.03E+01	2.63E-02	6.15E+00	0.00E+00	0.00E+00	4.10E+05	9.10E+02	2.30E+04	7.90E-01	8.00E-04	2.30E-01	4.30E+01	1.00E-03	2.20E+00	7.44E+00	1.86	4.30E-02	6.20E-02	8.40E-04	8.00E-02	1.30E-04	6.50E-04	6.20E-04	3.30E-05	1.10E-04	3.00E-05	1.10E-05	5.00E-05	1.00E-05	4.00E-05	1.00E-05	1.00E-05	0.00001	3.00E-05	9.00E-04	2.00E-05	1.00E-04	4.00E+00	3.70E+00	1.89E+02
SC05-Dec	0.00E+00	1.20E+01	7.34E-02	5.84E+00	0.00E+00	0.00E+00	4.50E+05	1.10E+02	2.70E+04	1.45E+00	1.00E-01	1.00E-01	4.10E+01	1.10E-03	2.30E+00	1.36E+01	3.4	4.20E-02	6.00E-02	1.00E-04	7.90E-02	1.50E-03	2.30E-03	4.80E-03	5.30E-04	2.10E-03	4.10E-04	9.35E-05	5.00E-04	6.80E-05	2.90E-04	1.40E-04	6.10E-05	0.000012	9.30E-05	2.10E-03	2.00E-05	1.00E-04	4.00E+00	3.50E+00	1.80E+02
SC06-Dec	0.00E+00	1.19E+01	7.75E-02	5.86E+00	0.00E+00	0.00E+00	2.90E+05	1.40E+02	3.20E+04	2.08E+00	1.20E-01	1.00E-01	4.10E+01	1.10E-03	2.20E+00	1.36E+01	3.4	4.20E-02	6.10E-02	1.00E-04	8.50E-02	1.70E-03	2.50E-03	5.20E-03	5.90E-04	2.30E-03	4.40E-04	1.10E-04	5.10E-04	7.80E-05	3.30E-04	1.60E-04	5.80E-05	0.00002	1.30E-04	2.40E-03	2.00E-05	1.00E-04	4.00E+00	4.60E+00	1.80E+02

Table B1.12 Model 2 WHAM Inputs

Description	SPM	Temp.	pCO2	pH	Part. Humic Acid	Part. Fulvic Acid	Part. Iron Oxide	Part. Manganese Oxide	Part. Aluminum Oxide	Colloidal Fulvic Acid	Al	K	Ca	Sc	Mn	Fe(II)	Fe(III)	Co	Ni	Cu	Zn	Y	La	Ce	Pr	Nd	Sm	Eu	Gd	Tb	Dy	Ho	Er	Tm	Yb	Lu	Pb	Th	Cl	NO3	SO4
	mg/l	deg C	atm		mg/l	mg/l	mg/l	mg/l	mg/l	mg/l	mg/l	mg/l	mg/l	mg/l	mg/l	mg/l	mg/l	mg/l	mg/l	mg/l	mg/l	mg/l	mg/l	mg/l	mg/l	mg/l	mg/l	mg/l	mg/l	mg/l	mg/l	mg/l	mg/l	mg/l	mg/l	mg/l	mg/l	mg/l	mg/l	mg/l	mg/l
SC01-Aug-PM	0.00E+00	28.97	0.0005	7.56	0.07	0.07	430,000	43,000	5,500	1.15	0.0062	0.72	44	8.20E-04	2	0.216	0.054	0.023	0.046	4.90E-04	0.05	2.60E-05	2.90E-05	2.60E-05	1.00E-06	9.00E-06	9.00E-06	3.60E-06	3.20E-06	8.70E-07	1.00E-06	1.90E-06	1.50E-06	0.00	2.10E-06	1.30E-06	8.10E-06	2.40E-05	4.00E+00	8.00E-01	2.07E+02
SC02-Aug-PM	0.00E+00	25.55	0.0017	7.18	0.04	0.04	380,000	61,000	14,000	1.15	0.001	0.68	41	7.10E-04	1.3	0.224	0.056	0.013	0.031	1.00E-04	0.036	2.10E-05	2.30E-05	1.80E-05	1.00E-06	9.00E-06	9.00E-06	2.40E-06	2.00E-06	1.00E-06	2.60E-06	8.60E-07	1.40E-06	0.00	1.30E-06	1.40E-06	2.00E-06	1.20E-05	4.00E+00	7.00E-01	2.19E+02
SC03-Aug-PM	0.00E+00	25.23	0.0057	6.47	0.04	0.04	460,000	8,500	10,000	0.85	0.0013	0.88	44	1.00E-03	3	0.632	0.158	0.053	0.067	1.00E-04	0.1	3.50E-04	5.00E-04	3.20E-04	2.00E-05	5.30E-05	9.00E-06	6.95E-06	2.20E-05	4.10E-06	1.70E-05	6.10E-06	1.20E-05	1.80E-06	6.90E-06	2.30E-06	2.00E-06	3.70E-05	4.00E+00	1.00E+00	2.13E+02
SC04-Aug-PM	0.00E+00	17.93	0.0354	5.81	2.85	2.85	140,000	220	54,000	0.9	0.1	0.57	42	1.00E-03	3	9.6	2.4	0.054	0.067	1.00E-04	0.28	1.80E-04	6.80E-04	4.80E-04	3.00E-05	8.70E-05	9.00E-06	4.50E-05	1.70E-05	1.70E-06	8.00E-06	2.90E-06	8.10E-06	1.20E-06	7.10E-06	2.00E-06	4.60E-06	7.90E-05	4.00E+00	8.00E-01	2.13E+02
SC05-Aug-PM	0.00E+00	13.91	0.0475	6.02	0.31	0.31	240,000	280	32,000	0.9	0.018	0.86	40	1.10E-03	2.6	15.2	3.8	0.059	0.075	1.00E-04	0.17	3.10E-03	4.50E-03	9.20E-03	1.00E-03	4.10E-03	6.60E-04	1.65E-04	8.40E-04	1.20E-04	5.50E-04	1.10E-04	2.90E-04	3.70E-05	2.10E-04	3.40E-05	1.30E-05	4.20E-04	4.00E+00	2.50E+00	2.25E+02
SC06-Aug-PM	0.00E+00	12.12	0.051	6.03	2.61	2.61	93,000	210	46,000	1.15	0.17	0.82	40	1.30E-03	2.9	16	4	0.064	0.082	4.80E-04	0.13	2.90E-03	3.90E-03	8.10E-03	9.50E-04	3.80E-03	6.80E-04	1.70E-04	8.60E-04	1.20E-04	5.80E-04	1.10E-04	3.10E-04	0.00	2.40E-04	3.70E-05	6.40E-05	2.40E-04	4.00E+00	3.80E+00	2.04E+02
SC02-Aug-AM	0.00E+00	21.08	0.0056	6.67	0.04	0.04	370,000	53,000	12,000	0.9	0.00076	0.78	47	8.50E-04	1.6	0.232	0.058	0.019	0.047	1.00E-04	0.052	3.00E-05	3.60E-05	2.40E-05	1.00E-06	9.00E-06	9.00E-06	4.05E-06	3.50E-06	9.00E-07	3.30E-06	1.70E-06	1.60E-06	1.00E-06	2.00E-06	1.30E-06	9.10E-06	1.00E-04	4.00E+00	9.00E-01	2.07E+02
SC05-Aug-AM	0.00E+00	12.1	0.0405	5.97	0.02	0.02	190,000	130	50,000	0.4	0.14	0.96	44	1.30E-03	2.9	16.8	4.2	0.066	0.083	1.00E-04	0.12	2.90E-03	3.90E-03	8.00E-03	9.40E-04	3.80E-03	6.90E-04	1.60E-04	8.00E-04	1.10E-04	5.60E-04	1.00E-04	3.10E-04	3.50E-05	2.40E-04	3.50E-05	3.60E-05	1.30E-04	4.00E+00	2.30E+00	2.16E+02
SC01-Dec	0.00E+00	8.46	0.0043	6.76	0.53	0.53	320,000	50,000	12,000	0.5	0.0008	0.47	43	8.00E-04	2.1	0.96	0.24	0.038	0.062	2.90E-04	0.078	2.10E-05	2.00E-05	5.00E-05	2.00E-06	6.00E-06	1.00E-05	2.00E-06	1.00E-05	2.00E-06	7.00E-06	2.00E-06	5.00E-06	4.00E-06	6.00E-06	4.00E-06	2.10E-04	1.00E-04	4.00E+00	1.60E+00	1.89E+02
SC02-Dec	0.00E+00	8.73	0.0062	6.65	0.19	0.19	370,000	23,000	12,000	0.44	0.0008	0.27	43	8.00E-04	2	1.6	0.4	0.037	0.058	5.60E-04	0.066	2.40E-05	3.00E-05	5.00E-05	2.00E-06	6.00E-06	1.00E-05	2.00E-06	1.00E-05	2.00E-06	7.00E-06	2.00E-06	5.00E-06	4.00E-06	6.00E-06	4.00E-06	2.00E-05	1.00E-04	4.00E+00	1.70E+00	1.89E+02
SC03-Dec	0.00E+00	8.81	0.011	6.44	0.1	0.1	450,000	11,000	13,000	0.5	0.0008	0.2	43	8.20E-04	2.1	4	1	0.042	0.062	5.00E-04	0.079	1.80E-04	2.40E-04	5.00E-05	1.20E-05	5.10E-05	1.00E-05	3.40E-06	1.20E-05	2.00E-06	1.30E-05	2.00E-05	8.50E-06	4.00E-06	6.70E-06	4.00E-06	2.70E-05	1.00E-04	4	2.7	186
SC04-Dec	0.00E+00	10.28	0.0263	6.15	0.1	0.1	410,000	910	23,000	0.79	0.0008	0.23	43	1.00E-03	2.2	7.44	1.86	0.043	0.062	8.40E-04	0.08	1.30E-04	6.50E-04	6.20E-04	3.30E-05	1.10E-04	3.00E-05	1.10E-05	5.00E-05	1.00E-05	4.00E-05	1.00E-05	1.00E-05	1.00E-05	3.00E-05	9.00E-04	2.00E-05	1.00E-04	4	3.7	189
SC05-Dec	0.00E+00	11.98	0.0734	5.84	0.17	0.17	450,000	110	27,000	1.45	0.1	0.1	41	1.10E-03	2.3	13.6	3.4	0.042	0.06	1.00E-04	0.079	1.50E-03	2.30E-03	4.80E-03	5.30E-04	2.10E-03	4.10E-04	9.35E-05	5.00E-04	6.80E-05	2.90E-04	1.40E-04	6.10E-05	1.20E-05	9.30E-05	2.10E-03	2.00E-05	1.00E-04	4	3.5	180
SC06-Dec	0.00E+00	11.89	0.0775	5.86	0.67	0.67	290,000	140	32,000	2.08	0.12	0.1	41	1.10E-03	2.2	13.6	3.4	0.042	0.061	1.00E-04	0.085	1.70E-03	2.50E-03	5.20E-03	5.90E-04	2.30E-03	4.40E-04	1.10E-04	5.10E-04	7.80E-05	3.30E-04	1.60E-04	5.80E-05	2.00E-05	1.30E-04	2.40E-03	2.00E-05	1.00E-04	4	4.6	180

LIZ ASHBY-THESIS

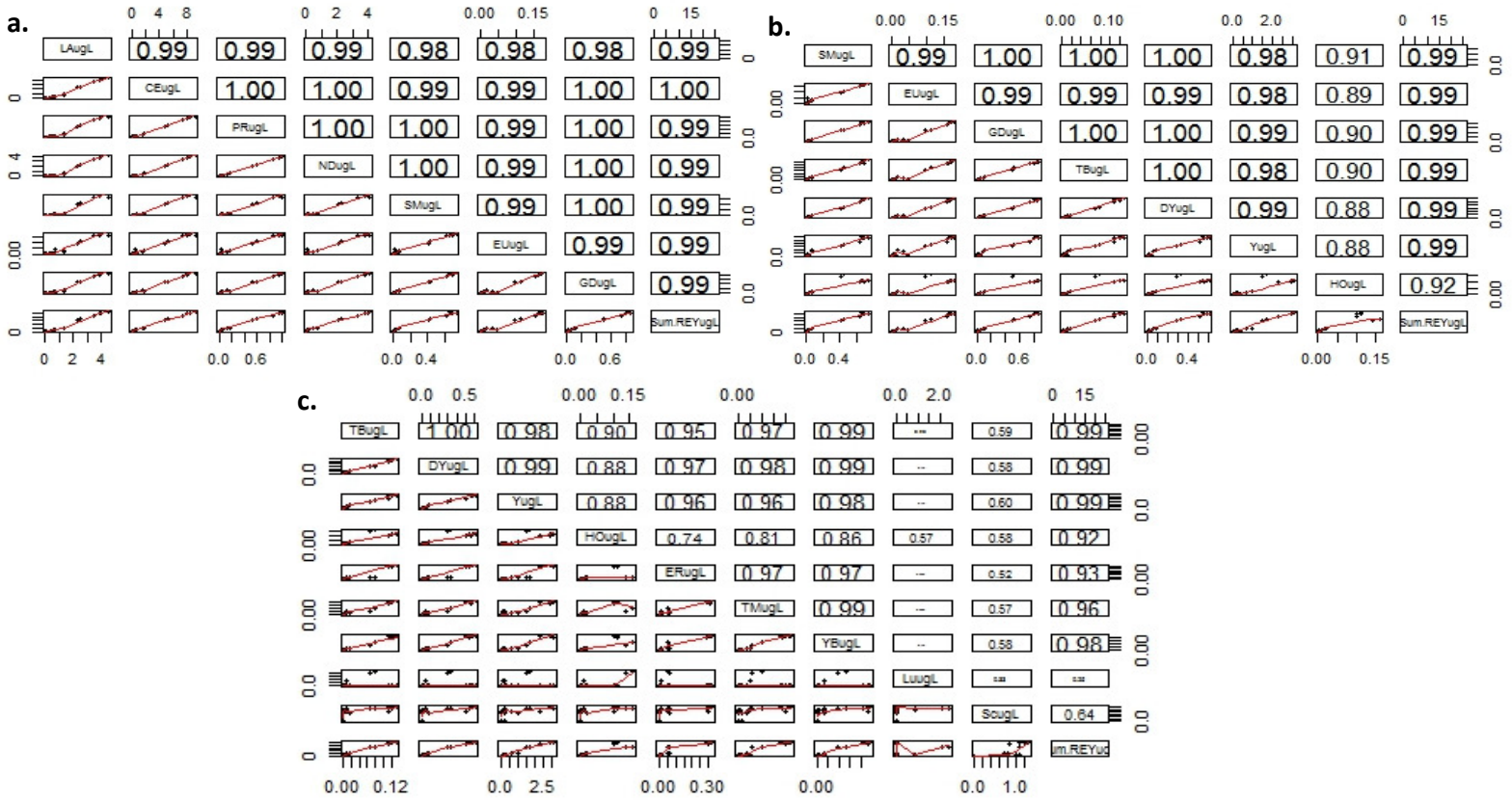

Figure B1.1 Scatterplots and Correlation Matrices for 0.45um filtered water: (a) LREYS; (b) MREYs; (c) HREYs

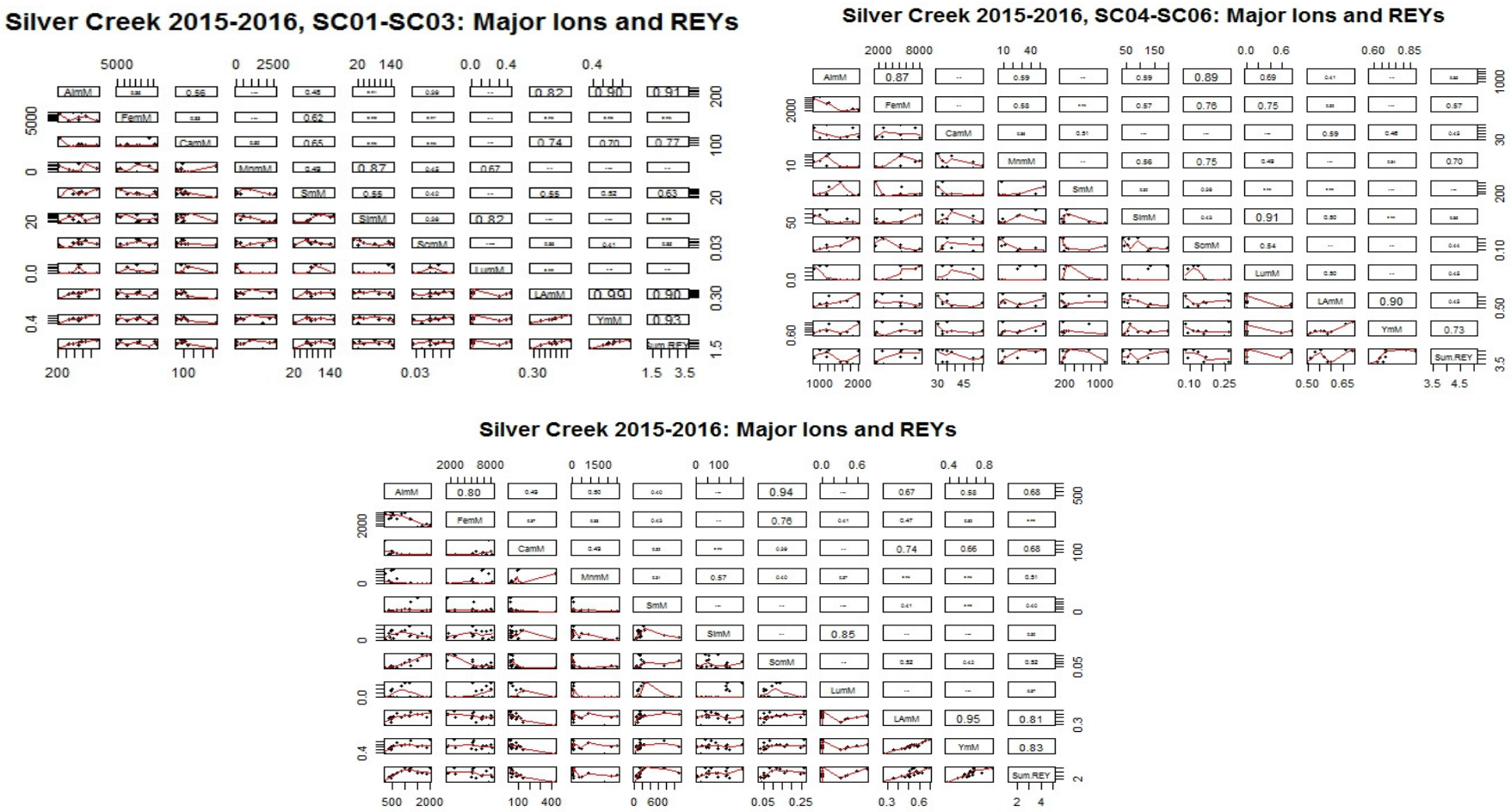

Figure B1.2 Scatterplots and Correlation Matrices for Major Ions and REYs (a) SC01, SC02, SC03; (b) SC04, SC05, SC06 and (c) all Silver Creek sites.

LIZ ASHBY-THESIS
TABLE Figure B2.3

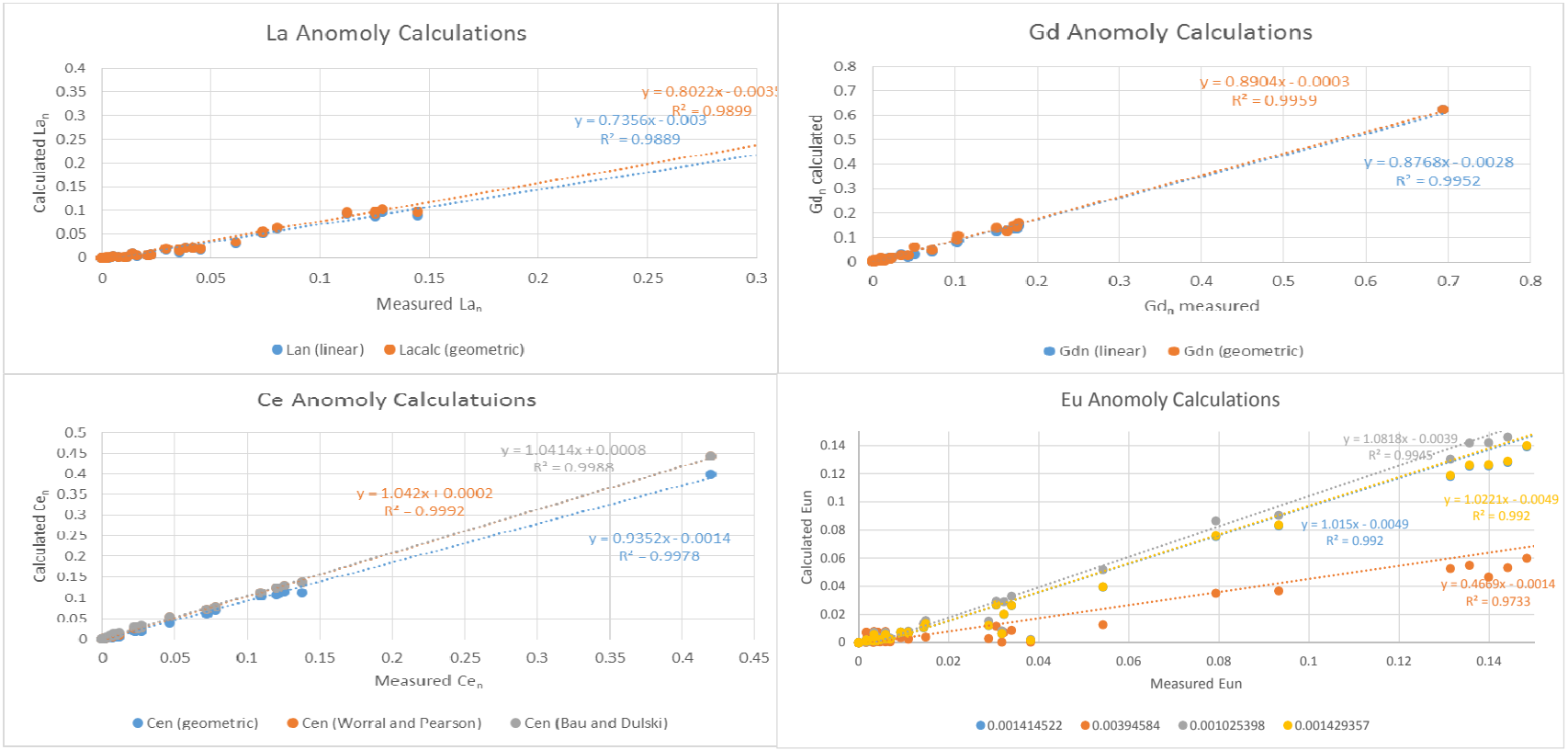

NOTES:
1. EQUATIONS FOR ANOMOLY CALCUATIONS ARE PROVIDED IN TABLE 4 IN THE TEXT.

Figure B1.3 Anomaly Calculation Verification - 0.45um Filtered Water

APPENDIX C

REY TOXICITY, BIOACCUMULATION AND LINKAGES TO MICROBIAL COMMUNITY COMPOSITION

LIZ ASHBY-THESIS
TABLE Appendix C.1

```
System information
==================
       Platform:     linux2
  Python version:     2.7.12 |Continuum Analytics, Inc.| (default, Jul  2 2016, 17:42:40)  [GCC 4.4.7 20120313 (Red Hat 4.4.7-1)]
Python executable:     /opt/global/qiime/qiime1/bin/python

QIIME default reference information
===================================
For details on what files are used as QIIME's default references, see here:
 https://github.com/biocore/qiime-default-reference/releases/tag/0.1.3

Dependency versions
===================
        QIIME library version:       1.9.1
         QIIME script version:       1.9.1
qiime-default-reference version:       0.1.3
              NumPy version:       1.10.4
              SciPy version:       0.17.1
             pandas version:       0.18.1
         matplotlib version:       1.4.3
        biom-format version:       2.1.5
              h5py version:       2.6.0 (HDF5 version: 1.8.16)
              qcli version:       0.1.1
               pyqi version:       0.3.2
         scikit-bio version:       0.2.3
            PyNAST version:       1.2.2
           Emperor version:       0.9.51
            burrito version:       0.9.1
     burrito-fillings version:       0.1.1
         sortmerna version:       SortMeRNA version 2.0, 29/11/2014
         sumaclust version:       SUMACLUST Version 1.0.00
            swarm version:       Swarm 1.2.19 [Mar  5 2016 16:56:02]
                gdata:       Installed.

QIIME config values
===================
For definitions of these settings and to learn how to configure QIIME, see here:
 http://qiime.org/install/qiime_config.html
 http://qiime.org/tutorials/parallel_qiime.html

               blastmat_dir:     None
    pick_otus_reference_seqs_fp:     /opt/global/qiime/qiime1/lib/python2.7/site-packages/qiime_default_reference/gg_13_8_otus/rep_set/97_otus.fasta
                 sc_queue:     all.q
    topiaryexplorer_project_dir:     None
   pynast_template_alignment_fp:     /opt/global/qiime/qiime1/lib/python2.7/site-packages/qiime_default_reference/gg_13_8_otus/rep_set_aligned/85_otus.pynast.fasta
           cluster_jobs_fp:     start_parallel_jobs.py
pynast_template_alignment_blastdb:     None
assign_taxonomy_reference_seqs_fp:     /opt/global/qiime/qiime1/lib/python2.7/site-packages/qiime_default_reference/gg_13_8_otus/rep_set/97_otus.fasta
              torque_queue:     friendlyq
             jobs_to_start:     1
               slurm_time:     None
       denoiser_min_per_core:     50
assign_taxonomy_id_to_taxonomy_fp:     /opt/global/qiime/qiime1/lib/python2.7/site-packages/qiime_default_reference/gg_13_8_otus/taxonomy/97_otu_taxonomy.txt
               temp_dir:     /tmp/
             slurm_memory:     None
              slurm_queue:     None
              blastall_fp:     blastall
          seconds_to_sleep:     1
```